

**EGR-mediated
relapse mechanisms
in infant t(4;11)
acute lymphoblastic leukemia**

Dissertation
zur Erlangung des Doktorgrades
der Naturwissenschaften

vorgelegt beim Fachbereich 14
Biochemie, Chemie und Pharmazie
der Johann Wolfgang Goethe – Universität
in Frankfurt am Main

von
Marius Külp
aus Aschaffenburg

Frankfurt 2022

D30

vom Fachbereich 14 Biochemie, Chemie und Pharmazie
der Johann Wolfgang Goethe – Universität
als Dissertation angenommen.

Dekan: Prof. Dr. Clemens Glaubitz

1. Gutachter: Prof. Dr. Rolf Marschalek
2. Gutachter: Prof. Dr. Robert Fürst

Datum der Disputation: 27.10.2022

für meinen Großvater Jochen Kulp

I. Table of contents

1	Introduction	1
1.1	Hematopoiesis	1
1.1.1	Hematopoietic hierarchy	1
1.1.2	Hematopoietic development	2
1.2	Infant acute leukemia	3
1.2.1	Epidemiology and clinical characteristics	3
1.2.2	Treatment	5
1.2.2.1	Risk stratification and induction therapy	5
1.2.2.2	Postinduction therapy	6
1.2.2.3	Hematopoietic stem cell transplantation	7
1.2.2.4	Relapse development and chemoresistance	8
1.2.2.5	Novel therapeutic opportunities	9
1.2.2.5.1	Epigenetic drugs	9
1.2.2.5.2	Targeting the leukemia microenvironment	10
1.2.2.5.3	Immunotherapy	10
1.2.3	Biology of infant t(4;11) ALL	11
1.2.3.1	The KMT2A recombinome and the translocation t(4;11)(q21;23)	11
1.2.3.2	Developmental and cellular origin of t(4;11)(q21;23)	12
1.2.3.3	Oncogenic mechanism of KMT2A::AFF1 and AFF1::KMT2A fusions	13
1.2.3.4	HOXA gene expression patterns in childhood t(4;11) ALL	15
1.2.3.5	The immediate early genes EGR1, EGR2 and EGR3	15
1.3	Objective of this project	17
2	Organisms, material, and methods	18
2.1	Organisms	18
2.1.1	Human cell lines	18
2.1.2	Bacterial strains	18
2.2	Material	18
2.2.1	Recombinant DNA	18
2.2.2	Oligonucleotides	18
2.2.3	Media and solutions	19
2.2.4	Antibodies	20
2.2.5	Chemicals and recombinant proteins	21
2.2.6	Commercial assays and kits	22
2.2.7	Consumables	22
2.2.8	Devices	23

2.2.9	Software	24
2.3	Methods	24
2.3.1	Cellular methods	24
2.3.1.1	Stable transgenesis of cell lines.....	24
2.3.1.1.1	Transfection of HEK 293T cells	24
2.3.1.1.2	Electroporation of SEM cells	24
2.3.1.2	Fluorescence microscopy	24
2.3.1.3	Cell culture.....	25
2.3.1.4	Human T-cell isolation.....	25
2.3.1.5	Co-culture study	25
2.3.1.6	Flow cytometry.....	26
2.3.2	Molecular methods	26
2.3.2.1	Standard methods	26
2.3.2.2	Massive analysis of cDNA ends sequencing (MACE-Seq).....	26
2.3.2.3	Gene expression analysis using qRT-PCR	27
2.3.2.4	Patient gene expression analysis using qRT-PCR	27
2.3.2.5	Protein expression analysis using western blot	27
2.3.2.6	Chromatin immunoprecipitation qRT-PCR and sequencing.....	28
2.3.3	Statistical data analysis.....	28
3	Results	29
3.1	Gene expression profiling of EGR1-3 overexpressing HEK293T cell culture models.....	29
3.1.1	Generation of EGR1-3 overexpressing HEK293T cell culture models	29
3.1.2	Massive analysis of cDNA ends sequencing (MACE-Seq)	30
3.1.3	Gene expression profile comparison of <i>EGR1-3</i> and <i>IRX1</i> using PCA.....	31
3.1.4	Qualitative analysis of MACE-Seq data	35
3.2	Generation of IRX1 and EGR3 overexpressing SEM cell culture models	35
3.2.1	Cloning of pSBtet_IRX1cFLAG_P.....	36
3.2.2	Establishment of stable cell culture models SEM::EGR3 and SEM::IRX1	36
3.3	Gene and protein expression analysis of SEM::EGR3 and SEM::IRX1 cell culture models	38
3.4	Characterization of ICOSLG upregulation through EGR3 overexpression	38
3.4.1	ChIP-qRT-PCR.....	38
3.4.2	ChIP-Seq.....	40
3.5	Gene expression analysis of infant t(4;11) ALL patients at diagnosis.....	41
3.5.1	Event-free survival analysis of infant t(4;11) ALL patients at diagnosis.....	45
3.5.1.1	Event-free survival depending on HOXA9 gene expression	46
3.5.1.2	Event-free survival depending on ICOSLG gene expression.....	46

3.6	Gene expression analysis of infant ALL patients at relapse	48
3.7	Primary T-cell co-culture study	50
4	Discussion.....	55
4.1	EGR3 as the main mediator of IRX1 signaling.....	55
4.2	Characterization of <i>ICOSLG</i> upregulation through EGR3 overexpression	56
4.3	Gene expression analysis using cell culture models and patient samples	57
4.4	Event-free survival depending on <i>HOXA9</i> gene expression.....	57
4.5	<i>IRX1</i> and <i>EGR3</i> expression depending on <i>HOXA9</i> gene expression.....	59
4.6	<i>ICOSLG</i> gene expression and relapse development	59
4.7	The role of ICOSLG in T-cell-mediated immunity	60
4.8	ICOSLG-mediated Treg expansion as a relapse mechanism in infant t(4;11) ALL	63
5	References.....	69
6	List of figures.....	94
7	List of tables.....	95
8	Acknowledgements	96
9	Declaration.....	97

II. Table of abbreviations

aa	amino acids
ALL	acute lymphoblastic leukemia
AML	acute myeloid leukemia
ampR	Ampicillin resistance
APC	antigen presenting cell
BM	bone marrow
bp	base pairs
BS	binding site
CAR	chimeric antigen receptor
cDNA	complementary DNA
ChIP	chromatin immunoprecipitation
ChIP-qRT-PCR	ChIP quantitative real time polymerase chain reaction
ChIP-Seq	ChIP-Sequencing
CI	confidence interval
DCAL	Diagnostic Center of Acute Leukemia
DNA DSB	DNA double-strand break
dNTP	deoxy nucleoside triphosphate
dx	diagnosis cohort
E	erythrocytes
EFS	event-free survival
ELISA	enzyme linked immunosorbent assay
FDNA	fusion-derived neoantigen
Fig.	Figure
FL	fetal liver
G	granulocytes
gDNA	genomic DNA
G-MDSC	granulocytic monocyte derived suppressor cells
i.m.	intramuscular
i.t.	intrathecal
i.v.	intravenous
iALL	infant acute lymphoblastic leukemia
kb	kilobases
kDa	kilo Dalton
KMT2A-r	KMT2A-rearrangements
LIC	leukemia initiating cells
log2fc	log2 fold change
LPS	lipopolysaccharides
mAb	monoclonal antibody
MACE	massive analysis of cDNA ends
MACE-Seq	massive analysis of cDNA ends sequencing
MHC	major histocompatibility complex
MRD	minimal residual disease
NGS	next generation sequencing
ORF	open reading frame

OS	overall survival
p.o.	peroral
PB	peripheral blood
PBMC	peripheral blood mononuclear cells
PCA	principal component analysis
PCR	polymerase chain reaction
PDX	patient derived xenograft
PP	primer pair
QC	quality control
qRT-PCR	quantitative real time polymerase chain reaction
rel	relapse cohort
RIN	RNA integrity number
RT	room temperature
s.c.	subcutaneous
SB	sleeping beauty
SDS-PAGE	SDS polyacrylamide gel electrophoresis
SE	standard error
t	translocation
TCR	T-cell receptor
TH	helper T-cells
TK	killer T-cells
Treg	regulatory T-cell
TSS	transcription start site
tx	transcription

III. Deutschsprachige Zusammenfassung

Leukämie ist durch die Störung der Homöostase des hierarchischen hämatopoetischen Systems gekennzeichnet, wodurch es zu einer übermäßigen Proliferation unreifer Blutzellen kommt. Dabei ist Leukämie die häufigste Krebserkrankung im Kindesalter. Innerhalb der deutschen Bevölkerung sind 29,5% aller Krebsdiagnosen bei Patienten unter 18 Jahren auf Leukämie zurückzuführen (Robert Koch-Institut, 2021).

Leukämie entwickelt sich aufgrund unterschiedlicher zytogenetischer Ereignisse, die entweder numerische Aberrationen einschließlich Hyperdiploidie oder strukturelle Aberrationen einschließlich Translokationen, Deletionen, Amplifikationen und Inversionen sind (De Lorenzo *et al.*, 2014; Mrózek *et al.*, 2004). Diese zytogenetischen Aberrationen bestimmen in den meisten Fällen einen bestimmten Leukämie-Subtyp und korrelieren mit der Prognose. Diese starke Korrelation zwischen einem oder wenigen zytogenetischen Ereignissen und dem Krankheitsverlauf steht in starkem Kontrast zu den meisten soliden Tumoren, die in der Mehrheit der Fälle durch die Akkumulation von Punkt-Mutationen gekennzeichnet sind. Zudem findet man in einigen Fällen aber auch dort chromosomale Translokationen. Veränderungen in soliden Tumoren weisen häufig auf genomische Instabilität hin, während bei Leukämien chromosomale Translokationen oft die einzige genetische Veränderung darstellen (Lengauer, 2001).

Säuglingsleukämie ist definiert durch den Erkrankungsbeginn im Alter unter einem Jahr und unterscheidet sich in vielen Merkmalen von Leukämie bei Kindern und Erwachsenen. Obwohl akute Säuglingsleukämie mit etwa 160 Fällen pro Jahr in den USA eine geringe Inzidenz aufweist (Howlader *et al.*, 2021), ist die Krankheit aufgrund hoher Rückfallraten und damit assoziierter Sterblichkeit verheerend (Pieters *et al.*, 2019, 2007; Quessada *et al.*, 2021). Leukämie kann in lymphoblastische (ALL) und myeloische (AML) Formen unterteilt werden. Der genomische Hintergrund der Säuglings-AML ist heterogen (Quessada *et al.*, 2021), wohingegen 70 – 80% aller Fälle von Säuglings-ALL (iALL) Translokationen des *KMT2A* Gens als ursächliche genomische Veränderungen aufweisen (*KMT2A-r*, früher *MLL*) (Pieters *et al.*, 2019, 2007). Die Dominanz von *KMT2A*-Rearrangements im Säuglingsalter ist einzigartig, so macht die Prävalenz von *KMT2A* Veränderungen bei pädiatrischer ALL nur etwa 5% aus (Behm *et al.*, 1996). Die Translokation t(4;11), die die Fusionsonkogene *KMT2A::AFF1* und *AFF1::KMT2A* erzeugt, ist die häufigste Art von *KMT2A*-rearrangierter Säuglings-ALL und tritt bei fast jedem zweiten *KMT2A*-rearrangierten Säuglings-ALL Patienten auf (Meyer *et al.*, 2018).

Klinisch weisen pädiatrische ALL-Patienten eine Vielzahl von Symptomen auf, darunter Hyperleukozytose, Fieber, Lethargie, Organomegalie, Hautläsionen und Zytopenie (Chessells *et al.*, 2002). Im Vergleich zu älteren Kindern zeigen Säuglinge mit ALL zusätzlich aggressivere Symptome wie eine sehr hohe Anzahl weißer Blutzellen (WBC), Hepatosplenomegalie und Beteiligung des Zentralnervensystems (ZNS) (Hilden *et al.*, 2006).

Zur Behandlung durchlaufen Säuglinge mit einer t(4;11) ALL eine in Induktions-, Konsolidierungs-, Reinduktions- und Erhaltungsphase gegliederte Chemotherapie, trotz derer 64% der Patienten innerhalb von vier Jahren nach der Diagnose ein „Ereignis“ einschließlich Rezidiv oder Tod erleiden. Das Gesamtüberleben drei Jahre nach einem Rezidiv beträgt nur 17% (Driessen *et al.*, 2016; Pieters *et al.*, 2019, 2007). Typischerweise erreichen die Patienten mit der Induktionstherapie schnell eine vollständige Remission (CR), erleiden jedoch bereits wenige Monate später trotz anhaltender Chemotherapie ein Rezidiv. Innerhalb dieser Zeit erwirbt die leukämische Population eine Chemoresistenz ohne, dass diese durch eine Zunahme an Sekundär-Mutationen erklärbar wäre.

Bei pädiatrischer ALL identifizierten Sequenzierungsstudien des gesamten Genoms Chemotherapie-induzierte Mutagenese als Hauptgrund für Arzneimittelresistenzen und Rezidiventwicklung (Li *et al.*, 2020). Im Gegensatz dazu zeigten genomweite Analysen von übereinstimmenden Säuglings-ALL-Patientenproben zu verschiedenen Zeitpunkten vor und zum Zeitpunkt des Rezidivs, dass die t(4;11)-ALL bei Säuglingen mit etwa 1,3 Mutationen im dominanten leukämischen Klon eine der niedrigsten Mutationslasten unter allen pädiatrischen Krebsarten aufweist (Agraz-Doblas *et al.*, 2019; Andersson *et al.*, 2015; Bardini *et al.*, 2011; Dobbins *et al.*, 2013; Mullighan *et al.*, 2007).

Aufgrund dessen stellt sich die Frage, durch welche molekularen Mechanismen Chemoresistenz erreicht wird.

Mittlerweile gilt als bewiesen, dass der t(4;11) Translokationsprozess pränatal *in utero* stattfindet. Greaves und Kollegen untersuchten die Zytogenetik von eineiigen Zwillingen, bei denen im Säuglings- und frühen Kindesalter eine konkordante ALL diagnostiziert wurde. Sie fanden heraus, dass die Leukämiezellen beider Geschwister den selben chromosomalen Bruchpunkt aufwiesen, was stark darauf hindeutete, dass die Translokation pränatal bei einem der Zwillinge stattfand und anschließend Leukämiezellen durch die gemeinsame Plazenta zum anderen Zwillings migrierten (Ford *et al.*, 1993; Greaves *et al.*, 2003; Greaves und Wiemels, 2003). Der pränatale Ursprung der Translokation wurde später für *KMT2A::AFF1* ALL durch retrospektive Studien von neonatalen Blutproben (Guthrie Cards) bestätigt.

In der Vergangenheit wurde die Überexpression des *HOXA* Genclusters als allgemeines Merkmal der *KMT2A*-rearrangierten akuten lymphoblastischen Leukämie angesehen, welches das Genexpressionsprofil der Krankheit definierte (Armstrong *et al.*, 2002; Ferrando *et al.*, 2003; Rozovskaia *et al.*, 2001). Darüber hinaus zeigten *Knockdown*-Experimente die ausgeprägte *HOXA9*-Abhängigkeit *KMT2A*-rearrangierter Zelllinien zur Vermeidung von Apoptose (Faber *et al.*, 2009). Dieses Dogma wurde 2009 in Frage gestellt, als Trentin *et al.* zwei unterschiedliche Genexpressionsmuster bei t(4;11) ALL im Säuglingsalter fanden (Trentin *et al.*, 2009). Die Patienten wurden gemäß ihrer *HOXA* Genexpression im Vergleich zu gesunden Kontrollen in eine *HOXA*^{lo}- und eine *HOXA*^{hi}-Gruppe eingeteilt. Nur die *HOXA*^{lo}, nicht aber die *HOXA*^{hi}-Patienten, zeigten eine Hochregulierung des *IRX1* Gens, das an der frühen embryonalen Segmentierung beteiligt ist (Bosse *et al.*, 1997). Zwei weitere Studien bestätigten diese Befunde und zeigten zusätzlich eine erhöhte Rezidivinzidenz (Stam *et al.*, 2010) bzw. ein schlechteres ereignisfreies Überleben (Kang *et al.*, 2012) von *HOXA*^{lo} Patienten. Kühn *et al.* zeigten in *in vitro* Experimenten, dass *IRX1*-Überexpression zu einer indirekten Hochregulierung der *Early Growth Response 1, 2* und *3* Gene (*EGR1*, *EGR2*, *EGR3*) führte. Diese Entdeckung ist die Grundlage des vorliegenden Promotionsvorhabens.

Trotz jüngster Fortschritte in der Therapie der pädiatrischen Leukämie durch die Anwendung von Kinase-Inhibitoren, Immuntherapie und verbesserter hämatopoetischer Stammzelltransplantation (HSZT) ist die *KMT2A*-rearrangierte ALL bei Säuglingen immer noch durch eine hohe Rezidivinzidenz gekennzeichnet, begleitet von einer Rezidiv-assoziierten Mortalität (Driessen *et al.*, 2016; Pieters *et al.*, 2019, 2007).

Dieses Promotionsprojekt zielte darauf ab, die molekularen Mechanismen, die zu einem Rezidiv der t(4;11) Säuglings-ALL führen, besser zu verstehen. Weiterhin sollte eine mögliche Korrelation zwischen der *HOXA*^{lo}-*IRX1*-*EGR*-Achse und der Rezidiventwicklung bei t(4;11) Säuglings-ALL untersucht werden. In diesem Zusammenhang sollte die Rolle der *EGR*-Gene evaluiert werden, um molekulare Targets zur potentiellen Prävention der Rezidivierung zu identifizieren.

Um zu untersuchen, ob die höhere Rezidivierungsrate von *IRX1*^{hi}/*HOXA*^{lo} Patienten durch die *EGR* Gene vermittelt werden könnte, wurden drei HEK293T Zellkulturmodelle generiert, die *EGR1*, *EGR2* oder *EGR3* überexprimierten. Anschließend wurden die Genexpressionsprofile dieser drei Zellkulturmodellen mittels *massive analysis of cDNA ends sequencing* (MACE-Seq) untersucht. Der Vergleich der Genexpressionsprofile mit dem eines *IRX1* Zellkulturmodells, das von Kühn *et al.* (2016) publiziert wurde, identifizierte *EGR3* als Hauptmediator der *IRX1*-induzierten Transkription. Um dies im zellulären Kontext der t(4;11) proB-ALL zu untersuchen, wurden *IRX1*- und *EGR3*-überexprimierende SEM-Zellkulturmodelle (SEM::*IRX1*, SEM::*EGR3*) etabliert und die Gen- und Proteinexpression untersucht. Die SEM Zelllinie weist den Geno- und Phänotyp der t(4;11) Säuglings-ALL auf. Die Gen- und Proteinexpressionsstudie führte zur Identifikation des Immunrezeptors *ICOSLG* als am stärksten hochreguliertes *EGR3*-Target. Chromatin-Immunpräzipitation (ChIP), gefolgt von qRT-PCR (ChIP-qRT-PCR) und *next generation sequencing* (ChIP-Seq), verifizierte, dass *EGR3* als Zinkfingertranskriptionsfaktor direkt den *ICOSLG* Promotor bindet und dadurch eine entsprechende Hochregulation bewirkte.

Die Ergebnisse aus den Zellkulturmodellen sollten durch Untersuchung primärer Patientenproben überprüft werden. Dafür wurde die Genexpression von 50 t(4;11) Säuglings-ALL-Patienten mittels qRT-PCR analysiert. Drei Studienzentren stellten dafür Patienten-RNA zur Verfügung, die zum Zeitpunkt der Diagnose aus peripherem Blut gewonnen wurde. Unter Verwendung der ΔC_T -Mittelwerte wurden Pearson-Korrelationstests durchgeführt, um Korrelationen zwischen den Genexpressionen von *IRX1*, *EGR3* und *ICOSLG* zu identifizieren. Die resultierende Pearson-Korrelationsmatrix zeigte positive Korrelationen für *IRX1/EGR3*, *EGR3/ICOSLG* und *IRX1/ICOSLG*. Dies bestätigte die Hochregulierung von (1) *EGR3* durch *IRX1*, wie von Kühn *et al.*, 2016 beschrieben, (2) *ICOSLG* durch *EGR3*, wie durch die SEM-Zellkulturmodelle suggeriert, und (3) *ICOSLG* durch *IRX1*. Damit wurde bestätigt, dass die mittels *in vitro* Untersuchungen identifizierte *IRX1-EGR3-ICOSLG* Achse auch tatsächlich in Patienten zu finden ist. Der höchste Korrelationswert wurde für die *EGR3/ICOSLG* Korrelation berechnet und war mit den ChIP-Experimenten in Einklang, die eine direkte Transaktivierung von *ICOSLG* durch *EGR3* zeigten.

Des Weiteren waren für 43 von 50 Patienten Überlebensdaten verfügbar, die eine Analyse des ereignisfreien Überlebens (EFS) ermöglichten, wobei EFS als die Zeit von der Diagnose bis zum ersten Ereignis (Induktionsversagen, Rezidiv, Tod oder Sekundärmalignizität) definiert wurde. Zur Untersuchung der zu Anfang beschriebenen höheren Rückfallraten der *HOXA*^{lo}-Patienten (Kang *et al.*, 2012; Stam *et al.*, 2010) wurde das EFS in Abhängigkeit der *HOXA9*-Genexpression bestimmt. Wie in der Literatur beschrieben, gruppieren sich die Patienten in eine *HOXA9*^{lo}- und eine *HOXA9*^{hi}-Gruppe. Die anschließende Kaplan-Meier-EFS-Analyse ergab, dass der zuvor berichtete EFS-Nachteil der *HOXA9*^{lo}-Gruppe mit einem 4-Jahres-EFS von $34,9 \pm 13,4\%$ im Vergleich zu $46,4 \pm 10,2\%$ der *HOXA9*^{hi}-Gruppe recht gering war. Außerdem waren die EFS-Kurven in einem Log-Rank-Test nicht signifikant unterschiedlich. Vorherige Studien bestätigend war das relativ erhöhte mittlere *IRX1*-Genexpressionsniveau der *HOXA9*^{lo}-Gruppe im Vergleich zur *HOXA9*^{hi}-Gruppe. Obwohl eine starke Korrelation zwischen den *IRX1*- und *EGR3*-Genexpressionen nachgewiesen wurde, zeigte die *HOXA9*^{lo}/*IRX1*^{hi}-Gruppe kein höheres *EGR3*-Genexpressionsniveau als die *HOXA9*^{hi}/*IRX1*^{lo}-Gruppe.

Um einen möglichen Beitrag der *ICOSLG*-Expression zur Therapieresistenz zu untersuchen, wurde eine EFS-Analyse unter Berücksichtigung der *ICOSLG*-Genexpression durchgeführt. Patienten mit einem *ICOSLG*-Expressionsniveau, welches das Expressionsniveau des SEM::*EGR3*-Zellkulturmodells erreichte oder überstieg, wurden als *ICOSLG*^{hi}-, die verbleibenden als *ICOSLG*^{lo}-Gruppe definiert. Die Kaplan-Meier-EFS-Analyse zeigte ein deutlich schlechteres EFS der *ICOSLG*^{hi}-Gruppe (n=7, 2y-EFS=0%) im Vergleich zur *ICOSLG*^{lo}-Gruppe (n=36, 2y-EFS= $58,8 \pm 8,8\%$). Dieser Unterschied wurde in einem Log-Rank-

Test als statistisch signifikant bestätigt. Zu beachten ist, dass die EFS-Analyse aufgrund der unterschiedlichen Gruppengröße ($n = 7$ vs. $n = 36$) verzerrt sein könnte. Eine potenzielle Verzerrung aufgrund des Patientenalters konnte jedoch ausgeschlossen werden, da sowohl die *ICOSLG*^{hi}- als auch die *ICOSLG*^{lo}-Gruppe aus Patienten bestanden, die zum Zeitpunkt der Diagnose jünger und älter als sechs Monate waren. In Übereinstimmung mit den vorherigen Untersuchungen der Genexpressionskorrelationen zeigte die *ICOSLG*^{hi}-Gruppe ($n=8$) aller Patienten ($n=50$) relativ erhöhte *EGR3*- und *IRX1*-Genexpressionsniveaus im Vergleich zur *ICOSLG*^{lo}-Gruppe. Insgesamt wurde also gezeigt, dass eine hohe *ICOSLG*-Genexpression zum Zeitpunkt der Diagnose mit einem schlechteren EFS bei Säuglingen mit *t(4;11)* ALL assoziiert war.

Daraus ergab sich die Frage, ob eine hohe *ICOSLG* Expression auch direkt mit der Entwicklung eines Rezidivs in Verbindung gebracht werden könnte. Zur Überprüfung dieser Hypothese wurden 18 RNA Proben von rezidierten *KMT2A*-r Säuglings-ALL Patienten untersucht, die zum Zeitpunkt des Rezidivs entnommen wurden („Rezidivkohorte“). Mittels qRT-PCR wurde die Genexpression von *HOXA9*, *IRX1*, *EGR3* und *ICOSLG* bestimmt. Diese Kohorte war unabhängig und nicht mit den Patienten der vorherigen Kohorte zum Zeitpunkt der Diagnose assoziiert. Die Genexpression der Rezidivkohorte wurde mit der Genexpression der Kohorte zum Zeitpunkt der Primärdiagnose („Diagnosekohorte“) verglichen. Dabei wurden ausschließlich die Patienten der Diagnosekohorte eingeschlossen, die auch ein Ereignis zeigten ($n=23$), um einen angemessenen, unverzerrten Vergleich beider Kohorten zu ermöglichen. Dabei wurde deutlich, dass die Rezidivkohorte im Vergleich zur Diagnosekohorte allgemein höhere *ICOSLG*- und *EGR3*-Genexpressionsniveaus aufwies. Wichtig dabei war, dass die mediane *ICOSLG*-Genexpression der Rezidivkohorte in etwa dem Niveau der *ICOSLG*^{hi}-Gruppe der Diagnosekohorte entsprach. Außerdem waren die Genexpressionen von *ICOSLG* und *EGR3* der Rezidivkohorte höher als die der Diagnosekohorte, während dies nicht für *IRX1* und *HOXA9* der Fall war. Insgesamt deuteten diese Befunde auf einen direkten Zusammenhang zwischen der *EGR3/ICOSLG*-Expression und einer Rezidivierung hin.

Daran anknüpfend wurde eine Hauptkomponentenanalyse (PCA) durchgeführt, um den Grad der Ähnlichkeit zwischen den Genexpressionsprofilen zu bestimmen. Die PCA zeigte eine hochgradige Ähnlichkeit zwischen der Gruppe von Patienten mit erhöhter *ICOSLG*-Expression zum Zeitpunkt der Diagnose und den Patienten zum Zeitpunkt des Rezidivs. Diese Ergebnisse deuten stark darauf hin, dass die *EGR3-ICOSLG*-Korrelation an der Rezidivierung beteiligt war und dass ein hohes *ICOSLG*-Expressionsniveau bei der Diagnose als Prädiktor für eine Rezidivierung beschrieben werden kann. Die Genexpressionsuntersuchungen der Patienten zum Zeitpunkt der Diagnose und zum Zeitpunkt des Rezidivs ergaben damit, dass erhöhte *EGR3*- und *ICOSLG*-Expressionen mit der Rezidivierung assoziiert waren und eine hohe *ICOSLG*-Expression zum Zeitpunkt der Diagnose ein Rezidiv vorhersagte. Ein kausaler Zusammenhang zwischen *EGR3/ICOSLG*-Expression und Rückfallbildung blieb jedoch zunächst unklar.

In der Literatur wurde eine erhöhte *ICOSLG*-Expression mit der Entwicklung regulatorischer T-Zellen (Treg) in der gesunden Knochenmarksnische (Lee *et al.*, 2017), beim Glioblastom (Iwata *et al.*, 2019), beim Melanom (Martin-Orozco *et al.*, 2010), bei Brustkrebs (Faget *et al.*, 2012) und bei akuter myeloischer Leukämie (AML) (Han *et al.*, 2018) in Verbindung gebracht. Daher entstand die Hypothese, dass die *ICOSLG*-Expression von *t(4;11)* ALL-Zellen, die sich in der Knochenmarksnische aufhalten, die Entwicklung benachbarter regulatorischer T-Zellen fördern könnte. In der Folge könnten ALL-Zellen vor einem Immunangriff geschützt sein, sodass die Rezidivierung ermöglicht werden könnte. Dementsprechend musste die Fähigkeit zur Induktion der Entwicklung regulatorischer T-Zellen durch *ICOSLG*-exprimierende *t(4;11)* ALL-Zellen evaluiert werden. Zu diesem Zweck wurde eine Co-Kultivierung von *EGR3*-überexprimierenden SEM-Zellen (SEM::*EGR3*) oder Leervektor-transfizierten SEM-Zellen

(SEM::mock) mit primären T-Zellen durchgeführt. Das Experiment wurde mit isolierten T-Zellen von sechs unabhängigen gesunden Spendern (HD1 – HD6) durchgeführt und führte zu einer Erhöhung des Anteils von CD25⁺FOXP3⁺ regulatorischen T-Zellen in der SEM::EGR3-Kokultur zwischen 7,96% und 23,94% im Vergleich zur SEM::mock-Co-Kultur. Dieses Ergebnis zeigte, dass die Überexpression von EGR3 in t(4;11) ALL-Zellen die schnelle Expansion regulatorischer T-Zellen bei Co-Kultivierung mit primären T-Zellen vermittelte.

Um die eingangs erläuterte Hypothese zu überprüfen, dass eine EGR3-vermittelte Hochregulation von ICOSLG zur Entwicklung regulatorischer T-Zellen führen könnte, wurde das Experiment mit HD1 – HD3 unter Zugabe eines neutralisierenden monoklonalen α -ICOSLG Antikörpers im Vergleich zu einem unspezifischen IgG1 Antikörper wiederholt. Die EGR3-vermittelte Entwicklung regulatorischer T-Zellen wurde durch den α -ICOSLG-Antikörper, aber nicht durch die IgG-Kontrollbehandlung beeinträchtigt, was stark darauf hindeutete, dass ICOSLG den Mediator der EGR3-induzierten Expansion regulatorischer T-Zellen darstellte. Dieses Ergebnis wurde durch die Quantifizierung der Zytokinspiegel in den Co-Kulturüberständen unter Verwendung von ELISA bestätigt. Die Anwendung des α -ICOSLG Antikörpers beeinflusste die IL-2-Spiegel der Co-Kulturüberstände nicht, führte aber zu einer signifikanten Abnahme der IL-10-Spiegel. IL-10 ist ein immunsuppressives Zytokin, das von regulatorischen T-Zellen sezerniert wird und als Indikator für deren Funktion dient (Maynard *et al.*, 2007). Somit wurde die α -ICOSLG-Behandlung als wirksam zur Beeinträchtigung der Entwicklung regulatorischer T-Zellen evaluiert, sowohl phänotypisch mittels Durchflusszytometrie, als auch funktionell durch ELISA. Final konnte gezeigt werden, dass in Übereinstimmung mit vorherigen Untersuchungen (Duhon *et al.*, 2012) die ICOS-Oberflächenexpression CD25⁺FOXP3⁺ regulatorischer T-Zellen höher als die der übrigen T-Zellen war.

Insgesamt zeigte dieses Promotionsprojekt, dass die ICOSLG-vermittelte Expansion regulatorischer T-Zellen zur Rezidivbildung beiträgt. Dies deutet darauf hin, dass dieser Mechanismus die Immunerkennung von ALL-Zellen beeinträchtigen könnte. Die Rekrutierung regulatorischer T-Zellen in direkter Nachbarschaft zu ALL-Zellen könnte somit ein Immunprivileg in der Knochenmarksnische etablieren. Dieser potentielle Immunumgehungsmechanismus könnte erklären, wie t(4;11)-ALL-Zellen eine Therapieresistenz ohne eine Zunahme von Sekundärmutationen erreichen. Wie oben beschrieben, wurde dieser Mechanismus bereits im gesunden Knochenmark, bei Brustkrebs, dem malignen Melanom, dem Glioblastom und der akuten myeloischen Leukämie beschrieben (Lee *et al.*, 2017; Iwata *et al.*, 2019; Martin-Orozco *et al.*, 2010; Faget *et al.*, 2012; Han *et al.*, 2018).

Im Detail zeigten *HOXA9*⁰-Patienten eine erhöhte *IRX1*-Genexpression, die mit einer Hochregulation von *EGR3* korrelierte. *EGR3* wiederum transaktivierte direkt die Expression des Immun-Checkpoints *ICOSLG*, wodurch die Expansion von stark immunsuppressiven IL-10-produzierenden regulatorischen T-Zellen induziert wurde. Diese regulatorischen T-Zellen könnten eine immunsuppressive Mikroumgebung in der Nische Leukämie-initiiierender Zellen (LIC) etablieren, wodurch es zu einem Wiederauftreten einer minimalen Resterkrankung (MRD) und in der Folge zu einem Rezidiv kommen könnte. Außerdem zeigte dieses Promotionsprojekt, dass eine erhöhte *ICOSLG*-Expression zum Zeitpunkt der Diagnose eine Rezidivierung vorhersagt und dass das *Targeting* des Immunrezeptors ICOSLG mit einem neutralisierenden monoklonalen Antikörper die ICOSLG-vermittelte Expansion regulatorischer T-Zellen *in vitro* beeinträchtigte. Diese Ergebnisse implizieren die ICOSLG-Checkpoint-Inhibition als potentielle therapeutische Möglichkeit zur Rezidivprävention und zur Behandlung von Rezidiv-assoziierten Therapieresistenzen. In der Folge liefert dieses Promotionsprojekt eine molekulare Begründung für die klinische Prüfung des gegen ICOSLG gerichteten, vollständig humanen monoklonalen Antikörpers Prezalumab zur Behandlung einer Therapieresistenz der t(4;11) ALL bei Säuglingen.

1 Introduction

1.1 Hematopoiesis

1.1.1 Hematopoietic hierarchy

The hematopoietic system is classically described as a hierarchical tree-like structure in which all blood cells are derived from different types of multipotent progenitor cells which in turn are descendants of hematopoietic stem cells (HSC) that have the ability to self-renew without differentiation (Abkowitz *et al.*, 2002; Morrison *et al.*, 1995). In this model, development of a HSC to a terminally differentiated effector cell type is a stepwise process characterized by increasing differentiation and lineage restriction, while the ability to self-renew is lost (**Figure 1**) (Chao *et al.*, 2008). HSC differentiate to multipotent progenitors (MPP) which depending on the cytokine milieu further develop into oligopotent common myeloid or lymphoid progenitors (CMP, CLP). The myeloid lineage is further segregated into megakaryocyte-erythrocyte-progenitors (MEP) and granulocyte-macrophage-progenitors (GMP). These oligopotent progenitors differentiate into lineage-restricted progenitors that in turn give rise to mature blood cells. In this context, HSC are defined as cells being able to recapitulate the whole hematopoietic system in irradiated immune-suppressed recipients upon transplantation (Chao *et al.*, 2008; Morrison *et al.*, 1995). The different populations of the hematopoietic system were defined through flow cytometric assessment of phenotypic markers (**Figure 1**).

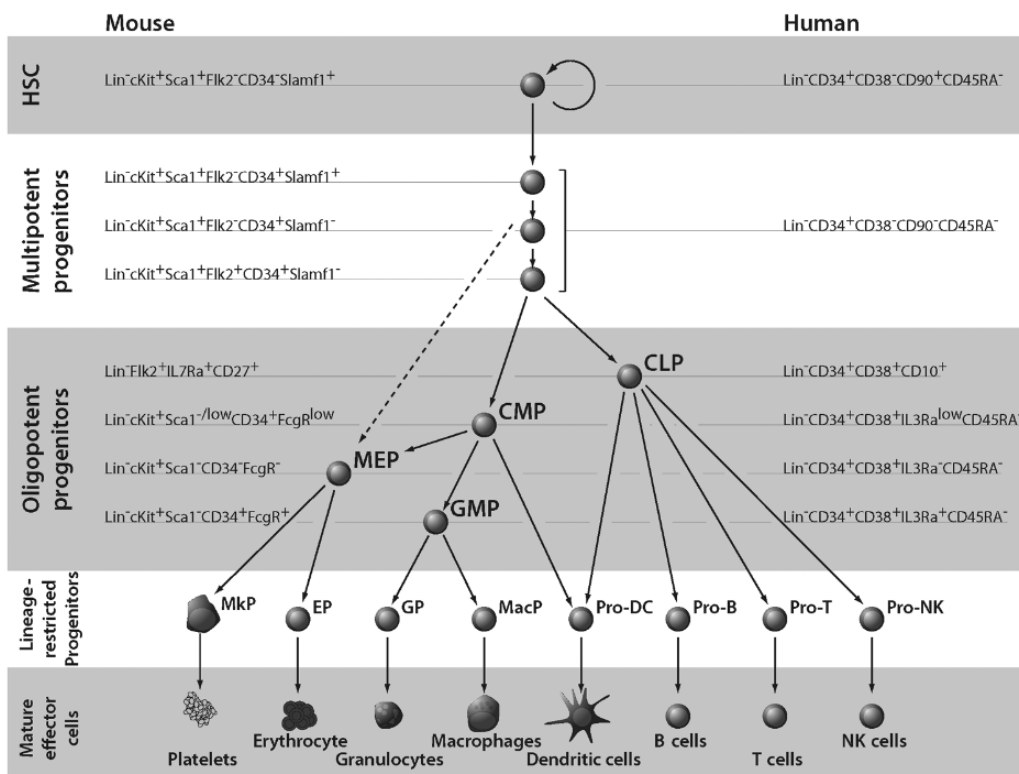


Figure 1. Taken from Chao *et al.*, 2008. The mouse and human multistep hematopoietic system. HSC = Hematopoietic stem cell. Lin = lineage markers. CLP = Common lymphoid progenitor. CMP = Common myeloid progenitor. MEP = Megakaryocyte-erythrocyte-progenitor. GMP = Granulocyte-macrophage-progenitor. MkpP = Megakaryocyte-progenitor. EP = Erythrocyte-progenitor. GP = Granulocyte-progenitor. MacP = Macrophage-progenitor. DC = Dendritic cell. NK = Natural killer.

In the last years, this stepwise model of hematopoiesis became challenged through the implementation of transcriptomic, flow cytometric and functional studies at the single-cell level. Those revealed that differentiating HSC do not necessarily have to pass through all distinct steps of differentiation and that cells defined as multipotent progenitors more represent a transition state of a continuous lineage

commitment process rather than a definitive cell type (Velten *et al.*, 2017). Furthermore, sophisticated studies identified dramatic changes of the blood hierarchy in fetal liver (FL) compared to that in adult bone marrow (BM). In the FL, oligopotent progenitors with myeloid-erythroid-megakaryocytic activity were identified whereas the adult BM was mainly composed of unilineage progenitors with myeloid or erythroid potential. As a result, a new hierarchic model of adult BM myeloid hematopoiesis was proposed which lacks oligopotent progenitor populations as intermediates between multipotent HSC and unipotent effector cells (**Figure 2**) (Notta *et al.*, 2016).

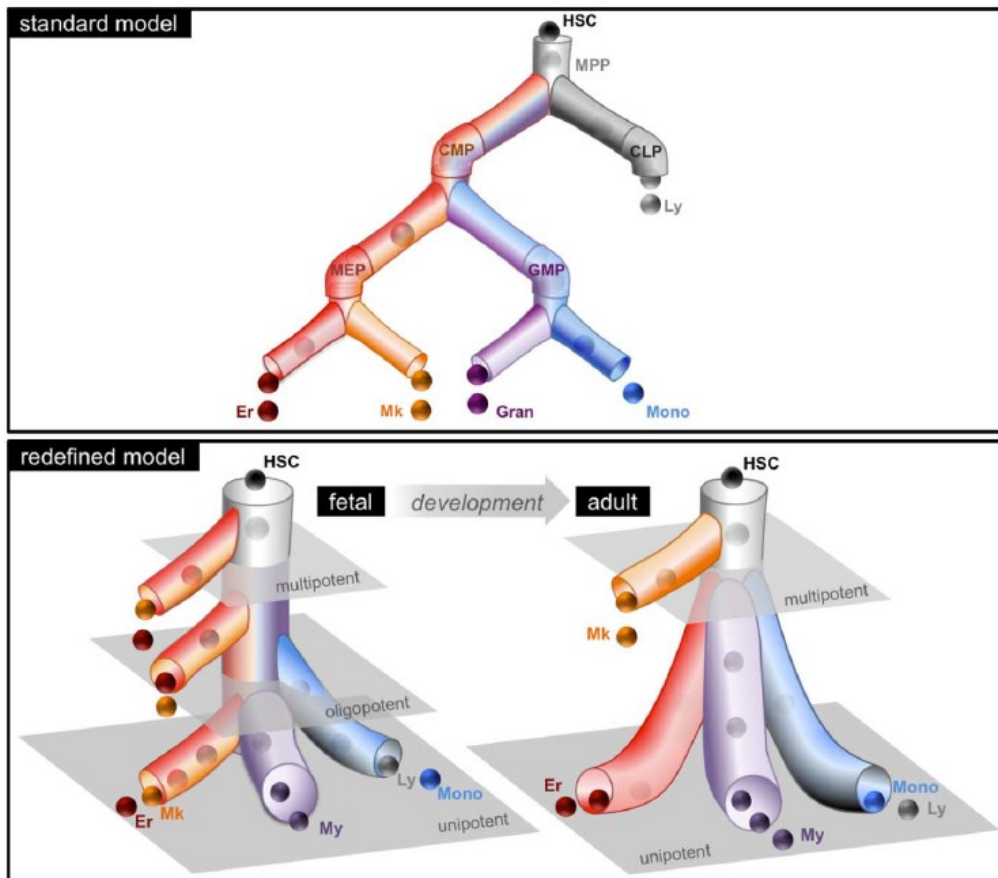


Figure 2. Taken from Notta *et al.*, 2016. The standard model of hematopoietic hierarchy (top) compared to the proposed redefined model in FL (bottom left) and adult BM (bottom right). Er = Erythrocytes. My = myeloid cells. Ly = lymphoid cells. Mono = Monocytes.

1.1.2 Hematopoietic development

Although HSC are frequently regarded as the origin of hematopoiesis, this does not apply during embryonic development. In mammals, embryonic development of the hematopoietic system proceeds in three waves: primitive, pro-definitive and definitive hematopoiesis (McGrath *et al.*, 2015; Palis, 2014). Primitive hematopoiesis in the mouse takes place in the yolk sac and gives rise to nucleated erythrocytes, megakaryocytes and macrophages at embryonic day 7 (E7) (Bertrand *et al.*, 2005; Chen *et al.*, 2011; Palis *et al.*, 1999). Nucleated erythrocytes meet the oxygenic demands of the growing embryo as oxygen diffusion from surrounding tissues becomes limited. Macrophages are required for tissue remodeling and defense, and megakaryocytes contribute to blood vessel maintenance (Bertrand *et al.*, 2005; Kingsley *et al.*, 2004). The subsequent second wave, the pro-definitive hematopoiesis, begins at E8.25 and is characterized by the emergence of erythromyeloid progenitors (EMP), lymphoid-primed multipotent progenitors (LMPP) and multilineage mesodermal progenitors (Azzoni *et al.*, 2014; Ghosn *et al.*, 2019). These cells develop through endothelial-to-hematopoietic transition (EHT) from the

hemogenic endothelium (Ottersbach, 2019) and sustain erythropoiesis, megakaryocyte, myeloid cell and NK cell development (Dege *et al.*, 2020; McGrath *et al.*, 2015). The first and second wave of embryonic hematopoiesis take place in the yolk sac, do not produce HSC, and thus are described as HSC-independent. The definitive hematopoiesis as the third wave begins with the emergence of HSC at E10.5 which develop through EHT in the aorta-gonad-mesonephros (AGM) region (Kissa and Herbomel, 2010; Medvinsky and Dzierzak, 1996; Müller *et al.*, 1994). Besides, HSC development has been detected in the umbilical arteries, embryonic head, and placenta (de Bruijn *et al.*, 2000; Z. Li *et al.*, 2012; Ottersbach and Dzierzak, 2005). At E12, HSC expand in the FL and home to and reside in the BM shortly prior to birth but throughout adulthood (Kumaravelu *et al.*, 2002). This definitive HSC-dependent hematopoiesis is structured as explained in 1.1.1.

In general, hematopoietic development is quite conserved in mammals. However, the described processes are well studied in mice, zebrafish, and other species, but only marginally in human tissues due to a lack of appropriate samples. The implementation of single-cell techniques and advanced *ex vivo* expansion protocols recently enabled first detailed comparisons between mouse and human embryonic hematopoiesis (Du *et al.*, 2021; Easterbrook *et al.*, 2019; Ivanovs *et al.*, 2020). In future, these novel techniques will enable a better understanding of human hematopoietic development.

1.2 Infant acute leukemia

Leukemia is characterized by the disruption of the hierarchical hematopoietic system-homeostasis resulting in the excessive proliferation of immature blast cells. Leukemia is the most prevalent childhood malignancy in the German population accounting for 29.5% of all cancer diagnoses in patients below 18 years of age (Robert Koch-Institut, 2021). Infant leukemia is an acute disease defined as leukemia diagnosed in children below 1 year of age and distinguishes in many characteristics from pediatric and adult leukemia. Although infant acute leukemia displays a relatively low incidence with approximately 160 cases per year in the US (Howlader *et al.*, 2021), the disease is devastating due to high relapse-rates, treatment-associated mortality, relapse-associated mortality and a lack of satisfactory treatment options (Pieters *et al.*, 2019, 2007; Quessada *et al.*, 2021).

1.2.1 Epidemiology and clinical characteristics

These ~160 cases per year of infant leukemia in the US can be subdivided into lymphoblastic (ALL) and myeloid (AML) leukemia. ALL has a slightly higher incidence with ~90 cases per year compared to AML with ~70 cases per year in the US (Howlader *et al.*, 2021). Due to the relatively low incidence, the numbers of the US population are in general more reliable than numbers from the smaller German population. The genomic background of infant AML is heterogenous (Quessada *et al.*, 2021), whereas 70 – 80% of all infant ALL (iALL) cases possess rearrangements of the *KMT2A* gene as causative genomic alteration (*KMT2A*-r, formerly *MLL*) (Pieters *et al.*, 2019, 2007). *KMT2A*-germline iALL patients display numerical aberrations including high hyperdiploidy in 23% of cases, or structural aberrations in 45% of cases. These include the translocations t(9;22), t(1;19), t(7;12), or other structural aberrations of tumor suppressor genes or oncogenes including *CDKN2A* deletions, *PAX5* deletions, *RUNX3* deletions, *GAS7* amplifications and deletions. 32% of *KMT2A*-germline iALL patients show no aberrations (De Lorenzo *et al.*, 2014; Linden *et al.*, 2016).

The dominance of *KMT2A*-r in infancy is unique, as the prevalence of *KMT2A* alterations in overall childhood ALL approximates only 5% (Behm *et al.*, 1996). Among *KMT2A*-r iALL, the translocation t(4;11) generating the fusion oncogenes *KMT2A::AFF1* and *AFF1::KMT2A* is the most frequent one accounting for almost every second case. Other translocations frequently occurring in *KMT2A*-r iALL are t(11;19) (*KMT2A::MLLT1*), t(9;11) (*KMT2A::MLLT3*) and t(10;11) (*KMT2A::MLLT10*) (**Figure 3A**) (Meyer *et al.*, 2018).

Clinically, pediatric ALL patients present a variety of symptoms including hyperleukocytosis, fever, lethargy, organomegaly, skin lesions and cytopenia (Chessells *et al.*, 2002). In comparison to older children, infants with ALL demonstrate more aggressive symptoms such as very high white blood count (WBC), hepatosplenomegaly and central nervous system (CNS) involvement (Hilden *et al.*, 2006).

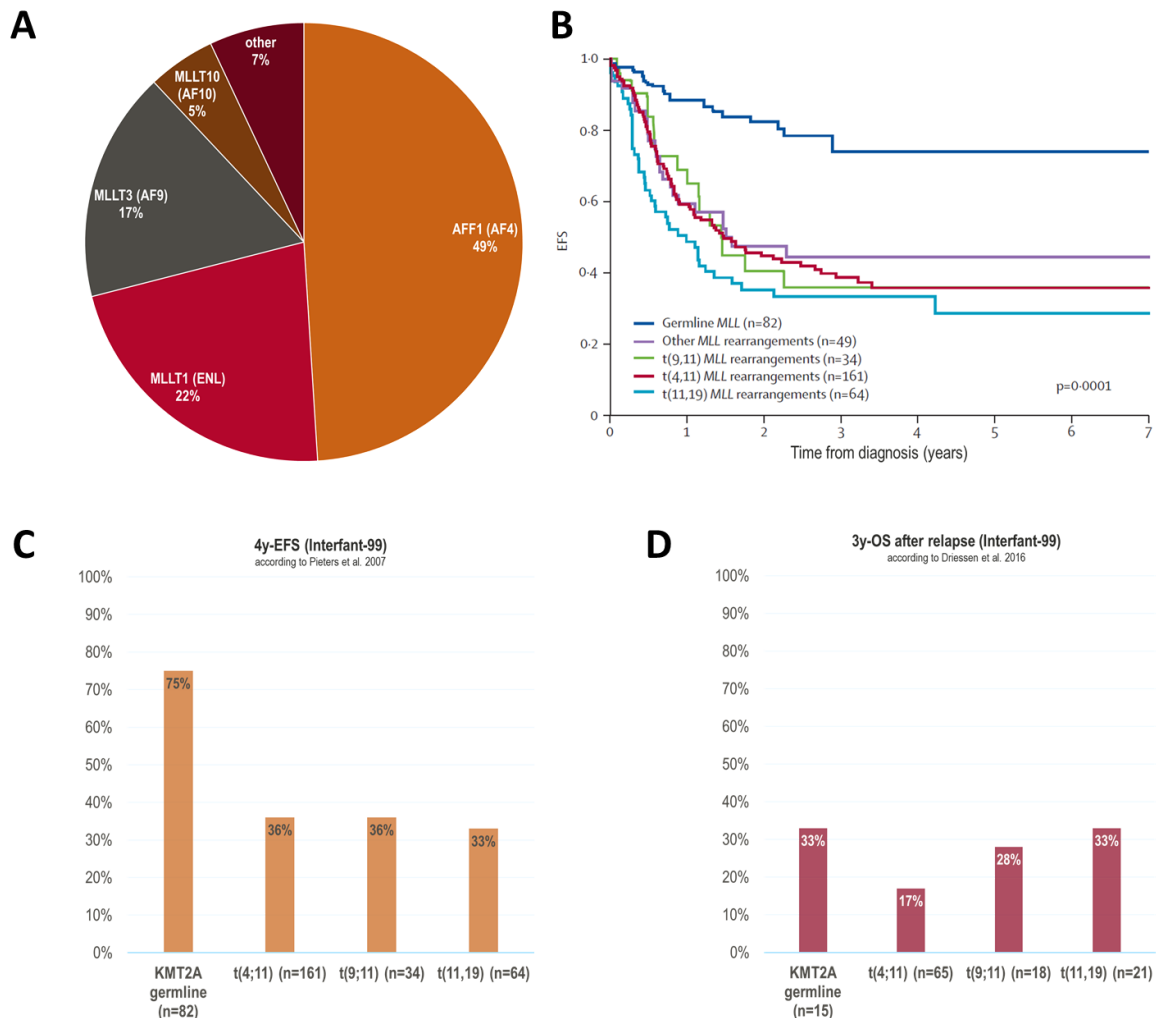


Figure 3. Epidemiology and clinical characteristics of infant *KMT2A*-r ALL.

A Quantitative distribution of *KMT2A*-r partner genes in infant ALL according to Meyer *et al.*, 2018. Former gene names in brackets. **B** Taken from Pieters *et al.*, 2007. Kaplan-Meier event-free survival (EFS) plot of iALL patients without and with *KMT2A*-r including t(9;11) (*KMT2A::MLLT3*), t(4;11) (*KMT2A::AFF1*) and t(11;19) (*KMT2A::MLLT1*). **C** 4-year EFS rates of the same patient groups according to Pieters *et al.*, 2007. **D** 3-year post-relapse overall survival (OS) rates of the patient groups according to Driessen *et al.*, 2016.

The Interfant-99 study enrolled 482 iALL patients between the years 1999 and 2005 and clearly demonstrated *KMT2A* rearrangements as very poor prognostic factors (**Figure 3B**) (Pieters *et al.*, 2007). Four years from diagnosis, *KMT2A*-germline patients demonstrated an event-free survival (EFS) of 75% whereas only 33 – 36% of patients with the most frequent *KMT2A* translocations t(4;11), t(9;11) and t(11;19) were event-free after the same time from diagnosis (**Figure 3C**). Events were defined as early death during induction, resistance to induction, relapse, death in continuous complete remission and second malignancy. Interfant-99 demonstrated in a large scale that most relapses of iALL happened within the first year from diagnosis while patients were still on treatment. In contrast, relapse in older children with ALL occurred mainly off treatment. Therefore, it is of special interest to regard the post-relapse outcome measured as overall survival (OS) of relapsed Interfant-99 patients three years from relapse diagnosis (**Figure 3D**) (Driessen *et al.*, 2016). Thereby, it became obvious that independent of

KMT2A-r, relapse was associated with a high mortality of at least 66%. In case of t(4;11), relapse-associated mortality after three years from relapse diagnosis was 83%. This is even more devastating reminding that *KMT2A-r* caused 70 - 80% of all iALL cases and possessed high relapse incidences with 4y-EFS between 33% and 36% as described above. In conclusion, there is a yet unmet need for targeted therapies preventing relapse formation in *KMT2A-r* infant ALL.

1.2.2 Treatment

1.2.2.1 Risk stratification and induction therapy

Treatment of infant ALL mainly relies on chemotherapy regimen that were assessed by three international groups who conduct clinical trials for infant ALL: the European “Interfant” with the Interfant-06 trial following the Interfant-99 trial, the North American “Children’s Oncology Group” (COG) with the AALL0631 trial and the “Japanese Pediatric Leukemia Study Group” (JPLSG) with the MLL-10 trial (Brown *et al.*, 2021; Pieters *et al.*, 2019, 2007; Salzer *et al.*, 2015; Tomizawa *et al.*, 2020).

All three groups implemented a risk stratification which classified patients as high, intermediate or low risk based on the outcome predictors *KMT2A* status, age, white blood count (WBC), central nervous system (CNS) involvement and Prednisone response (Pieters *et al.*, 2019; Salzer *et al.*, 2015; Tomizawa *et al.*, 2020) (**Table 1**). Based on risk stratification, patients underwent an induction therapy regimen which COG and JPLSG adapted from Interfant-99 due to raised toxicity of the former more intensified COG induction regimen (Salzer *et al.*, 2015). The risk stratification step is necessary to decrease the relapse incidence of high risk patients due to insufficient chemotherapy while minimizing the probability of therapy-related mortality of low risk patients due to excessive chemotherapy.

Table 1. Risk stratification of Interfant-06, COG (AALL0631) and JPLSG (MLL-10). Adapted from Brown *et al.*, 2019.

Risk group	Interfant-06	COG (AALL0631)	JPLSG (MLL-10)	approx. EFS
high	<i>KMT2A-r</i> age < 6 months WBC ≥ 300,000/μL poor PRED response	<i>KMT2A-r</i> age < 3 months	<i>KMT2A-r</i> age < 6 months CNS leukemia	20 %
intermediate	<i>KMT2A-r</i> and not high risk	<i>KMT2A-r</i> and not high risk	<i>KMT2A-r</i> and not high risk	50%
low	wildtype <i>KMT2A</i>	wildtype <i>KMT2A</i>	wildtype <i>KMT2A</i>	75%

The aim of induction therapy is to achieve a complete remission (CR) that was defined as fewer than 5% leukemic cells in BM, hematopoiesis in regeneration, and no evidence of remaining leukemic cells outside the BM (Pieters *et al.*, 2007). Induction therapy began with a 7-day Prednisone (PRED) prophase with oral or i.v. PRED doses of 60 mg/m²/day (**Figure 4**). This cytoreductive phase aimed to gently decrease the leukemic burden avoiding a tumor lysis syndrome due to massive leukemia cell death. With day 8 and until day 36, PRED became replaced by oral or i.v. Dexamethasone (DEXA) doses of 6 mg/m²/day and chemotherapy was launched with Vincristine (VCR) administered weekly as i.v. pushes of 1.5 mg/m² on days 8, 15, 22 and 29. Also, 75 mg/m² Cytarabine (ARA-C) was i.v. administered daily for two weeks from day 8 to 21. Daunorubicin (DNR) 30 mg/m² treatment was performed at days 8 and 9. Asparaginase (L-ASP) was administered in a dose of 10,000 U/m² at days 15, 18, 22, 25, 29 and 33. Methotrexate (MTX) (6 mg) and PRED (6 mg) were administered intrathecally at days 1 and 29, and in case of initial CNS leukemia additionally at days 8 and 22. ARA-C (15 mg) and PRED (6 mg) were administered at day 15 intrathecally. Intrathecal doses did not depend on body surface area. Response to PRED treatment was assessed at day 8 and enabled additional risk stratification (Brown *et al.*, 2019; Pieters *et al.*, 2007).

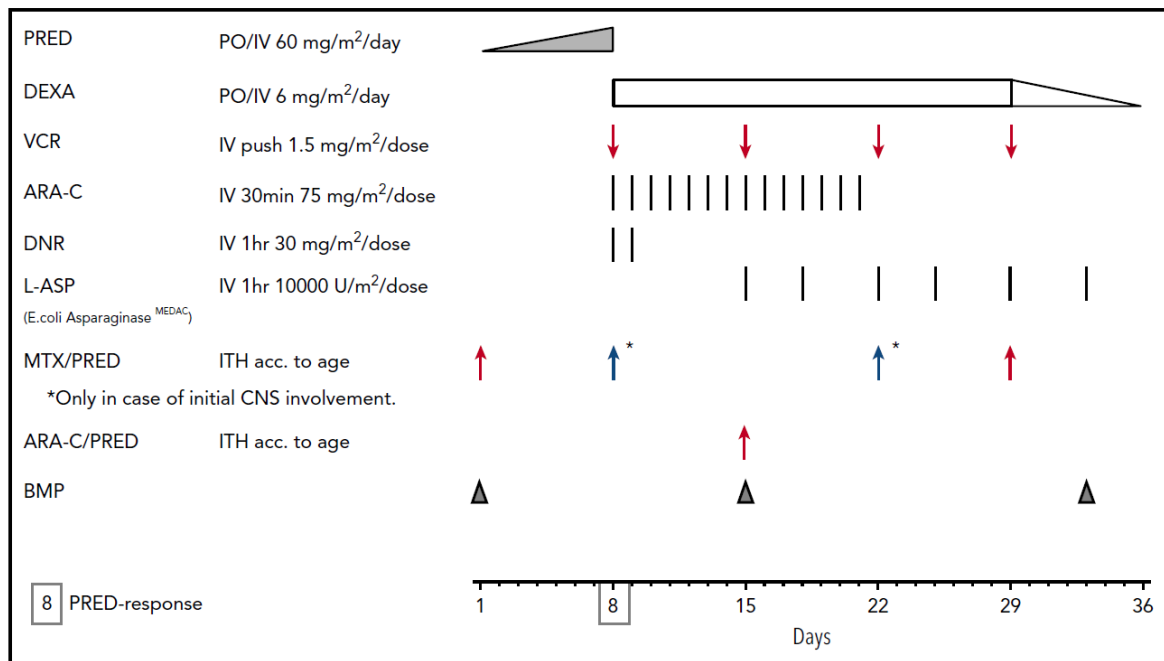


Figure 4. Interfant induction protocol. Abbreviations as stated in the text. Taken from Brown *et al.*, 2019 and based on Pieters *et al.*, 2007.

1.2.2.2 Postinduction therapy

Interfant-99 enrolled 482 patients and followed a hybrid treatment protocol in which the 5 weeks induction phase was followed by a 4 weeks consolidation phase with MARAM treatment including 6-Mercaptopurine p.o., MTX i.v. and i.t., PRED i.t., ARA-C i.t. and L-ASP i.v. or i.m. (**Figure 5**). Consolidation was followed by a 7 weeks enduring reinduction phase with OCTADD treatment involving DEXA p.o., 6-Tioguanine p.o., VCR i.v., DNR i.v., ARA-C i.v. and i.t., and Cyclophosphamide i.v.. High risk patients with available donor were considered for hematopoietic stem cell transplantation (HSCT) after reinduction. An optional intensification phase following reinduction consisted of MARAM treatment plus VCR i.v. (VIMARAM). Subsequently, low-risk patients underwent a maintenance phase composed of three cycles of 14 weeks 6-Mercaptopurine p.o., MTX p.o., DEXA p.o., VCR i.v., MTX + PRED i.t., ARA-C + PRED i.t. treatment (maintenance IA), high-risk patients were additionally treated with Etoposide i.v. and ARA-C i.v. during each cycle (maintenance IB). The second phase of maintenance for all patients was composed of 6-Mercaptopurine p.o. and MTX p.o. treatment until 104 weeks from diagnosis (Pieters *et al.*, 2007).

The subsequent Interfant-06 trial enrolled 651 patients and compared a “lymphoid style” consolidation consisting of ARA-C, 6-Mercaptopurine and Cyclophosphamide (IB treatment) with a “myeloid style” consolidation based on ARA-C, DNR, Etoposide (ADE treatment) and ARA-C, Mitoxantrone and Etoposide (MAE treatment). The myeloid-directed therapy was investigated since *KMT2A-r* occurred also in AML (Meyer *et al.*, 2018), *KMT2A-r* iALL was reported to be sensitive to the myeloid-targeting drug ARA-C (Ramakers-van Woerden *et al.*, 2004; Stam *et al.*, 2003) and frequently co-expressed myeloid markers (Pieters *et al.*, 2019). Interfant-06 revealed that the “myeloid style” protocol did not significantly improve outcomes compared to the “lymphoid style” protocol (6y-EFS 54.4±4.0% vs. 47.1±4.2%, p=0.2706). Additionally, EFS was not improved compared to Interfant-99 (6y-EFS 46.1 vs. 46.5%) (Pieters *et al.*, 2019, 2007). However, Interfant-06 disclosed that patients with high minimal residual disease (MRD) at the end of induction (EOI) might benefit from “myeloid style” consolidation whereas patients with low EOI MRD might benefit from “lymphoid style” consolidation (Stutterheim *et al.*, 2021).

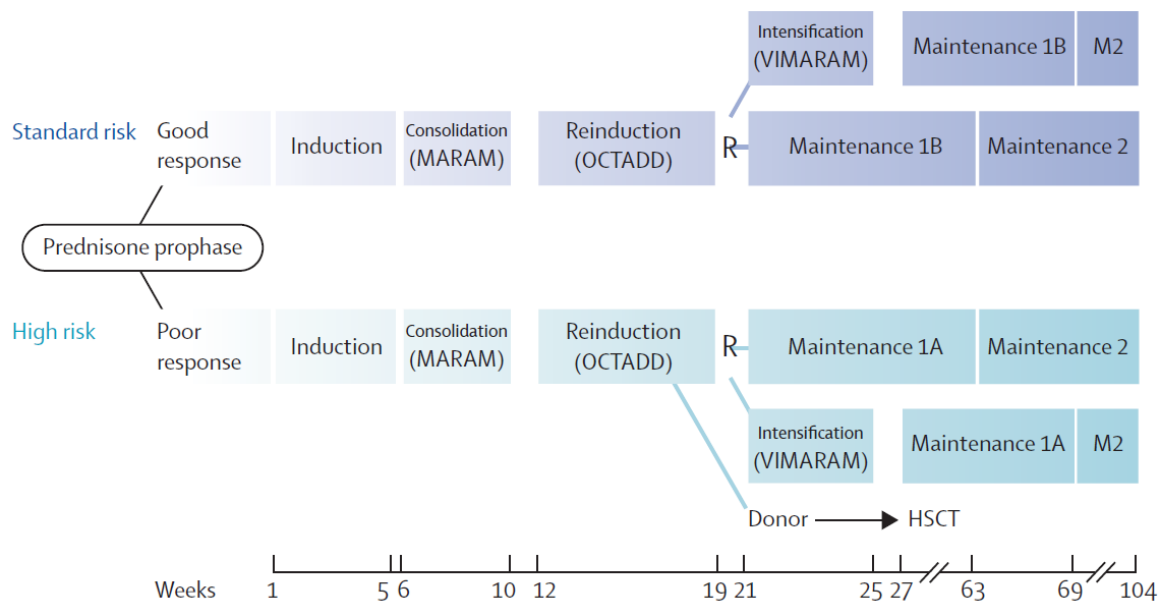


Figure 5. Interfant-99 protocol. Abbreviations as stated in the text. Taken from Pieters *et al.*, 2007.

The COG AALL0631 trial was the first to evaluate a molecularly targeted agent in frontline iALL treatment. The study assessed whether the implementation of the *Fms like tyrosine kinase 3* (FLT3) inhibitor Lestaurtinib in postinduction therapy could improve outcomes (Brown *et al.*, 2021). Various studies indicated overexpression of FLT3 in *KMT2A-r* iALL and that high FLT3 expression was retrospectively linked to poor outcome (Armstrong *et al.*, 2002; Chillón *et al.*, 2012; Kang *et al.*, 2012; Stam *et al.*, 2010, 2007). FLT3 overexpression was due to activating mutations (Armstrong *et al.*, 2003; Taketani *et al.*, 2004) or co-expression of FLT3 ligand resulting in autocrine activation (Brown *et al.*, 2005). Unfortunately, the study disclosed no clinical benefit of standard chemotherapy plus Lestaurtinib compared to standard chemotherapy without the kinase inhibitor (3y-EFS 36±6% vs. 39±7%, $p = 0.67$) (Brown *et al.*, 2021).

1.2.2.3 Hematopoietic stem cell transplantation

Hematopoietic stem cell transplantation (HSCT) was implemented differently in the most recent trials. Interfant-99 did not disclose improved outcomes of those patients who underwent HSCT of the intermediate risk group (Pieters *et al.*, 2007), but has proven clinical benefit from HSCT for high risk patients with *KMT2A-r* and two additional poor prognostic factors including age < 6 months, poor steroid response or high WBC (Mann *et al.*, 2010). Interfant-06 considered all high risk and MRD⁺ patients after MARAM for HSCT. Of 142 high risk patients, only 76 received HSCT due to the very early occurrence of events (mainly relapse) prior to HSCT. Therefore, HSCT patients represented a positively selected group and formal outcome comparison could be biased. Nonetheless, 81% of intermediate risk patients who underwent HSCT relapsed and 14% of all HSCT patients died due to HSCT-related toxicities (Pieters *et al.*, 2019). These clinical observations suggested a restriction of HSCT to very high risk patients.

A smaller observational study of the COG suggested no benefit from HSCT for iALL patients (Dreyer *et al.*, 2011) and thus, COG's AALL0631 generally did not consider HSCT for any patient subgroup (Brown *et al.*, 2021). In contrast, JPLSG considered HSCT for all high risk patients in MLL-10 (Tomizawa *et al.*, 2020). MLL-10 revealed that patients of the high risk group can benefit from HSCT if an appropriate conditioning regimen was applied. However, the authors stated that life-threatening toxicities suggest a very restrictive application of HSCT in iALL (Takachi *et al.*, 2021).

In summary, HSCT is not indicated for the majority of iALL patients and neither for the whole high risk group. Only patients at very high risk could benefit from transplantation, however, the challenge

remained to perform HSCT in first CR but prior to relapse. If HSCT was applied, related toxicities were life threatening and an appropriate conditioning regimen was required. This situation definitely demands novel therapeutic opportunities.

1.2.2.4 Relapse development and chemoresistance

A retrospective study investigated the outcome of relapsed infants treated on Interfant-99 and characterized the clinical picture of relapse (Driessen *et al.*, 2016). The study included 202 relapsed patients, 38% and 63% of the standard risk (good PRED response) and high risk group (poor PRED response), respectively (**Figure 5**). 72% of relapses occurred in the BM, the remaining in CNS, skin, testes or combined BM and extramedullary. 57% of relapses occurred in the first year from diagnosis while patients were still on treatment. The time to relapse (TTR) ranged from 1.7 to 50.7 months resulting in a median of 10.0 months, the standard risk group displayed a median TTR of 12 months, whereas the high risk group had a median TTR of 9 months. *KMT2A*-germline patients relapsed significantly later (more than 24 months) than *KMT2A*-r patients. The OS after three years from relapse (3y-OS) was $20.9 \pm 3.5\%$. *KMT2A*-germline patients demonstrated a 3y-OS of $33.3 \pm 12.9\%$ (10 deaths of 15 patients) compared to t(4;11) patients with a 3y-OS of $16.9 \pm 6.2\%$ (54 deaths of 65 patients) (**Figure 3D**). Although this did not reach statistical significance, relapse within 12 months from diagnosis, which was directly associated with *KMT2A*-r, displayed inferior 3y-OS ($17.5 \pm 5.6\%$) compared to patients relapsing within 12 – 24 ($25.5 \pm 7.0\%$) or later than 24 months ($44.4 \pm 9.7\%$) from diagnosis, respectively. This analysis validated the clinical picture of *KMT2A*-r iALL previously seen in smaller cohorts (Tomizawa *et al.*, 2009): patients rapidly achieve CR during induction therapy but relapse frequently within the first year from diagnosis while still being on treatment. This observation suggested that not the bulk leukemia is responsible for relapse, rather a small cellular subgroup becoming chemoresistant over time.

The remaining question is how chemoresistance is molecularly achieved. For ALL in general, whole-genome sequencing revealed chemotherapy-induced mutagenesis as a major reason for drug resistance resulting in relapse (Li *et al.*, 2020). In contrast, genome-wide analyses of matched iALL patient samples at different time points prior to and at relapse demonstrated that infant t(4;11) ALL possesses one of the lowest mutational burden among all pediatric cancer types with approximately 1.3 non-silent mutations in the dominant leukemic clone (Agraz-Doblas *et al.*, 2019; Andersson *et al.*, 2015; Bardini *et al.*, 2011; Dobbins *et al.*, 2013; Mullighan *et al.*, 2007). Secondary mutations were frequently in *KRAS* and *NRAS* but have been identified to be subclonal and lost at relapse in most cases (Agraz-Doblas *et al.*, 2019; Driessen *et al.*, 2013; Prell *et al.*, 2013). This indicated that secondary mutations probably occurred due to the excessive cycling activity of the dominant leukemic clone and did not act as additional driver mutations necessary for leukemic progression or re-emergence as relapse. As a result, chemoresistance is unlikely to be achieved by the acquisition of or selection for secondary mutations as common in non-infant ALL (Li *et al.*, 2020).

Epigenetic studies revealed that relapse in childhood ALL went along with DNA hypermethylation (Bhatla *et al.*, 2012; Hogan *et al.*, 2011; Schafer *et al.*, 2010; Stumpel *et al.*, 2009). These studies suggested that chemoresistance could be supported by epigenetic instead of somatic changes potentially explaining the low incidence of somatic mutations at time of relapse. This would also be in line with the function of *KMT2A* as an epigenetic regulator (see 1.2.3.3). These studies therefore concluded that treatment with epigenetic agents could improve patient outcomes.

Another possible explanation for relapse development without increase in somatic mutations is subclonality. Although t(4;11) leukemia cells at different stages of maturation were characterized to possess stem cell capabilities (Aoki *et al.*, 2015; Kong *et al.*, 2008; le Viseur *et al.*, 2008), recent single-cell analyses uncovered that relapsing leukemia cells show upregulated genes related to glucocorticoid resistance, stemness and quiescence (Candelli *et al.*, 2022; Chen *et al.*, 2022). This is in line with

previous studies linking quiescent subclones to relapse and steroid resistance (Bardini *et al.*, 2015). As a result, chemotherapy could select for more quiescent, stem-cell like subclones potentially being responsible for relapse development.

Finally, therapy resistance could also be explained through interactions of leukemic cells with their microenvironment in the BM niche. The niche provides an environment composed of several different cell types secreting a multitude of cytokines thereby regulating HSC quiescence, self-renewal and proliferation (Pinho and Frenette, 2019). Meanwhile it is known that B-cell leukemia initiating cells (LIC) occupy the BM niche in response to induction therapy (Duan *et al.*, 2014). In this context, BM stromal cells support LIC through secretion of the HSC-regulating cytokine CXCL12 binding to CXCR4 on the LIC surface, and through transfer of mitochondria enabling LIC to cope with oxidative stress (Usmani *et al.*, 2019). Mitochondrial transfer from BM stromal cells to LIC is also known in AML (Marlein *et al.*, 2017). Studies demonstrated that the interaction between stromal cells and LIC through CXCL12 secretion as well as mitochondrial transfer were related to therapy resistance in AML and pediatric KMT2A-r ALL (Saito *et al.*, 2021; Sison *et al.*, 2013b). Furthermore, it has been shown that leukemic cells upregulate CXCR4 in response to therapy in AML and KMT2A-r ALL (Sison *et al.*, 2014, 2013a). Besides, ALL cells interact with mesenchymal stem cells (MSC) which provide asparagine to leukemia cells, thereby circumventing Asparaginase treatment (Iwamoto *et al.*, 2007). Of note, this is not the only mechanism of Asparaginase resistance as it can also be achieved through GSK3 α mediated proteasomal degradation resulting in catabolic asparagine provision within ALL cells (Hinze *et al.*, 2019). In addition, ALL cells interact with immunosuppressive cells including regulatory T-cells (Treg) and granulocytic monocyte derived suppressor cells (G-MDSC) that interfere with immune recognition of ALL cells through BM residing T-cells, NK-cells and macrophages (Curran *et al.*, 2017; Feuerer *et al.*, 2003, 2001; Pastorczak *et al.*, 2021; Zou *et al.*, 2004). In this context, stem-cell like blasts in KMT2A-r iALL were uncovered to suppress NK- and NKT-cells through yet unknown mechanisms (Chen *et al.*, 2022). Thus, the distinct interactions between KMT2A-r LIC and BM-residing immune cells remain to be investigated.

In summary, besides epigenetic alterations and subclonality, the BM microenvironment has been characterized as a mediator of therapy resistance by different means. Regarding the complexity of the BM niche, further yet unknown mechanisms of microenvironmental protection leading to chemoresistance are likely to exist.

1.2.2.5 Novel therapeutic opportunities

Several new therapeutic opportunities for the treatment of infant KMT2A-r leukemia emerged from *in vitro* and *in vivo* studies and entered clinical investigation in the recent years. These comprise epigenetic drugs, immunotherapies and drugs targeting the leukemic microenvironment in the BM niche. Unfortunately, a “breakthrough therapy” leading to enduring clinical remission without relapse development or severe toxicities has not been identified up to now.

1.2.2.5.1 Epigenetic drugs

KMT2A-r leukemia reaches oncogenicity through the assembly of a multiprotein complex aberrantly regulating gene expression through epigenetic alterations including histone methylation and acetylation (see 1.2.3.3). One of the recruited proteins is the H3K79 methyltransferase DOT1L (Bernt *et al.*, 2011; Deshpande *et al.*, 2013; Nguyen *et al.*, 2011). DOT1L inhibitors showed preclinical efficacy in terms of preventing H3K79 methylation and achieving antileukemic activity in KMT2A-r patient derived xenografts (PDX) (Daigle *et al.*, 2013, 2011; Perner *et al.*, 2020). The DOT1L inhibitor Pinometostat demonstrated moderate clinical efficacy in a trial including 25 adult KMT2A-r leukemia patients (Stein *et al.*, 2018) but unfortunately no clinical benefit in a trial with 18 childhood relapsed/refractory KMT2A-r leukemia patients (Shukla *et al.*, 2016).

The *Bromodomain and extra terminal* (BET) protein family has a chromatin reader function and is part of the KMT2A-r multiprotein complex. In this context, BET inhibition has been identified as an effective treatment for KMT2A::AFF1 and KMT2A::MLLT3 leukemia *in vitro* and *in vivo* (Dawson *et al.*, 2011). The first clinical trials showed tolerability and antileukemic effects of BET inhibitors in adult relapsed/refractory AML (Berthon *et al.*, 2016; Borthakur *et al.*, 2021).

CpG island hypermethylation of promoters and microRNA genes has been identified as an epigenetic hallmark in t(4;11) and t(11;19) infant ALL (Stumpel *et al.*, 2011, 2009). Furthermore, a correlation between promoter hypermethylation and poor survival of Interfant-99 patients has been demonstrated retrospectively, and *in vitro* experiments disclosed antileukemic efficacy of the demethylating agent Zebularine (Stumpel *et al.*, 2009). Besides, the demethylating agent Decitabine was proven antileukemic in KMT2A-r cell lines and PDX models of B-cell precursor ALL (Roelf *et al.*, 2018). Due to these encouraging preclinical studies, two clinical trials investigating the antileukemic efficacy of the demethylating drug Azacitidine in infant ALL were launched by COG and JPLSG, respectively (Brown *et al.*, 2019).

Deacetylation of histones mediated by histone deacetylases (HDAC) leads to gene silencing through highly condensed chromatin (Ropero and Esteller, 2007). It has been shown that treatment with HDAC inhibitors (HDACi) reversed promoter hypomethylation and thus activation of oncogenes related to KMT2A::AFF1 expression in primary iALL patient samples and t(4;11) cell lines (Stumpel *et al.*, 2012). The same has been shown in childhood ALL (Bhatla *et al.*, 2012). *In vivo* PDX mouse models demonstrated the antileukemic efficacy of the HDACi Panobinostat (Garrido Castro *et al.*, 2018). The combination of the demethylating agent Decitabine with the HDACi Vorinostat showed efficacy in a trial with 23 childhood ALL patients but unfortunately severe fungal infections were common and questioned the safety of the drug combination (Burke *et al.*, 2020). Thus, the safety of HDACi in combination with other chemotherapeutic drugs for the treatment of pediatric ALL remains to be demonstrated. However, a first trial investigating the implementation of Vorinostat into the chemotherapy backbone for the treatment of infant ALL is already recruiting (NCT02553460, clinicaltrials.gov).

1.2.2.5.2 Targeting the leukemia microenvironment

Secretion of the HSC-regulating cytokine CXCL12 through the BM stromal microenvironment was linked to resistance of LIC against the FLT3 inhibitor Lestaurtinib in pediatric KMT2A-r ALL (Sison *et al.*, 2013b). This study used a mouse xenograft model to demonstrate that Lestaurtinib resistance was overcome through administration of the CXCR4 inhibitor Plerixafor, which was later also shown for PDX models of infant KMT2A-r ALL (Sison *et al.*, 2014). Furthermore, the CXCR4 inhibitor POL5551 was proven effective against chemoresistance of primary pediatric and infant KMT2A-r ALL patient samples in *in vitro* and PDX models (Sison *et al.*, 2015). These studies led to clinical investigation of Plerixafor in combination with Cytarabine and Etoposide in pediatric relapsed/refractory acute leukemias which disclosed modest clinical responses (Cooper *et al.*, 2017). Unfortunately, this trial did not include infant KMT2A-r patients.

1.2.2.5.3 Immunotherapy

The success story of immunotherapies including the bispecific antibody Blinatumomab (von Stackelberg *et al.*, 2016) and the chimeric antigen receptor (CAR) T-cell therapy Tisagenlecleucel (Maude *et al.*, 2018) for the treatment of pediatric B-ALL accelerated the investigation of their clinical potential for the treatment of infant ALL. Unfortunately, several case reports indicated that treatment of KMT2A-r iALL with CD19 targeting therapies like Blinatumomab and Tisagenlecleucel resulted in lineage switch from lymphoblastic to myeloid leukemia without clinical benefit (Gardner *et al.*, 2016; Mejstříková *et al.*, 2017; Rayes *et al.*, 2016). Single-cell experiments suggested that stem-cell like blasts

possessing increased lineage plasticity could be responsible for lineage switch in infant KMT2A-r ALL (Chen *et al.*, 2022). Nevertheless, a clinical trial investigating Blinatumomab combined with the Interfant-06 backbone is ongoing (NTR6359, trialregister.nl).

Besides lineage switch, the complex and time-consuming manufacturing process of CAR T-cells is very challenging especially if T-cells are derived from heavily pretreated infants. To solve this problem, for two iALL patients, a CD19 CAR was transduced into human leukocyte antigen (HLA)-mismatched donor T-cells that were simultaneously T-cell receptor (TCR) and CD52 knocked out (Qasim *et al.*, 2017). The disruption of both allogeneic rejection factors prevented graft-versus-host-disease (GVHD) and a 4-week remission was achieved that enabled allogeneic HSCT. Genome-edited donor derived allogeneic CD19 CAR T-cells showed antileukemic effects and a manageable safety profile in two phase I trials for the treatment of B-ALL in children and adults (Benjamin *et al.*, 2020). These encouraging results could lead to further development and investigation of donor derived CAR T-cell therapies for the treatment of infant ALL.

The CD22 targeting antibody-drug-conjugate Inotuzumab-Ozogamicin achieved very promising results in a phase II trial of relapsed/refractory B-ALL in non-infants (O'Brien *et al.*, 2022). Unfortunately, KMT2A-r iALL cells were characterized to express low levels of CD22, thus decreasing the probability of a clinical benefit through treatment with Inotuzumab-Ozogamicin (Shah *et al.*, 2015).

In summary, profound lineage plasticity, intraleukemic heterogeneity regarding CD19 and CD22 surface expression, and severe pretreatments are the major challenges for the successful implementation of immunotherapies into treatment protocols for infant KMT2A-r ALL.

1.2.3 Biology of infant t(4;11) ALL

1.2.3.1 The *KMT2A* recombinome and the translocation t(4;11)(q21;23)

Leukemia develops due to distinct cytogenetic events which are either numerical aberrations including hyperdiploidy, or structural aberrations including translocations, deletions, amplifications and inversions (De Lorenzo *et al.*, 2014; Mrózek *et al.*, 2004). These cytogenetic aberrations determine in most cases a distinct leukemia subtype and correlate with prognosis. As an example, t(4;11) in infants leads in 95% of cases to ALL with a B-cell progenitor phenotype (proB ALL) (**Figure 6**) (Meyer *et al.*, 2018). This strong correlation between one or few cytogenetic events and disease characteristics is a major contrast to most solid tumors, which are characterized by an accumulation of mutations including unbalanced chromosomal translocations and diverse karyotypes. These alterations are indicative for genomic instability, whereas in infant ALL, translocations are regarded as a single-hit being sufficient for leukemogenesis in most cases (Lengauer, 2001).

The *KMT2A* recombinome of acute leukemias has been mapped in detail by the Diagnostic Center of Acute Leukemia (DCAL) (Meyer *et al.*, 2018). Currently, 104 different *KMT2A* in-frame fusions are listed in the DCAL database (May 2022). Of 2345 patients analyzed until 2017, 36% displayed *KMT2A::AFF1* fusions. Subdividing these by age revealed that 42% were infant, 41% adult and 18% pediatric patients. In all three age groups, ALL was the dominant phenotype accounting for 91% - 99% of these cases (**Figure 6**). Noteworthy, not all rearrangements of *KMT2A* lead to balanced in-frame translocations. Complex three-way translocations, out-of-frame fusions and *KMT2A* internal inversions represent ~11% of the *KMT2A* recombinome of 2017 (Kowarz *et al.*, 2007; Meyer *et al.*, 2018).

The chromosomal translocation t(4;11)(q21;23) occurs through DNA double-strand breaks (DSB) followed by illegitimate recombination events (Betti *et al.*, 2001; Gillert *et al.*, 1999; Reichel *et al.*, 2001, 1998). The DNA DSB appear within the *KMT2A* gene on band 23 of the q-arm of chromosome 11 (11q23), and within the *AFF1* gene on band 21 of the q-arm of chromosome 4 (4q21). Subsequently, the non-homologues-end-joining (NHEJ) DNA DSB repair machinery illegitimately recombines the

broken chromosomes leading to the gene fusions *KMT2A::AFF1* and the reciprocal counterpart *AFF1::KMT2A*. Since apoptotic stimuli were shown to induce *KMT2A* translocations, it has been proposed that the DNA DSB occur due to early apoptotic DNA fragmentation processes in cells that subsequently evade further execution of apoptosis and survive (Betti *et al.*, 2003, 2001; Stanulla *et al.*, 1997). Importantly, studies demonstrated that the presence of the translocation-derived fusion genes is sufficient to induce leukemogenesis, as other aberrations that could serve as a second-hit in a potential multistep oncogenesis process do not occur (Agraz-Doblas *et al.*, 2019; Andersson *et al.*, 2015; Bardini *et al.*, 2011).

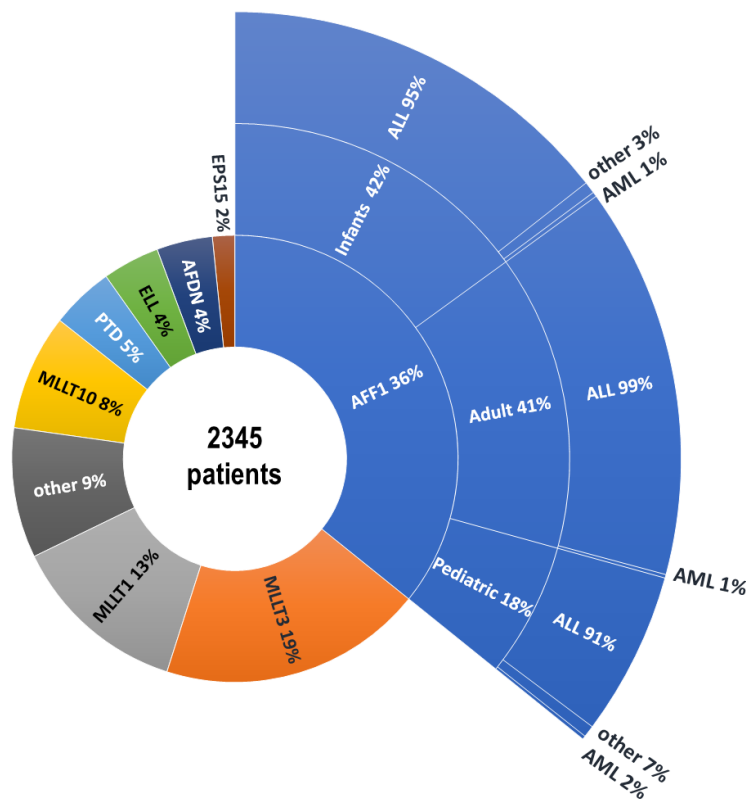


Figure 6. The *KMT2A* recombinome of acute leukemia. Distribution of *KMT2A*-r partner genes of 2345 patients analyzed in the DCAL until 2017. Frequency of age and phenotypic subgroups of *KMT2A::AFF1* leukemia. Other phenotypic subtypes include myelodysplastic syndrome (MDS) and biphenotypic leukemia. Adapted from Meyer *et al.*, 2018.

1.2.3.2 Developmental and cellular origin of t(4;11)(q21;23)

There is strong evidence that the described t(4;11)(q21;23) translocation process takes place prenatally *in utero*. Greaves and colleagues investigated the cytogenetics of monozygotic twins diagnosed with concordant ALL during infancy and early childhood. They found that the leukemic cells of both siblings displayed the same chromosomal breakpoint which strongly suggested that the translocation happened prenatally in one of the twins and subsequently, leukemic cells seeded to the other twin via migration through the shared placenta (Ford *et al.*, 1993; Greaves *et al.*, 2003; Greaves and Wiemels, 2003). The prenatal origin of the translocation was later corroborated by non-twinning *KMT2A::AFF1* ALL through retrospective studies of neonatal blood spots (Guthrie cards) that were taken within hours after birth. Greaves and colleagues showed that these neonatal blood spots of patients diagnosed with B-ALL between 5 months and 2 years of age already displayed the gene fusions prior to diagnosis (Gale *et al.*, 1997). With this, they demonstrated evidence for the occurrence of t(4;11) *in utero*.

The cellular origin of translocation is a matter of debate since decades. In 2005, Hotfilder, Vormoor and colleagues showed that the translocation t(4;11) was present in 68% of primitive lymphoid-restricted CD34⁺CD19⁻ iALL patient cells (Hotfilder *et al.*, 2005). CD34 is an HSC marker and CD19 a lymphoblastic marker, indicating bulk proB cells. This study on intratumoral heterogeneity of infant t(4;11) ALL uncovered that sorted t(4;11)-carrying HSC were restricted to lymphoid lineage when seeded in semisolid methylcellulose cultures supplemented with myeloid growth factors. In line with that, genome-wide analyses of 124 iALL patients revealed transcriptomic similarities between t(4;11)⁺ iALL cells and immature human fetal liver hematopoietic stem and progenitor cells (HSPC) (Agraz-Doblas *et al.*, 2019). Using a CRISPR/Cas9 *KMT2A::AFF1* knock-in model of primary human fetal liver hematopoietic cells, Rice *et al.* showed that fetal gene expression programs shape the distinct molecular profile and drive oncogenesis of t(4;11) iALL (Rice *et al.*, 2021). Furthermore, a study implementing single-cell transcriptomics of 1,665 leukemia patients disclosed high similarity between early lymphoid progenitor cells (ELP) and *KMT2A*-r iALL cells in contrast to *KMT2A*-germline ALL cells (Khabirova *et al.*, 2022). Thereby, t(4;11) displayed the strongest ELP signal among all *KMT2A*-r iALL subtypes. In summary, several independent studies involving different experimental procedures point to fetal liver derived hematopoietic progenitor cells as the most likely cellular origin of transformation in t(4;11) iALL. However, the finding that mesenchymal stem cells (MSC) of t(4;11) iALL patients also expressed *KMT2A::AFF1* points to a shared preleukemic cell as origin of transformation (Menendez *et al.*, 2009). Noteworthy, this study involved only four t(4;11) iALL patients.

The intratumoral heterogeneity of t(4;11) iALL is of special interest considering that not only CD34⁺ but also CD34⁻ leukemic cells, including CD19⁺ blasts of various differentiation stages, were reported to hold stem cell capabilities in t(4;11) iALL (Aoki *et al.*, 2015; Kong *et al.*, 2008; le Viseur *et al.*, 2008). Stem cells are able to self-renew without differentiation and HSPC additionally to recapitulate the hematopoietic system upon transplantation in an immunocompromised irradiated recipient. In the cited studies, these capabilities have been validated using xenotransplantation of patient-derived leukemic cells in NOD/SCID mice. Accordingly, these experiments suggest that in t(4;11) iALL, stemness is not restricted to phenotypically (CD34⁺) identified HSPC. This implies that t(4;11)⁺ cells at different stages of differentiation could serve as leukemia initiating cells (LIC). In AML, the presence of leukemia stem cells (LSC) that occupy the HSC niche within the BM and outcompete healthy HSC has been demonstrated in several studies (Bonnet and Dick, 1997; Boyd *et al.*, 2014; Kumar *et al.*, 2018; Medyouf, 2017). Accordingly, the AML bulk leukemia cells descending from AML LSC do not possess stem cell capabilities. This is a major seminal difference between AML and *KMT2A*-r ALL.

1.2.3.3 Oncogenic mechanism of *KMT2A::AFF1* and *AFF1::KMT2A* fusions

Wild type *lysine methyltransferase 2A* (*KMT2A*, formerly *MLL*) encodes a protein with several conserved domains of various functions: N-terminal AT-hook motifs bind AT rich DNA sequences (Zeleznik-Le *et al.*, 1994), the DNA methyltransferase homology domain suppresses transcription (Xia *et al.*, 2003), four PHD domains mediate protein binding (Fair *et al.*, 2001), a transactivation domain recruits the nuclear coactivator CREBBP (Ernst *et al.*, 2001), and a C-terminal SET domain methylates histone 3 at lysine 4 (H3K4me) (Milne *et al.*, 2002; Nakamura *et al.*, 2002; Patel *et al.*, 2009). *KMT2A* protein is processed by Taspase1 leading to the two fragments p320 and p180 which heterodimerize (Hsieh *et al.*, 2003; Sabiani *et al.*, 2015; Yokoyama *et al.*, 2002). The p320/p180 dimer itself confers weak methyltransferase activity but increases the latter through formation of a multiprotein complex involving LEDGF, MEN1, PP2A, GADD34, PAF, CYP33, CREBBP, MOF, WDR5, ASH2L, SRY-30 (SOX30), RbBP5 and the polycomb group complex composed of BMI1, HPC2, HDAC1/2 and CtBP (Adler *et al.*, 1999, 1997; Cao *et al.*, 2010; Dou *et al.*, 2006, 2005; Milne *et al.*, 2010; Muntean *et al.*, 2010; Nakamura *et al.*, 2002; Southall *et al.*, 2009; Wysocka *et al.*, 2005; Xia *et al.*, 2003; Yokoyama *et al.*, 2004, 2002). This *KMT2A* multiprotein complex binds to active promoter regions to subsequently mark these through chromatin

modifications (de Boer *et al.*, 2013). In this context, the N-terminal KMT2A portion binds chromatin signatures and the C-terminal region mediates acetylation and methylation of histones (Marschalek, 2011; Sanjuan-Pla *et al.*, 2015). Binding of CYP33 to the PHD domain mediates conformational changes that turn the KMT2A multiprotein complex from transcriptional activation to transcriptional repression through recruitment of the Polycomb-group complex (Park *et al.*, 2010). This results in the deacetylation of nucleosomes and transcription factors thereby repressing transcription (Hom *et al.*, 2010; Schraets *et al.*, 2003; Wang *et al.*, 2010). In summary, KMT2A can be described as an epigenetic regulator mediating transcriptional activation or repression of target genes. This is achieved through indexing of transcriptionally active and inactive chromatin domains via histone lysine methylation and acetylation (Pokholok *et al.*, 2005; Santos-Rosa *et al.*, 2002). Through this, KMT2A regulates especially HSC program genes during hematopoietic development (Milne, 2017; Wilkinson *et al.*, 2013; Yeoh *et al.*, 2002; Yokoyama, 2021).

The DNA DSB required for the translocation t(4;11)(q21;23) almost exclusively take place in the breakpoint cluster region 1 (BCR1) of *KMT2A*, predominantly located between introns 9 and 11 (Meyer *et al.*, 2018). This breakpoint location results in the separation of chromatin binding capability of the N-terminal domains from histone modification capability of the C-terminal domains. Besides, the CYP33 dependent “switch” from transcriptional activation to repression becomes destroyed through translocation (Rössler and Marschalek, 2013; Sanjuan-Pla *et al.*, 2015). Fusion of the N-terminal KMT2A part to the C-terminal part of AFF1 results in the formation of the chimeric oncoprotein KMT2A::AFF1. AFF1 is a regulator of RNA polymerase II (RNAP2) through binding of the P-TEFb elongation factor, ENL proteins and the SL1 complex of RNA polymerase I to form a super elongation complex (Lin *et al.*, 2010; Luo *et al.*, 2012; Okuda *et al.*, 2015; Yokoyama *et al.*, 2010). The combination of the KMT2A chromatin binding and AFF1 transcriptional activation capabilities leads to aberrant transcriptional hyperactivation of KMT2A target genes including those facilitating HSC capabilities especially self-renewal without differentiation (Kühn *et al.*, 2016; Yeoh *et al.*, 2002). Besides the cell of origin, this may additionally explain the stem cell identity of t(4;11)⁺ blasts at various stages of differentiation.

The role of the reciprocal fusion protein AFF1::KMT2A in this oncogenic mechanism is a matter of debate. AFF1::KMT2A is found in about 80% of patients whereas KMT2A::AFF1 is detected in every patient with t(4;11)(q21;23) (Kowarz *et al.*, 2007; Trentin *et al.*, 2009). Patients with detectable reciprocal fusion protein were reported to display superior event-free and overall survival rates (Agraz-Doblas *et al.*, 2019). Furthermore, knockdown experiments revealed that t(4;11) cell lines were shown to be independent of AFF1::KMT2A expression while being addicted to KMT2A::AFF1 expression (Kumar *et al.*, 2011). Additionally, AFF1::KMT2A was not sufficient to induce leukemogenesis in cord blood HSC (Prieto *et al.*, 2017). These observations point to a minor role of AFF1::KMT2A for leukemogenesis and pathogenesis of t(4;11) ALL. On the other hand, the target gene *RUNX1* has been shown to be activated through a cooperating effect of both fusion proteins (Wilkinson *et al.*, 2013) and the reciprocal fusion protein alone was capable to drive ALL onset in mice (Bursen *et al.*, 2010). However, in this mouse model KMT2A::AFF1 alone did not lead to leukemogenesis within 13 months of observation which conflicts the clinical and epidemiological observation that KMT2A::AFF1 was detected in every t(4;11) ALL patient questioning the validity of this mouse model. Additionally, leukemia onset of both fusions and the reciprocal alone took more than six months not representing the short latency period of childhood and infant t(4;11) ALL. Anyhow, KMT2A::AFF1 ALL is regarded to be the most difficult *KMT2A*-r leukemia to model in the murine system (Milne, 2017). Moreover, human embryonic stem cell (ESC) based KMT2A::AFF1 and AFF1::KMT2A *in vitro* and *in vivo* models disclosed a cooperative effect of both fusions promoting the emergence of hemato-endothelial precursors and enhancing blood cell proliferation (Bueno *et al.*, 2019). Based on *in vitro* gene expression studies, it has been proposed that the reciprocal fusion is mandatory for initial transformation of the cell of origin but unessential for further

leukemogenesis and subsequently lost in a clonal evolutionary process (Wilhelm and Marschalek, 2021).

1.2.3.4 *HOXA* gene expression patterns in childhood t(4;11) ALL

In the past, overexpression of the *HOXA* gene cluster was regarded as a general characteristic of KMT2A-r ALL defining the distinct gene expression profile of the disease (Armstrong *et al.*, 2002; Ferrando *et al.*, 2003; Rozovskaia *et al.*, 2001). Furthermore, knockdown experiments revealed the distinct dependency of KMT2A-r cell lines on *HOXA9* expression to avoid apoptosis (Faber *et al.*, 2009).

This dogma became challenged in 2009 when Trentin *et al.* reported the presence of two distinct gene expression patterns in childhood t(4;11) ALL (Trentin *et al.*, 2009). Patients were clustered according to their *HOXA* gene expression related to healthy controls into a *HOXA*^{lo} and a *HOXA*^{hi} group. Low *HOXA* gene expression was exclusively found in infants whereas high *HOXA* gene expression emerged in infant and childhood patients. *HOXA*^{lo} but not *HOXA*^{hi} patients showed upregulation of the *Iroquois homeobox 1 (IRX1)* gene which is involved in early embryonic patterning (Bosse *et al.*, 1997). Two studies confirmed these findings and additionally revealed an elevated relapse incidence (Stam *et al.*, 2010) or poorer EFS (Kang *et al.*, 2012) of *HOXA*^{lo} patients, respectively. Agraz-Doblas *et al.* linked the presence of the reciprocal *AFF1::KMT2A* fusion to high *HOXA* gene expression and thus, better outcome (Agraz-Doblas *et al.*, 2019). Symeonidou *et al.* confirmed the presence of *HOXA*^{lo}/*IRX1*^{hi} and *HOXA*^{hi}/*IRX1*^{lo} gene expression patterns in infant t(4;11) ALL and speculated that *HOXA*^{lo}/*IRX1*^{hi} patients' leukemia may derived from an earlier cell of origin explaining different gene expression and worse outcome (Symeonidou and Ottersbach, 2021). Kühn *et al.* demonstrated in *in vitro* experiments that *IRX1* overexpression led to an indirect upregulation of the immediate early genes *Early growth response 1, 2 and 3 (EGR1, EGR2, EGR3)* potentially involved in a stem-cell identity expression program explaining inferior outcome. This discovery is the basis of this doctoral project.

1.2.3.5 The immediate early genes *EGR1, EGR2* and *EGR3*

Immediate early genes are rapidly and transiently upregulated upon stimulation of a cell by various stimuli including hormones, stress or growth factors (Healy *et al.*, 2013). The *early growth response* gene family is composed of the four members *EGR1, EGR2, EGR3* and *EGR4* encoding transcription factors with a highly conserved DNA binding domain (DBD) composed of three C2H2 zinc fingers (ZF) (Beckmann and Wilce, 1997; O'Donovan *et al.*, 2000; Russo *et al.*, 1995). *EGR1, EGR2* and *EGR3* possess a relatively similar protein structure (**Figure 7**). However, they differ in their count and location of activation domains and overall protein size. *EGR1* is composed of 543 amino acids (aa) and has a molecular weight of 58 kDa, followed by *EGR2* with 476 aa and 51 kDa and *EGR3* with 387 aa and 43 kDa. *EGR1* has four activation domains, of which one is C-terminal of the DBD, whereas *EGR2* and *EGR3* possess two activation domains N-terminal related to the DBD. All three transcription factors have a repressor domain (R1) that interacts with the transcriptional repressor proteins *NGFI-A binding protein 1* and *2 (NAB1, NAB2)*. The interaction of *NAB1* and *NAB2* or their murine homologues with *EGR* proteins have been shown to repress *EGR* function (Russo *et al.*, 1995; Svaren *et al.*, 1996; Swirnow *et al.*, 1998). In later studies, *NAB* proteins were demonstrated to act as coactivators or repressors of *EGR* proteins, depending on the target gene (Desmazières *et al.*, 2008; Le *et al.*, 2005). Initially, all *EGR* proteins were reported to bind a distinct consensus sequence, the *EGR* response element (Beckmann and Wilce, 1997), ChIP-Seq studies meanwhile revealed slight differences in the binding motifs of *EGR1, EGR2* and *EGR3* as the consensus sequence of the JASPAR transcription factor database shows (**Figure 7**). This also revealed that the binding motifs of *EGR2* and *EGR3* are closer to each other than to *EGR1*.

The EGR proteins were identified as important regulators in the central nervous system with the observation that stimulation of neurons by different neurotransmitters lead to immediate upregulation of *EGR1* (Cole *et al.*, 1989; Wisden *et al.*, 1990). In this context, *EGR1* was disclosed to be involved in mediation of neural plasticity (Davis *et al.*, 2003; Knapska and Kaczmarek, 2004; Williams *et al.*, 1995; Yamagata *et al.*, 1994), regulation of the circadian rhythm (Lin *et al.*, 1997) and hindbrain development (Schneider-Maunoury *et al.*, 1993).

Importantly, *Egr1* was characterized as a controller of proliferation and localization of murine HSC (Min *et al.*, 2008). In this study, *Egr1* knockout mice showed increased HSC proliferation in the BM and elevated numbers of HSC in PB without raising the overall HSC count. This indicated a role of *Egr1* as a mediator of HSC quiescence and negative regulator of HSC mobilization. Similarly, knockdown experiments in mice uncovered *Egr3* as an inhibitor of HSC proliferation (Cheng *et al.*, 2015). Besides, *EGR1* was associated with proliferation and stem cell identity of glioblastoma stem cells (Riddick *et al.*, 2017; Sakakini *et al.*, 2016).

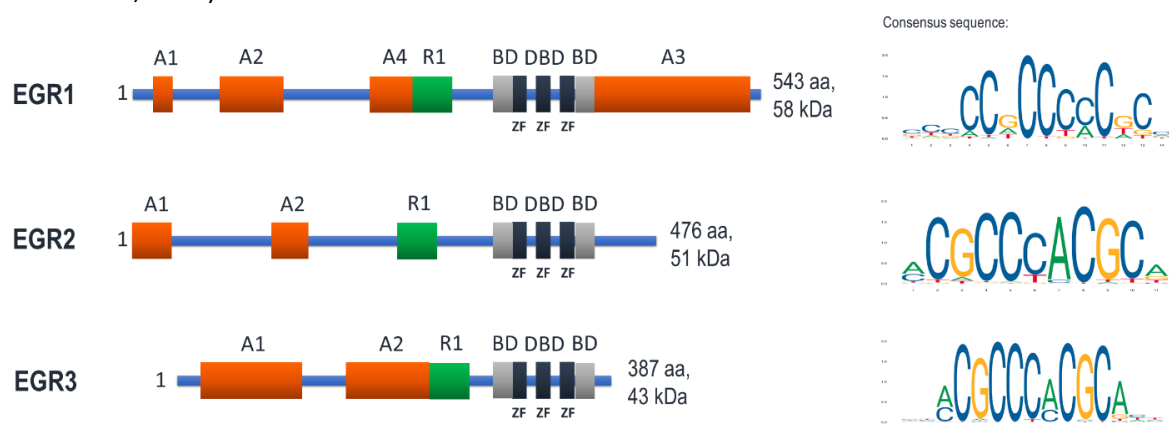


Figure 7. Schematic protein structure and consensus binding sequence of *EGR1*, *EGR2* and *EGR3*. Protein structure adapted from Beckmann and Wilce, 1997; O'Donovan *et al.*, 2000; Russo *et al.*, 1995. Consensus sequences taken from transcription factor database JASPAR 2020® (Sandelin *et al.*, 2004). A = activation domain. R = repressor domain. BD = basic domain. DBD = DNA binding domain. ZF = zinc finger.

In T-cells, *Egr2* and *Egr3* act as repressors of T-cell activation through upregulation of Fas ligand (Mittelstadt and Ashwell, 1999, 1998) and the E3 ubiquitin ligase Cbl-b which subsequently ubiquitinates factors involved in T-cell receptor signaling including PI3KR1 (Safford *et al.*, 2005). Besides, studies suggest a role of *Egr* proteins in T- and B-cell development (Li *et al.*, 2011) as well as thymocyte development (Carter *et al.*, 2007).

Another study reported a correlation between high *EGR3* expression and poor prognosis in glioblastoma (GBM) patients with *MGMT* promoter hypermethylation (Knudsen *et al.*, 2020). This hypermethylation leads to epigenetic silencing of the DNA repair enzyme O⁶-methylguanine DNA methyltransferase (*MGMT*) which is related to good Temozolomide response in GBM (Chinot *et al.*, 2007). Knudsen *et al.* identified *EGR3* as a poor prognostic factor in the group of patients with *MGMT* promoter hypermethylation that usually respond well to Temozolomide. Therefore, the authors hypothesized *EGR3* could be implicated in Temozolomide resistance. *EGR3* was previously correlated with Docetaxel resistance in breast invasive ductal cancer (Li *et al.*, 2017) and endocrine treatment resistance in breast cancer (Varešlija *et al.*, 2016).

In summary, the early growth transcription factors are implicated in many different functions and expressed in several different tissues. Throughout the reviewed studies, the disclosed function of the three transcription factors highly depended on the cellular and tissue context. Correspondingly, *EGR1* (synonyms: NGFI-A, ETR103, KROX-24, ZIF-268, ZNF225) has been described as “a gene with as many names as biological functions” (DeLigio and Zorio, 2009).

1.3 Objective of this project

KMT2A-rearrangements are causative for 70-80% all infant acute lymphoblastic leukemias (Pieters *et al.*, 2019, 2007). Among these, the translocation t(4;11)(q21;23) generating the oncogenic fusion genes *KMT2A::AFF1* and *AFF1::KMT2A* is the most frequent one, accounting for almost every second case of *KMT2A-r* infant ALL (Meyer *et al.*, 2018). Despite passing a multimodal chemotherapy, 64% of patients achieve an event including relapse or death within four years from diagnosis, and overall survival three years from relapse remains poor with only 17% (Driessen *et al.*, 2016; Pieters *et al.*, 2019, 2007). Various studies have shown that relapse and therapy resistance were not mediated by chemotherapy-induced mutagenesis as there was no accumulation of secondary mutations in the dominant leukemic clone between diagnosis and relapse (Agraz-Doblas *et al.*, 2019; Andersson *et al.*, 2015; Bardini *et al.*, 2011; Dobbins *et al.*, 2013; Driessen *et al.*, 2013; Mullighan *et al.*, 2007).

Intriguingly, exclusively infant t(4;11) ALL patients were reported to subdivide in two groups depending on the level of *HOXA* gene cluster expression (Trentin *et al.*, 2009). The *HOXA*^{lo} group displayed a high expression of *IRX1* and the *HOXA*^{hi} group a low expression of *IRX1* (Symeonidou and Ottersbach, 2021; Trentin *et al.*, 2009). Importantly, the *HOXA*^{lo}/*IRX1*^{hi} group was characterized to possess a strongly elevated relapse incidence compared to the *HOXA*^{hi}/*IRX1*^{lo} group (Kang *et al.*, 2012; Stam *et al.*, 2010). *IRX1* was identified to upregulate the *Early growth response* genes *EGR1*, *EGR2* and *EGR3* (Kühn *et al.*, 2016).

The doctoral project “EGR-mediated relapse mechanisms in infant t(4;11) acute lymphoblastic leukemia” aimed to investigate a potential correlation between the *HOXA*^{lo}-*IRX1*-*EGR* axis and relapse development in infant t(4;11) ALL. The primary objective was to clarify through which molecular mechanism(s) relapse development despite continuous chemotherapy could be achieved. In this context, the role of the *EGR* genes has been investigated. In addition, this project aimed to disclose molecular targets which could offer novel therapeutic interventions to interfere with therapy resistance and relapse formation.

2 Organisms, material, and methods

2.1 Organisms

2.1.1 Human cell lines

Stable cell culture models were established using the human cell lines HEK 293T (ACC 635) or SEM (ACC 546) (**Table 2**).

Table 2. Stable cell lines established using the sleeping beauty (SB) transposon system.

Cell line	SB plasmid	Application
HEK::mock	pSBtet_ohneLuc_P	gene expression profiling
HEK::EGR1	pSBtet_EGR1cFLAG_P	
HEK::EGR2	pSBtet_EGR2cFLAG_P	
HEK::EGR3	pSBtet_EGR3cFLAG_P	
SEM::mock	pSBtet_ohneLuc_P	gene and protein expression analysis, ChIP-qRT-PCR/ChIP-Seq, primary T-cell co-culture
SEM::EGR3	pSBtet_EGR3cFLAG_P	
SEM::IRX1	pSBtet_IRX1cFLAG_P	
SEM::GFP	pSBtet_GP	

2.1.2 Bacterial strains

The bacterial strain used for cloning was NEB 5-alpha competent *Escherichia coli*; DH5α derivative (C2987, NEB).

2.2 Material

2.2.1 Recombinant DNA

Table 3. Recombinant DNA used in this thesis.

Vector	Source	Identifier
pSBtet_Puro	Kowarz <i>et al.</i> , 2015	AddGene #60507
pSBtet_GP	Kowarz <i>et al.</i> , 2015	AddGene #60495
SP1-SB100X	Moudgil <i>et al.</i> , 2020	AddGene #154887
pSBtet_EGR1cFLAG_P	Dr. Anna Lena Siemund	n/a
pSBtet_EGR2cFLAG_P	Dr. Anna Lena Siemund	n/a
pSBtet_EGR3cFLAG_P	Dr. Anna Lena Siemund	n/a
pITR-ABCD_IRX1cFLAG_GP	Kühn <i>et al.</i> , 2016; Kühn, 2017	n/a

2.2.2 Oligonucleotides

Table 4. Oligonucleotides used in this thesis.

Name	Sequence (5' -> 3')	Application
GAPDH_fwd_short	GGTCACCAGGGCTGC	PCR, qRT-PCR
GAPDH_rev_short	CGTTCTCAGCCTTGA	PCR, qRT-PCR
IRX1_fwd_short	GGATCTCAGCCTTCTCG	qRT-PCR, PCR, proof of expression
IRX1_rev_short	GTGGAGACCTGCGTGAGG	qRT-PCR, PCR, proof of expression
EGR1_fwd_short	CTTCAACCCTCAGGCGGACA	qRT-PCR, PCR, proof of expression
EGR1_rev_short	GTTTGGCTGGGGTAACTGGT	qRT-PCR, PCR, proof of expression

Name	Sequence (5' -> 3')	Application
EGR2_fwd_short	ACGTCGGTGACCATCTTTCC	qRT-PCR, PCR, proof of expression
EGR2_rev_short	TGGGAGATCCAACGACCTCT	qRT-PCR, PCR, proof of expression
EGR3_fwd_short	CAGCGACTCGGTAGTCCATT	qRT-PCR, PCR, proof of expression
EGR3_rev_short	TAGGTCACGGTCTTGTGCGC	qRT-PCR, PCR, proof of expression
LGALS1_fwd_short	GTGTGCAACAGCAAGGACG	qRT-PCR
LGALS1_rev_short	TATCCATCTGGCAGCTTGACG	qRT-PCR
ICOSLG_fwd_short	AGTCCGGAGACAGAGCTCAC	qRT-PCR
ICOSLG_rev_short	CAGTCTGGGAGTCCATGCTC	qRT-PCR
TGFB1_fwd_short	CTGGACACGCAGTACAGCAA	qRT-PCR
TGFB1_rev_short	CGCACGATCATGTTGGACAG	qRT-PCR
IL6R_fwd_short	AGCCTCCAGTGAAGATTC	qRT-PCR
IL6R_rev_short	GCATGCTTGTCTTGCTTCC	qRT-PCR
HOXA9_fwd_short	CCACGCTTGACACTCACA	qRT-PCR
HOXA9_rev_short	AGTTGGCTGCTGGGTATTG	qRT-PCR
ICOSLG_fwd_ChIP1	ACCGGGACCCATGGCA	ChIP-qRT-PCR
ICOSLG_rev_ChIP1	CTCCCTCCTCCAGCGTTC	ChIP-qRT-PCR
ICOSLG_fwd_ChIP2	GTGAGCCGGGAAGGA	ChIP-qRT-PCR
ICOSLG_rev_ChIP2	ATGGGTCCCAGTCCCA	ChIP-qRT-PCR
ICOSLG_fwd_ChIP3	GCAGAGCCGAACCTTCCG	ChIP-qRT-PCR
ICOSLG_rev_ChIP3	TGGAGGCAGCCGTGTC	ChIP-qRT-PCR
ICOSLG_fwd_ChIP4	CCTCAGAGCCAGTGTAAAGC	ChIP-qRT-PCR
ICOSLG_rev_ChIP4	CGCATGCATGAATGGAAGGA	ChIP-qRT-PCR
ICOSLG_fwd_ChIP5	GCCCTGCCAGCTCTT	ChIP-qRT-PCR
ICOSLG_rev_ChIP5	CAGGCCACGCTGAGAGAC	ChIP-qRT-PCR
ICOSLG_fwd_ChIP6	GCTCTCAAGGCCAGCTG	ChIP-qRT-PCR
ICOSLG_rev_ChIP6	AAGCTGTACTCTGGTTCA	ChIP-qRT-PCR

2.2.3 Media and solutions

Table 5. Media and solutions used in this thesis.

Media/Solution	Source/Manufacture	Application
5 % BSA in TBS-T	5 % BSA dissolved in TBS-T (w/v)	western blot
0.5 % BSA in TBS-T	0.5 % BSA dissolved in TBS-T (w/v)	flow cytometry staining, T-cell isolation
Ampicillin	dissolved in MQ-H ₂ O	<i>E. coli</i> selection
anode buffer 1	300 mM Tris, 20 % Methanol (v/v), pH=10.4	western blot
anode buffer 2	25 mM Tris, 20 % Methanol (v/v), pH=10.4	western blot
Brilliant Stain Buffer	563794, BD	flow cytometry staining
ChIP elution buffer	100 mM NaHCO ₃ , 1 % SDS (w/v)	ChIP
ChIP wash buffer	20 mM Tris-HCl, 150 mM NaCl, 2 mM EDTA, 1 % Triton X-100 (v/v), 0.1 % SDS (w/v) pH=8.0	ChIP
DMEM low Glucose	DMEM-HPA, Capricorn	cell culture media
DMEM high glucose	DMEM-HA, Capricorn	cell culture media
DMEM high modified	SH30022.01, VWR	ChIP
RPMI 1640	RPMI-HA, Capricorn	cell culture
Dulbecco's PBS	Capricorn	cell culture wash buffer

Media/Solution	Source/Manufacture	Application
fetal bovine serum (FBS)	FBS-11A, Capricorn	cell culture media ingredient
RBC lysis buffer	J62990.AP, Alfa Aesar	T-cell isolation
Lymphosep	L0560-500, Biowest	T-cell isolation
cathode buffer	25 mM Tris, 40 mM ϵ -Aminocapronsäure, 20 % Methanol (v/v), pH=9.4	western blot
cryo media	90 % FBS (v/v), 10 % DMSO (v/v)	cryo conservation of cells
cell lysis buffer	150 mM NaCl, 10 mM Tris-HCl, 1 mM EDTA, 1 mM EGTA, 1 % Triton X-100 (v/v), 0.5 % NP40 (v/v), 1x protease inhibitor cocktail (added freshly)	cell lysis
Penicillin/ Streptomycin	PS-B, Capricorn	cell culture antibiotics
Puromycin	dissolved in MQ-H ₂ O	selection of transfected cells
RIPA (-SDS) buffer	50 mM Tris-HCl, 150 mM NaCl, 2 mM EDTA, 1 % NP-40 (v/v), 0.5 % Deoxycholat (w/v), pH=8.0	ChIP
RLN buffer	50 mM Tris-HCl, 140 mM NaCl ₂ , 1.5 mM MgCl ₂ , 0.5 % NP-40 (v/v) pH=8.0	RNA extraction
SDS running buffer	190 mM Glycin, 25 mM Tris-HCl, 0.1 % SDS (w/v)	SDS-PAGE
TBE buffer	100 mM Tris-HCl, 50 mM H ₃ BO ₃ , 2 mM EDTA	agarose gel electrophoresis
TBS-T	150 mM NaCl, 10 mM Tris-HCl, 0.1 % Tween® 20 (v/v)	western blot
Towbin buffer	25 mM Tris, 192 mM Glycin, 15% methanol, 0.01% SDS, pH=8.3	western blot
YT	1.2 % Bacto™ Trypton (w/v), 0.5 % NaCl (w/v), 0.5 % Hefeextrakt (w/v)	<i>E. coli</i> media
YT/YTamp agar	YT/ YTamp media, 1 % Bacto™ Agar (w/v)	solid <i>E. coli</i> media
YT _{amp}	YT media, 100 µg/ml Ampicillin	selection media for AmpR clones

2.2.4 Antibodies

Table 6. Antibodies used in this thesis.

Antibody	Source	Identifier
Goat Anti-Rabbit IgG, polyclonal antibody, Horseradish Peroxidase conjugated (1:10000; WB)	abcam	Abcam ab6721, RRID:AB_955447
DYKDDDDK Tag (D6W5B) Rabbit, monoclonal antibody, unconjugated (1/1,000 WB and ChIP)	Cell Signaling Technology	Cell Signaling Technology 14793, RRID: AB_2572291
Rabbit Anti-Actin, polyclonal antibody, unconjugated (1/1,000 WB)	Sigma-Aldrich	Sigma-Aldrich A2066, RRID: AB_476693
Rabbit Recombinant Anti-ICOS Ligand/ICOSL, monoclonal antibody, unconjugated (1/1,000 WB)	abcam	ab209262
Mouse Anti-Human CD3, monoclonal antibody, APC-H7 conjugated (flow cytometry)	BD	BD Biosciences 560176, RRID: AB_1645475
Mouse Anti-Human CD4, monoclonal antibody, PE-Cy7 conjugated (flow cytometry)	BD	BD Biosciences 557852, RRID: AB_396897
Mouse Anti-Human CD8, monoclonal antibody, BV510 conjugated (flow cytometry)	BD	BD Biosciences 563919, RRID: AB_2722546
Mouse Anti-Human CD25 (IL-2 Receptor α), monoclonal antibody, BV421 conjugated (flow cytometry)	BD	BD Biosciences 564033, RRID: AB_2738555
Mouse Anti-Human FoxP3, monoclonal antibody, AF647 conjugated (flow cytometry)	BD	BD Biosciences 561184, RRID: AB_10584328
Mouse Anti-Human CD278 (ICOS), monoclonal antibody, BB515 conjugated (flow cytometry)	BD	BD Biosciences 564549, RRID: AB_2738840
Mouse Anti-Human B7-h2, monoclonal antibody, neutralizing, unconjugated (neutralization assays)	RnD Systems	R and D Systems MAB165, RRID: AB_2122734
Mouse IgG1 kappa isotype control, functional grade (neutralization assays)	Thermo Fisher	Thermo Fisher 16-4714-85, RRID: AB_470162

2.2.5 Chemicals and recombinant proteins

Table 7. Chemicals and recombinant proteins used in this thesis.

Chemical/Protein	Source	Identifier
Q5® High-Fidelity DNA Polymerase	NEB	NEB M0491L
SuperScript™ II Reverse Transcriptase	Invitrogen	Invitrogen 18064071
Annexin V Pacific Blue	Invitrogen	Invitrogen A35122
7-AAD	Miltenyi Biotec	Miltenyi Biotec 130-111-568
Sfil restriction enzyme	NEB	NEB R0123L
T4 DNA ligase	NEB	NEB M0202S
Clarity Max Western ECL Substrate	Bio-Rad	Bio-Rad 1705061
Protease inhibitor cocktail tablets	Roche	Roche 4693116001
DNase I	Qiagen	Qiagen 79254
Go-Taq polymerase	Promega	Promega M7801
ORA qPCR Green ROX H Mix	HighQu	HighQu QPD020
Proteinase K	Roth	Roth 7528.3
RNase A	Qiagen	Qiagen 19101
RNasin®	Promega	Promega N2511
Accutase®	Capricorn	Capricorn ACC-1B
Agarose	Invitrogen	Invitrogen 10264544
Ampicillin	Roth	Roth HP62.1
Big Dye™ Terminator v3.1	Thermo Fisher	Thermo Fisher 4337457
Di(N-succinimidyl) glutarat	Sigma Aldrich	Sigma Aldrich 80424
Human BD Fc Block™	BD	BD 564219
dNTP	Roche	Roche 3622614001
Doxycyclin hydrochlorid	Sigma Aldrich	Sigma Aldrich D3447
DTT	Invitrogen	Invitrogen R0862
EDTA	Roth	Roth 8043.2
EGTA	Roth	Roth 3054.3
Ethanol	Roth	Roth P075.4
Ethidium bromide	Sigma Aldrich	Sigma Aldrich E1510-10ML
Formaldehyd	Sigma Aldrich	Sigma Aldrich F8775
Glycin	Roth	Roth 3790.1
HEPES	Capricorn	Capricorn HEP-B
Herring sperm DNA	Promega	Promega D1816
Hi-Di™ Formamid	Thermo Fisher	Applied Biosystems™ 4311320
Color Protein Standard Broad Range	NEB	NEB P7719S
L-glutamin	Capricorn	Capricorn STA-B
Isopropanol	Roth	Roth 9781.1
Metafectene Pro®	Biontexas	Biontexas T040-1.0
Methanol	Sigma Aldrich	Sigma Aldrich 82762
MgCl ₂	Merck	Merck M7304
NaCl	Roth	Roth HN00.2
NaOH	Roth	Roth 6771.1
Sodium acetate	Merck	Merck S2889
NP-40	VWR	VWR 492016-100
Trypan Blue Stain (0.4%)	Gibco	Gibco 15250061
Puromycin dihydrochloride	Sigma Aldrich	Sigma Aldrich P8833

Chemical/Protein	Source	Identifier
Bovine serum albumine (BSA)	Roth	Roth 8076.5
Roti®-Load 1 (4x)	Roth	Roth K929.2
SDS	Biomol	Biomol 04051.1
TRIS	Roth	Roth 4855.1
Triton™ X-100	Sigma Aldrich	Sigma Aldrich T8787
Tween® 20	Sigma Aldrich	Sigma Aldrich P9416
2-Mercaptoethanol	Roth	Roth 4227.3
6-Amino caproic acid	VWR	VWR SIALA2504-100G

2.2.6 Commercial assays and kits

Table 8. Commercial assays and kits used in this thesis.

Assay/Kit	Source	Identifier
Amata™ Cell Line Nucleofector™ Kit R	Lonza	Lonza VCA-1001
ChIP DNA Clean & Concentrator™ Kit	Zymo Research	Zymo Research D5205
QIAquick PCR & Gel Cleanup Kit	Qiagen	Qiagen 28506
Amata™ Cell Line Nucleofector™ Kit R	Lonza	Lonza VCA-1001
Pierce™ BCA Protein Assay Kit	Thermo Fisher	Thermo Fisher 23225
IL-10 (human) ELISA Kit	Enzo	Enzo ADI-900-036
IL-2 ELISA Kit (human)	Aviva	Aviva OKBB00179
MiSeq Reagent Kit v2	Illumina	Illumina MS-102-2003
Accel-NGS® 2S plus DNA library Kit	Swift Biosciences	Swift Biosciences 21024
Swift Unique Dual Indexing Primer Kit	Swift Biosciences	Swift Biosciences X9096
Accel-NGS 2S Truncated Adapters	Swift Biosciences	Swift Biosciences 28196
PureYield™ Plasmid Midiprep Kit	Promega	Promega A2492
RNeasy Mini Kit	Qiagen	Qiagen 74104
RNA ScreenTape Analysis	Agilent	Agilent 5067-5576, -5577, -5578
DNA ScreenTape Analysis D1000	Agilent	Agilent 5067-5582, -5583, -5586, -5602
Transcription Factor Buffer Set	BD	BD 562574
CD8 MicroBeads human	Miltenyi	Miltenyi 130-045-201
CD4 MicroBeads human	Miltenyi	Miltenyi 130-045-101
T Cell Activation/Expansion Kit human	Miltenyi	Miltenyi 130-091-441

2.2.7 Consumables

Table 9. Consumables used in this thesis.

Consumable	Source	Identifier
1 kb ladder	NEB	NEB N3232L
100 bp ladder	NEB	NEB N3231L
50 bp ladder	NEB	NEB N3236L
cell culture 6-well plates	Greiner Bio One	Greiner Bio One 657960
cell culture 10 cm plates	Greiner Bio One	Greiner Bio One 664950
50 mL cell culture flasks	Greiner Bio One	Greiner Bio One 690985
250 mL cell culture flasks	Greiner Bio One	Greiner Bio One 658195
low binding tube	Biozym	Biozym 710176

Consumable	Source	Identifier
reaction tubes 50 mL, 15 mL, 5 mL, 2 mL, 1.5 mL, 0.2 mL	Greiner Bio One	Greiner Bio One 227270, 188261-N, 622201, 623201, 616261, 671201
qRT-PCR 96-well plates	Bio-Rad	Bio-Rad #MLL9651
adhesive sealing film for qRT-PCR	Nerbe Plus	Nerbe Plus 04-095-0060
cryo tube for cell culture 2 mL	Greiner Bio One	Greiner Bio One 126278
Protein G magnetic beads	NEB	NEB S1430S
Low Fluorescence PVDF Western Membrane	Abcam	Abcam Cat# ab133411
Mini-PROTEAN TGX Stain-Free Gels 4-15%	Bio-Rad	Bio-Rad 4568085
pipette 5 mL, 10 mL, 25 mL	Greiner Bio One	Greiner Bio One 606160, 607160, 760160-TRI
MS columns	Miltenyi	Miltenyi 130-042-201

2.2.8 Devices

Table 10. Devices used in this thesis.

Device	Manufacturer
SeqStudio Genetic Analyzer	Thermo Fisher
MiSeq	Illumina
Precision balance TE123SE-OCE	Sartorius
TC20 Automated Cell Counter	Bio-Rad
Cell incubator HERAcCell 240	Thermo Fisher
Light microscope	Nikon
Ice machine	Ziegler
Fluorescence microscope Observer Z1	Carl Zeiss
Chemi Doc XRS+	Bio-Rad
Heating block	VWR
Magnetic rack	NEB
FACSVerse™	BD
Mini PROTEAN Tetra Cell	Bio-Rad
Nano photometer	Implen
OctoMACS™ Separator	Miltenyi
MACS® MultiStand	Miltenyi
Nucleofector™ 2b	Lonza
PCR cycler	Applied Biosystems
Orbital shaker iQ	QInstruments
Varioskan Flash	Thermo Fisher
Roller shaker SRT6D	Stuart
Rotator SB3	Stuart
Shaking incubator CH4103	Infros
StepOnePlus Real Time PCR cycler	Applied Biosystems
Laminar flow bench SterilGard	The Baker Company
Tape Station 2200	Agilent
Thermo shaker Compact	Eppendorf
Vacuum pump VAC-MAN	Promega
Vortexer REAX 2000	Heidolph
Water bath SE-20C	Julabo
Tilting table	Heidolph

Device	Manufacturer
Different centrifuges	Eppendorf 5415D, 5425 VWR Galaxy Mini Star Beckmann L-70, J6-HC, J2-HS, SW40

2.2.9 Software

Table 11. Software used in this thesis.

Software	Source
GraphPad Prism 7.01	GraphPad Software
ClustVis (Metsalu and Vilo, 2015)	open source
Integrative Genomics Viewer (IGV)	open source
JASPAR 2020 (Sandelin <i>et al.</i> , 2004)	open source
Microsoft Office 365®	Microsoft
Volocity 4.2.1	Improvision
Fiji (ImageJ)	open source

2.3 Methods

2.3.1 Cellular methods

2.3.1.1 Stable transgenesis of cell lines

Stable transgenesis of HEK 293T and SEM cell lines was achieved using the sleeping beauty transposon system (**Figure 8A**) (Kowarz *et al.*, 2015).

2.3.1.1.1 Transfection of HEK 293T cells

Transfection of HEK 293T cells was performed using the lipid-based transfection reagent Metafectene Pro®. 1×10^5 cells per well were seeded in a 6-well plate a day before transfection. A total of 2 µg DNA was transfected: 1.9 µg SB-plasmid and 0.1 µg of SB-transposase encoding plasmid SP1-SB100X. The respective volumes of both plasmids were filled *ad* 100 µL with PBS and in a separate batch 6 µL Metafectene Pro® added to 94 µL PBS. Subsequently, the plasmid containing batch (100 µL) was added to the Metafectene Pro® containing batch (100 µL) and incubated at RT for 20 min. Within this time, the DNA became incorporated into liposomes that enabled trafficking through cell and nuclear membranes. Afterwards, loaded liposomes were dropwise added to the media of the seeded HEK 293T cells.

2.3.1.1.2 Electroporation of SEM cells

SEM cells were electroporated using the Lonza Nucleofector™ 2b device together with the Lonza Kit R and the nucleofection program T-016 according to the manufacturer's recommendations. The nucleofection program T-016 was evaluated as most effective for electroporation of the SEM cell line by Dr. Alessa Kühn (Kühn, 2017). 0.1 µg sleeping beauty transposase plasmid SP1-SB100X together with 1.9 µg one of the SB-plasmids were used to electroporate 2×10^6 SEM cells.

2.3.1.2 Fluorescence microscopy

The fluorescence microscope Observer Z1 (Carl Zeiss) was used for microscopic imaging. Fluorescent and phase contrast imaging was performed using the software Volocity 4.2.1 (Improvision) and Fiji (ImageJ). GFP signals were excited at 483 nm causing an emission maximum at 506 nm measured using a GFP HC filter.

2.3.1.3 Cell culture

HEK 293T cells, SEM cells and isolated primary T-cells were kept at 37°C in 5% CO₂ and a relative humidity of 95%. All cells were cultivated under sterile conditions and counted using TC10™ Automated Cell Counter following Trypan blue staining. HEK 293T cells were maintained as adherent culture on cell culture plates in DMEM low glucose supplemented with 10% FBS, 2 mM L-glutamine, 100 U/mL Penicillin and 100 U/mL Streptomycin, preheated to 37°C prior to use. Cells were passaged three times per week with complete media exchange through detachment using Accutase® after washing with PBS. SEM cells were maintained as suspension culture in RPMI 1640 supplemented with 10% FBS, 2 mM L-glutamine, 100 U/ml Penicillin and 100 µg/ml Streptomycin, preheated to 37°C prior to use. Cells were passaged twice a week with complete media exchange maintaining a density of ~1-3 x 10⁶ cells/mL. For this, cell suspension was centrifuged at 200 x g for 5 min and the cell pellet was resuspended in prewarmed media. Primary T-cells were maintained as suspension culture in DMEM high glucose supplemented with 10% human plasma (derived from each donor), 2 mM L-glutamine, 100 U/ml Penicillin and 100 µg/ml Streptomycin, preheated to 37°C prior to use. T-cells were immediately activated following isolation and underwent co-culture experiments, thus no passaging was necessary. Induction of transgene expression of generated sleeping beauty transposon based cell culture models was performed by addition of 1 µg/mL Doxycycline into the media. If not otherwise stated, experimental readout was undertaken after 48h of induction with Doxycycline.

2.3.1.4 Human T-cell isolation

PBMC were isolated from peripheral blood (PB) of healthy adult donors using density gradient centrifugation. Therefore, 15 mL PB were diluted with 20 mL PBS supplemented with 0.5% BSA and overlaid with Lymphocyte Separation Media followed by 30 min centrifugation at 400 x g without break leading to separation of plasma and PBMC from remaining blood cells. Plasma was stored for T-cell culture media preparation. PBMC layer was transferred to another tube and resuspended in 50 mL PBS supplemented with 0.5% BSA followed by centrifugation at 400 x g for 5 min with break. Pellet was resuspended in 10 mL RBC lysis buffer and 10 min incubated at RT to lyse remaining erythrocytes. Afterwards, cell suspension was washed with 30 mL PBS supplemented with 0.5% BSA and isolated PBMC were counted. CD4⁺ and CD8⁺ cells were magnetically separated using CD4 MicroBeads or CD8 MicroBeads, MS columns and OctoMACS™ separator fixed to MACS® MultiStand according to the manufacturer's protocols. Purity of T-cell isolation was assessed using flow cytometry and a minimum purity of 85% was tolerated (**Figure 22B**).

2.3.1.5 Co-culture study

1x10⁶ SEM::EGR3 or SEM::mock were co-cultured for 48h with 5x10⁵ CD4⁺ T-cells and 5x10⁵ CD8⁺ T-cells in 1 mL of DMEM high glucose supplemented with 10% human plasma (derived from each donor), 2 mM L-glutamine, 100 U/ml Penicillin and 100 µg/ml Streptomycin, preheated to 37°C prior to use. T-lymphocytes were isolated from PBMC of healthy donors using magnetic bead separation as already described. Prior to co-culture, isolated T-cells were stimulated using the T-cell Activation/Expansion Kit human for 24h according to the manufacturer's recommendations. SEM::EGR3 and SEM::mock were induced with 1 µg/mL Doxycycline 24h prior to co-culture. In case of antibody treatment experiments, 20 µg/mL neutralizing monoclonal mouse α-human ICOSLG antibody (RnD Systems®) or mouse IgG1 isotype control (Invitrogen™) were added 2h prior to co-culture. After 48h of co-culture, cells were collected and stained with FACS antibodies and supernatant immediately frozen in liquid nitrogen and stored for ELISA experiments.

2.3.1.6 Flow cytometry

Cells were blocked using Human BD Fc Block™ (BD) and stained with FACS antibodies (BD) according to the manufacturer's recommendations. Half of the cell suspension was stained with α -CD3, -CD4, -CD8, Annexin V and 7-AAD to assess the viability of the T-cells after co-culture. The remaining cells were stained with α -CD3, -CD4, -CD8, -CD25, -ICOS, fixed, permeabilized and stained with α -FOXP3. Cells were analysed with a BD FACSVerse™. The gating strategy is explained in **Figure 23A**. Used antibodies are described in **Table 6**.

2.3.2 Molecular methods

2.3.2.1 Standard methods

The following methods were performed according to the respective manufacturer's recommendations or according to the lab protocols of Green and Sambrook, 2012:

- plasmid MidiPrep (Promega)
- preparation of plasmid-DNA miniprepates from *E. coli*
- alcoholic precipitation of nucleic acids
- agarose gel electrophoresis
- gel extraction and PCR purification using QIAquick PCR & Gel Cleanup Kit (Qiagen)
- DNA ligation using T4 DNA ligase (NEB)
- PCR
- qRT-PCR with StepOnePlus system
- BigDye™ Terminator v3.1 Cycle Sequencing Kit (Thermo Fisher)
- extra- and intracellular flow cytometry staining using FACS antibodies (BD), Brilliant Stain Buffer (BD) and Transcription Factor Buffer Set (BD)
- photometric quantification of nucleic acids
- protein extraction from mammalian cells
- protein quantification using Pierce™ BCA Protein Assay Kit
- western blot and protein detection with Chemi Doc XRS+ system (Bio-Rad)
- DNA digestion using SfiI
- bacterial transformation via heat shock
- RNA extraction from mammalian cells using RNeasy Mini Kit (Qiagen)
- cDNA synthesis using SuperScript™ II Reverse Transcriptase (Invitrogen)
- Pierce™ BCA protein assay (Thermo Fisher)
- IL-10 (human) ELISA Kit (Enzo)
- IL-2 ELISA Kit (human) (Aviva)

2.3.2.2 Massive analysis of cDNA ends sequencing (MACE-Seq)

Gene expression studies were performed using MACE-Seq which is a variant of 3' single end mRNA sequencing that enables high resolution transcription profiling. For that purpose, extracted RNA needed to meet quality demands that were assessed by means of RNA screen tape analysis. This QC method calculates the ratio of 18S to 28S rRNA (ribosomal ratio) resembling the integrity of the RNA sample because RNA degradation becomes obvious as a decrease in the 18S to 28S ribosomal band ratio. Screen tape analysis was performed using the bioanalyzer Agilent 2200 TapeStation that electrophoretically separates RNA samples on mini gels and subsequently detects laser induced fluorescence. As a result, RNA quality could be estimated using the gel image, electropherogram and the RNA integrity number (RIN). RIN is automatically calculated by the TapeStation software following an

algorithm that considers the ribosomal ratio as well as signal areas and intensities, and represents RNA quality ranging from 1 (total degradation) to 10 (no degradation). For MACE-Seq, a RIN value of 7.0 or higher was considered as tolerable. The RNA samples were delivered to GenXPro GmbH who carried out library preparation and NGS run including bioinformatic analysis.

2.3.2.3 Gene expression analysis using qRT-PCR

cDNA was synthesized using SuperScript™ II Reverse Transcriptase (Invitrogen) according to the manufacturer's protocol. qRT-PCR was performed in triplicates using the StepOnePlus system, the ORA qPCR Green ROX H Mix and the primer oligonucleotides listed in **Table 4**. The used PCR program started with one cycle of initial denaturation at 95°C for 10 min followed by 40 cycles of denaturation at 95°C for 15 s and elongation at 60°C for 1 min. Subsequently, a melt curve was run to check for potential mispriming. ΔC_T values were calculated with *GAPDH* expression as a reference. $\Delta\Delta C_T$ mean values were calculated with ΔC_T mean values of the empty vector control cell models HEK::mock or SEM::mock as a reference.

2.3.2.4 Patient gene expression analysis using qRT-PCR

Patient RNA samples were provided by the study centers listed in **Table 12**. For all patients analyzed, informed consent was obtained by the study centers. All patients were diagnosed with ALL between 0 and 12 months of age (infants) and displayed a pro-B phenotype. RNA was extracted from peripheral blood either at day of initial diagnosis ("diagnosis cohort" / "dx", n=50) or relapse diagnosis ("relapse cohort" / "rel", n=18) by the respective study centers. The dx cohort is solely composed of t(4;11) samples, the rel cohort is composed of the fusions KMT2A::AFF1/t(4;11) (n=14), KMT2A::MLL1/t(11;19) (n=3) and KMT2A::MLL3/t(9;11) (n=1). Detailed patient characteristics are summarized in **Tables 19** and **20**. To assess patient gene expression, cDNA was synthesized out of 1 µg RNA and *HOXA9*, *IRX1*, *EGR3* and *ICOSLG* gene expressions were measured as triplicates using qRT-PCR. ΔC_T mean values were calculated using *GAPDH* expression as a reference and relative expressions were calculated as ratio (reference/target) = $2^{CT(GAPDH) - CT(target)} = 2^{-\Delta CT}$. If available, clinical outcome was provided by the study centers.

Table 12. Patients assigned to study centers that provided RNA samples. Patients 1 – 50 belong to the dx cohort, patients REZ1 – REZ18 belong to the rel cohort.

Patient no.	Study center	Contact
1 -14	Centro Ricerca Tettamanti, Pediatrics, University of Milano-Bicocca, San Gerardo Hospital, Monza, Italy	Dr. Michela Bardini, Prof. Dr. Gianni Cazzaniga
15-29	Department of Genetics, University Hospital Robert Debré, Paris, France	Dr. Aurélie Caye-Eude, Prof. Dr. Hélène Cavé
30 - 50	Department of Pediatrics, University Medical Center Schleswig-Holstein, Kiel, Germany	Dr. Julia Alten, Prof. Dr. Gunnar Cario
REZ1 – REZ18	Department of Pediatric Oncology and Hematology, Charité Campus Virchow Clinic, Berlin, Germany	PD Dr. Cornelia Eckert

2.3.2.5 Protein expression analysis using western blot

Extracted protein lysate was quantified using the Pierce™ BCA protein assay kit and denatured at 95°C for 5 min upon addition of Roti®-Load 1 loading dye. A volume equivalent to a defined protein mass and 5 µL of Color Protein Standard Broad Range (NEB) were loaded onto an SDS gel followed by SDS-PAGE using the Mini PROTEAN Tetra Cell system (Bio-Rad). Afterwards, tank blotting onto a PVDF membrane was performed in Towbin buffer pH=8.3 at 110V for 70 min with constant cooling. Subsequently, the membrane was blocked in TBS-T + 5% BSA under constant agitation at RT for 1h and incubated over night with primary antibody in TBS-T + 5% BSA. Completing the incubation, the membrane

was washed four times with TBS-T followed by incubation with secondary antibody in TBS-T + 5% BSA for 1h at RT. Finally, the membrane was washed four times with TBS-T and detected using Clarity Max Western ECL Substrate (Bio-Rad) and the Chemi Doc XRS+ system (Bio-Rad).

2.3.2.6 Chromatin immunoprecipitation qRT-PCR and sequencing

For chromatin immunoprecipitation (ChIP), 2×10^7 SEM::mock or SEM::EGR3 cells were used after 48h of transgene expression induction with Doxycycline 1 $\mu\text{g}/\text{mL}$. ChIP-qRT-PCR was performed according to the protocol from Kühn, 2017.

For ChIP sequencing (ChIP-Seq), the same immunoprecipitated gDNA as for ChIP-qRT-PCR was used. The NGS library preparation was carried out using the Accel-NGS[®] 2S plus DNA library kit (Swift Biosciences) and Accel-NGS[®] 2S Truncated Adaptors (Swift Biosciences) according to the manufacturer's protocols with indexing performed by PCR (10 cycles). The NGS run was conducted using the MiSeq system (Illumina) and the MiSeq Reagent Kit v2 (Illumina). Dr. Patrizia Larghero applied the bioinformatic pipeline generating bam files with reads mapped to the human genome hg38 visualized using the Integrative Genomics Viewer (IGV).

2.3.3 Statistical data analysis

Statistical tests were performed using GraphPad Prism 7.01 with the settings indicated in figure legends. Level of significance was indicated with asterisks representing p-values: ns = $p > 0.05$; * = $p \leq 0.05$; ** = $p \leq 0.01$; *** = $p \leq 0.001$; **** = $p \leq 0.0001$. Principal component analysis (PCA) was conducted as a singular value decomposition using ClustVis (Metsalu and Vilo, 2015). Unit variance scaling for rows was applied. The PCA heatmaps were generated with *average* as clustering method for rows and columns, *correlation* as clustering distance for rows, and *Manhattan* as clustering distance for columns if not stated otherwise.

Kaplan-Meier plotting for survival analyses was performed using GraphPad Prism 7.01. EFS was defined as the time from diagnosis to first failure including induction failure, relapse, death, or second malignant neoplasm according to the Interfant-99 protocol (Pieters *et al.*, 2007). Time was censored at last follow-up if no events were observed. Curves were estimated with Kaplan-Meier and standard errors (SE) calculated according to Greenwood, and subsequently compared using the log-rank test.

3 Results

3.1 Gene expression profiling of EGR1-3 overexpressing HEK293T cell culture models

EGR1-3 have been reported to be upregulated upon IRX1-overexpression in HEK293T and SEM cell culture models (Kühn *et al.*, 2016; Kühn, 2017). To investigate whether the higher relapse rate of IRX1^{hi}/HOXA^{lo} patients could be mediated by the *EGR* genes, three HEK293T cell culture models expressing *EGR1*, *EGR2* or *EGR3* were generated, and their gene expression profiles assessed using MACE-Seq followed by differential gene expression analysis.

3.1.1 Generation of EGR1-3 overexpressing HEK293T cell culture models

Stable cell lines with a Doxycycline-inducible transgene expression were established using the sleeping beauty transposon system. Dr. Anna Lena Siemund generated the *EGR1*, *EGR2* and *EGR3* ORF-containing sleeping beauty plasmids pSBtet_EGR1cFLAG_P, pSBtet_EGR2cFLAG_P, pSBtet_EGR3cFLAG_P, and the empty vector control pSBtet_ohneLuc_P (mock) (**FIGURE 8A**). HEK293T cells were co-transfected with one of the EGR sleeping beauty vectors or mock control, and the SB-transposase encoding plasmid SP1-SB100X. The transposase mediated the stable integration of the SB expression cassette into the genome. As the integration cassette encodes the *puromycin-N-acetyltransferase* ORF, three 48h puromycin 2 µg/mL treatments enabled the selection of successfully transfected cells. This led to the establishment of four stable cell lines: HEK::EGR1, HEK::EGR2, HEK::EGR3 and HEK::mock.

To proof transgene transcription, cells were treated with Doxycycline to induce transgene expression, and incubated for 48h. Afterwards, RNA was extracted and subsequently written into cDNA to assess transgene transcription using PCR with *EGR1-3* specific primer pairs. *GAPDH* primers served as a positive control and water instead of cDNA as a negative control (H₂O). RNA was tested for DNA impurities. As seen in **Figure 8B**, all cell lines expressed the respective transgene and *GAPDH*, whereas no amplification took place in the water control. Subsequently, qRT-PCR was performed to quantify transgene transcription. *GAPDH* transcription served as a reference to calculate the ΔC_T value for each transcript, and respective HEK::mock ΔC_T values were used as a reference to calculate $\Delta\Delta C_T$ values which enabled quantification and comparison of transgene transcription levels (**Figure 8C**). Thereby, HEK::EGR2 exhibited the strongest transgene transcription ($\Delta\Delta C_T$ mean(EGR2) = 11.145±0.089) followed by HEK::EGR3 ($\Delta\Delta C_T$ mean(EGR3) = 10.522±0.097) and HEK::EGR1 ($\Delta\Delta C_T$ mean(EGR1) = 8.693±0.075).

Finally, cell lines were tested for protein expression using western blotting. Therefore, protein lysates were generated 48h after induction of transgene expression and the amount of protein was quantified using a BCA assay. Subsequently, 15 µL of protein lysate were loaded onto an SDS-gradient gel 4-15% followed by SDS-PAGE, tank blotting, and detection of α -FLAG and α -Actin signal. The amount of 15 µL was equal to 44.25 µg of HEK::EGR1, 25.02 µg of HEK::EGR2 and 30.90 µg of HEK::EGR3 lysates. The lysates were not adjusted to the same protein mass since prior experiments with adjusted volumes corresponding to 10 µg and 20 µg protein failed to yield a detectable EGR1cFLAG and EGR2cFLAG signal. As shown in **Figure 8D**, all transgenes became translated into detectable FLAG-tagged protein, although EGR1cFLAG and EGR2cFLAG displayed a clearly thinner α -FLAG band than EGR3cFLAG. In contrast, HEK::EGR1 exhibited the strongest Actin band indicating the higher amount of loaded protein (44.25 µg). Taken together, these findings revealed a higher protein expression level of EGR3cFLAG compared to EGR1cFLAG and EGR2cFLAG despite comparable transcript levels (**Figure 8C**). EGR1 has a predicted protein mass of 58 kDa but EGR1cFLAG appeared as a double band at ~58 kDa and ~85 kDa

which is in line with previous studies (Day *et al.*, 1990). EGR2cFLAG and EGR3cFLAG became detected at slightly higher protein masses than predicted (EGR2: 51 kDa, EGR3: 43 kDa).

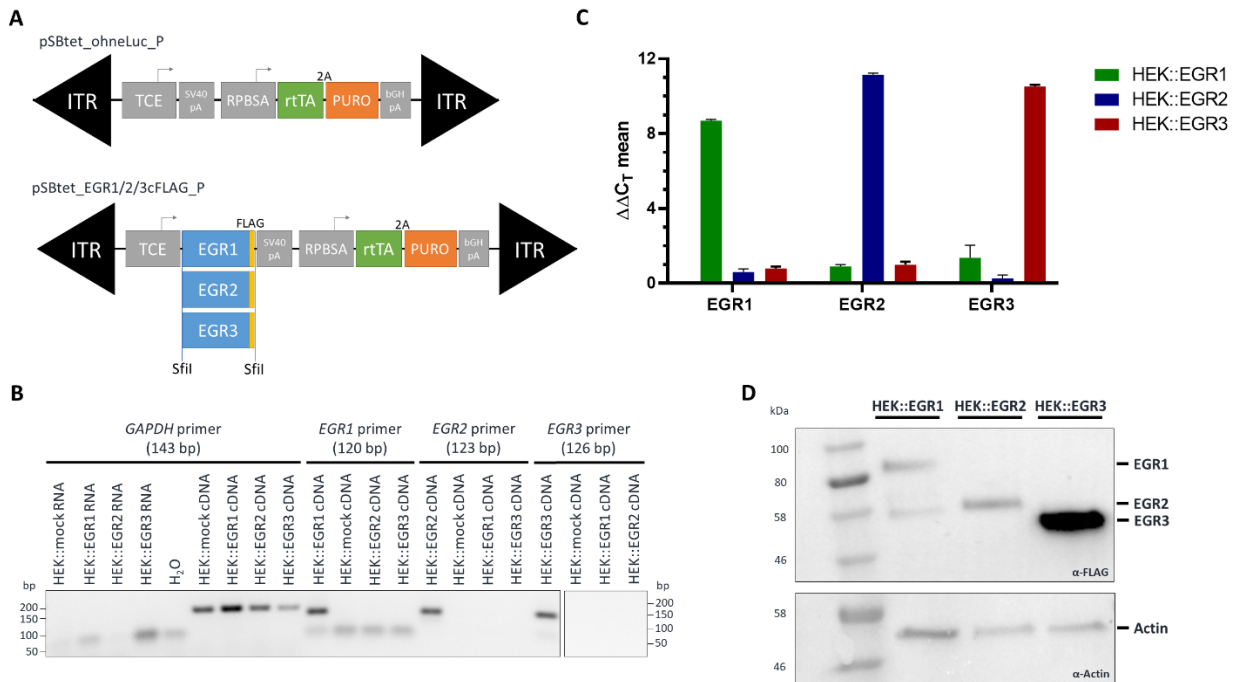


Figure 8. A Schematic structure of sleeping beauty constructs. pSBtet_ohneLuc_P served as an empty vector control (mock). pSBtet_EGR1/2/3cFLAG_P contains an expression cassette flanked by transposon derived inverted terminal repeats (ITR) that mediate genomic integration of intermediate DNA segments. EGR1/2/3 ORF fused to C-terminal FLAG-tags are under control of Tetracycline response element and minimal CMV promoter enhanced (TCE promoter), and downstream followed by SV40 polyA sequence. The synthetic RPBSA promoter controls constitutive expression of a bicistronic cassette containing the reverse Tetracycline transactivator (rtTA) and *puromycin-N-acetyltransferase* ORF (PURO) divided by a 2A sequence and followed by bGH polyA sequence. **B** PCR with transcript-specific primer pairs and subsequent 2% agarose gel electrophoresis revealed transgene transcription of HEK::EGR1, HEK::EGR2 and HEK::EGR3. RNA was tested for DNA impurities and *GAPDH* transcription served as a positive control. **C** $\Delta\Delta C_T$ mean values \pm standard errors calculated after qRT-PCR of HEK::EGR1, HEK::EGR2 and HEK::EGR3 visualize *EGR1*, *EGR2* and *EGR3* transcription levels. **D** Western blotting using an α -FLAG antibody revealed protein expression of transgenes. Actin was detected as a loading control. Tank blotting onto a PVDF membrane was performed in Towbin buffer pH=8.3, 110V, 70 min with constant cooling. α -FLAG 1/200 in TBS-T/BSA, α -Actin 1/1,000 in TBS-T/BSA, α -rabbit 1/10,000 in TBS-T/BSA.

3.1.2 Massive analysis of cDNA ends sequencing (MACE-Seq)

MACE-Seq was performed as described in 2.3.2.2. For that purpose, RNA was extracted from the four generated cell lines in triplicates 48h after induction with Doxycycline following RNA quality control by means of RNA screen tape analysis. RNA samples for MACE-Seq and corresponding RIN values are summarized in **Table 13**. Library preparation and NGS run including a bioinformatic pipeline were performed by GenXPro GmbH. The company applied the common DESeq2 method for differential gene expression analysis and provided the HEK::mock-related log₂ fold change value (log₂fc) for 28,918 transcripts including p-values and raw read counts.

Table 13. Summary of RNA sample characteristics for MACE-Seq.

Sample no.	Cell line	Charge	Date of RNA prep	Concentration [$\mu\text{g}/\mu\text{L}$]	Sample volume [μL]	RIN value
1	HEK::mock			0.032	5	7.1
2	HEK::EGR1	1	19.02.2020	0.038	5	8.6
3	HEK::EGR2			0.152	5	8.4
4	HEK::EGR3			0.025	8	8.0
5	HEK::mock			0.151	5	8.7
6	HEK::EGR1	2	26.02.2020	0.060	5	8.5
7	HEK::EGR2			0.072	5	7.9
8	HEK::EGR3			0.053	5	9.5
9	HEK::mock			0.319	5	9.8
10	HEK::EGR1	3	28.04.2020	0.319	5	9.7
11	HEK::EGR2			0.278	5	9.8
12	HEK::EGR3			0.088	5	9.7

3.1.3 Gene expression profile comparison of *EGR1-3* and *IRX1* using PCA

The *EGR1-3* gene expression profiles (MACE data) were compared to the gene expression data of transiently transfected HEK293T cells overexpressing *IRX1* (Affymetrix HG-U133Plus 2.0 data). These *IRX1* gene expression data were derived from Kühn *et al.*, 2016. The $\log_2\text{fc}$ values of the MACE *EGR1-3* datasets were assigned to all more than two-fold up- or downregulated genes of the *IRX1* Affymetrix data set ($\log_2\text{fc} \geq 1$ or $\log_2\text{fc} \leq -1$). Only genes included in both, MACE and Affymetrix data, were used for principal component analysis (PCA) resulting in an assignment involving 156 differentially expressed genes (**Table 14**). Using the open-source online tool ClustVis (Metsalu and Vilo, 2015), a PCA was performed as singular value decomposition (SVD), and unit variance scaling for rows was applied. The resulting variance explained by three dimensions (principal components 1-3) is summarized in **Table 15** and the PC coordinates of the data sets *EGR1-3* and *IRX1* in **Table 16**. Plotting of the four data sets within a coordinate system spanned by PC1 (x axis) and PC2 (y axis) resembling 85% of total variance is displayed in **Figure 9A**. As obvious, *EGR1* and *EGR2* data sets clustered closely together in distance to the *EGR3* and *IRX1* datasets. The *EGR3* dataset was the closest to *IRX1*, both differed mainly along PC2, and to a lesser extent along PC1. The described cluster pattern indicated that the *EGR3* data set possessed the highest grade of similarity related to the *IRX1* data set concerning the analyzed genes (**Table 14**).

To enable a more sophisticated and detailed comparison between the gene expression profiles, a PCA heatmap was generated (**Figure 9B**). Through this, the similarity in gene expression patterns between the datasets *EGR1* and *EGR2* on the one hand, and *IRX1* and *EGR3* on the other hand was demonstrated along the included 156 differentially expressed genes. As displayed, the *IRX1* gene expression profile was mimicked stronger by the *EGR3* profile than by *EGR1* and *EGR2* profiles. As a result, *EGR3* was identified as the main mediator of *IRX1*-induced transcription among the investigated *EGR* genes. However, differences in the level of up- and downregulation between *IRX1* and *EGR3* profiles, or even completely contrary expressed genes were present indicating that not the complete *IRX1* gene expression profile was mediated by *EGR3* expression.

Table 14. Selected genes and respective log₂fc values of *IRX1* (Affymetrix) and *EGR1-3* (MACE) data sets. Differential gene expression is indicated as mean log₂fc value of normalized triplicates. Positive log₂fc values report transcriptional upregulation, negative log₂fc values report transcriptional downregulation.

Gene symbol	IRX1 log ₂ fc	EGR1 log ₂ fc	EGR2 log ₂ fc	EGR3 log ₂ fc
IL11	5.2015	3.4308	3.4728	6.2614
LGALS1	4.7142	0.4105	0.5799	1.4637
KISS1R	4.5057	3.3372	3.6997	6.6231
TGFB1	4.2505	0.4877	0.0308	1.1876
GADD45B	4.0162	3.1156	2.6593	4.6417
RHEBL1	3.8320	1.7768	1.6867	3.3372
SOX8	3.7508	1.5471	0.8901	1.7734
EGR3	3.7480	-0.0130	1.1127	7.7437
SNAI1	3.6395	2.2931	3.3746	4.8602
MAFF	3.5681	1.1098	2.2166	3.3685
PHLDA2	3.1990	1.2684	1.2129	2.1569
NES	3.1747	-0.0022	1.7031	1.8096
BAIAP2	3.0136	1.5908	1.2549	2.2499
ID1	2.8701	0.7325	0.4545	1.2673
MICALL2	2.8359	1.0421	2.5642	2.5332
DHRS2	2.7732	1.8348	3.9886	4.2005
FOS	2.6745	2.0493	2.1248	3.4501
IER5L	2.6637	0.6642	1.2010	2.0970
CCND1	2.6039	1.8962	1.3952	2.1201
DISP2	2.5818	0.2007	-0.3406	0.7848
TNFSF9	2.5694	0.1734	1.5677	1.7562
CDKN2D	2.4726	0.1442	1.1532	1.2146
CPEB4	2.4230	-0.5121	0.1288	0.5719
NPPC	2.2829	1.4733	0.8761	1.8940
TMEM52	2.2617	0.5995	1.9272	2.1932
KCNC1	2.1943	0.4681	0.7644	1.5528
NPTX2	2.1848	1.0332	1.2843	2.2467
ISYNA1	2.1191	0.7806	1.1451	1.1866
RASD1	2.1036	0.9266	1.1818	2.9346
RASIP1	2.0796	0.5853	1.0919	1.7037
PDGFA	2.0504	1.5352	1.5320	1.9641
GALNS	2.0468	0.7402	0.6288	0.8786
COL1A1	2.0275	0.0602	0.3256	0.7048
ICAM3	2.0111	0.2048	0.0233	1.1083
C3	2.0089	1.3268	1.2038	3.1273
SPATA2L	1.9951	0.4342	0.5744	0.8147
CXCR4	1.9857	1.5802	2.3670	2.7628
TTC7A	1.9650	1.0531	0.3250	0.6890
IER3	1.9309	1.3608	1.2309	2.6105
VGF	1.9073	2.9254	2.0491	4.6188
NOTCH1	1.8910	0.5136	1.0381	1.1203
UBASH3B	1.8842	0.6139	0.5831	1.4013
ABAT	1.8723	0.3865	0.7424	1.7203
KAZALD1	1.8601	0.9671	0.9230	1.6603
MIDN	1.8567	1.0347	0.4135	1.8294
C9orf116	1.8552	-0.0171	0.8112	0.9378
FAM200A	1.8387	0.0541	0.1803	0.8772
FSCN1	1.8353	1.6923	1.1700	2.4205
DOK4	1.8299	0.3039	0.7713	1.1465
EGR1	1.8292	5.6100	0.1402	0.8410
EPHA2	1.7976	0.6117	1.2743	1.9678
LBH	1.7828	2.6522	2.5417	3.5738
CDKN1C	1.7705	3.4181	1.7093	3.2832
AQP3	1.7677	0.2811	0.4963	2.1712
HES4	1.7600	0.4237	0.2588	1.0958
APOE	1.7519	0.5196	0.0918	2.2825

Gene symbol	IRX1 log2fc	EGR1 log2fc	EGR2 log2fc	EGR3 log2fc
TNNI3	1.7284	0.1793	0.6093	1.3300
ZFP36	1.7170	0.3062	1.4813	3.1630
NRARP	1.7089	1.7232	1.1548	1.5862
SPHK1	1.6878	2.0015	1.9291	3.0122
ADAMTS1	1.6852	1.2049	1.1648	1.4267
FLNA	1.6796	0.9475	0.4017	1.3839
GPX3	1.6462	-0.2625	0.0214	1.1407
LMNA	1.6455	-0.1460	0.3117	0.4928
ELFN1	1.6356	1.9917	3.4788	4.4117
LRP10	1.6086	0.2388	-0.3594	0.4606
GDPD5	1.5440	0.4719	0.1459	0.9414
TRIB1	1.5420	2.1820	1.2845	2.1210
PLK3	1.5326	-3.3956	0.0703	0.5510
FLNC	1.5299	0.3668	1.0516	1.4034
B4GALNT1	1.5220	1.4086	0.6358	1.8667
PIM1	1.4883	0.4803	0.7214	1.0949
DUSP1	1.4790	0.8578	0.5570	1.5805
ZNF862	1.4737	-0.8355	0.1014	0.7616
UCN	1.4615	-0.1691	0.8215	0.8094
METRNL	1.4422	1.5289	1.1799	1.4091
DLL1	1.4267	0.9893	0.0784	2.6962
C6orf203	1.4115	0.9298	0.8165	1.2805
FAM43A	1.4062	0.3460	1.0743	1.3662
NPTX1	1.3995	1.2856	0.4939	1.2083
SERTAD1	1.3953	0.8079	0.7972	1.9771
MAGEB2	1.3894	0.4357	0.8707	1.6966
SLC25A29	1.3875	0.9172	1.5172	1.3391
AXIN2	1.3859	0.8940	0.5716	0.9017
GPRC5B	1.3828	-0.2342	0.0178	0.4829
CA11	1.3646	0.7532	-0.4994	1.2945
ARRDC4	1.3620	0.5207	0.2162	0.8915
PPFIA3	1.3547	0.0156	0.1919	0.5633
CXXC5	1.3535	2.6507	1.3929	2.1259
ASGR1	1.3518	0.9482	0.5358	1.7022
CAMKV	1.3308	1.1299	1.0757	1.6187
ZNF30	1.3258	0.9149	0.9913	1.2676
LHX1	1.3253	1.0813	0.8079	1.5320
ELF4	1.2943	0.6232	0.5859	1.0655
ENO2	1.2922	0.4132	1.2815	1.5375
TUBA4A	1.2881	-0.2890	0.7410	1.6282
DUSP5	1.2827	1.9187	1.4894	2.2370
ZFAND2A	1.2787	0.5797	1.2285	1.3764
EFNB1	1.2666	0.7865	0.3888	1.1560
MCAM	1.2645	0.4090	0.5267	0.9405
MAFB	1.2642	1.2978	1.2911	1.4247
UBASH3B	1.2628	0.6139	0.5831	1.4013
SOCS2	1.2020	0.3192	-0.4010	0.8724
PPFIA3	1.1894	0.0156	0.1919	0.5633
IL6R	1.1798	0.8684	0.9504	1.6794
IFFO2	1.1551	0.5885	-0.1949	0.6407
SSTR2	1.1391	-0.5813	-0.1373	1.1419
KRT18	1.1307	0.9926	0.2383	0.6940
ZCCHC12	1.1277	3.4597	3.0346	2.9455
IL27RA	1.1273	0.8647	1.3994	1.5196
DPYSL4	1.1213	1.6892	1.5950	1.5736
TFPT	1.1075	0.8390	0.8943	1.3099
ITGA7	1.1016	0.4840	1.2080	1.3970
CRYGS	1.0912	1.1204	0.9179	1.3015
CRTAC1	1.0878	3.2246	2.9296	4.5312
COL18A1	1.0769	0.9425	0.3603	1.1053

Gene symbol	IRX1 log2fc	EGR1 log2fc	EGR2 log2fc	EGR3 log2fc
APOC1	1.0758	0.3491	0.6871	1.3665
ID4	1.0568	1.2734	1.4097	1.8880
ZNF324	1.0529	0.2622	0.5784	0.7123
ZBTB3	1.0399	-0.1367	0.3409	0.6606
JAG1	1.0394	1.3578	-0.4142	2.3306
ASPHD1	1.0115	2.3669	1.6230	3.0041
AIF1L	1.0073	0.8188	1.1131	1.2006
TGS1	-1.0051	-0.5253	-0.7665	-0.9693
ZADH2	-1.0111	-0.5781	-0.7611	-1.1127
SASS6	-1.0136	-0.2016	-0.3336	-0.5763
RAB33B	-1.0233	0.0593	-0.3362	-0.6009
RGS17	-1.0276	0.0247	-0.3497	-0.1372
TIA1	-1.0552	-0.2069	-0.5952	-0.7127
TMEM136	-1.0753	-0.0327	0.0669	-0.1038
HOXA10	-1.0861	-0.2534	-0.4788	-0.4171
ZNF639	-1.1392	-0.6138	-0.7170	-0.5730
SESN1	-1.1412	-0.0605	0.3571	-0.5390
MAP3K1	-1.1480	-0.4967	-0.5519	-0.7122
GJA1	-1.1506	-0.1204	-0.2176	-0.7144
KAT2B	-1.1535	-0.5684	-0.4232	-0.8681
MECOM	-1.1585	-0.3874	0.2991	-0.6016
RGMB	-1.2270	-0.1749	-0.5845	-0.7385
SPIN4	-1.2504	-0.2435	-0.8780	-0.9491
CALD1	-1.3209	-0.3553	-0.2803	-0.7304
DNAJB4	-1.3401	-0.3498	0.1603	-0.2601
GNAI1	-1.3664	-0.4455	-0.5784	-0.5062
RIPK2	-1.3784	-0.3558	-0.4749	-0.7537
EPHA7	-1.3840	-0.6887	-0.6350	-1.1431
DICER1	-1.4208	-0.3616	-0.4017	-0.6584
SLC1A3	-1.4281	-0.2007	-0.3364	-1.0197
TSHZ1	-1.4953	-0.6574	-0.7641	-1.1503
ACVR2A	-1.4974	-0.6100	-0.6611	-0.7175
HOXA5	-1.5170	-0.2754	-0.7305	-1.0232
FIGN	-1.5389	-0.2946	-0.4757	-1.2156
MEF2C	-1.5714	0.0590	-1.0198	-0.5766
CXorf57	-1.5783	-0.0623	-0.4078	-0.9390
NR2F1	-1.5874	-0.6978	-1.2651	-1.1242
ARHGAP18	-1.6095	-0.4453	-0.6475	-1.2347
MBNL2	-1.6579	-0.8281	0.5134	-0.8722
CLIP1	-1.8202	-0.5189	-0.3420	-1.0873

Table 15. Individual and cumulative variance expressed by three dimensions (principal components PC1 - PC3).

	PC1	PC2	PC3
Individual	0.66	0.19	0.15
Cumulative	0.66	0.85	1.00

Table 16. Principal component coordinates of each data set.

	PC1	PC2	PC3
IRX1 log2fc	-11.95	-4.92	0.94
EGR1 log2fc	9.65	-0.96	5.61
EGR2 log2fc	7.00	-1.89	-6.3
EGR3 log2fc	-4.69	7.77	-0.25

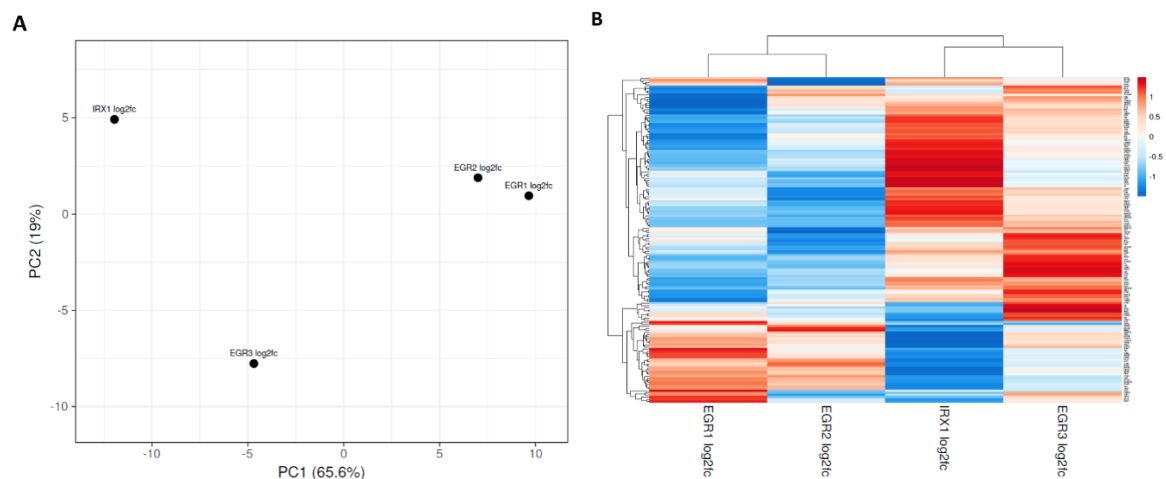


Figure 9. Principal component analysis (PCA) comparing the grade of similarity between the IRX1 and EGR1-3 gene expression data sets.

A Coordinate system along principal component 1 (PC1) spanning 65.6% of total variance and principal component 2 (PC2) spanning 19% of total variance. **B** PCA Heatmap visualizing differentially expressed genes in detail and clustering along columns (data sets) and rows (genes).

3.1.4 Qualitative analysis of MACE-Seq data

EGR3 expression has been linked to prevention of autoimmunity and restriction of immune activity in murine B- and T-cells (Anderson *et al.*, 2006; Collins *et al.*, 2008; S. Li *et al.*, 2012; Parkinson *et al.*, 2014; Safford *et al.*, 2005). In concordance, MACE-Seq and differential gene expression analysis revealed up-regulation of several immune related genes by EGR3 and IRX1 summarized in **Table 17**.

Table 17. Immune related genes upregulated in EGR3 MACE data and IRX1 Affymetrix data. Level of significance is indicated with asterisks representing p-values: ns = $p > 0.05$; * = $p \leq 0.05$; ** = $p \leq 0.01$; *** = $p \leq 0.001$; **** = $p \leq 0.0001$.

Gene symbol	IRX1 log2fc	EGR1 log2fc	EGR2 log2fc	EGR3 log2fc
LGALS1	4.7 ****	ns	0.6 *	1.5 ****
ICOSLG	ns	1.5 *	ns	2.2 **
TGFB1	4.3 ***	ns	ns	1.2 *
IL6R	1.2 **	ns	ns	1.7 **

This set of immune related genes upregulated exclusively through IRX1 or EGR3 overexpression in HEK293T cells lead to the hypothesis that the relatively higher relapse incidence in $HOXA^{lo}/IRX1^{hi}$ infant t(4;11) ALL patients could be operated by EGR3 through upregulation of factors interacting with T-cells. An immune evasion mechanism could explain the development of relapse despite continuous chemotherapy and without accumulation of secondary mutations in the dominant leukemic clone. To investigate this assumption, the upregulation of the listed genes first needed to be verified in the t(4;11) pro-B cellular context. This was achieved by two means: Firstly, the establishment of EGR3 and IRX1 overexpressing cell culture models with the t(4;11) pro-B phenotypic cell line SEM, and secondly, a gene expression analysis of patient-derived material.

3.2 Generation of IRX1 and EGR3 overexpressing SEM cell culture models

Stable SEM cell culture models were generated through electroporation with the sleeping beauty plasmids pSBtet_EGR3cFLAG_P (cell line SEM::EGR3), pSBtet_IRX1cFLAG_P (cell line SEM::IRX1) and empty vector plasmid pSBtet_ohneLuc_P (cell line SEM::mock). pSBtet_IRX1cFLAG_P needed to be cloned

because only the GFP containing plasmid pITR-ABCD_IRX1cFLAG_GP was available, generated by Dr. Alessa Kühn (Kühn *et al.*, 2016; Kühn, 2017).

3.2.1 Cloning of pSBtet_IRX1cFLAG_P

The open reading frame of *IRX1* C-terminally fused to a FLAG-tag (IRX1cFLAG) was cleaved out of the available plasmid pITR-ABCD_IRX1cFLAG_GP through overnight digestion with *Sfi*I. The fragment was electrophoretically separated using an agarose gel, visualized using ethidium bromide and subsequently extracted. pSBtet_EGR3cFLAG_P was digested the same way to extract the desired GFP-less linearized vector backbone pSBtet_P. Afterwards, the eluted fragment IRX1cFLAG and the linearized vector backbone pSBtet_P were ligated, leading to pSBtet_IRX1cFLAG_P. Competent *E. coli* (NEB® stable) became transformed with the plasmid and the selected clone was sequence-validated.

3.2.2 Establishment of stable cell culture models SEM::EGR3 and SEM::IRX1

The sleeping beauty plasmids pSBtet_ohneLuc_Puro (SEM::mock), pSBtet_EGR3cFLAG_Puro (SEM::EGR3) and pSBtet_IRX1cFLAG_Puro (SEM::IRX1) were electroporated with the transposase encoding plasmid SP1-SB100X as explained in 2.3.1.1.2. The SB-plasmids do not have a fluorescence marker in their backbone to avoid interference in multicolor flow cytometry. To monitor transfection and selection efficiency with a fluorescence microscope, the plasmid pSBtet_GP containing a GFP marker in the backbone was electroporated and treated equally thereby leading to a reporter cell line (SEM::GFP). Cells were selected six times (once to twice per week) with Puromycin 2 µg/mL for 24-48h until all SEM::GFP reporter cells displayed green fluorescence (**Figure 10**).

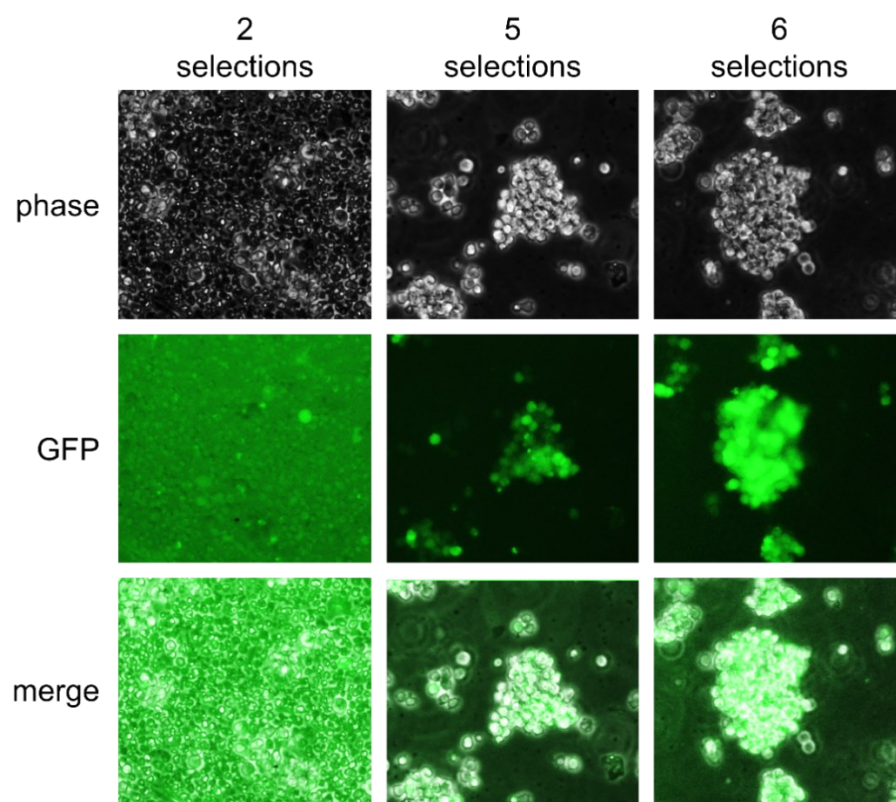


Figure 10. SEM::GFP reporter cell line was monitored using fluorescence microscopy to surveil transfection and selection efficiency during establishment of SEM cell culture models SEM::mock, SEM::EGR3 and SEM::IRX1. Upper panel: phase contrast. Central panel: GFP signal. Bottom panel: overlay of phase contrast and GFP signal (merge). After two selections, the majority of cells died due to Puromycin treatment and only

a small fraction of living cells was GFP⁺ (left column). Completing five selections, most cells were viable and formed clusters indicating proliferation, ~90% of cells were GFP⁺ (central column). Finally, all cells were GFP⁺ and proliferated after six selections (right column).

To proof transgene transcription, cells were induced with Doxycycline, and RNA extracted after 48h. Upon cDNA synthesis, transgene transcription was monitored using PCR and quantified using qRT-PCR. PCR and subsequent agarose gel electrophoresis disclosed transcription of the transgenes and confirmed purity of extracted RNA (**Figure 11A**). qRT-PCR revealed a $\Delta\Delta C_T$ mean value of 12.025 ± 0.215 for *EGR3* expression of the SEM::*EGR3* cell line, and 5.922 ± 0.167 for *IRX1* expression of the SEM::*IRX1* cell line. Gene expression quantification of SEM::*IRX1* confirmed additionally the upregulation of *EGR3* through *IRX1* overexpression, indicated by a $\Delta\Delta C_T$ mean value of 1.265 ± 0.246 (**Figure 11B**). Although *EGR3* transcription level of SEM::*EGR3* was approximately twice the level of *IRX1* transcription of SEM::*IRX1*, western blotting did not suggest a stronger protein expression of *EGR3* compared to *IRX1*. The induction of *EGR3* protein expression through *IRX1* overexpression in SEM::*IRX1* is not visible on this western blot since the used antibody targets the FLAG-tag of both transgenes and thus, wild-type proteins were not detected (**Figure 11C**).

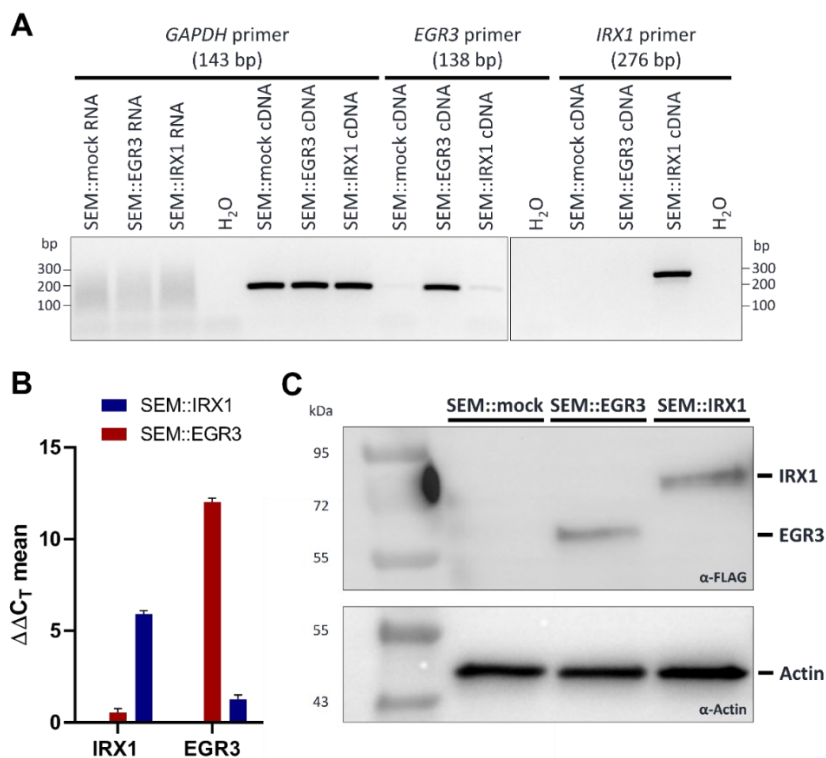


Figure 11. Proof of transgene expression for cell lines SEM::mock, SEM::EGR3 and SEM::IRX1.

A Transgene expression was proven by PCR with transgene specific primer pairs and followed by 2% agarose gel electrophoresis. *GAPDH* amplification served as a positive control, water (H₂O) as a negative control. RNA was tested for impurities. **B** qRT-PCR enabled quantification of *IRX1* and *EGR3* transcription levels through $\Delta\Delta C_T$ mean value calculation for cell lines SEM::*IRX1* (blue) and SEM::*EGR3* (red). *GAPDH* transcription served as an internal reference (ΔC_T calculation) and the respective transcription levels of SEM::mock as external references ($\Delta\Delta C_T$ calculation). **C** Western blotting using an α -FLAG antibody revealed equal protein expression of transgenes. Actin served as a loading control. 20 μ g of protein lysate were loaded onto 4-15% SDS gradient gel. Tank blotting onto a PVDF membrane was performed in Towbin buffer pH=8.3, 110V, 70 min with constant cooling. Primary antibodies 1/1,000 in TBS-T/BSA, α -rabbit 1/10,000 in TBS-T/BSA.

3.3 Gene and protein expression analysis of SEM::EGR3 and SEM::IRX1 cell culture models

The established cell lines SEM::EGR3 and SEM::IRX1 were investigated for the transcription levels of the immune-related genes, that were suggested by MACE/Affymetrix-Seq to be upregulated through EGR3 or IRX1 overexpression in HEK293T cells (Table 17). Therefore, RNA was extracted from cells after 48h of transgene expression induction followed by cDNA synthesis. Subsequently, qRT-PCR was performed with transcript specific primer pairs (Figure 12A). In contrast to the gene expression analysis of the HEK293T cell culture models, SEM cell culture models indicated only the upregulation of *ICOSLG* and *IL6R* through IRX1 or EGR3 overexpression, respectively. Thereby, SEM::EGR3 upregulated *ICOSLG* approximately three times more than SEM::IRX1 ($\Delta\Delta C_T$ mean of 3.240 ± 0.157 vs. 0.919 ± 0.158), whereas SEM::IRX1 upregulated *IL6R* approximately three times more than SEM::EGR3 ($\Delta\Delta C_T$ mean of 3.098 ± 0.202 vs. 0.748 ± 0.209). The upregulation of *ICOSLG* detected by qRT-PCR was subsequently corroborated on the protein level by western blot with an α -ICOSLG antibody (Figure 12B). As a result, ICOSLG was validated as a downstream target of EGR3 in the pro-B t(4;11) cellular context.

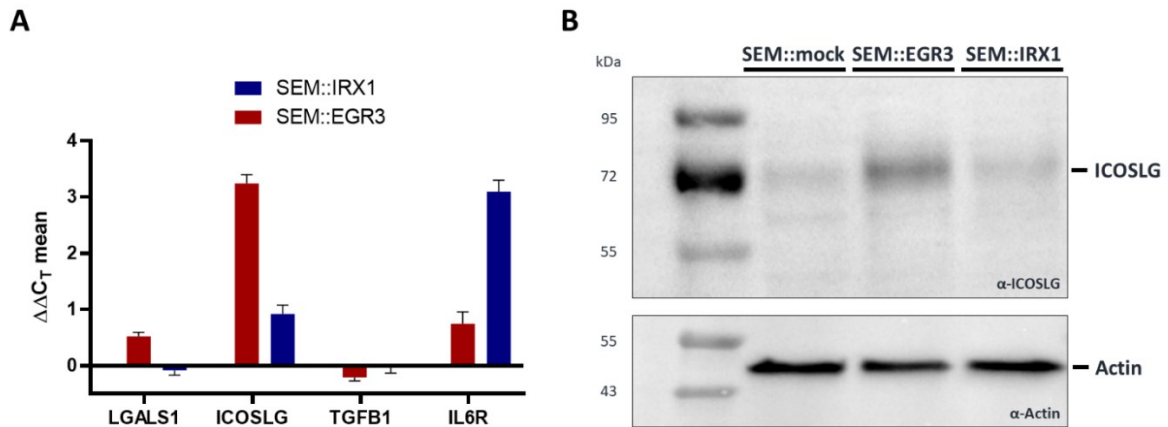


Figure 12. Gene and protein expression analysis of SEM::EGR3 and SEM::IRX1 cell culture models.

A qRT-PCR enabled comparison of transcription levels of immune related genes in SEM::IRX1 (blue) and SEM::EGR3 (red). $\Delta\Delta C_T$ mean values were calculated related to *GAPDH* transcription level and SEM::mock.

B Western blotting using an α -ICOSLG antibody corroborated ICOSLG upregulation through EGR3 overexpression on the protein level. Faint ICOSLG bands of SEM::mock and SEM::IRX1 are due to basal ICOSLG expression in SEM cells. Actin served as a loading control. 20 μ g of protein lysate were loaded onto 4-15% SDS gradient gel. Tank blotting onto a PVDF membrane was performed in Towbin buffer pH=8.3, 110V, 70 min with constant cooling. Primary antibodies 1/1,000 in TBS-T/BSA, α -rabbit 1/10,000 in TBS-T/BSA.

3.4 Characterization of ICOSLG upregulation through EGR3 overexpression

With the identification of ICOSLG as a target of EGR3, the question raised whether EGR3 as a zinc finger transcription factor binds directly to the *ICOSLG* promoter or upregulates unknown intermediate factors that in turn directly transactivate *ICOSLG*. To address this question, chromatin immunoprecipitation (ChIP) followed by qRT-PCR (ChIP-qRT-PCR) and next generation sequencing (ChIP-Seq) was performed.

3.4.1 ChIP-qRT-PCR

Initially, an *in silico* EGR3 binding site prediction was performed using the online database JASPAR 2020 (Sandelin *et al.*, 2004) in order to identify potential EGR3 binding sites in the *ICOSLG* promoter area. The genomic sequence -2000 bp until +1000 bp relative to *ICOSLG* transcription start site (TSS) was entered and the tool compared this input sequence with the consensus binding sequence of EGR3.

This led to the prediction of nine potential EGR3 binding sites (BS1 - BS9) with a relative score above 0.80 (Table 18).

Table 18. Predicted binding sites of EGR3 -2000 bp until +1000 bp relative to *ICOSLG* TSS. The relative score was calculated by JASPAR 2020 and indicated the grade of similarity between predicted binding site sequence and EGR3 consensus binding sequence.

	Relative score	Strand	Sequence
BS1	0.9399	-	GCCCCCCCCGCACG
BS2	0.8345	-	CCCCGCCCCGAGCC
BS3	0.8266	-	CCCCGCCCCGGCCT
BS4	0.8244	-	GCCCCCCCCACCTA
BS5	0.8132	-	CCCCGTCCCCGCCCC
BS6	0.8103	+	GCCCTCCCCACACA
BS7	0.8094	-	GGCCGCCCCGGCGCC
BS8	0.8079	-	TGCCGTCCACGCCCC
BS9	0.8020	+	CCCCGCCCTGCCAG

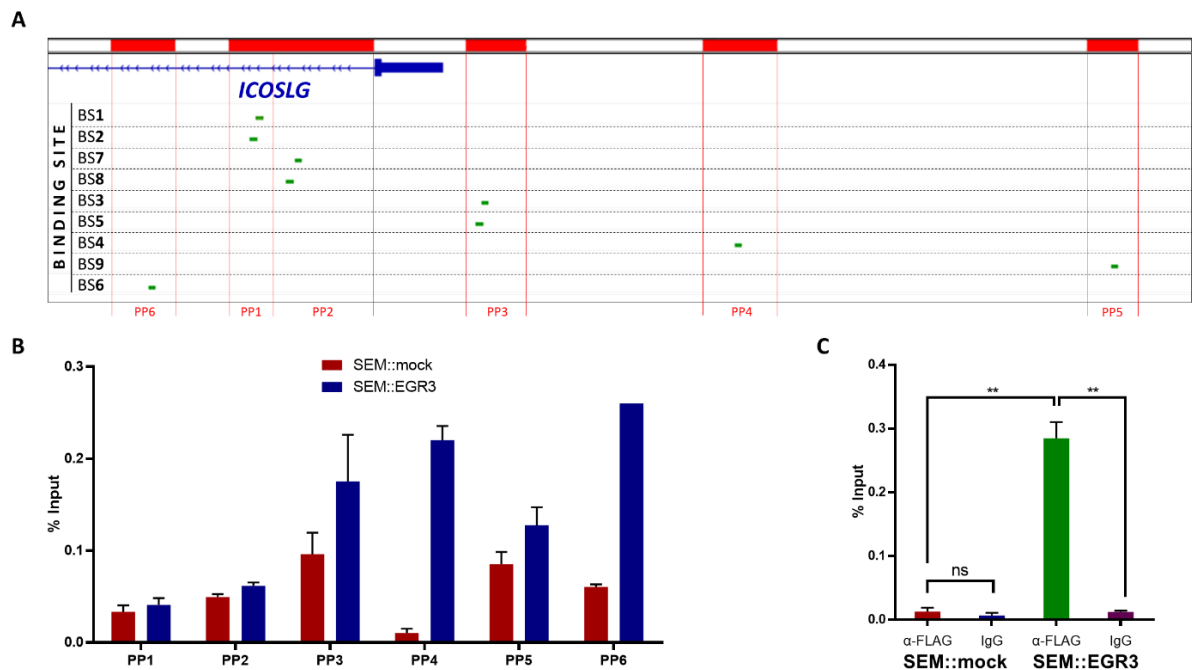


Figure 13. ChIP-qRT-PCR of predicted EGR3 binding sites at *ICOSLG* promoter.

A Snapshot from IGV (hg38) with location of *in silico* predicted EGR3 binding sites BS1 - BS9 (green) and DNA sections covered by primer pairs PP1 – PP6 (red). *ICOSLG* gene is illustrated in blue with exon 1 as a bar and intron 1 as a line. **B** Percent input values ± standard error of PP1 – PP6 for SEM::mock α-FLAG immunoprecipitate (red) and SEM::EGR3 α-FLAG immunoprecipitate (blue). **C** Percent input values ± standard error of PP4. α-FLAG immunoprecipitates of SEM::mock and SEM::EGR3 were compared to respective non-specific IgG control immunoprecipitates. Two-tailed unpaired t- tests with Welch's correction indicated a significant difference between SEM::EGR3 α-FLAG vs. IgG ($p=0.0082$) and SEM::EGR3 α-FLAG vs. SEM::mock α-FLAG ($p=0.0063$), whereas no significant difference between SEM::mock α-FLAG vs. IgG was detected ($p=0.4452$).

Six primer pairs (PP1 - PP6) were designed to cover BS1 - BS9 (Figure 13A) and ChIP of SEM::mock and SEM::EGR3 48h past transgene induction was performed using an α-FLAG antibody. The percent input method of Thermo Fisher Scientific was used to compare the amount of precipitated gDNA related to respective input samples (sonicated lysate without immunoprecipitation). As seen in Figure 13B,

amplification with PP4 revealed a higher amount of precipitated gDNA fragments in SEM::EGR3 compared to SEM::mock thereby indicating binding of EGR3cFLAG in the genomic area covered by PP4. Subsequently, the experiment was replicated with a non-specific IgG isotype control antibody in comparison to α -FLAG to evaluate potential non-specific antibody binding (**Figure 13C**). This disclosed a significantly higher percent input value of SEM::EGR3 α -FLAG immunoprecipitate compared to SEM::EGR3 IgG immunoprecipitate (antibody control) and SEM::mock α -FLAG immunoprecipitate (EGR3 control). Accordingly, a direct binding of EGR3 to *ICOSLG* promoter in the genomic area covered by PP4 (**Figure 13A**) was shown.

3.4.2 ChIP-Seq

ChIP-Seq was performed with SEM::EGR3 α -FLAG immunoprecipitate compared to SEM::EGR3 input. Reads were aligned and mapped to the human genome (hg38) by Dr. Patrizia Larghero. As visible in **Figure 14**, many reads of α -FLAG immunoprecipitate mapped selectively in the *ICOSLG* promoter area whereas reads of the input sample were distributed and did not accumulate at the promoter area. In conclusion, ChIP-Seq corroborated the finding that EGR3 binds directly to the *ICOSLG* promoter.

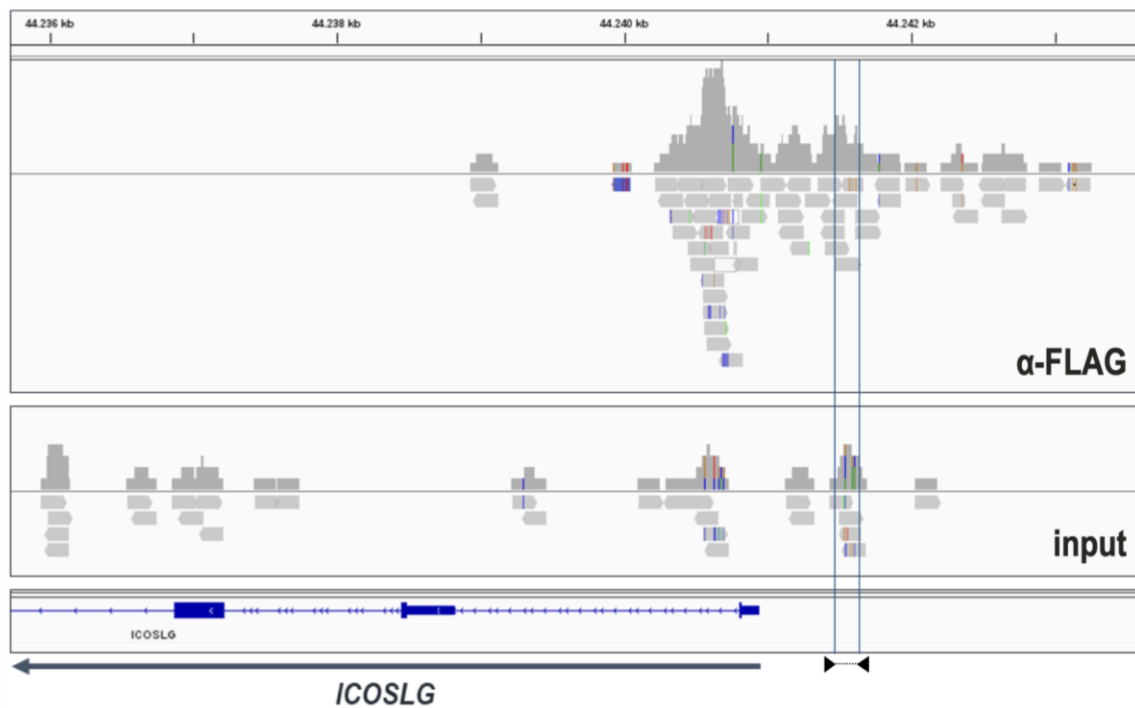


Figure 14. IGV snapshot of *ICOSLG* promoter area with ChIP-Seq reads of SEM::EGR3 α -FLAG immunoprecipitate compared to input aligned and mapped to the human genome (hg38). The area covered by PP4 is marked with arrows.

3.5 Gene expression analysis of infant t(4;11) ALL patients at diagnosis

The gene and protein expression analysis combined with ChIP-qRT-PCR and -Sequencing of a stable SEM cell culture model overexpressing EGR3 indicated the direct transactivation of *ICOSLG* through EGR3 in the t(4;11) proB cellular context. To inspect whether this regulation also applies to the clinic, gene expression of 50 infant t(4;11) ALL patients was analyzed using qRT-PCR. Although mainly *ICOSLG* was upregulated through EGR3 overexpression in the SEM cell model, the remaining immune-related genes (**Table 17**) were included as well to confirm the results of the SEM cell model gene expression analysis (**Figure 12A**).

For all patient samples informed consent was obtained by the study centers that provided samples (University Medical Center Schleswig Holstein, Kiel, Germany; University of Milan-Bicocca, Monza, Italy; University Hospital Robert Debré, Paris, France). The study centers isolated RNA from peripheral blood (PB) that was taken at the day of initial diagnosis and provided the RNA samples and clinical data. All patients were diagnosed between 0 – 12 months of age (infants) and displayed a t(4;11) translocation and proB ALL phenotype.

RNA was written into cDNA and qRT-PCR performed assessing the *HOXA9*, *IRX1*, *EGR3*, *ICOSLG*, *LGALS1*, *TGFB1* and *IL6R* gene expression levels relative to *GAPDH*. Patient characteristics and ΔC_T mean values representing gene expression levels are summarized in **Table 19**.

The study involved 29 female and 21 male patients. The patient age distribution was balanced and suggested no overrepresentation of a distinct age group (**Figure 15**).

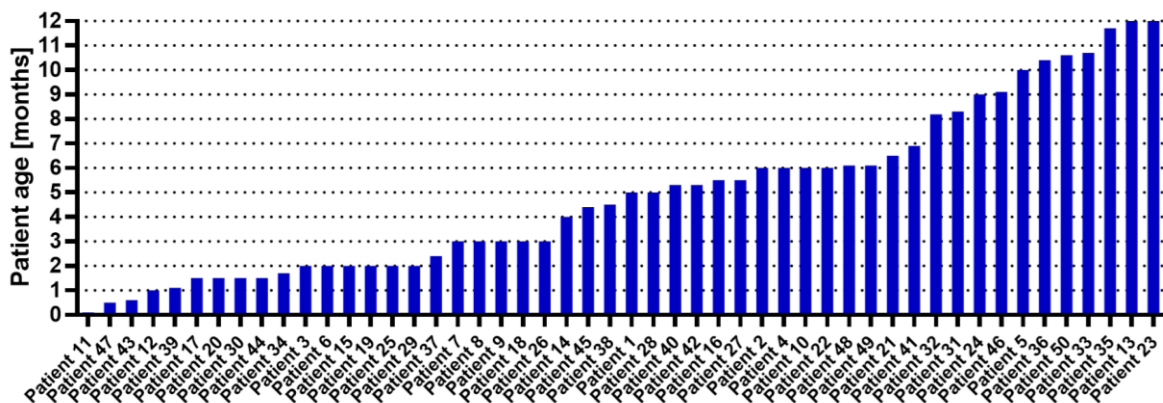


Figure 15. Patient age distribution.

Using the ΔC_T mean values of **Table 19**, Pearson correlation testing was performed to identify potential correlations between the gene expressions of *IRX1*, *EGR3*, *ICOSLG*, *LGALS1*, *TGFB1* and *IL6R*. The resulting Pearson correlation matrix (**Figure 16**) disclosed positive correlations for *IRX1/EGR3* (Pearson $r=0.451$, $p=9.98 \times 10^{-4}$), *EGR3/ICOSLG* (Pearson $r=0.644$, $p=4.54 \times 10^{-7}$) and *IRX1/ICOSLG* (Pearson $r=0.476$, $p=4.75 \times 10^{-4}$). This confirmed the upregulation of (1) EGR3 through IRX1 as described by Kühn *et al.*, 2016, (2) *ICOSLG* through EGR3 as indicated by SEM cell culture model and (3) *ICOSLG* through IRX1 verifying the suggested IRX1-EGR3-*ICOSLG* axis. The highest Pearson r value for EGR3/*ICOSLG* correlation was in line with the ChIP experiments indicating a direct transactivation of *ICOSLG* through EGR3. Besides, weak positive correlations became suggested for *IRX1/IL6R* (Pearson $r=0.371$, $p=0.01$), *EGR3/IL6R* (Pearson $r=0.357$, $p=0.01$), *EGR3/TGFB1* (Pearson $r=0.365$, $p=0.01$) and *IL6R/TGFB1* (Pearson $r=0.404$, $p=3.6 \times 10^{-3}$). *LGALS1* was denoted to be negatively correlated with *IRX1* (Pearson $r= -0.343$, $p=0.01$), *EGR3* (Pearson $r= -0.458$, $p=8.15 \times 10^{-4}$) and *ICOSLG* (Pearson $r= -0.445$, $p=1.21 \times 10^{-3}$). The Pearson correlations of *IRX1*, *EGR3* and *ICOSLG* were additionally visualized in volcano plots (**Figure 17A-C**) and patient dot plots (**Figure 17D-F**).

Table 19. Patient characteristics (n=50). Samples were taken from PB at the day of diagnosis. Gene expression values are indicated as ΔC_T mean of three technical replicates. F=female (n=29), M=male (n=21). / indicates that no outcome and treatment information were available.

Patient no.	Patient age [months]	Treatment protocol	sex	Time to event (last follow-up) [months]	<i>HOXA9</i> ΔC_T Mean	<i>IRX1</i> ΔC_T Mean	<i>EGR3</i> ΔC_T Mean	<i>ICOSLG</i> ΔC_T Mean	<i>LGALS1</i> ΔC_T Mean	<i>TGFB1</i> ΔC_T Mean	<i>IL6R</i> ΔC_T Mean
1	5.0	Interfant-06	F	(40.1)	13.3592	6.1705	8.1850	7.6499	1.9095	2.5480	10.7413
2	6.0	/	F	/	3.9204	7.7667	11.2758	8.0223	0.4124	1.1581	8.9073
3	2.0	Interfant-06	F	(23.6)	12.9546	7.1581	9.3618	7.1255	1.2583	2.6229	10.0329
4	6.0	Interfant-06	M	(17.1)	11.5783	7.9774	11.1637	7.8868	1.0367	1.7933	9.9919
5	10.0	/	M	/	3.5974	8.3317	8.8214	6.0364	1.2839	1.8193	11.2044
6	2.0	Interfant-06	M	(83.6)	4.9698	9.5555	11.5618	6.8416	1.8881	2.4003	10.6343
7	3.0	Interfant-06	F	(5.6)	11.0093	5.1167	8.5196	5.6658	0.2451	2.5425	7.2017
8	3.0	Interfant-06	F	(1.2)	4.9163	6.4184	8.2271	4.8055	1.6906	1.7833	7.6261
9	3.0	Interfant-06	M	(2.5)	4.5976	9.0338	8.0114	9.8380	1.7727	2.8336	6.7825
10	6.0	Interfant-06	F	9.5 (10.7)	5.0818	8.4812	12.3136	9.3984	0.8736	2.7232	8.4588
11	0.1	/	F	/	8.6964	8.0250	11.2989	9.9469	2.2966	5.0809	9.7797
12	1.0	/	M	/	12.3443	6.0576	11.6236	8.4245	2.7931	4.2476	9.4431
13	12.0	/	F	/	2.2824	7.9734	9.1826	7.9894	0.3829	0.9746	6.8897
14	4.0	/	F	/	11.4825	6.3166	11.4695	9.0590	1.9298	1.7006	9.5289
15	2.0	Interfant-06	M	6.0 (6.0)	4.6973	5.9447	13.3440	8.7451	1.4748	2.8882	5.6165
16	5.5	Interfant-06	M	9.5 (15.0)	6.2129	6.5399	9.5330	8.2498	-1.1884	2.4243	6.6974
17	1.5	Interfant-06	F	10.0 (13.0)	6.0703	4.9900	6.2132	4.0517	3.2334	3.4241	6.3793
18	3.0	Interfant-06	F	6.0 (11.5)	2.0906	8.4791	9.4723	8.5023	0.0054	1.5295	6.4675
19	2.0	Interfant-06	F	10.5 (19)	7.8537	3.1429	7.2056	5.2518	2.9979	2.9744	6.3224

Patient no.	Patient age [months]	Treatment protocol	sex	Time to event (last follow-up) [months]	<i>HOXA9</i> ΔC_T Mean	<i>IRX1</i> ΔC_T Mean	<i>EGR3</i> ΔC_T Mean	<i>ICOSLG</i> ΔC_T Mean	<i>LGALS1</i> ΔC_T Mean	<i>TGFB1</i> ΔC_T Mean	<i>IL6R</i> ΔC_T Mean
20	1.5	Interfant-06	M	26.5 (41.0)	4.4627	8.3685	11.2026	7.5564	1.6763	3.7679	10.3557
21	6.5	Interfant-06	M	24.0 (32.8)	11.2673	5.3156	8.7817	8.6026	1.1984	0.5756	5.9375
22	6.0	Interfant-06	F	19.5 (23.5)	11.5891	7.0636	10.0553	7.8697	1.8581	1.0288	7.8379
23	12.0	Interfant-06	F	32.0 (60.6)	11.1226	4.2582	8.0600	7.3822	0.8995	0.4484	6.8650
24	9.0	Interfant-06	M	(84.9)	8.7665	2.2034	7.0569	5.8906	3.5974	-0.9682	5.8935
25	2.0	Interfant-06	F	(118.8)	4.6017	7.1138	10.2925	7.1171	0.9684	1.7201	6.9823
26	3.0	Interfant-06	M	8.0 (108.5)	13.0872	5.9083	8.7375	8.5604	3.1732	1.5346	6.7797
27	5.5	Interfant-06	M	(9.0)	5.9626	8.1536	9.1105	8.6464	0.6725	0.4871	5.4908
28	5.0	Interfant-06	M	17.0 (33.0)	5.9922	4.8934	5.0456	3.8081	2.4379	1.0869	5.5554
29	2.0	Interfant-06	F	56.0 (58.6)	5.3297	8.4461	9.3271	8.9127	1.8728	1.0541	8.4662
30	1.5	Interfant-06	F	(146.1)	5.8358	8.0518	9.8910	8.1978	1.4358	1.9338	6.9138
31	8.3	Interfant-06	F	(109.3)	2.2195	6.2132	6.5075	6.2880	0.7614	0.7850	5.8221
32	8.2	Interfant-06	M	(95.9)	1.7726	7.4956	7.2074	7.4143	0.7116	1.5468	4.8458
33	10.7	Interfant-06	M	8.8 (8.8)	2.6953	3.0935	2.4138	4.9064	5.0513	1.2514	6.0852
34	1.7	Interfant-06	F	(91.5)	3.8579	7.1200	6.2540	7.6448	1.1743	1.9610	6.8876
35	11.7	Interfant-06	F	(73.2)	2.9311	7.9152	10.9273	7.2855	0.2957	1.1438	6.3915
36	10.4	Interfant-06	F	(75.9)	5.7541	8.8581	10.4144	9.1282	0.8518	2.3135	8.4111
37	2.4	Interfant-06	F	(73.8)	13.3331	6.1426	9.8438	9.0200	0.7787	2.3130	8.9769
38	4.5	Interfant-06	M	16.1 (63.5)	4.6562	8.9152	11.4891	8.7484	0.0676	1.9520	7.5241
39	1.1	Interfant-06	F	3.3 (15.7)	12.9071	6.3552	11.9464	9.3496	1.1245	2.6300	7.2875
40	5.3	Interfant-06	M	(58.7)	5.4284	8.4380	10.3705	8.3493	1.0471	2.2064	6.9109

Patient no.	Patient age [months]	Treatment protocol	sex	Time to event (last follow-up) [months]	<i>HOXA9</i> ΔC_T Mean	<i>IRX1</i> ΔC_T Mean	<i>EGR3</i> ΔC_T Mean	<i>ICOSLG</i> ΔC_T Mean	<i>LGALS1</i> ΔC_T Mean	<i>TGFB1</i> ΔC_T Mean	<i>IL6R</i> ΔC_T Mean
41	6.9	Interfant-06	F	(63.2)	9.2472	8.5374	9.7053	6.0532	3.9702	2.6845	8.8912
42	5.3	Interfant-06	M	(60.7)	3.4737	7.4371	9.5640	7.1599	1.5483	1.8940	5.9846
43	0.6	Interfant-06	F	5.0 (11.9)	7.9122	6.2711	8.6364	8.0174	1.1722	2.5610	7.9737
44	1.5	Interfant-06	M	17.3 (18.3)	8.1333	8.0008	9.5745	7.1672	1.9211	2.9547	9.0455
45	4.4	Interfant-06	M	6.6 (10.8)	4.2993	8.0016	10.2528	8.4346	0.7570	1.4843	6.4437
46	9.1	Interfant-06	F	39.7 (45.2)	3.1663	7.7915	9.3985	8.2159	2.1566	2.2845	5.8910
47	0.5	Interfant-06	F	8.7 (13.3)	6.2701	6.5276	9.9358	7.8396	1.2066	2.5907	6.8413
48	6.1	AIEOP-BFM ALL 2017	F	6.6	12.6734	4.2609	9.4741	4.7534	1.8121	1.8669	5.9915
49	6.1	AIEOP-BFM ALL 2017	F	8.3	4.5847	8.1496	10.5529	7.6922	1.4470	3.0814	6.2429
50	10.6	/	M	/	5.0774	9.4705	5.1199	5.4875	3.7999	1.3113	8.2715

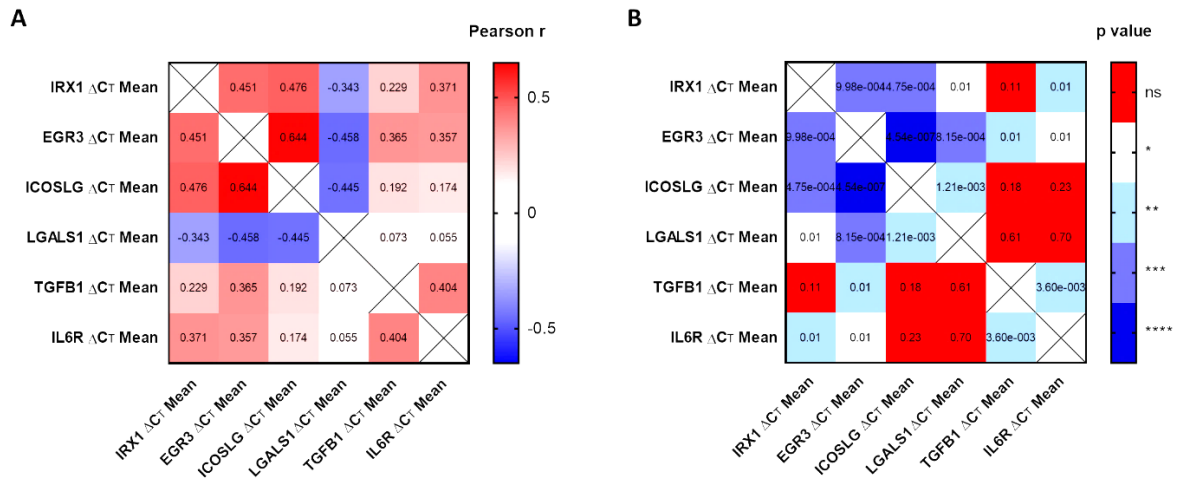


Figure 16. Pearson correlation matrix of ΔC_T mean values from **Table 19** (A) and respective p values (B).

The SEM cell model suggested a positive correlation between IRX1-EGR3-ICOSLG which was confirmed through the patient gene expression study. However, SEM::EGR3 led to a slight upregulation of LGALS1 (**Figure 12A**) which was in the patient study negatively related to EGR3 expression. Furthermore, both SEM cell culture models denoted a minimally negative regulation of TGFB1 by EGR3 and IRX1 (**Figure 12A**), which was not confirmed with patient data. In summary, Pearson correlation testing of patient samples verified the suggested IRX1-EGR3-ICOSLG axis in infant t(4;11) ALL.

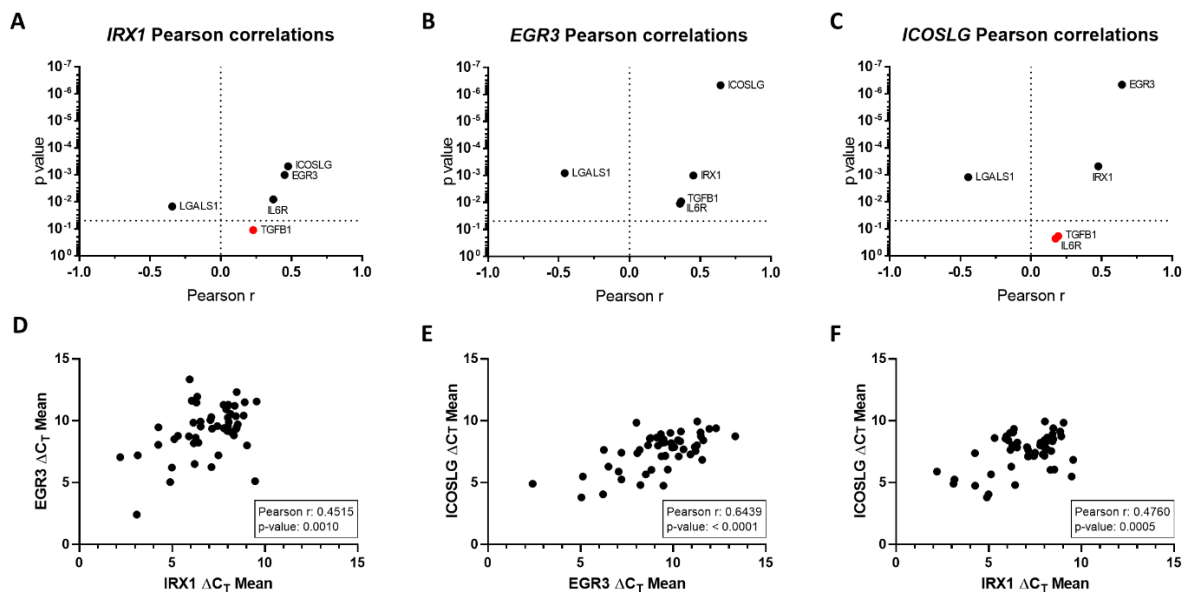


Figure 17. Pearson correlations of IRX1, EGR3 and ICOSLG.

A-C Pearson correlations visualized as volcano plots. p value ≥ 0.05 as threshold for non-significance is drawn as a line from y axis, and non-significant correlation dots are marked in red. **D-E** Pearson correlations illustrated as dot plots with patients assigned to gene expressions indicated by axis labels.

3.5.1 Event-free survival analysis of infant t(4;11) ALL patients at diagnosis

Outcome data were available for 43 of 50 patients (**Table 19**) enabling an event-free survival (EFS) analysis with EFS defined as the time from diagnosis to first failure (induction failure, relapse, death, or second malignant neoplasm). Infant t(4;11) patients were reported to cluster into a $HOXA^{hi}/IRX1^{lo}$ and a $HOXA^{lo}/IRX1^{hi}$ group (Symeonidou and Ottersbach, 2021; Trentin *et al.*, 2009), with higher relapse rates of the $HOXA^{lo}$ patients (Kang *et al.*, 2012; Stam *et al.*, 2010). Therefore, EFS depending on $HOXA9$ gene expression was investigated.

3.5.1.1 Event-free survival depending on *HOXA9* gene expression

As illustrated in **Figure 18A**, patients that did not achieve an event ($n=12$) as well as patients that displayed an event ($n=23$) within five years from diagnosis both clustered into a $HOXA9^{lo}$ and a $HOXA9^{hi}$ group. Subsequent Kaplan-Meier EFS analysis including all patients ($n=43$) revealed that the previously reported EFS disadvantage of the $HOXA9^{lo}$ group was quite modest with a four-year EFS (4y-EFS) of $34.9\pm 13.4\%$ compared to $46.4\pm 10.2\%$ for the $HOXA9^{hi}$ group. The EFS curves were not significantly different in a log-rank test ($p=0.6929$) (**Figure 18B**). In line with previous studies was the relatively elevated median *IRX1* gene expression level of the $HOXA9^{lo}$ group in comparison to the $HOXA9^{hi}$ group ($p=0.0012$) (**Figure 18C**). Although a strong correlation between *IRX1* and *EGR3* gene expressions in infant $t(4;11)$ ALL was demonstrated (**Figure 17D**), the $HOXA9^{lo}/IRX1^{hi}$ group displayed no higher median *EGR3* gene expression level than the $HOXA9^{hi}/IRX1^{lo}$ group ($p=0.5397$) (**Figure 18D**). In conclusion, $HOXA9^{lo}$ patients showed only slightly inferior EFS than $HOXA9^{hi}$ patients.

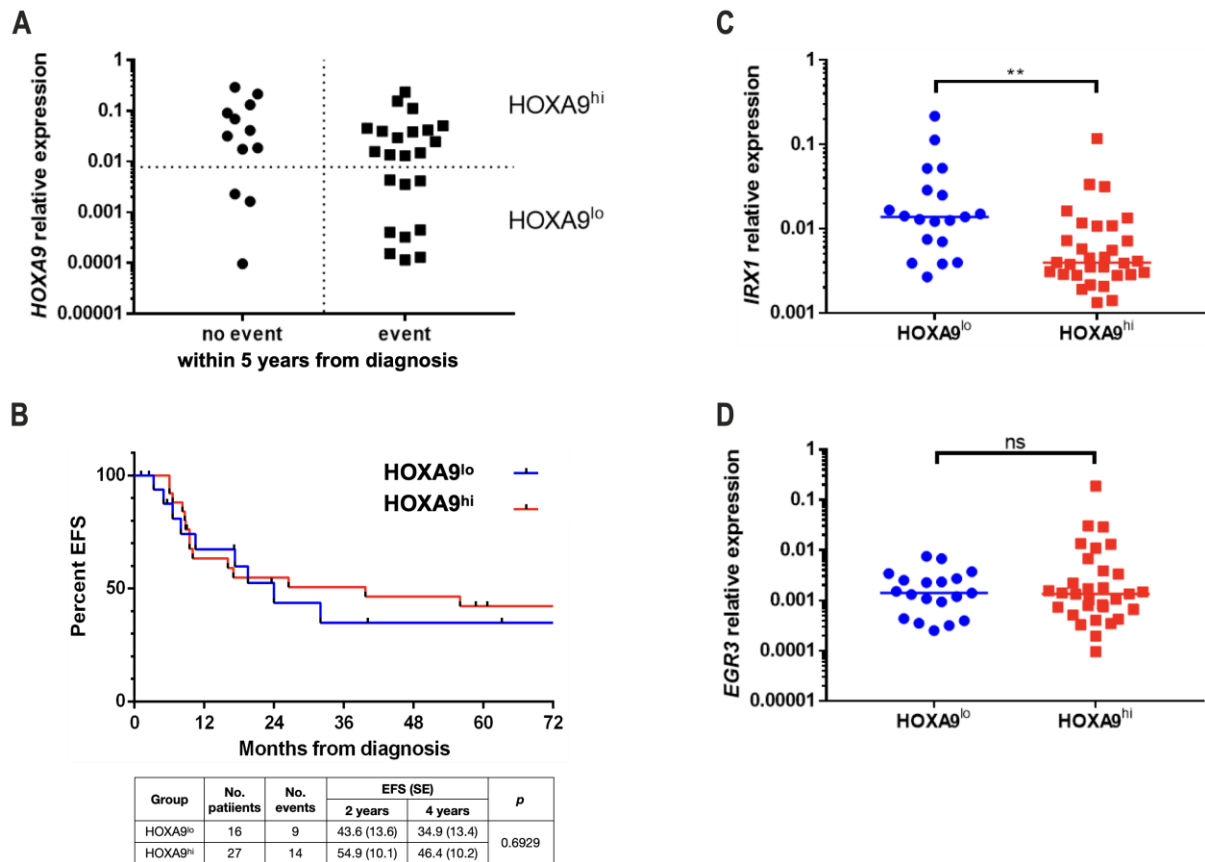


Figure 18. EFS depending on *HOXA9* gene expression.

A Division of patients into a group that achieved no event ($n=12$) and a group that displayed an event within five years from diagnosis ($n=23$) enabled subgrouping of patients depending on *HOXA9* transcription level into a $HOXA9^{lo}$ and $HOXA9^{hi}$ cluster. **B** Kaplan-Meier EFS analysis revealed slightly inferior EFS of the $HOXA9^{lo}$ group without reaching statistical significance in a log-rank-test ($p=0.6929$). Group characteristics are specified in the table below. $HOXA9^{lo}$ patients exhibited a relatively higher *IRX1* ($p=0.012$) (**C**) but not *EGR3* ($p=0.5397$) (**D**) gene expression level. Statistical testing was performed using two-tailed unpaired t-tests.

3.5.1.2 Event-free survival depending on *ICOSLG* gene expression

To investigate a potential contribution of *ICOSLG* expression on therapy resistance, an EFS analysis was performed considering *ICOSLG* gene expression. Therefore, patients of the “no event group”

(n=12) and “event group” (n=23) were assigned to respective *ICOSLG* gene expression levels (Figure 19A).

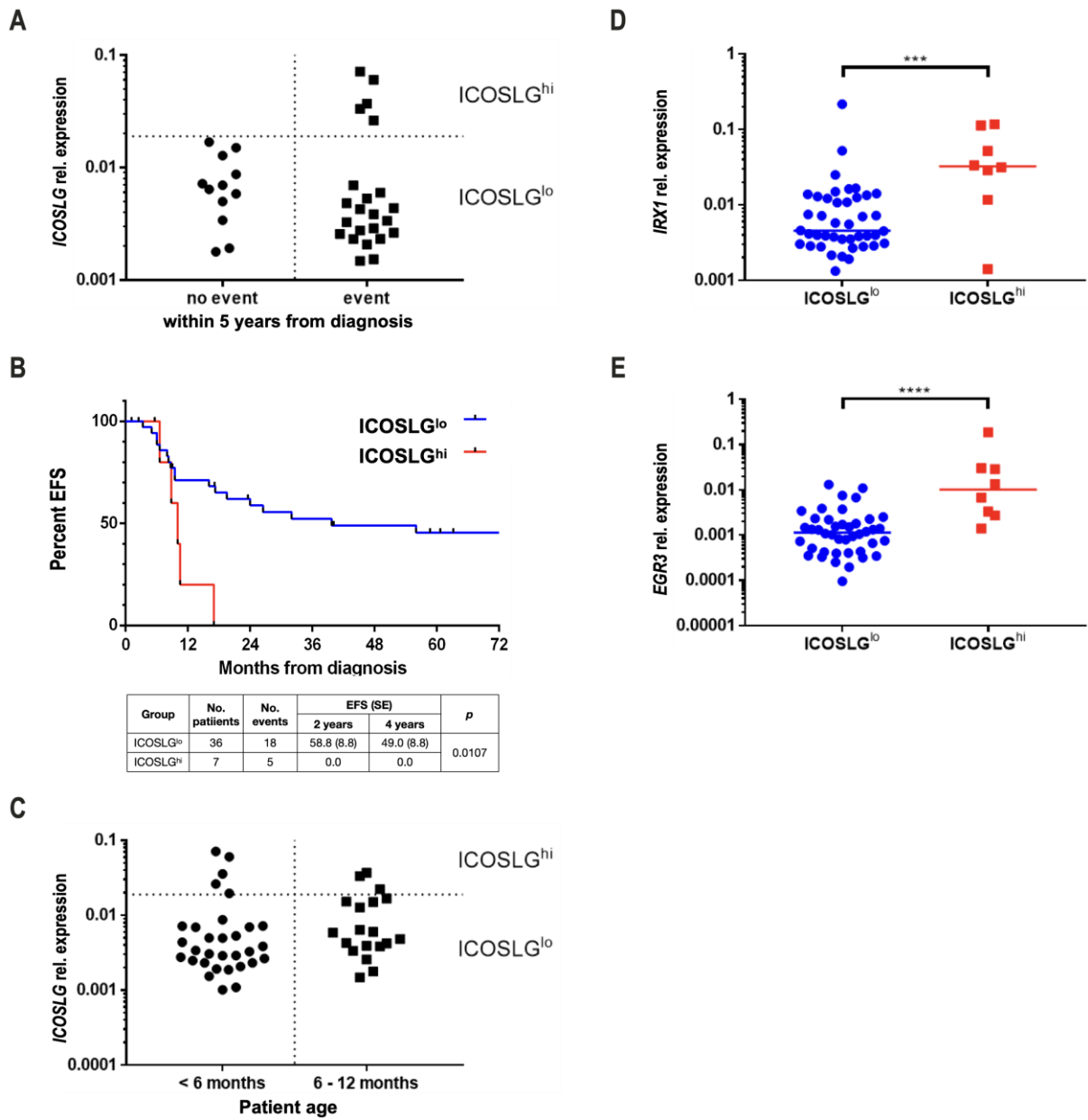


Figure 19. EFS depending on *ICOSLG* gene expression.

A Assignment of the “no event group” (n=12) and the “event group” (n=23) to respective *ICOSLG* expression levels disclosed division of the “event group” into an *ICOSLG*^{hi} and an *ICOSLG*^{lo} subgroup. **B** Kaplan-Meier EFS analysis revealed significantly inferior EFS of the *ICOSLG*^{hi} group in a log-rank-test (p=0.0107). Group characteristics are specified in the table below. **C** Patients separated by age were assigned to *ICOSLG* gene expression levels demonstrating that the *ICOSLG*^{hi} group was composed of patients younger and older than 6 months. *ICOSLG*^{hi} patients exhibited relatively higher *IRX1* (p=0.0006) (**D**) and *EGR3* (p<0.0001) (**E**) gene expression levels. Statistical testing was performed as two-tailed unpaired t-tests.

Patients with an *ICOSLG* expression level reaching or exceeding that one of the SEM::EGR3 cell culture model (rel. expression = 0.02) were regarded as *ICOSLG*^{hi}. Importantly, patients of the “event group” clustered into an *ICOSLG*^{hi} and an *ICOSLG*^{lo} group whereas the “no event group” consisted exclusively of *ICOSLG*^{lo} patients. In line with this observation, the Kaplan-Meier EFS analysis revealed clearly inferior EFS of the *ICOSLG*^{hi} group (n=7, 2y-EFS=0%) compared to the *ICOSLG*^{lo} group (n=36, 2y-

EFS=58.8±8.8%) (**Figure 19B**). This difference was confirmed to be statistically significant in a log-rank-test ($p=0.0107$). Of note, the EFS analysis could be biased due to the difference in group size ($n=7$ vs. $n=36$). However, a potential bias due to patient age could be excluded as both the *ICOSLG*^{hi} and the *ICOSLG*^{lo} group are composed of patients younger and older than six months (**Figure 19C**). Consistent with the previous investigations of gene expression correlations, the *ICOSLG*^{hi} group ($n=8$) of all patients ($n=50$) exhibited relatively elevated *EGR3* ($p=0.0006$) and *IRX1* ($p<0.0001$) gene expression levels compared to the *ICOSLG*^{lo} group (**Figure 19D,E**). In summary, high *ICOSLG* expression was associated with inferior EFS.

3.6 Gene expression analysis of infant ALL patients at relapse

With the observation that high *ICOSLG* gene expression at diagnosis was associated with inferior EFS in infant t(4;11) ALL, the question raised whether *ICOSLG*^{hi} could be directly linked to relapse development. To examine this thesis, 18 infant ALL patient samples taken at relapse diagnosis (“relapse cohort” / “rel”) were investigated for gene expression of *HOXA9*, *IRX1*, *EGR3* and *ICOSLG*. This cohort was independent and not related to the patients at diagnosis of the previous cohort. Informed consent was obtained for all patients by the providing study center (Department of Pediatric Oncology and Hematology, Charité University Clinic, Berlin, Germany). The “rel” cohort ($n=18$) consisted of infant proB ALL patients with the fusions *KMT2A::AFF1/t(4;11)* ($n=14$), *KMT2A::MLL1/t(11;19)* ($n=3$) and *KMT2A::MLL3/t(9;11)* ($n=1$). Patient characteristics are summarized in **Table 20**. The study center extracted RNA from PB and provided the samples for investigation. cDNA was synthesized out of RNA and gene expression measured in triplicates using qRT-PCR with *GAPDH* as reference for calculation of ΔC_T values.

Table 20. Patient characteristics of the “relapse cohort” ($n=18$). Samples were taken from PB at the day of relapse diagnosis. Gene expression values are indicated as ΔC_T mean of three technical replicates. F=female ($n=10$), M=male ($n=8$).

Patient no.	Age at primary diagnosis [months]	<i>KMT2A</i> -r partner	sex	<i>HOXA9</i> ΔC_T Mean	<i>IRX1</i> ΔC_T Mean	<i>EGR3</i> ΔC_T Mean	<i>ICOSLG</i> ΔC_T Mean
REZ1	1.3	<i>AFF1</i>	F	2.0164	5.1564	2.8329	6.6125
REZ2	2.9	<i>MLL1</i>	M	5.5175	6.9523	4.1774	7.6475
REZ3	3.8	<i>AFF1</i>	F	10.2331	2.5280	4.3014	5.3886
REZ4	2.5	<i>AFF1</i>	F	7.7676	2.6212	6.6574	4.6624
REZ5	1.2	<i>AFF1</i>	F	3.0343	6.7165	1.1889	5.4212
REZ6	10.7	<i>MLL1</i>	M	7.7594	4.8719	5.1781	5.7146
REZ7	4.3	<i>MLL1</i>	M	-0.4711	4.3449	3.7298	2.8993
REZ8	3.6	<i>MLL3</i>	F	6.2062	6.1063	4.7424	5.8926
REZ9	9.1	<i>AFF1</i>	F	10.7240	4.1039	2.2761	4.2876
REZ10	0.7	<i>AFF1</i>	F	8.6099	2.5404	1.6308	4.4925
REZ11	4.4	<i>AFF1</i>	M	3.0476	5.1591	6.5653	4.7486
REZ12	4.2	<i>AFF1</i>	M	1.7890	6.1005	5.0302	5.8425
REZ13	2.0	<i>AFF1</i>	F	10.5380	1.7080	2.5849	5.5004
REZ14	3.1	<i>AFF1</i>	F	11.7303	9.2469	8.4397	4.8532
REZ15	7.6	<i>AFF1</i>	F	7.3905	6.9466	7.8336	2.7011

Patient no.	Age at primary diagnosis [months]	<i>KMT2A-r</i> partner	sex	<i>HOXA9</i> ΔC_T Mean	<i>IRX1</i> ΔC_T Mean	<i>EGR3</i> ΔC_T Mean	<i>ICOSLG</i> ΔC_T Mean
REZ16	6.7	<i>AFF1</i>	M	7.3009	9.9403	9.5416	4.6631
REZ17	5.3	<i>AFF1</i>	M	4.8711	8.6455	9.8667	3.9622
REZ18	7.2	<i>AFF1</i>	M	14.5412	9.5706	6.7247	3.3545

Gene expression of the “relapse cohort” (“rel”) was compared to gene expression of the cohort from primary diagnosis (“diagnosis cohort” / “dx”) using a heatmap (**Figure 20A**). For that purpose, exclusively those patients of the “diagnosis cohort” were included that achieved an event (n=23), in order to enable an appropriate, unbiased comparison of both cohorts. It became obvious that the “rel” cohort displayed generally higher *ICOSLG* and *EGR3* gene expression levels compared to the “dx” cohort. Importantly, the median *ICOSLG* gene expression of the “rel” cohort approximated the level of the *ICOSLG*^{hi} group of the “dx” cohort (**Figure 20B**). The relatively higher levels of *ICOSLG* (**Figure 20B**) and *EGR3* (**Figure 20C**) gene expression of the “rel” cohort achieved significance in unpaired t-tests ($p < 0.0001$), whereas no difference was identified considering *IRX1* ($p = 0.2737$) (**Figure 20D**) and *HOXA9* ($p = 0.8374$) (**Figure 20E**) gene expression levels. Altogether, these findings pointed to a direct linkage between *EGR3/ICOSLG* expression and relapse formation.

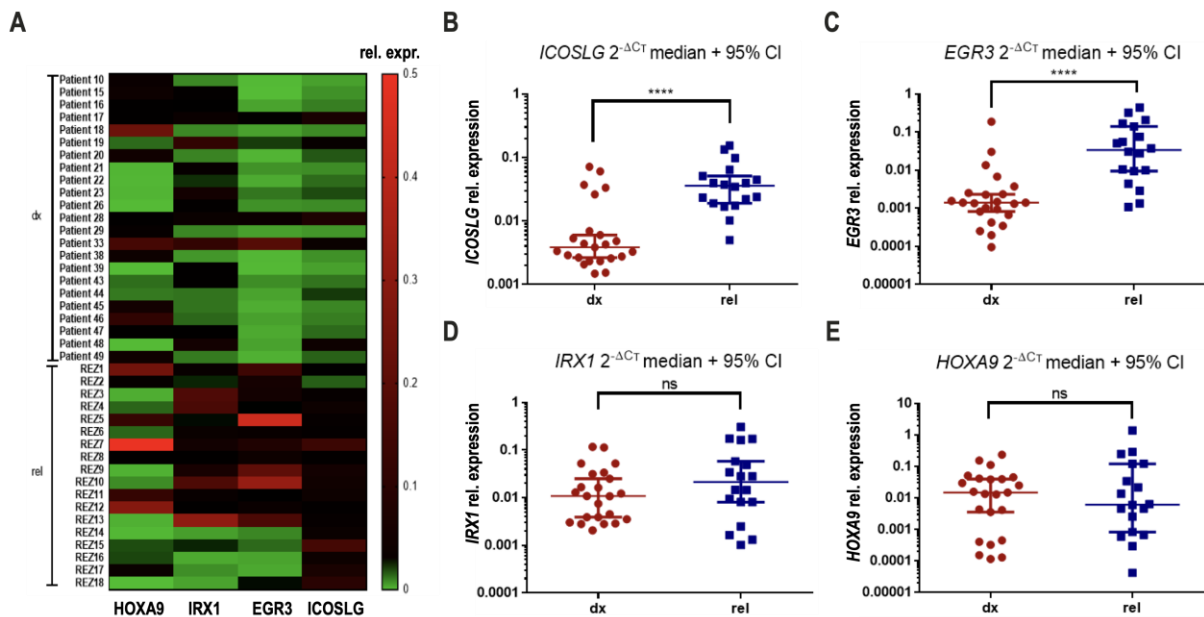


Figure 20. Gene expression comparison of “relapse” and “diagnosis” cohort.

A Heatmap displaying *HOXA9*, *IRX1*, *EGR3* and *ICOSLG* expression levels of the “diagnosis cohort” (“dx”, patients achieving an event, n=23) and the “relapse cohort” (“rel”, n=18). High relative expression (rel. expr.) is indicated in red. *ICOSLG* (**B**) and *EGR3* (**C**) median relative expression levels of the “rel” cohort were significantly higher than those of the “dx” cohort in unpaired t-tests ($p < 0.0001$). This was not the case for *IRX1* (**D**) ($p = 0.2737$) and *HOXA9* (**E**) ($p = 0.8374$) expressions. CI = confidence interval.

Because the *ICOSLG* expression level of the “rel” cohort approximated the level of the *ICOSLG*^{hi} group of the “dx” cohort (**Figure 20B**), a principal component analysis (PCA) was performed to inspect the grade of similarity between the gene expression profiles of these groups. The individual and cumulative variance expressed through PC1 - PC3 are shown in **Table 21**.

Table 21. Individual and cumulative variance expressed by three dimensions (principal components PC1 - PC3).

	PC1	PC2	PC3
Individual	0.68	0.22	0.10
Cumulative	0.68	0.90	1.00

Gene expression profiles assigned to “dx” *ICOSLG*^{hi}, “dx” *ICOSLG*^{lo}, and “rel” were plotted in a coordinate system along PC1 and PC2 (**Figure 21A**). This demonstrated coherent clustering and overlap of “dx” *ICOSLG*^{hi} (red) with “rel” (green) whereas “dx” *ICOSLG*^{lo} (blue) clustered besides with only minimal overlap. Additionally, the PCA heatmap illustrated the consistent gene expression profile of “dx” *ICOSLG*^{hi} and “rel” (green) in contrast to that one of “dx” *ICOSLG*^{lo} (blue) (**Figure 21B**).

In summary, PCA disclosed a high grade of similarity regarding *EGR3* and *ICOSLG* expressions between the group of patients with elevated *ICOSLG* expression at diagnosis and the patients at relapse. These results strongly suggest that the *EGR3*-*ICOSLG* relation is involved in relapse development, and that a high *ICOSLG* expression level at diagnosis can be described as a predictor for relapse.

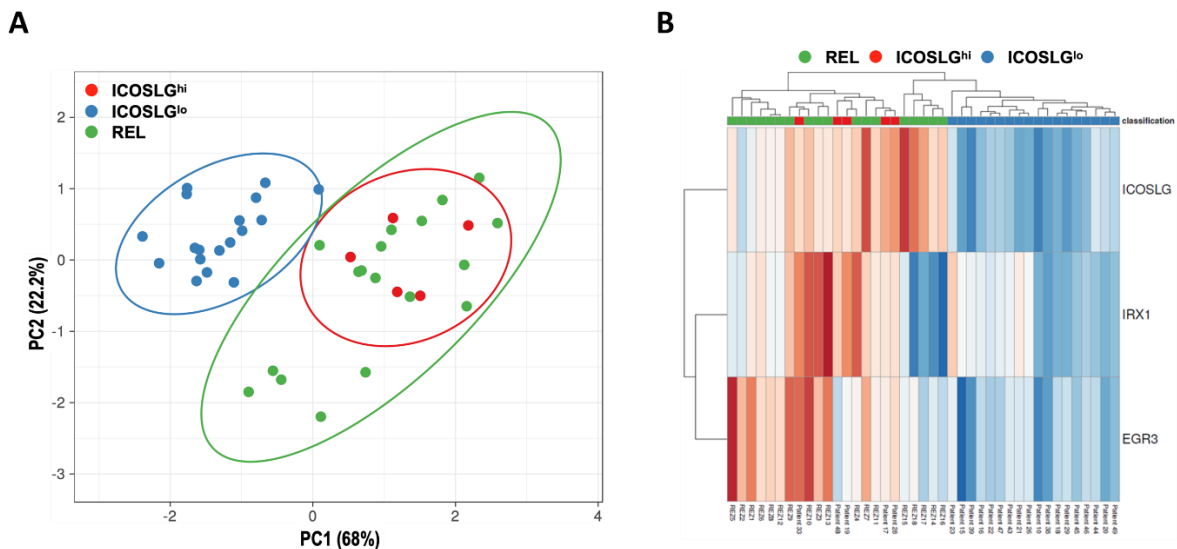


Figure 21. Principal component analysis (PCA) comparing the grade of similarity between “dx” *ICOSLG*^{hi}, “dx” *ICOSLG*^{lo}, and “rel”.

A Coordinate system along PC1 spanning 68% of total variance and PC2 spanning 22.2% of total variance. Patients assigned to “dx” *ICOSLG*^{hi} are labeled in red, those of “dx” *ICOSLG*^{lo} in blue, and “rel” patients in green. Prediction ellipses are such that the probability that a new patient from the same group will be covered by the ellipse is 95%. **B** PCA heatmap illustrating patient clustering in detail.

3.7 Primary T-cell co-culture study

The gene expression investigations of patients at diagnosis and at relapse revealed that elevated *EGR3* and *ICOSLG* expressions were relapse-associated, and high *ICOSLG* expression at diagnosis predictive for relapse. However, a causal relationship between *EGR3*/*ICOSLG* expression and relapse formation remained unclear.

ICOSLG expression was linked to the induction of regulatory T-cell (Treg) development in the healthy BM niche (Lee *et al.*, 2017), glioblastoma (Iwata *et al.*, 2019), melanoma (Martin-Orozco *et al.*, 2010), breast cancer (Faget *et al.*, 2012) and acute myeloid leukemia (AML) (Han *et al.*, 2018). Therefore, the hypothesis emerged that *ICOSLG* expression of t(4;11) ALL cells residing in the BM niche could promote adjacent Treg development thereby protecting ALL cells from immune attack which could enable relapse formation. Accordingly, the capability to induce Treg development by t(4;11) ALL cells expressing *ICOSLG* needed to be evaluated. For that purpose, co-culture of SEM::*EGR3* and SEM::mock cell culture

models with primary T-cells was performed. **Figure 22A** summarizes the applied workflow. Peripheral Blood (PB) of healthy adult donors was fractionated via gradient centrifugation and the layer of peripheral blood mononuclear cells (PBMC) was manually extracted. Subsequently, CD4⁺ and CD8⁺ T-cells were magnetically separated, and purity assessed using flow cytometry (**Figure 22B**). A minimum purity of 85% was tolerated and T-cells activated using α -CD2/-3/-28 coated beads for 16h to mimic T-cell receptor (TCR) stimulation thus enabling non-isogenic experiments without necessity of MHC-matching. This was followed by a 48h co-culture of 50% SEM::EGR3/SEM::mock with 25% CD4⁺ and 25% CD8⁺ T-cells. Afterwards, the fraction of Tregs was quantified using flow cytometry, and IL-2 and IL-10 cytokine levels of the co-culture supernatants measured by enzyme linked immunosorbent assays (ELISA).

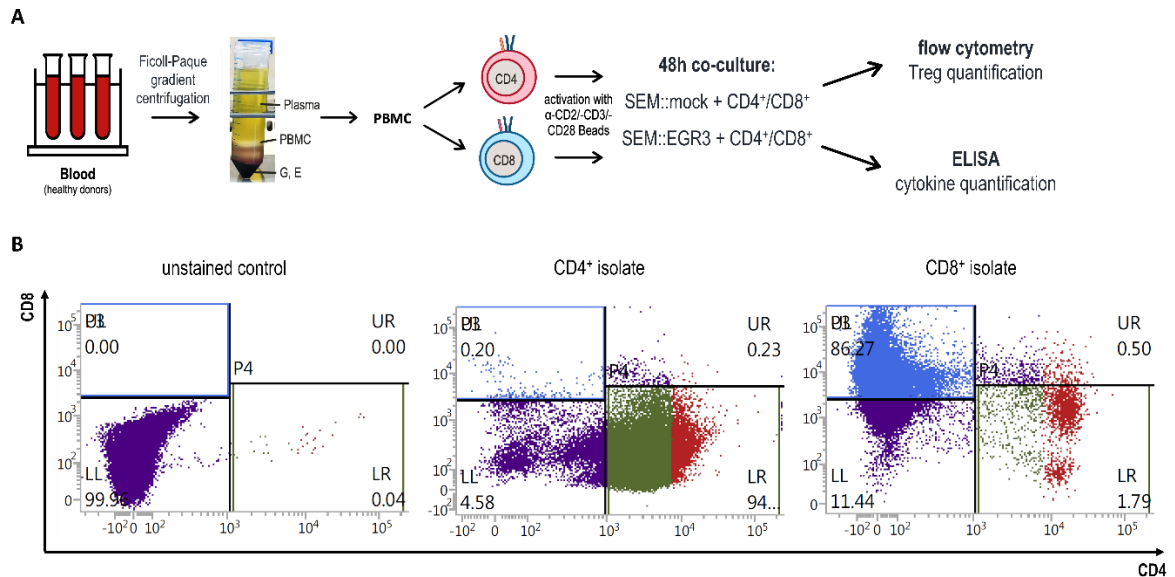


Figure 22. T-cell co-culture: experimental procedure.

A Operational workflow. PBMC = peripheral blood mononuclear cells. G = granulocytes. E = erythrocytes.

B Dot plots as an example for purity assessment after magnetic separation of CD4⁺ and CD8⁺ T-cells. Unstained control enabled gate setting.

The gating strategy for flow cytometric Treg quantification is explained in **Figure 23A**. Monitoring of T-cell viability after co-culture using Annexin V and 7-AAD staining yielded a viability above 70% of CD4⁺ and CD8⁺ T-cells in every experiment. Tregs were measured as the percentage of CD25⁺FOXP3⁺ cells among the fraction of CD3⁺CD4⁺ cells (**Figure 23A**). The experiment was performed with isolated T-cells of six independent healthy donors (HD1 – HD6) and resulted in an increase in the percentage of CD25⁺FOXP3⁺ Tregs in the SEM::EGR3 co-culture of 7.96% to 23.94% compared to SEM::mock co-culture. The geometric mean of SEM::EGR3 Treg percentage to SEM::mock Treg percentage was 1.14 ± 0.009991 ($p=0.0023$) (**Figure 23B**). This result indicated that the overexpression of EGR3 in t(4;11) ALL cells mediated the rapid expansion of Tregs upon co-culture with primary T-cells.

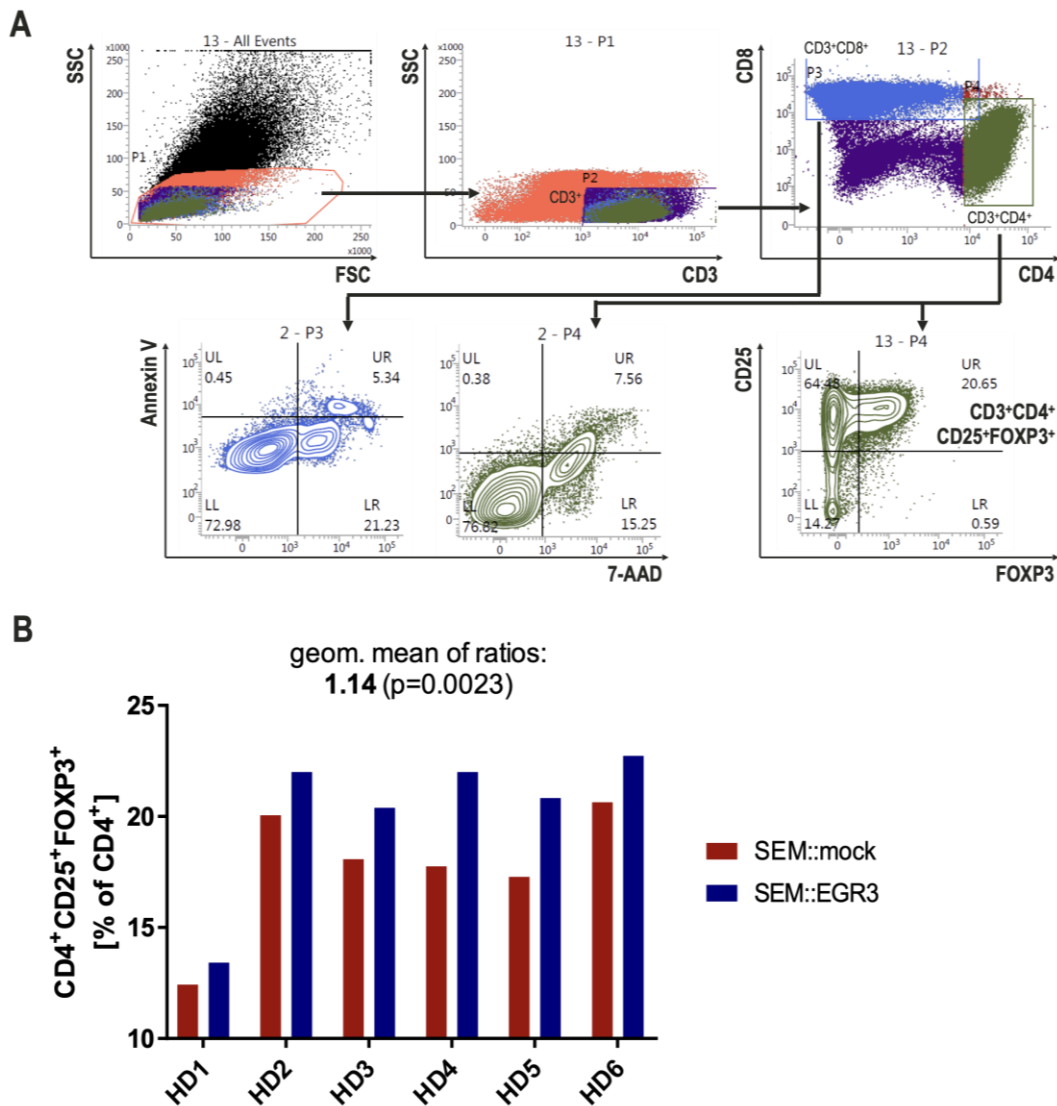


Figure 23. Results of co-culture experiments.

A Flow cytometry gating strategy. Cells with low granularity were gated out of all cells. Subsequently, CD3⁺ cells were selected in order to separate CD4⁺ and CD8⁺ cells. Viability after co-culture of these populations was assed using Annexin V and 7-AAD staining to ensure that the majority of T-cells was alive throughout co-culture. The percentage of CD25⁺FOXP3⁺ Tregs was quantified among the CD4⁺ population. **B** Percentages of CD25⁺FOXP3⁺ Tregs among CD4⁺ T-cells after co-culturing T-cells from six healthy donors (HD1 – HD6) with SEM::mock or SEM::EGR3 cell culture models. SEM::EGR3 co-culture lead to 7.96% to 23.94% more Tregs than SEM::mock co-culture (geometric mean: 1.14±0.009991, p=0.0023 in a two-tailed ratio paired t-test).

To inspect the initially explained hypothesis that EGR3-mediated upregulation of ICOSLG could lead to Treg development, the experiment was replicated with HD1 – HD3 under addition of a neutralizing α -ICOSLG monoclonal antibody (mAb) in comparison to a non-specific IgG1 isotype control. The EGR3-mediated Treg development became impaired through α -ICOSLG antibody but not IgG control treatment, strongly suggesting that ICOSLG was the mediator of EGR3-induced Treg expansion (**Figure 24A**). This result was corroborated through quantification of cytokine levels in the co-culture supernatants using ELISA. Administration of α -ICOSLG did not affect the IL-2 levels of co-culture supernatants (**Figure 24B**) but led to a significant decrease of the IL-10 level (**Figure 24C**). IL-10 is an immunosuppressive cytokine secreted by Tregs and serves as an indicator for Treg function (Maynard *et al.*, 2007). Thus, α -ICOSLG treatment was proven efficient in impairing Treg development phenotypically by flow cytometry and functionally by ELISA. Paradoxically, α -ICOSLG antibody treatment also led to an apparent

increase in the fraction of Tregs when administered to the media of SEM::mock co-culture which anyway did not affect the decreased IL-10 level through ICOSLG blockade.

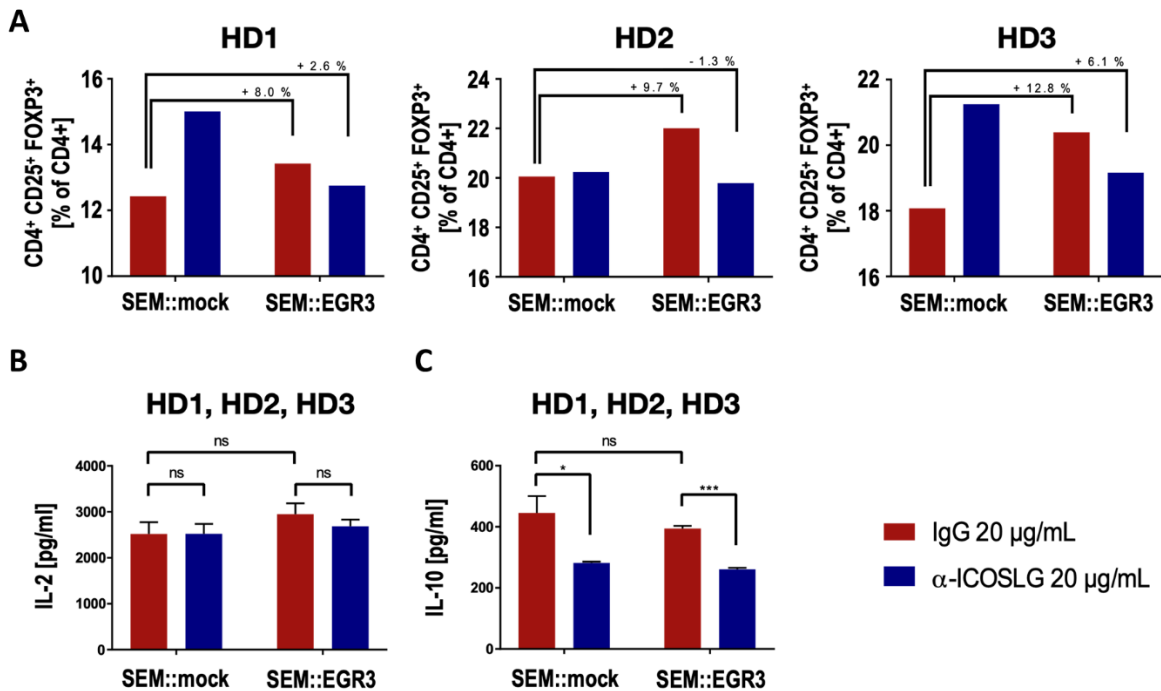


Figure 24. Consequences of ICOSLG blockade on Treg development.

A Percentages of CD25⁺FOXP3⁺ Tregs for co-culture of HD1 – HD3 under addition of 20 µg/mL IgG1 isotype control (red) or neutralizing monoclonal α-ICOSLG antibody (blue). **B** IL-2 and **C** IL-10 levels in co-culture supernatants. ICOSLG blockade strongly decreased IL-10 levels of SEM::mock ($p=0.0424$) and SEM::EGR3 ($p=0.0002$) co-cultures (multiple t-tests).

Finally, the question appeared why ICOSLG expressing ALL cells specifically expand Tregs and not other T-cell subsets. It has been reported that Tregs in the PB of healthy individuals possess a higher ICOS surface expression compared to non-regulatory T-cell subsets (Duhon *et al.*, 2012). To investigate if this could be the reason for the preferential Treg expansion, the ICOS surface expression of Tregs that developed during co-culture was quantified using flow cytometry. This uncovered that CD25⁺FOXP3⁺ cells displayed a higher ICOS surface expression than CD25⁺FOXP3⁻ and CD25⁻FOXP3⁻ cells within the CD4⁺ subset (**Figure 25**). Importantly, this was neither affected by the co-cultured cell model (SEM::mock vs SEM::EGR3) nor by different antibody treatments (IgG vs α-ICOSLG). Consequently, the higher ICOS surface expression of Tregs in comparison to other T-cell subsets was likely the explanation for the preferential expansion of Tregs through ICOSLG expression.

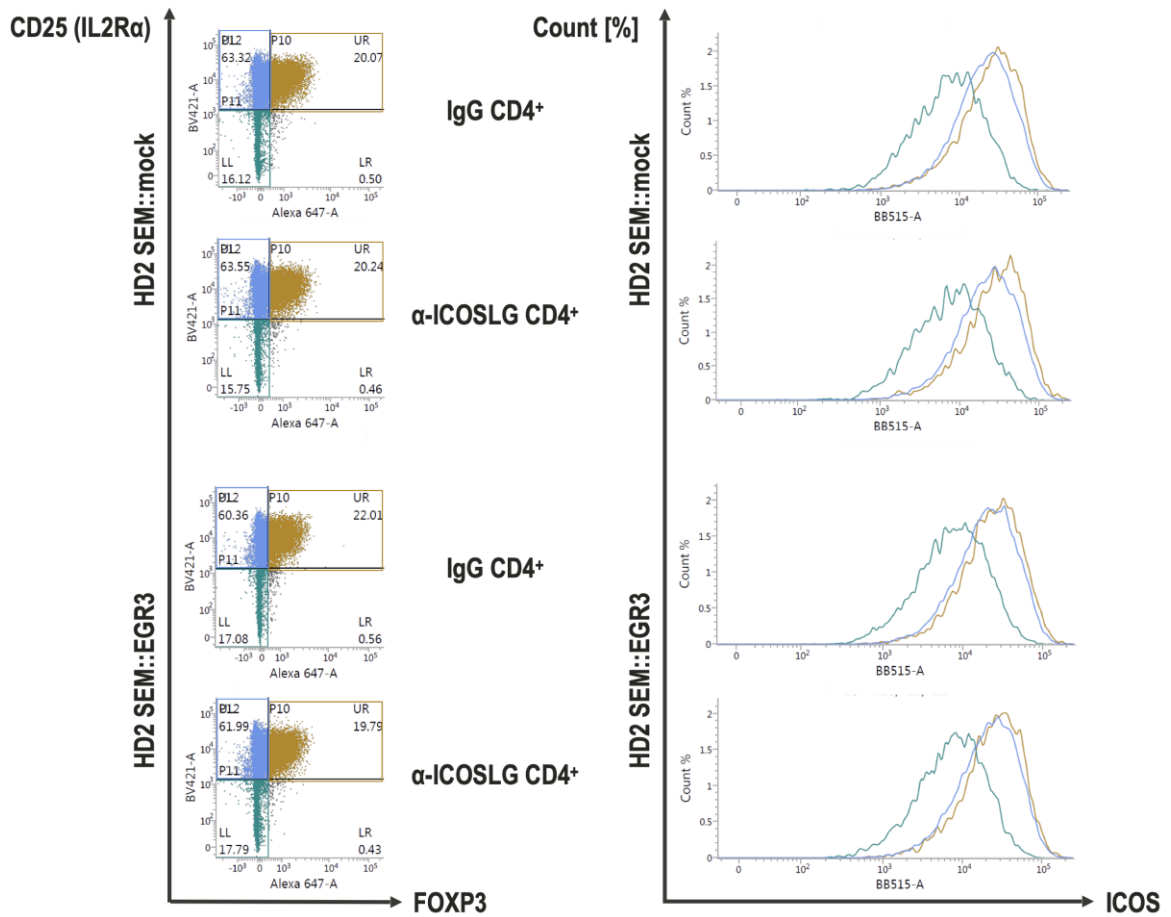


Figure 25. ICOS surface expression among different T-cell subsets. Representative dot plots of the CD3⁺CD4⁺ subset of HD2 are shown. CD25⁺FOXP3⁺ Tregs (yellow), CD25⁺FOXP3⁻ (blue) and CD25⁻FOXP3⁻ (turquoise) cells were gated (left) and their respective ICOS surface expression displayed in a comparative plot (right). CD25⁺FOXP3⁺ Tregs showed the highest ICOS expression, followed by CD25⁺FOXP3⁻ cells. CD25⁻FOXP3⁻ cells clearly displayed the lowest ICOS surface expression.

4 Discussion

Despite recent advancements in the therapy of pediatric leukemia through the application of kinase inhibitors, immunotherapy and improved HSCT, infant *KMT2A*-rearranged ALL is still characterized by a high relapse incidence accompanied by relapse-associated mortality being responsible for very poor patient outcome (Driessen *et al.*, 2016; Pieters *et al.*, 2019, 2007). The disappointing clinical situation that therapeutic innovations already successfully implemented in the therapy of pediatric leukemia did not result in clinical benefit when translated to infant patients led to the description of *KMT2A*-r infant leukemia as “a thorn in the side of a remarkable success story” (Rice and Roy, 2020).

This doctoral project aimed to better understand the molecular mechanisms leading to relapse in t(4;11) iALL and the distinct role of the immediate early genes *EGR1*, *EGR2* and *EGR3* in disease progression.

4.1 EGR3 as the main mediator of IRX1 signaling

The establishment of HEK293T cell culture models stably expressing *EGR1*, *EGR2* or *EGR3* enabled a comparison of the *EGR1-3* gene expression profiles with that one of *IRX1* which has been characterized by Kühn *et al.*, 2016. A principal component analysis (PCA) including 156 differentially expressed genes disclosed the *EGR3* profile as displaying the highest grade of similarity to the *IRX1* profile among the *EGR* cell culture models (**Figure 9**). This led to the conclusion that *EGR3* is the most important downstream mediator of *IRX1* among the investigated *EGR* genes which is in line with the observation that *IRX1* overexpression in HEK293T and SEM cells upregulated *EGR3* the most (Kühn *et al.*, 2016; Kühn, 2017).

A relative uncertainty in the HEK293T cell culture models was the difference in protein expression levels of the transgenes. The protein level of *EGR3* in the respective cell model detected by western blot was remarkably higher compared to *EGR1* and *EGR2* (**Figure 8D**). This indicated a stronger protein expression of *EGR3* although the *EGR1-3* transcript levels detected by qRT-PCR were comparable suggesting differences either in extent of translation or protein stability (**Figure 8C**). The protein expression level discrepancy cannot be explained by different antibody affinities as all three proteins were FLAG-tagged and detected with the same α -FLAG antibody. Theoretically, a higher amount of protein could lead to low affinity binding towards sequences not fully recapitulating the consensus binding sequence of the transcription factor. Thus, it is not clear whether the differences in protein expression levels affected the gene expression profile comparison and whether the protein expression difference represents the real leukemic situation or is a weakness of the experimental set-up.

EGR1 was detected as two bands approximately at 58 kDa and 85 kDa which is concordant with reports of these two *EGR1* species in PC12 cells (Day *et al.*, 1990). The study reported that a 54 kDa isoform is solely cytoplasmic and derived from the exclusively nuclear found 85 kDa isoform through truncation of the C-terminal portion. In the HEK293T cell model, the FLAG-tag was located at the C-terminus, thus a C-terminal truncated isoform would not be detected, even not if both isoforms would dimerize as the SDS-PAGE was performed under reducing and denaturing conditions. Posttranslational modifications have been reported to affect *EGR1* activity: SUMOylation and ubiquitination of *EGR1* led to proteasomal degradation, but went along with a protein size shift from approximately 80 kDa to 90 kDa, not explaining the 58 kDa band (Manente *et al.*, 2011). In 2019, a novel *EGR1* splicing isoform has been identified and characterized (Aliperti *et al.*, 2019). The isoform *EGR1* Δ 141–278 lacked 414 base pairs in exon 2 belonging to the first N-terminal activation domain and transfection of HEK293T cells with the canonical *EGR1* or *EGR1* Δ 141–278 resulted in a double band at ~55 kDa and ~85 kDa in case of the canonical *EGR1*, and a single band at ~55 kDa for *EGR1* Δ 141–278 (Aliperti *et al.*, 2019). The study

reported that both isoforms were able to enter the nucleus but EGR1 Δ 141–278 was shown to transactivate the target genes *ARC* and *SIK1* to a significantly lower extent than canonical EGR1. In conclusion, it is very likely that the EGR1 double band of **Figure 8D** is due to protein expression of the canonical EGR1 (85 kDa) and the alternative splicing isoform EGR1 Δ 141–278 (58 kDa). The transcript level assessed in **Figure 8C** was measured using qRT-PCR with oligonucleotide primers spanning the only exon junction of the transcript, while the truncated area Δ 141–278 is downstream of the reverse primer and thus qRT-PCR did not distinguish between the alternatively spliced and canonical transcripts. Accordingly, the transcript levels displayed in **Figure 8C** refer to both protein isoforms with the 58 kDa isoform having a weaker transactivation activity according to Aliperti *et al.*, 2019. This could also explain the transcriptional differences of EGR1 and EGR3 suggested by the PCA (**Figure 9**).

Apart from the difference in protein expression levels, an important weakness of the HEK293T cell culture model was the cell type. HEK293T cells are in general easy to transfect and cultivate but do not represent the pheno- or genotype of t(4;11) ALL. Therefore, the SEM cell culture models were established to compare the gene and protein expression of the immune-related genes identified using the HEK293T model (**Table 17**). This disclosed that only *ICOSLG* and *IL6R* but not *LGALS1* and *TGFB1* transcript levels were upregulated through EGR3 or IRX1 overexpression in the t(4;11) cellular context. Since *ICOSLG* was approximately three times stronger upregulated by EGR3 compared to IRX1, whereas the situation for *IL6R* was the opposite, *ICOSLG* was subsequently in focus of the project (**Figure 12A**).

Of note, overexpression of a transgene, in contrast to a knock-in, usually leads to non-physiologically high amounts of transcript and protein probably affecting the respective cell. Nevertheless, if interpreted appropriately, gene overexpression models are valuable tools to identify downstream signaling effectors although validation through analysis of primary patient samples is recommended (Prelich, 2012). In addition, the sleeping beauty transposon system possesses the advantage of a close-to-random integration profile (Kebriaei *et al.*, 2017) in contrast to viral transduction systems that have been reported to integrate into promoters of oncogenes resulting in malignancy (Hacein-Bey-Abina *et al.*, 2008, 2003; Howe *et al.*, 2008).

4.2 Characterization of *ICOSLG* upregulation through EGR3 overexpression

The direct binding of EGR3 to the *ICOSLG* promoter has been disclosed initially by ChIP-qRT-PCR and was later corroborated by ChIP-Seq. These experiments were performed using the SEM::EGR3 cell culture model because the t(4;11) cellular context determines chromatin accessibility through characteristic epigenetic marks including trimethylation of histone 3 at lysine-4 (H3K4me3) among others (Chang *et al.*, 2010; Prange *et al.*, 2017). Chromatin accessibility is a prerequisite for transcription factor binding and thus, the t(4;11) epigenetic background of the SEM cell line was necessary to identify binding sites of EGR3 in the *ICOSLG* promoter area.

A general disadvantage of ChIP-qRT-PCR is that the result highly depends on appropriate primer annealing to intronic sequences that are frequently characterized by regions with a high GC content. These GC-rich sections frequently fold into complex secondary structures and respective primers are prone to dimerization (Green and Sambrook, 2019). Data analyses with the integrative genomics viewer (IGV) in hg38 showed a GC-content of 65% for PP4 target sequence compared to 81% for PP1 and PP2 target sequences (**Figure 13A**). This difference in GC-content could affect primer annealing and thus explain why using ChIP-qRT-PCR only PP4 indicated EGR3 binding, whereas ChIP-Seq disclosed a distribution of aligned reads to the *ICOSLG* promoter area correlating with the that one of the *in silico* predicted theoretical binding sites (**Figure 13A** and **Figure 14**).

4.3 Gene expression analysis using cell culture models and patient samples

Pearson correlation testing using the gene expression data derived from the cohort of 50 patients at diagnosis confirmed the correlations of the IRX1-EGR3-ICOSLG axis which were initially suggested by HEK293T and SEM cell culture models. In contrast, other suggested correlations were not confirmed by the patient gene expression study. *LGALS1* was indicated to be upregulated through IRX1 and EGR3 overexpression in HEK293T cell culture models (**Table 17**) which was corroborated by SEM::EGR3 but not SEM::IRX1 (**Figure 12A**). However, the patient study indicated a negative correlation between *LGALS1* and *EGR3* or *IRX1* (**Figure 16**). Furthermore, HEK::IRX1 and HEK::EGR3 suggested an upregulation of *TGFB1* (**Table 17**) which was not confirmed by the SEM cell models (**Figure 12A**). Nevertheless, the patient study revealed a positive correlation between *EGR3* and *TGFB1* (**Figure 16**). In case of *IL6R*, the HEK293T cell models suggested an upregulation through IRX1 or EGR3 overexpression (**Table 17**) which was confirmed by the SEM cell models that indicated an approximately three times stronger upregulation by SEM::IRX1 compared to SEM::EGR3 (**Figure 12A**). The patient data in turn demonstrated only a weak correlation between *IL6R* and *IRX1* or *EGR3* (**Figure 16**).

These disparities between the three gene expression analyses indicate that the expression of a gene highly depends on the cellular context. HEK293T cell models are convenient in terms of establishment and cultivation but do neither possess a leukemic phenotype nor the translocation t(4;11). The SEM cell culture models mimic the cell identity of infant t(4;11) ALL very well considering the proB phenotype and the t(4;11) rearrangement although the SEM cell line was established from PB of a 5-year old ALL patient and not an infant patient (Greil *et al.*, 1994). The HEK293T and SEM cell culture models have in common that the genes of interest were massively overexpressed exceeding natural expression levels even in leukemic cells. This overexpression provoked changes in the cellular signaling network which could be analyzed by various means in order to deduct to signaling pathways and interactors (Prelich, 2012). The patient samples enabled a direct examination of the cell culture model derived data for identification of correlations that also apply in the clinic. Anyhow, due to the general heterogeneity of patient derived data, the inclusion of 50 patients into the diagnosis cohort was necessary although the diagnosis cohort was solely composed of t(4;11) infant ALL patients with a proB phenotype. However, also the patient study possessed some weaknesses including the lack of cellular samples to measure protein (surface) expression, the lack of matched samples from BM and PB to investigate potential differences in the expression depending on the leukemic compartment and the lack of matched RNA samples from the same patient at different time points to enable a longitudinal expression study. These issues were due to the dearth of patient samples resulting from the low incidence of the disease also explaining that the inclusion of only 50 RNA patient samples required the involvement of three different study centers.

In summary, gene expression data derived from cell culture models overexpressing IRX1 or EGR3 identified a set of immune-related genes of which *ICOSLG* was verified as a downstream mediator of EGR3 among a cohort of 50 patients. The comparison of cell culture model derived data with primary patient data enabled the identification and verification of *ICOSLG* as a prognostic biomarker and therapeutic target. Disparities between the cell culture models and patient data underlined the importance of a verification of model data using primary data.

4.4 Event-free survival depending on *HOXA9* gene expression

The EFS analysis of patients assigned to the *HOXA9*^{hi} or *HOXA9*^{lo} group revealed only a slight EFS disadvantage of *HOXA9*^{lo} patients which did not reach statistical significance (**Figure 18B**). This result contradicts the study of Stam *et al.* demonstrating that *HOXA*^{lo} patients displayed a higher relapse

incidence than $HOXA^{hi}$ patients (Stam *et al.*, 2010). However, Stam *et al.* considered the expression of $HOXA9$, $HOXA7$, $HOXA10$, $HOXA5$ and $HOXA3$, whereas the present study solely considered $HOXA9$ expression to discriminate patients. Nevertheless, for 28 of 29 patients in the study of Stam *et al.*, the expression of $HOXA9$ was representative for all $HOXA$ genes indicating that both studies are indeed comparable.

Another major difference is that the present study compared event-free survival (EFS) whereas Stam *et al.* assessed relapse-free survival (RFS) to compare the outcome of $HOXA^{lo}$ versus $HOXA^{hi}$ patients. In the present study, events were defined according to Interfant-99 and -06 as early death during induction, resistance to induction, relapse, death in continuous complete remission and second malignancy. In contrast, RFS considers solely relapse or death. 41 of 43 patients of the present study were included in Interfant-06 and thus, the cohort was representative for the events of the Interfant-06 high risk group. In this group, 88% of events were relapses, 7.5% were deaths in CR and 4.5% were deaths in continuous complete remission. No resistance to induction or second malignancy was reported (Pieters *et al.*, 2019). Accordingly, EFS assessed in the present study and RFS reported by Stam *et al.* covered both only relapse and death as events. Therefore, the outcome data of both studies are comparable.

In addition, treatment differences could explain the outcome disparities between the present study and that one of Stam *et al.* In the present study, 41 patients were included in Interfant-06 and 2 patients included in AIEOP-BFM ALL 2017 (Table 19). The cohort from Stam and colleagues was included in Interfant-99. Importantly, Interfant-99 and Interfant-06 demonstrated similar outcomes for $t(4;11)^+$ patients with Interfant-99 reporting a 4y-EFS of $35.8 \pm 4.5\%$ and Interfant-06 reporting a 4y-EFS of $34.3 \pm 3.4\%$ (Pieters *et al.*, 2019, 2007). The AIEOP-BFM ALL 2017 trial will be completed in 2028 and did not publish intermediate results yet (NCT03643276 at clinicaltrials.gov, 13.05.2022). As a result, the different treatment protocols applied to patients are unlikely to explain the discrepancy between both studies.

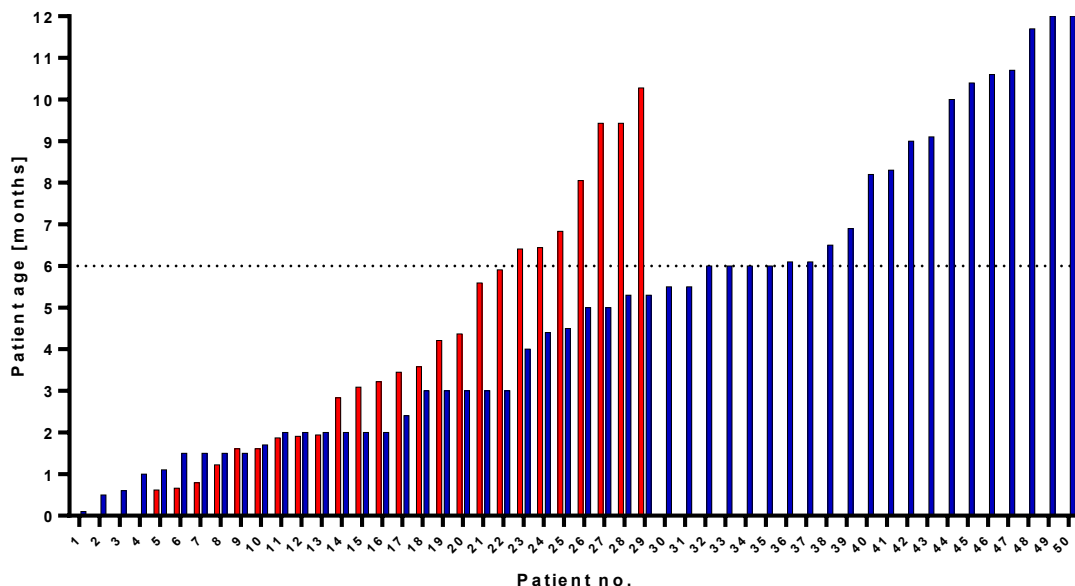


Figure 26. Patient age distribution of Stam *et al.*, 2010 (red, n=29 patients) compared to own data (blue, n=50 patients).

Finally, another important difference between both studies is the number of investigated patients. Stam *et al.* included 23 patients in the RFS analysis, n=12 $HOXA^{lo}$ and n=11 $HOXA^{hi}$, whereas the present EFS study involved 43 patients, n=16 $HOXA9^{lo}$ and n=27 $HOXA9^{hi}$. The lower number of included

patients in the Stam *et al.* study, especially in case of the $HOXA^{hi}$ patients, could have led to a biased estimation of RFS. Furthermore, the present study displayed a $HOXA^{lo}$ percentage of 37.2% which is close to the $HOXA^{lo}$ fraction of all patients including those without available outcome data (n=50) being 38% (19 of 50 patients). This is another contrast to the Stam *et al.* study, which displayed a $HOXA^{lo}$ fraction of 52.2%. In line with this discrepancy, both studies differed in their patient age distributions (**Figure 26**). In the study of Stam *et al.* 75.9% of patients were below 6 months of age at diagnosis, whereas the present study involved 62% of patients below 6 months of age. If the $HOXA^{lo}$ expression pattern were the result of an earlier cell of origin as assumed by Symeonidou and Ottersbach (2021), this could explain that a cohort with a higher fraction of patients below 6 months of age showed a larger $HOXA^{lo}$ percentage.

In summary, the study of Stam *et al.* and the present study differ most notably in the number of included patients, the ratio of $HOXA^{lo}$ to $HOXA^{hi}$ group size, and the patient age distribution. These fundamental differences could have led to the described discrepancy in outcome between both studies, although this can only be assumed.

4.5 *IRX1* and *EGR3* expression depending on *HOXA9* gene expression

The gene expression analysis of patients assigned to the $HOXA^{hi}$ or $HOXA^{lo}$ group disclosed a significantly elevated *IRX1* gene expression of the $HOXA^{lo}$ group (**Figure 18C**). This inverse correlation of *HOXA9* and *IRX1* gene expression in infant t(4;11) ALL is in concordance with four previous studies examining between 20 and 47 patients (Kang *et al.*, 2012; Stam *et al.*, 2010; Symeonidou and Ottersbach, 2021; Trentin *et al.*, 2009). Although *IRX1* and *EGR3* expression were shown to strongly correlate among the 50 patients (**Figure 16**), the median *EGR3* expression was not significantly different when comparing the $HOXA^{hi}$ and $HOXA^{lo}$ group (**Figure 18D**).

Based on the study of Kühn *et al.* (2016) showing that *IRX1* overexpression led to the upregulation of *EGR1*, *EGR2* and *EGR3* *in vitro*, this doctoral project aimed to clarify whether the expression of the *EGR* genes could be responsible for the supposed higher relapse rate of $HOXA^{lo}$ patients. The lack of association between low *HOXA9* gene expression and elevated *EGR3* expression in the investigated patient cohort strongly suggests that *EGR3* is not implicated in the apparent EFS disadvantage of $HOXA^{lo}$ patients.

4.6 *ICOSLG* gene expression and relapse development

In contrast to *HOXA9* expression, patient discrimination depending on the *ICOSLG* expression level uncovered significant EFS differences. All $ICOSLG^{hi}$ patients failed within 17 months from diagnosis, whereas the $ICOSLG^{lo}$ patients achieved a remarkable 4y-EFS of $49 \pm 8.8\%$ (**Figure 19B**). This EFS difference was not affected by patient age (**Figure 19C**), but the very small size of the $ICOSLG^{hi}$ group (n=7) could have led to a biased result. Nevertheless, in line with Pearson correlation testing (**Figure 16**), *IRX1* and *EGR3* expression levels were significantly elevated in $ICOSLG^{hi}$ patients thereby pointing to an involvement of the *IRX1*-*EGR3*-*ICOSLG* axis in relapse development (**Figure 19D,E**). This became corroborated through comparison of the *HOXA9*, *IRX1*, *EGR3* and *ICOSLG* gene expressions between the cohort of patients at diagnosis (dx, n=23) and the cohort of patients at relapse (rel, n=18) demonstrating that high *EGR3* and *ICOSLG* expressions were relapse-associated (**Figure 20A-C**). Importantly, the diagnosis cohort was solely composed of t(4;11) iALL patients, whereas due to a dearth of samples only 14 of 18 patients (78%) of the relapse cohort were t(4;11) cases. The cohort additionally consisted of three t(11;19) (17%) cases and one t(9;11) (6%) case. Nevertheless, the t(11;19) and t(9;11) patients met all other patient characteristics and did obviously not stand out regarding the gene expression

profile illustrated by the heatmap, suggesting that a comparison of both cohorts was appropriate (**Figure 20A**).

Contrarily to *EGR3* and *ICOSLG*, the median *IRX1* and *HOXA9* expression levels were not significantly different when comparing the patients at relapse and those at diagnosis (**Figure 20D,E**). However, as *IRX1* expression was elevated in the *ICOSLG*^{hi} group of the cohort at diagnosis, the transcription factor should still be considered being implicated in relapse formation, even not in a direct association but through upregulation of *EGR3* that in turn transactivates *ICOSLG*. This became underpinned by the PCA with patients assigned either to the relapse cohort or to the *ICOSLG*^{hi} or *ICOSLG*^{lo} group of the diagnosis cohort, showing that the separation of patients depending on their *ICOSLG* expression level at diagnosis led to coherent clustering of the *ICOSLG*^{hi} group with the relapse cohort (**Figure 21A**). Through this, the *ICOSLG* expression level at diagnosis was identified as an adverse prognostic biomarker predictive for relapse formation.

A molecular explanation for the link between *EGR3/ICOSLG* expression and relapse formation emerged with the identification that *EGR3*-mediated *ICOSLG* upregulation led to relative outgrowth of regulatory T-cells (Tregs) upon co-culture of SEM::*EGR3* with primary activated CD4⁺ and CD8⁺ T-cells (**Figure 23** and **Figure 24**). To appropriately evaluate this, the role of *ICOSLG* in T-cell-mediated immunity needs to be discussed.

4.7 The role of *ICOSLG* in T-cell-mediated immunity

The *Inducible T-cell costimulator ligand* (*ICOSLG*) is a member of the B7 family of immune receptors and shares partial sequence identity with CD80 and CD86 (Coyle and Gutierrez-Ramos, 2001). Besides *ICOSLG*, CD80 and CD86, the *Programmed cell death ligands 1* and *2* (PD-L1, PD-L2) also belong to the B7 family (Greaves and Gribben, 2013). *ICOSLG* is a costimulatory immune receptor expressed by antigen presenting cells (APC) including B-cells and binds the *Inducible T-cell costimulator* (*ICOS*) (Coyle and Gutierrez-Ramos, 2001; Yoshinaga *et al.*, 1999). *ICOS* belongs to the CD28 superfamily of immune receptors and is expressed at marginal levels on resting memory T-cells but binding to *ICOSLG* results in rapid upregulation of *ICOS* expression (Hutloff *et al.*, 1999; Khayyamian *et al.*, 2002). Besides, *ICOS* expression defines a highly suppressive IL-10 producing Treg subset (Ito *et al.*, 2008). In addition, *ICOSLG* has recently been described to bind Osteopontin by a different domain than that binding *ICOS* (Raineri *et al.*, 2020). In the hematopoietic system, *ICOSLG* displays the highest expression on proB-cells which is also the phenotype of infant t(4;11) ALL cells (**Figure 27**).

Costimulatory and coinhibitory immune receptor interactions are important secondary signals balancing the activation of T-cells besides the T-cell receptor (TCR) / major histocompatibility complex (MHC) interaction thereby finetuning immune activation. In this context, *ICOSLG* expression on BM-resident mesenchymal stem cells (MSC) has been shown to induce the development of Tregs (Lee *et al.*, 2017). Lee *et al.* demonstrated that MSC upregulated *ICOSLG* and subsequently induced Treg development through *ICOSLG/ICOS* binding under inflammatory conditions mimicked through IL1 β , TNF- α or lipopolysaccharide (LPS) treatment.

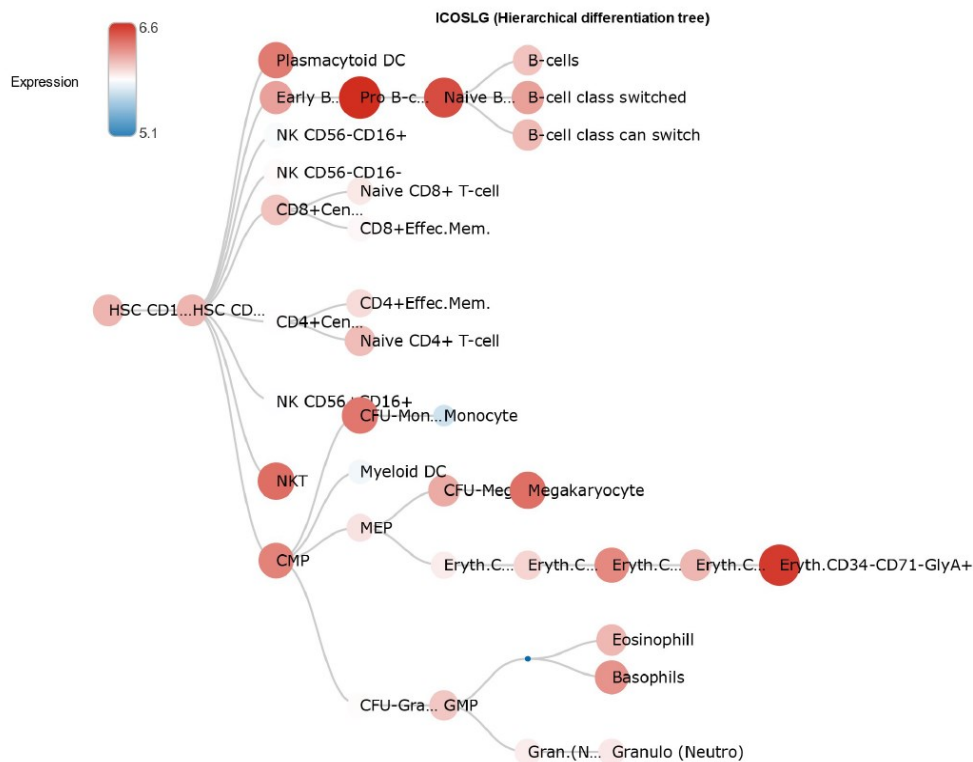


Figure 27. ICOSLG expression in cells of the hematopoietic system. Taken from bloodspot.eu (Bagger *et al.*, 2016).

Moreover, Lee *et al.* identified that the ICOSLG/ICOS interaction activated the PI3K/Akt signaling pathway in CD4⁺ T-cells to mediate their differentiation into regulatory subsets producing IL-10 (Lee *et al.*, 2017). This observation is in concordance with studies showing that in Tregs ICOSLG/ICOS binding caused sustained PI3K/Akt activation which mediated suppressive activity and survival of Tregs (Fos *et al.*, 2008; Li and Xiong, 2020). The *phosphatidylinositol 3 kinase* (PI3K) is composed of a regulatory subunit (p85 α , p55 α , p50 α , p85 β or p55 γ) and a catalytic subunit (p110 α , p110 β or p110 δ) (Okkenhaug and Vanhaesebroeck, 2003). It has been demonstrated that ICOSLG binding leads to homodimerization of ICOS resulting in its phosphorylation at the YMFM motif which binds the PI3K regulatory subunit p85 α or p50 α thereby recruiting the catalytic subunit (p110) which catalyzes the phosphorylation of *phosphatidylinositol bisphosphate* (PIP2) to *phosphatidylinositol trisphosphate* (PIP3) that in turn phosphorylates and activates Akt (**Figure 28**) (Li and Xiong, 2020; Okkenhaug and Vanhaesebroeck, 2003). Comparisons between naïve T-cells and Tregs uncovered that in Tregs mTORC1 mediates phosphorylation of its substrates S6 and 4E-BP1 which has been suggested to be required for homeostasis and suppressive capability of Tregs through regulation of lipid metabolism (**Figure 28**) (Zeng *et al.*, 2013). Furthermore, Akt activation fosters Treg survival through two distinct mechanisms. First, Akt inhibits GSK3 β resulting in prevention of degradation of the anti-apoptotic protein Mcl-1 (Ahmad *et al.*, 2017; Pierson *et al.*, 2013). Second, ICOS⁺ Tregs displayed elevated levels of the anti-apoptotic protein Bcl-2 upon Akt activation (**Figure 28**) (Kornete *et al.*, 2012; Li and Xiong, 2020; Smigiel *et al.*, 2014). Besides anti-apoptotic and metabolic consequences, ICOS-PI3K signaling mediates complex formation of the transcription factors FOXP3 and *Nuclear factor of activated T-cells* (NFAT), thereby outcompeting binding of AP-1 to NFAT (Chen *et al.*, 2018; Zheng *et al.*, 2013). AP-1 and FOXP3 are competitors of NFAT binding being necessary to operate transcriptional activation (Rudensky *et al.*, 2006; Wu *et al.*, 2006). Murine studies have shown that ICOS activation on Tregs led to upregulation of the highly suppressive FOXP3::NFAT target genes *IL-10*, *IL-4* and *TGFB1* and downregulation of the AP-1::NFAT target genes

IL-2 and *IL-6* (**Figure 28**) (Chen *et al.*, 2018). Through this switch, ICOS fosters the transformation of naïve T-cells to Tregs. Finally, ICOS expression has been identified as a driver of CXCR3 expression which is a known receptor for chemoattraction and migration towards inflammatory tissues (**Figure 28**) (Kornete *et al.*, 2015).

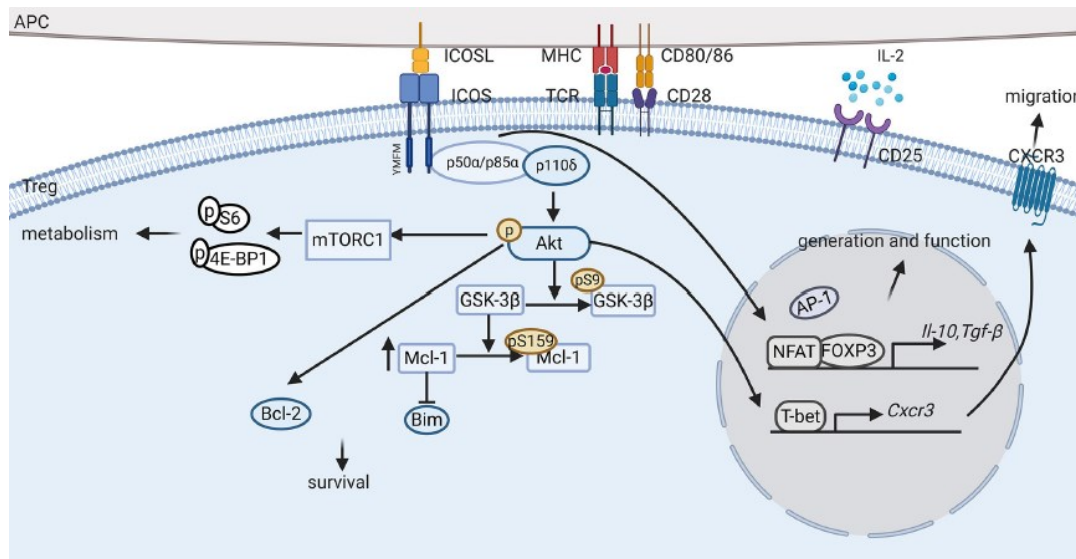


Figure 28. Signaling pathways activated in Tregs upon ICOSL/ICOS binding. Taken from Li and Xiong, 2020.

Following the discussion of ICOS expression, it is important to mention that ICOSL has been identified as being expressed on different kinds of tumors leading to expansion of Tregs in the tumor microenvironment. Initially, this has been described for gastric cancer (Chen *et al.*, 2003) and stage IV metastatic melanoma cells (Martin-Orozco *et al.*, 2010). Of note, both studies proved IL-10 production leading to immune suppression of tumor infiltrating lymphocytes (TIL) as a hallmark of ICOSL-mediated Treg expansion. Comparable with the observation that ICOSL expression on healthy BM-resident MSC resulted in Treg induction (Lee *et al.*, 2017), ICOSL was also found to be expressed on stem-like glioblastoma (GBM) cells promoting Treg expansion (Iwata *et al.*, 2019). This study revealed that Tregs were IL-10 producing, pro-tumorigenic and negatively correlated to OS in a cohort of 71 GBM patients. Interestingly, another study demonstrated that ICOSL expression could promote immune escape of tumor cells even if not the tumor itself expressed ICOSL. Faget *et al.* found that ICOSL expressing plasmacytoid dendritic cells (pDC) co-localized with breast cancer cells and promoted ICOS⁺ Treg accumulation through ICOS/ICOSL binding (Faget *et al.*, 2012). This “bystander effect” was shown to foster immune escape through IL-10 production and among 120 breast cancer patients the presence of ICOS⁺ Tregs was linked to inferior EFS and OS. These results underlined the importance of the tumor microenvironment for immune evasion and patient outcome in solid cancers. However, ICOSL-mediated Treg expansion has also been characterized to take place in the microenvironment of hematologic malignancy. Han *et al.* demonstrated the expression of ICOSL on AML cells which mediated Treg expansion in the BM microenvironment (Han *et al.*, 2018). Furthermore, the study corroborated previous investigations suggesting that AML patients displayed a higher fraction of BM-residing Tregs (Shenghui *et al.*, 2011). Furthermore, Han *et al.* verified that the ICOSL expression level of BM-located AML cells, as well as the frequencies of ICOS⁺ Tregs, were all associated with inferior disease-free survival (DFS). In addition, the study reported that IL-10 secretion of ICOS⁺ Tregs led to proliferation of AML cell lines *in vitro*.

In summary, the expression of ICOSLG on tumor cells or their “bystanders” led to Treg induction and expansion upon ICOS binding in different solid and liquid cancers. In all discussed studies, this interaction resulted in local immune evasion accompanied by markedly poorer patient outcome.

4.8 ICOSLG-mediated Treg expansion as a relapse mechanism in infant t(4;11) ALL

The co-culture experiments of EGR3-overexpressing SEM cells with elevated ICOSLG expression revealed that the previously described mechanism of ICOSLG-mediated Treg induction also applies to infant t(4;11) ALL.

Importantly, co-culture experiments were performed with primary T-cells activated with α -CD2/3/28 coated beads to enable MHC-unmatched experiments. This implied that almost all T-cells subsequently interacting with leukemia cells became activated which is very unlikely to occur in reality. In addition, CD28-based T-cell activation goes along with ICOS upregulation which could have led to an overestimation of ICOSLG responsiveness in the co-culture experiments (Greenwald *et al.*, 2005). Nevertheless, CD4⁺ and CD8⁺ T-cells are known to enter the BM from vasculature and to become primed through BM-resident DC which has been shown to result in T-cell activation and primary immune responses (Feuerer *et al.*, 2003, 2001). Thus, bead-based T-cell activation in the co-culture experiments probably mimicked DC-based T-cell activation in the BM and therefore, the measured effects appear authentic. Another weakness of the co-culture study is that due to the lack of an available cell sorter, T-cells were magnetically enriched instead of sorted, resulting in impurities of up to 15% (**Figure 22B**). As the microscopic observation after enrichment did not reveal a significant co-isolation of differently shaped cells, it is very likely that co-isolated cells were CD4 and/or CD8 negative T-cells. Due to massive proliferation of responsive T-cells during bead activation, non-responsive CD4⁻CD8⁻ T-cells were probably overgrown. However, these assumptions were not verified experimentally.

Moreover, a relative difference between Treg development of SEM::mock treated with α -ICOSLG antibody in case of HD1 and HD3 but not HD2 co-culture was observed (**Figure 24A**). This could be due to differences in T-cell activation (variations of the bead to cell ratio), T-cell isolation (purity of isolated T-cells) or the general condition of T-cells (naïve vs. exhausted). Furthermore, the experiment depended on the viability and ICOSLG expression of SEM cells. Additionally, off-target effects of excess antibody potentially could have led to apparent Treg development.

Surprisingly, also co-culture with SEM::mock cells resulted in expansion of Tregs despite a lack of EGR3-overexpression (**Figure 23**). This could be explained by the basal expression of ICOSLG on SEM cells as suggested by the map of ICOSLG expression among the hematopoietic system (**Figure 27**) and as verified by western blot of the SEM::mock cell culture model (**Figure 12B**). Importantly, elevated ICOSLG expression was always accompanied by increased Treg development. Furthermore, the ICOSLG expression level of SEM::EGR3 defined the threshold for assignment of patients to the ICOSLG^{hi} group in the patient gene expression study, indicating that the *in vitro* co-culture experiments represented the minimal Treg expansion assumed to occur in reality.

Moreover, the co-culture study disclosed the highest ICOS surface expression of FOXP3⁺CD25⁺ Tregs compared to FOXP3⁻CD25⁺ and FOXP3⁻CD25⁻ T-cells. This reflects the results of previous investigations (Duhon *et al.*, 2012). In mice, high ICOS surface expression among Tregs has been shown to determine stronger suppressive and proliferative capabilities and prolonged survival which has been corroborated in human studies (Chen *et al.*, 2012; Vocanson *et al.*, 2010).

Anyhow, the co-culture study did not investigate whether the relative outgrowth of Tregs was due to excessive proliferation of already existing Tregs or due to conversion of naïve T-cells to regulatory ones. Lee *et al.* described Treg expansion in the BM because of ICOSLG expression on adjacent MSC (Lee *et al.*, 2017). In this study, the authors stated that Tregs probably differentiated from naïve T-cells instead

of proliferating from existing Tregs. They came to this conclusion since repetition of their co-culture experiments with doubled amounts of T-cells that subsequently underwent co-culture did not result in increased Treg percentages after co-culture. In addition, they performed co-cultures with and without prior depletion of CD25⁺ T-cells and did not measure differences in the amount of Tregs after co-culture. Although such experiments were not performed within this doctoral project, due to the similarity of the experimental setup to the study of Lee *et al.*, it is likely that the described Treg expansion after co-culture with SEM cells was due to a differentiation process of naïve T-cells. Differentiation of naïve T-cells to Tregs upon ICOS/ICOSLG binding is known to be mediated by PI3K/Akt signaling as described above.

In conclusion, the co-culture experiments strongly suggest causality between the disclosed elevated *ICOSLG* expression level at diagnosis in some patients and their inferior EFS. Thus, *ICOSLG*-mediated Treg expansion has been identified as a contributor to relapse in infant t(4;11) ALL rendering the *ICOSLG* expression level at diagnosis a valuable prognostic marker. In addition, the immune checkpoint *ICOSLG* has been characterized as a therapeutic antibody target whose blocking impaired Treg development and thus treatment with α -*ICOSLG* antibodies holds promise to prevent relapse in the clinic.

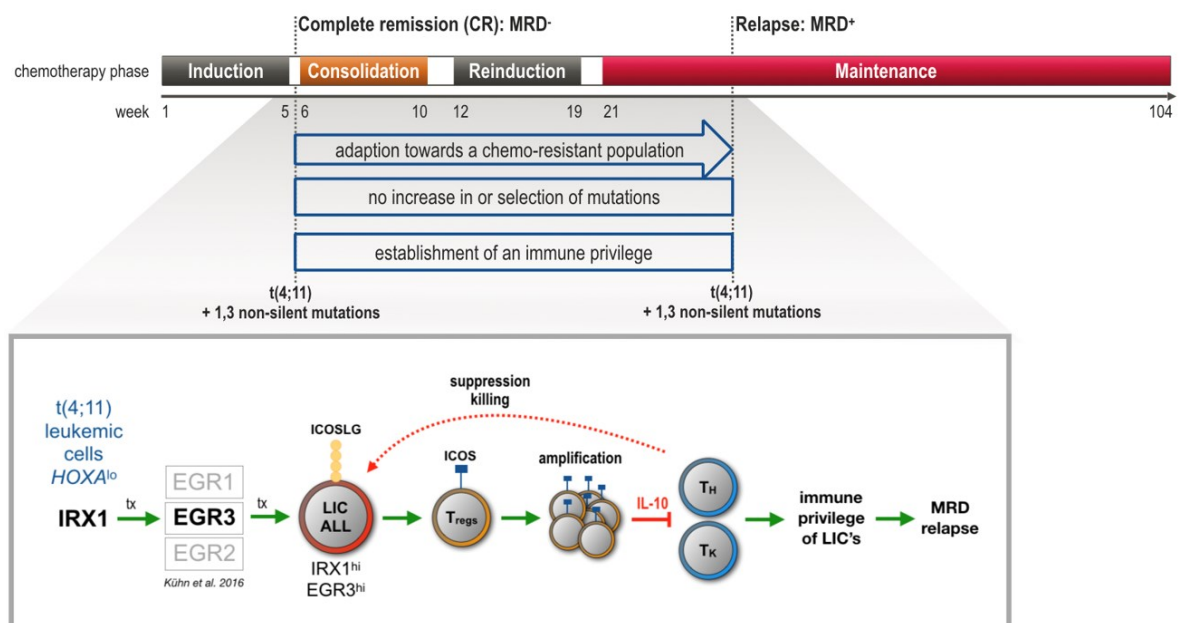


Figure 29. Proposed immune-evasion relapse mechanism.

t(4;11) iALL Patients undergo a chemotherapy structured in induction, consolidation, reinduction and maintenance phases. Typically, patients achieve complete remission (CR) rapidly with induction therapy but suffer from relapse only months later despite maintained chemotherapy. Within this time, the leukemic population acquires chemo-resistance without an increase in or selection of mutations. The results of this doctoral project point to an immune-evasion relapse mechanism as a possible explanation for the described clinical situation. This mechanism relies on the establishment of an immune privilege in the BM niche to prevent immune attack of leukemia initiating cells (LIC). In detail, *HOXA10* patients display elevated *IRX1* gene expression which correlates with *EGR3* upregulation. *EGR3* in turn directly transactivates the expression of the immune checkpoint *ICOSLG* which induces the expansion of highly suppressive IL-10 producing Tregs. These Tregs could acquire an immune suppressive microenvironment in the LIC niche leading to minimal residual disease (MRD) reemerging as relapse. tx = transcription. T_H = helper T-cell. T_K = killer T-cell.

Infant t(4;11) ALL has been identified to possess one of the lowest mutational burdens among pediatric cancers, displaying only 1.3 non-silent mutations in the dominant leukemic clone (Agraz-Doblas *et al.*, 2019; Andersson *et al.*, 2015; Bardini *et al.*, 2011; Dobbins *et al.*, 2013; Mullighan *et al.*, 2007).

Moreover, patients suffer from relapse only months after diagnosis despite rapid achievement of complete remission and maintenance of a multimodal chemotherapy without accumulation of secondary mutations (Driessen *et al.*, 2016; Pieters *et al.*, 2019, 2007). This doctoral project identified that ICOSLG-mediated Treg expansion contributes to relapse formation suggesting that this mechanism could interfere with immune recognition of ALL cells. Acquisition of regulatory T-cells adjacent to ALL cells could establish an immune privilege in the BM niche. This putative immune evasion mechanism could explain how t(4;11) ALL cells achieve therapy resistance without an increase in secondary mutations (**Figure 29**).

This hypothesis supposes that t(4;11) ALL cells lead to T-cell responses in the BM despite their low mutational burden. Rarity of mutations is usually considered to determine immune invisibility due to a lack of altered MHC-presented peptides serving as tumor neoantigens (Goodman *et al.*, 2017; Hugo *et al.*, 2016; Rizvi *et al.*, 2015). Considering the relative mutational silence of t(4;11) iALL at diagnosis and at relapse, the most likely source of immunogenic neoantigens is the fusion protein KMT2A::AFF1 and, in case of balanced translocations, the reciprocal fusion protein AFF1::KMT2A. It has been shown that such fusion-derived neoantigens (FDNA) led to specific CD8⁺ T-cell responses in pediatric ETV6::RUNX1 ALL (Zamora *et al.*, 2019). In addition, a patient with head and neck squamous cell carcinoma (HNSCC) and lung metastases was reported to respond surprisingly well to immune checkpoint inhibition (Pembrolizumab) due to the presence of the oncogenic fusion DEK::AFF2 (Yang *et al.*, 2019). In this study, Yang *et al.* demonstrated that FDNA stimulated T-cell responses, and the study provided evidence of immune surveillance causing a negative selection pressure against FDNA bearing tumor cells. This explained the successful checkpoint inhibitor treatment resulting in disappearance of the primary tumor and metastases. Unfortunately, the immunogenicity of t(4;11) fusion peptides and their ability to function as FDNA have not been investigated yet.

Another prerequisite for the above mentioned hypothesis is that FDNA become presented by t(4;11) ALL cells rendering them recognizable for T-cell attack. So far, no studies were conducted to evaluate this. However, very recently it has been uncovered that HSPC constitutively present antigens via MHC-II thereby enabling immune surveillance of the stem cell pool (Hernández-Malmierca *et al.*, 2022). The study found that CD4⁺ T-cells eliminated transformed HSPC and thus prevented leukemia. This remarkable study strongly suggests that leukemia developing from HSPC generally requires immune evasion strategies. In addition, the study highlighted the importance of T-cells for regulating the integrity of the HSC pool. As discussed in the introduction, the cell of origin of the translocation t(4;11) leading to iALL likely belongs to the HSPC pool of the fetal liver (see 1.2.3.2). The study of Hernández-Malmierca *et al.* was performed with murine HSPC derived from BM and not fetal liver. Thus, it remains unclear whether the described MHC-II-dependent immune surveillance mechanism also applies to fetal liver derived HSPC including the t(4;11) cell of origin.

ICOS⁺FOXP3⁺ Tregs are important immune regulators during fetal development since the neonatal thymus and cord blood were both characterized to contain ICOS⁺FOXP3⁺ Tregs (Ito *et al.*, 2008; Takahata *et al.*, 2004). Interestingly, the percentage of ICOS⁺ Tregs in the newborn's thymus exceeds that one of adult PB, and ICOS⁺ Tregs express the thymus emigration marker CD31 (Ito *et al.*, 2008; Takahata *et al.*, 2004). This suggests that ICOS⁺ Tregs are directly derived from the thymus and do not convert from ICOS⁻ Tregs. Besides, fetal T-cells have been identified to adopt a regulatory phenotype more easily compared to adult T-cells which is in line with the general need for immune tolerability during fetal development (Mold *et al.*, 2010). During gestation, fetal tissues are surrounded by placental extravillous trophoblast cells (EVT) which express high levels of ICOSLG throughout pregnancy (Petroff *et al.*, 2005). EVT protect the fetus from the mother's semi-foreign immune system. In this context, ICOSLG

expression has been validated as a mediator of tolerance at the fetomaternal interface (Riella *et al.*, 2013). Furthermore, EVT are known mediators of decidual Treg invasion to the fetomaternal interface leading to local suppression of T-cell activity by secretion of IL-10 (Aluvihare *et al.*, 2004; Du *et al.*, 2014; Salvany-Celades *et al.*, 2019; Svensson-Arvelund *et al.*, 2015; Tilburgs *et al.*, 2008). In summary, the ICOSLG/ICOS interaction is a mediator of Treg invasion and differentiation at the fetomaternal interface thereby guarding fetal tissues against potential attack by the mother's T-cells. Regarding infant ALL, this implies that during *in utero* transformation of the t(4;11) cell of origin, the ICOSLG/ICOS interaction applies a local immune privilege to the fetomaternal interface, comparable to the proposed BM niche immune privilege resulting in relapse. Accordingly, it could well be that during relapse formation, the ICOSLG-mediated Treg development in the BM reflects the ICOSLG-mediated immune privilege established during pregnancy. As a consequence, the establishment of an immune privilege in the BM niche could be a prerequisite for relapse development, as the immune suppressive conditions during fetal development could be a prerequisite for survival of t(4;11)-transformed preleukemic cells. In other words, t(4;11) iALL could depend on an immune privilege first to occur *in utero*, and second to re-emerge as relapse in the BM. This implies that turning the leukemic BM niche towards immune-susceptibility holds promise to prevent relapse and to overcome therapy-resistance of relapsed patients. However, this hypothesis requires experimental verification.

The importance of an immune privileged microenvironment in the BM niche for ALL cell survival originates from the function of the BM as a primary and secondary immune organ. The BM has been characterized as a primary immune organ because it provides the specialized niche in which HSC reside, survive, and maintain hematopoiesis throughout life (Chen *et al.*, 2016; Morrison and Scadden, 2014). In addition, the BM was identified to be a secondary immune organ with the observation that it is part of the lymphocyte recirculation network (Osmond, 1994). CD4⁺ and CD8⁺ T-cells migrate into the BM from blood vessels, become primed by BM-residing APC resulting in primary immune reactions and memory T-cell formation (Feuerer *et al.*, 2003, 2001). Additionally, Tregs have been shown to accumulate in the BM following chemoattraction by CXCL12 (Zou *et al.*, 2004). Furthermore, Tregs were identified to colocalize with HSC providing an immune suppressive microenvironment in the niche and maintaining HSC quiescence (Fujisaki *et al.*, 2011; Hirata *et al.*, 2019, 2018). These studies imply a fine-tuned balance between immune surveillance and immune tolerance essential for HSC regulation. Through the observed ICOSLG-mediated Treg expansion, infant t(4;11) ALL cells could be capable to reprogram the BM microenvironment towards immune tolerability. This could especially be important as massive leukemia cell death with chemotherapy onset presumably triggers processing of FDNA by APC and subsequently priming of naïve T-cells according to the concept of the cancer-immunity cycle (Chen and Mellman, 2013).

Through the combination of cell culture model data with primary patient data, this project revealed *EGR3* as a transactivator of *ICOSLG* expression and verified the known upregulation of *EGR3* through *IRX1* in the context of t(4;11) iALL. Regarding this, an unaddressed question is the reason for the elevated *EGR3/ICOSLG* expression levels in a small group of patients of the diagnosis cohort (defined as the *ICOSLG*^{hi} group) (**Figure 19A,E**). Elevated *ICOSLG* expression at diagnosis could be indicative for a positive immune selection of *ICOSLG*⁺ ALL cells. The observation that at relapse all patients displayed elevated *ICOSLG* expression levels suggests the establishment of an immune privileged microenvironment to be a prerequisite for relapse development. This would explain the short EFS of *ICOSLG*^{hi} patients and could indicate that *ICOSLG*^{lo} patients at the timepoint of diagnosis had not yet acquired an immune evasive microenvironment resulting in longer EFS. It could well be that the leukemic population of *ICOSLG*^{lo} patients consist to a small extent of a minor subgroup of *ICOSLG*⁺ ALL cells which had

not been immune selected at diagnosis but become the major phenotype at relapse upon immune selection in the BM niche. In line with that, ALL initiating cells were characterized to occupy the BM niche in response to chemotherapy thereby perturbing hematopoiesis resulting in apoptosis of healthy HSC (Burt *et al.*, 2019; Duan *et al.*, 2014; Tang *et al.*, 2018). The special role of the BM for relapse development in infant ALL becomes obvious considering that Interfant-99 characterized 72% of relapses as isolated BM relapses (Driessen *et al.*, 2016). This is in concordance with the ALL-REZ BFM 90 study reporting the BM as major relapse compartment for pediatric ALL (Tallen *et al.*, 2010).

Interestingly, some of the relapse cohort patients displayed an apparent lack of correlation between the *IRX1/EGR3* and *ICOSLG* expressions in the heatmap (**Figure 20A**). Regarding this issue, it should be considered that *ICOSLG* was identified as the final mediator of Treg development and immune evasion, therefore a selection of *ICOSLG*⁺ ALL cells is likely to take place in the BM niche. Probably, this selection does not directly depend on *EGR3* or *IRX1* expression. *ICOSLG* is known to be upregulated through TNF- α , IL-1 β and LPS treatments (Chen *et al.*, 2018; Gao *et al.*, 2017; Han *et al.*, 2018) and via transactivation by p65 (NF κ B) (Maurer *et al.*, 2020). Accordingly, inflammatory conditions mediated by BM-resident immune cells could also cause *ICOSLG* upregulation. As a result, high *IRX1* expression leading to the upregulation of *EGR3* should be regarded as an initial event that subsequently leads to a positive selection of *ICOSLG*⁺ leukemia cells. The maintenance of the condition could then be maintained by inflammatory processes. However, it should be considered that iALL patients receive an anti-inflammatory treatment in the shape of glucocorticoid administration throughout the complete chemotherapy usually suppressing inflammation (Pieters *et al.*, 2019, 2007). Nonetheless, it has not been investigated whether this applies also to the BM niche. Furthermore, it is not unlikely that other yet unknown leukemia or chemotherapy associated regulators could transactivate *ICOSLG*.

In conclusion, this doctoral project demonstrated that elevated *ICOSLG* expression at diagnosis is predictive for relapse formation and that *ICOSLG*-targeting with a neutralizing mAb impaired *ICOSLG*-mediated Treg expansion *in vitro*. These results imply *ICOSLG* checkpoint inhibition as a potential therapeutic opportunity to prevent relapse and to treat relapse-associated therapy resistance. Therefore, the *ICOSLG*-targeting fully human mAb Prezalumab should undergo clinical investigation for the treatment of infant t(4;11) ALL. The safety and efficacy of Prezalumab (AMG557 / MEDI5872) have been investigated for the treatment of autoimmune diseases including systemic lupus erythematosus (SLE) and active lupus arthritis in three phase I trials registered as NCT02391259, NCT00774943 and NCT01683695 (Cheng *et al.*, 2018; Sullivan *et al.*, 2016). The first two studies compared the safety and tolerability of single (1.8 - 210 mg s.c. or 18 mg i.v.) vs. multiple (6 - 210 mg s.c. every other week) dose administration of Prezalumab among 112 adult SLE patients. The safety for both dosing regimens was disclosed and only non-neutralizing α -Prezalumab antibodies were detected. The third study verified the long-term safety and tolerability of Prezalumab treatment in a cohort of 10 patients monitored for 23 weeks. Unfortunately, Prezalumab failed to reach the primary endpoints in a phase IIa trial for the treatment of primary Sjögren's syndrome questioning the efficacy of the checkpoint inhibitor for the treatment of autoimmune diseases (NCT02334306) (Mariette *et al.*, 2019; Pontarini *et al.*, 2020). Following this mid-phase fail, no further clinical investigation of Prezalumab was conducted.

Anyhow, the safety and tolerability of Prezalumab has not been investigated in children or infants up to now. Nevertheless, the checkpoint inhibitor Pembrolizumab targeting PD-L1 was proven safe for the treatment of children older than six months with advanced melanoma or PD-L1 positive solid tumor or lymphoma in the phase I/II trial KEYNOTE-051 (NCT02332668) (Geoerger *et al.*, 2020). The study included only three patients aged 6 months – 2 years, besides 22 aged 2 – 5 years, 25 aged 6 – 9 years and 104 aged 10 – 17 years. Serious adverse events including pyrexia, hypertension and pleural

effusion were observed in only 9% of patients. Moreover, the PD-1 checkpoint inhibitor Nivolumab was clinically investigated for the treatment of lymphoma in children older than 1 year in a phase I/II trial and demonstrated safety and tolerability (Davis *et al.*, 2020). These studies express that checkpoint inhibition is at the very beginning of clinical investigation in young children and infants but so far it is promising that severe side effects potentially limiting the feasibility of checkpoint inhibition in very young patients have not been observed. Nonetheless, the safety and tolerability of Prezalumab remains to be demonstrated in pediatric patients.

In summary, this doctoral project provides a molecular rationale for the clinical investigation of Prezalumab in the context of infant t(4;11) ALL. The results underline the importance of considering interactions between leukemia and immune cells to fully understand the unique biology of infant *KMT2A*-r leukemias. Moreover, the project reinforced the concept of immune evasion as a means to reach therapy resistance and relapse formation in infant hematologic diseases.

5 References

- Abkowitz, J.L., Catlin, S.N., McCallie, M.T., Gutter, P., 2002. Evidence that the number of hematopoietic stem cells per animal is conserved in mammals. *Blood* 100, 2665–2667. <https://doi.org/10.1182/blood-2002-03-0822>
- Adler, H.T., Chinery, R., Wu, D.Y., Kussick, S.J., Payne, J.M., Fornace, A.J., Tkachuk, D.C., 1999. Leukemic HRX fusion proteins inhibit GADD34-induced apoptosis and associate with the GADD34 and hSNF5/INI1 proteins. *Mol. Cell. Biol.* 19, 7050–7060. <https://doi.org/10.1128/MCB.19.10.7050>
- Adler, H.T., Nallaseth, F.S., Walter, G., Tkachuk, D.C., 1997. HRX leukemic fusion proteins form a heterocomplex with the leukemia-associated protein SET and protein phosphatase 2A. *J. Biol. Chem.* 272, 28407–28414. <https://doi.org/10.1074/jbc.272.45.28407>
- Agraz-Doblas, A., Bueno, C., Bashford-Rogers, R., Roy, A., Schneider, P., Bardini, M., Ballerini, P., Cazzaniga, G., Moreno, T., Revilla, C., Gut, M., Valsecchi, M.G., Roberts, I., Pieters, R., De Lorenzo, P., Varela, I., Menendez, P., Stam, R.W., 2019. Unraveling the cellular origin and clinical prognostic markers of infant B-cell acute lymphoblastic leukemia using genome-wide analysis. *Haematologica* 104, 1176–1188. <https://doi.org/10.3324/haematol.2018.206375>
- Ahmad, S., Abu-Eid, R., Shrimali, R., Webb, M., Verma, V., Doroodchi, A., Berrong, Z., Samara, R., Rodriguez, P.C., Mkrtichyan, M., Khleif, S.N., 2017. Differential PI3K δ Signaling in CD4+ T-cell Subsets Enables Selective Targeting of T Regulatory Cells to Enhance Cancer Immunotherapy. *Cancer Res.* 77, 1892–1904. <https://doi.org/10.1158/0008-5472.CAN-16-1839>
- Aliperti, V., Sgueglia, G., Aniello, F., Vitale, E., Fucci, L., Donizetti, A., 2019. Identification, Characterization, and Regulatory Mechanisms of a Novel EGR1 Splicing Isoform. *Int. J. Mol. Sci.* 20, 1548. <https://doi.org/10.3390/ijms20071548>
- Aluvihare, V.R., Kallikourdis, M., Betz, A.G., 2004. Regulatory T cells mediate maternal tolerance to the fetus. *Nat. Immunol.* 5, 266–271. <https://doi.org/10.1038/ni1037>
- Anderson, P.O., Manzo, B.A., Sundstedt, A., Minaee, S., Symonds, A., Khalid, S., Rodriguez-Cabezas, M.E., Nicolson, K., Li, S., Wraith, D.C., Wang, P., 2006. Persistent antigenic stimulation alters the transcription program in T cells, resulting in antigen-specific tolerance. *Eur. J. Immunol.* 36, 1374–1385. <https://doi.org/10.1002/eji.200635883>
- Andersson, A.K., Ma, J., Wang, J., Chen, X., Gedman, A.L., Dang, J., Nakitandwe, J., Holmfeldt, L., Parker, M., Easton, J., Huether, R., Kriwacki, R., Rusch, M., Wu, G., Li, Y., Mulder, H., Raimondi, S., Pounds, S., Kang, G., Shi, L., Becksfors, J., Gupta, P., Payne-Turner, D., Vadodaria, B., Boggs, K., Yergeau, D., Manne, J., Song, G., Edmonson, M., Nagahawatte, P., Wei, L., Cheng, C., Pei, D., Sutton, R., Venn, N.C., Chetcuti, A., Rush, A., Catchpoole, D., Heldrup, J., Fioretos, T., Lu, C., Ding, L., Pui, C.-H., Shurtleff, S., Mullighan, C.G., Mardis, E.R., Wilson, R.K., Gruber, T.A., Zhang, J., Downing, J.R., 2015. The landscape of somatic mutations in infant MLL-rearranged acute lymphoblastic leukemias. *Nat. Genet.* 47, 330–337. <https://doi.org/10.1038/ng.3230>
- Aoki, Y., Watanabe, T., Saito, Y., Kuroki, Y., Hijikata, A., Takagi, M., Tomizawa, D., Eguchi, M., Eguchi-Ishimae, M., Kaneko, A., Ono, R., Sato, K., Suzuki, N., Fujiki, S., Koh, K., Ishii, E., Shultz, L.D., Ohara, O., Mizutani, S., Ishikawa, F., 2015. Identification of CD34+ and CD34- leukemia-initiating cells in MLL-rearranged human acute lymphoblastic leukemia. *Blood* 125, 967–980. <https://doi.org/10.1182/blood-2014-03-563304>
- Armstrong, S.A., Kung, A.L., Mabon, M.E., Silverman, L.B., Stam, R.W., Boer, M.L.D., Pieters, R., Kersey, J.H., Sallan, S.E., Fletcher, J.A., Golub, T.R., Griffin, J.D., Korsmeyer, S.J., 2003. Inhibition of FLT3 in MLL: Validation of a therapeutic target identified by gene expression based classification. *Cancer Cell* 3, 173–183. [https://doi.org/10.1016/S1535-6108\(03\)00003-5](https://doi.org/10.1016/S1535-6108(03)00003-5)

Armstrong, S.A., Staunton, J.E., Silverman, L.B., Pieters, R., den Boer, M.L., Minden, M.D., Sallan, S.E., Lander, E.S., Golub, T.R., Korsmeyer, S.J., 2002. MLL translocations specify a distinct gene expression profile that distinguishes a unique leukemia. *Nat. Genet.* 30, 41–47. <https://doi.org/10.1038/ng765>

Azzoni, E., Conti, V., Campana, L., Dellavalle, A., Adams, R.H., Cossu, G., Brunelli, S., 2014. Hemogenic endothelium generates mesoangioblasts that contribute to several mesodermal lineages in vivo. *Dev. Camb. Engl.* 141, 1821–1834. <https://doi.org/10.1242/dev.103242>

Bagger, F.O., Sasivarevic, D., Sohi, S.H., Laursen, L.G., Pundhir, S., S nderby, C.K., Winther, O., Rapin, N., Porse, B.T., 2016. BloodSpot: a database of gene expression profiles and transcriptional programs for healthy and malignant haematopoiesis. *Nucleic Acids Res.* 44, D917–D924. <https://doi.org/10.1093/nar/gkv1101>

Bardini, M., Galbiati, M., Lettieri, A., Bungaro, S., Gorletta, T.A., Biondi, A., Cazzaniga, G., 2011. Implementation of array based whole-genome high-resolution technologies confirms the absence of secondary copy-number alterations in MLL-AF4-positive infant ALL patients. *Leukemia* 25, 175–178. <https://doi.org/10.1038/leu.2010.232>

Bardini, M., Woll, P.S., Corral, L., Luc, S., Wittmann, L., Ma, Z., Lo Nigro, L., Basso, G., Biondi, A., Cazzaniga, G., Jacobsen, S.E.W., 2015. Clonal variegation and dynamic competition of leukemia-initiating cells in infant acute lymphoblastic leukemia with MLL rearrangement. *Leukemia* 29, 38–50. <https://doi.org/10.1038/leu.2014.154>

Beckmann, A.M., Wilce, P.A., 1997. Egr transcription factors in the nervous system. *Neurochem. Int.* 31, 477–510; discussion 517-516. [https://doi.org/10.1016/s0197-0186\(96\)00136-2](https://doi.org/10.1016/s0197-0186(96)00136-2)

Behm, F.G., Raimondi, S.C., Frestedt, J.L., Liu, Q., Crist, W.M., Downing, J.R., Rivera, G.K., Kersey, J.H., Pui, C.H., 1996. Rearrangement of the MLL gene confers a poor prognosis in childhood acute lymphoblastic leukemia, regardless of presenting age. *Blood* 87, 2870–2877.

Benjamin, R., Graham, C., Yallop, D., Jozwik, A., Mirci-Danicar, O.C., Lucchini, G., Pinner, D., Jain, N., Kantarjian, H., Boissel, N., Maus, M.V., Frigault, M.J., Baruchel, A., Mohty, M., Gianella-Borradori, A., Binlich, F., Balandraud, S., Vitry, F., Thomas, E., Philippe, A., Fouliard, S., Dupouy, S., Marchiq, I., Almena-Carrasco, M., Ferry, N., Arnould, S., Konto, C., Veys, P., Qasim, W., Benjamin, R., Graham, C., Yallop, D., Jozwik, A., Pagliuca, A., Mufti, G., Patten, P., Kassam, S., Devereux, S., Kazmi, M., Cuthill, K., Potter, V., Kuhn, A., Metaxa, V., Bonganay, L., Stewart, O., Ellard, R., Catt, L., Lewis, J., Farzaneh, F., Chappell, J., Mason, A., Chu, V., Dunlop, A., Saleem, A., Cheung, G., Munro, H., Giemza, E., Qasim, W., Veys, P., Ciocarlie, O., Lucchini, G., Pinner, D., Chu, J., Amrolia, P., Rao, K., Chiesa, R., Silva, J., Hill, A., Finch, M., Young, L., Hara, H., Samarasinghe, S., Rao, A., Vora, A., Gilmour, K., Rivat, C., Murphy, C., Ahsan, G., Shamsah, R.S., James, J., Inglott, S., Wright, G., Adams, S., Izotova, N., Jain, N., Konopleva, M., Wierda, W., Jabbour, E., Kantarjian, H., Kebrieai, P., Jones, E., McGee, K., Maus, M., Frigault, M., Brown, J., Toncheva, V., Casey, K., Hock, H., McKeown, M.A., Mathews, R., Spitzer, T., Boissel, N., Raffoux, E., Lenglin , E., Itzykson, R., Rabian, F., Larghero, J., Madelaine, I., Azoulay, E., Clappier, E., Caillat-Zucman, S., Meunier, M., Celli-Lebras, K., Tremorin, M.-T., Baruchel, A., Yakouben, K., Mechinaud-Heloury, F., Grain, A., Alimi, A., Roupret, J., Chaillou, D., Larghero, J., Madelaine, I., Cav , H., Caye-Eude, A., Fenneteau, O., Laine, E., Naudin, J., Mohty, M., Brissot, E., Dulery, R., Malard, F., Mediavilla, C., Bonnin, A., Vekhoff, A., Ledraa, T., Larghero, J., Dagueneil-Nguyen, A., 2020. Genome-edited, donor-derived allogeneic anti-CD19 chimeric antigen receptor T cells in paediatric and adult B-cell acute lymphoblastic leukaemia: results of two phase 1 studies. *The Lancet* 396, 1885–1894. [https://doi.org/10.1016/S0140-6736\(20\)32334-5](https://doi.org/10.1016/S0140-6736(20)32334-5)

Bernt, K.M., Zhu, N., Sinha, A.U., Vempati, S., Faber, J., Krivtsov, A.V., Feng, Z., Punt, N., Daigle, A., Bullinger, L., Pollock, R.M., Richon, V.M., Kung, A.L., Armstrong, S.A., 2011. MLL-rearranged leukemia is dependent on aberrant H3K79 methylation by DOT1L. *Cancer Cell* 20, 66–78. <https://doi.org/10.1016/j.ccr.2011.06.010>

Berthon, C., Raffoux, E., Thomas, X., Vey, N., Gomez-Roca, C., Yee, K., Taussig, D.C., Rezai, K., Roumier, C., Herait, P., Kahatt, C., Quesnel, B., Michallet, M., Recher, C., Lokiec, F., Preudhomme, C., Dombret, H., 2016. Bromodomain inhibitor OTX015 in patients with acute leukaemia: a dose-escalation, phase 1 study. *Lancet Haematol.* 3, e186-195. [https://doi.org/10.1016/S2352-3026\(15\)00247-1](https://doi.org/10.1016/S2352-3026(15)00247-1)

Bertrand, J.Y., Jalil, A., Klaine, M., Jung, S., Cumano, A., Godin, I., 2005. Three pathways to mature macrophages in the early mouse yolk sac. *Blood* 106, 3004–3011. <https://doi.org/10.1182/blood-2005-02-0461>

Betti, C.J., Villalobos, M.J., Diaz, M.O., Vaughan, A.T., 2001. Apoptotic triggers initiate translocations within the MLL gene involving the nonhomologous end joining repair system. *Cancer Res.* 61, 4550–4555.

Betti, C.J., Villalobos, M.J., Diaz, M.O., Vaughan, A.T.M., 2003. Apoptotic stimuli initiate MLL-AF9 translocations that are transcribed in cells capable of division. *Cancer Res.* 63, 1377–1381.

Bhatla, T., Wang, J., Morrison, D.J., Raetz, E.A., Burke, M.J., Brown, P., Carroll, W.L., 2012. Epigenetic reprogramming reverses the relapse-specific gene expression signature and restores chemosensitivity in childhood B-lymphoblastic leukemia. *Blood* 119, 5201–5210. <https://doi.org/10.1182/blood-2012-01-401687>

Bonnet, D., Dick, J.E., 1997. Human acute myeloid leukemia is organized as a hierarchy that originates from a primitive hematopoietic cell. *Nat. Med.* 3, 730–737. <https://doi.org/10.1038/nm0797-730>

Borthakur, G., Odenike, O., Aldoss, I., Rizzieri, D.A., Prebet, T., Chen, C., Popovic, R., Modi, D.A., Joshi, R.H., Wolff, J.E., Jonas, B.A., 2021. A phase 1 study of the pan-bromodomain and extraterminal inhibitor mivebresib (ABBV-075) alone or in combination with venetoclax in patients with relapsed/refractory acute myeloid leukemia. *Cancer* 127, 2943–2953. <https://doi.org/10.1002/cncr.33590>

Bosse, A., Zülch, A., Becker, M.B., Torres, M., Gómez-Skarmeta, J.L., Modolell, J., Gruss, P., 1997. Identification of the vertebrate Iroquois homeobox gene family with overlapping expression during early development of the nervous system. *Mech. Dev.* 69, 169–181. [https://doi.org/10.1016/s0925-4773\(97\)00165-2](https://doi.org/10.1016/s0925-4773(97)00165-2)

Boyd, A.L., Campbell, C.J.V., Hopkins, C.I., Fiebig-Comyn, A., Russell, J., Ulemek, J., Foley, R., Leber, B., Xenocostas, A., Collins, T.J., Bhatia, M., 2014. Niche displacement of human leukemic stem cells uniquely allows their competitive replacement with healthy HSPCs. *J. Exp. Med.* 211, 1925–1935. <https://doi.org/10.1084/jem.20140131>

Brown, P., Levis, M., Shurtleff, S., Campana, D., Downing, J., Small, D., 2005. FLT3 inhibition selectively kills childhood acute lymphoblastic leukemia cells with high levels of FLT3 expression. *Blood* 105, 812–820. <https://doi.org/10.1182/blood-2004-06-2498>

Brown, P., Pieters, R., Biondi, A., 2019. How I treat infant leukemia. *Blood* 133, 205–214. <https://doi.org/10.1182/blood-2018-04-785980>

Brown, P.A., Kairalla, J.A., Hilden, J.M., Dreyer, Z.E., Carroll, A.J., Heerema, N.A., Wang, C., Devidas, M., Gore, L., Salzer, W.L., Winick, N.J., Carroll, W.L., Raetz, E.A., Borowitz, M.J., Small, D., Loh, M.L., Hunger, S.P., 2021. FLT3 inhibitor lestaurtinib plus chemotherapy for newly diagnosed KMT2A-rearranged infant acute lymphoblastic leukemia: Children’s Oncology Group trial AALL0631. *Leukemia* 35, 1279–1290. <https://doi.org/10.1038/s41375-021-01177-6>

Bueno, C., Calero-Nieto, F.J., Wang, X., Valdés-Mas, R., Gutiérrez-Agüera, F., Roca-Ho, H., Ayllon, V., Real, P.J., Arambilet, D., Espinosa, L., Torres-Ruiz, R., Agraz-Doblas, A., Varela, I., Boer, J. de, Bigas, A., Gottgens, B., Marschalek, R., Menendez, P., 2019. Enhanced hemato-endothelial specification during human embryonic differentiation through developmental cooperation between AF4-MLL and MLL-AF4 fusions. *Haematologica* 104, 1189–1201. <https://doi.org/10.3324/haematol.2018.202044>

Burke, M.J., Kostadinov, R., Sposto, R., Gore, L., Kelley, S.M., Rabik, C., Trepel, J.B., Lee, M.-J., Yuno, A., Lee, S., Bhojwani, D., Jeha, S., Chang, B.H., Sulis, M.L., Hermiston, M.L., Gaynon, P., Huynh, V., Verma, A., Gardner, R., Heym, K.M., Dennis, R.M., Ziegler, D.S., Laetsch, T.W., Oesterheld, J.E., Dubois, S.G., Pollard, J.A., Glade-Bender, J., Cooper, T.M., Kaplan, J.A., Farooqi, M.S., Yoo, B., Guest, E., Wayne, A.S., Brown, P.A., 2020. Decitabine and Vorinostat with Chemotherapy in Relapsed Pediatric Acute Lymphoblastic Leukemia: A TACL Pilot Study. *Clin. Cancer Res. Off. J. Am. Assoc. Cancer Res.* 26, 2297–2307. <https://doi.org/10.1158/1078-0432.CCR-19-1251>

Bursen, A., Schwabe, K., Rüster, B., Henschler, R., Ruthardt, M., Dingermann, T., Marschalek, R., 2010. The AF4.MLL fusion protein is capable of inducing ALL in mice without requirement of MLL.AF4. *Blood* 115, 3570–3579. <https://doi.org/10.1182/blood-2009-06-229542>

Burt, R., Dey, A., Aref, S., Aguiar, M., Akarca, A., Bailey, K., Day, W., Hooper, S., Kirkwood, A., Kirschner, K., Lee, S.-W., Lo Celso, C., Manji, J., Mansour, M.R., Marafioti, T., Mitchell, R.J., Muirhead, R.C., Cheuk Yan Ng, K., Pospori, C., Puccio, I., Zuborne-Alapi, K., Sahai, E., Fielding, A.K., 2019. Activated stromal cells transfer mitochondria to rescue acute lymphoblastic leukemia cells from oxidative stress. *Blood* 134, 1415–1429. <https://doi.org/10.1182/blood.2019001398>

Candelli, T., Schneider, P., Garrido Castro, P., Jones, L.A., Bodewes, E., Rockx-Brouwer, D., Pieters, R., Holstege, F.C.P., Margaritis, T., Stam, R.W., 2022. Identification and characterization of relapse-initiating cells in MLL-rearranged infant ALL by single-cell transcriptomics. *Leukemia* 36, 58–67. <https://doi.org/10.1038/s41375-021-01341-y>

Cao, F., Chen, Y., Cierpicki, T., Liu, Y., Basrur, V., Lei, M., Dou, Y., 2010. An Ash2L/RbBP5 heterodimer stimulates the MLL1 methyltransferase activity through coordinated substrate interactions with the MLL1 SET domain. *PLoS One* 5, e14102. <https://doi.org/10.1371/journal.pone.0014102>

Carter, J.H., Lefebvre, J.M., Wiest, D.L., Tourtellotte, W.G., 2007. Redundant role for early growth response transcriptional regulators in thymocyte differentiation and survival. *J. Immunol. Baltim. Md* 1950 178, 6796–6805. <https://doi.org/10.4049/jimmunol.178.11.6796>

Chang, P.-Y., Hom, R.A., Musselman, C.A., Zhu, L., Kuo, A., Gozani, O., Kutateladze, T.G., Cleary, M.L., 2010. Binding of the MLL PHD3 Finger to Histone H3K4me3 Is Required for MLL-Dependent Gene Transcription. *J. Mol. Biol.* 400, 137–144. <https://doi.org/10.1016/j.jmb.2010.05.005>

Chao, M.P., Seita, J., Weissman, I.L., 2008. Establishment of a normal hematopoietic and leukemia stem cell hierarchy. *Cold Spring Harb. Symp. Quant. Biol.* 73, 439–449. <https://doi.org/10.1101/sqb.2008.73.031>

Chen, Changya, Yu, W., Alikarami, F., Qiu, Q., Chen, Chia-hui, Flournoy, J., Gao, P., Uzun, Y., Fang, L., Davenport, J.W., Hu, Y., Zhu, Q., Wang, K., Libbrecht, C., Felmeister, A., Rozich, I., Ding, Y., Hunger, S.P., Felix, C.A., Wu, H., Brown, P.A., Guest, E.M., Barrett, D.M., Bernt, K.M., Tan, K., 2022. Single-cell multi-omics reveals increased plasticity, resistant populations, and stem-cell-like blasts in KMT2A-rearranged leukemia. *Blood* 139, 2198–2211. <https://doi.org/10.1182/blood.2021013442>

Chen, D.S., Mellman, I., 2013. Oncology Meets Immunology: The Cancer-Immunity Cycle. *Immunity* 39, 1–10. <https://doi.org/10.1016/j.immuni.2013.07.012>

Chen, J.Y., Miyanishi, M., Wang, S.K., Yamazaki, S., Sinha, R., Kao, K.S., Seita, J., Sahoo, D., Nakauchi, H., Weissman, I.L., 2016. Hoxb5 marks long-term haematopoietic stem cells and reveals a homogenous perivascular niche. *Nature* 530, 223–227. <https://doi.org/10.1038/nature16943>

Chen, M.J., Li, Y., De Obaldia, M.E., Yang, Q., Yzaguirre, A.D., Yamada-Inagawa, T., Vink, C.S., Bhandoola, A., Dzierzak, E., Speck, N.A., 2011. Erythroid/Myeloid Progenitors and Hematopoietic Stem Cells Originate from Distinct Populations of Endothelial Cells. *Cell Stem Cell* 9, 541–552. <https://doi.org/10.1016/j.stem.2011.10.003>

- Chen, Q., Mo, L., Cai, X., Wei, L., Xie, Z., Li, H., Li, J., Hu, Z., 2018. ICOS signal facilitates Foxp3 transcription to favor suppressive function of regulatory T cells. *Int. J. Med. Sci.* 15, 666–673. <https://doi.org/10.7150/ijms.23940>
- Chen, X.-L., Cao, X.-D., Kang, A.-J., Wang, K.-M., Su, B.-S., Wang, Y.-L., 2003. In situ expression and significance of B7 costimulatory molecules within tissues of human gastric carcinoma. *World J. Gastroenterol.* 9, 1370–1373. <https://doi.org/10.3748/wjg.v9.i6.1370>
- Chen, Y., Shen, S., Gorentla, B.K., Gao, J., Zhong, X.-P., 2012. Murine Regulatory T Cells Contain Hyperproliferative and Death-Prone Subsets with Differential ICOS Expression. *J. Immunol.* 188, 1698–1707. <https://doi.org/10.4049/jimmunol.1102448>
- Cheng, H., Hao, S., Liu, Y., Pang, Y., Ma, S., Dong, F., Xu, J., Zheng, G., Li, S., Yuan, W., Cheng, T., 2015. Leukemic marrow infiltration reveals a novel role for Egr3 as a potent inhibitor of normal hematopoietic stem cell proliferation. *Blood* 126, 1302–1313. <https://doi.org/10.1182/blood-2015-01-623645>
- Cheng, L.E., Amoura, Z., Cheah, B., Hiepe, F., Sullivan, B.A., Zhou, L., Arnold, G.E., Tsuji, W.H., Merrill, J.T., Chung, J.B., 2018. Brief Report: A Randomized, Double-Blind, Parallel-Group, Placebo-Controlled, Multiple-Dose Study to Evaluate AMG 557 in Patients With Systemic Lupus Erythematosus and Active Lupus Arthritis. *Arthritis Rheumatol.* 70, 1071–1076. <https://doi.org/10.1002/art.40479>
- Chessells, J.M., Harrison, C.J., Kempski, H., Webb, D.K.H., Wheatley, K., Hann, I.M., Stevens, R.F., Harrison, G., Gibson, B.E., 2002. Clinical features, cytogenetics and outcome in acute lymphoblastic and myeloid leukaemia of infancy: report from the MRC Childhood Leukaemia working party. *Leukemia* 16, 776–784. <https://doi.org/10.1038/sj.leu.2402468>
- Chillón, M.C., Gómez-Casares, M.T., López-Jorge, C.E., Rodríguez-Medina, C., Molines, A., Sarasquete, M.E., Alcoceba, M., Miguel, J.D.G.-S., Bueno, C., Montes, R., Ramos, F., Rodríguez, J.N., Giraldo, P., Ramírez, M., García-Delgado, R., Fuster, J.L., González-Díaz, M., Menendez, P., 2012. Prognostic significance of FLT3 mutational status and expression levels in MLL-AF4+ and MLL-germline acute lymphoblastic leukemia. *Leukemia* 26, 2360–2366. <https://doi.org/10.1038/leu.2012.161>
- Chinot, O.L., Barrié, M., Fuentes, S., Eudes, N., Lancelot, S., Metellus, P., Muracciole, X., Braguer, D., Ouafik, L., Martin, P.-M., Dufour, H., Figarella-Branger, D., 2007. Correlation Between O⁶-Methylguanine-DNA Methyltransferase and Survival in Inoperable Newly Diagnosed Glioblastoma Patients Treated With Neoadjuvant Temozolomide. *J. Clin. Oncol.* 25, 1470–1475. <https://doi.org/10.1200/JCO.2006.07.4807>
- Cole, A.J., Saffen, D.W., Baraban, J.M., Worley, P.F., 1989. Rapid increase of an immediate early gene messenger RNA in hippocampal neurons by synaptic NMDA receptor activation. *Nature* 340, 474–476. <https://doi.org/10.1038/340474a0>
- Collins, S., Lutz, M.A., Zarek, P.E., Anders, R.A., Kersh, G.J., Powell, J.D., 2008. Opposing regulation of T cell function by Egr-1/NAB2 and Egr-2/Egr-3. *Eur. J. Immunol.* 38, 528–536. <https://doi.org/10.1002/eji.200737157>
- Cooper, T.M., Sison, E.A.R., Baker, S.D., Li, L., Ahmed, A., Trippett, T., Gore, L., Macy, M.E., Narendran, A., August, K., Absalon, M.J., Boklan, J., Pollard, J., Magoon, D., Brown, P.A., 2017. A phase 1 study of the CXCR4 antagonist plerixafor in combination with high-dose cytarabine and etoposide in children with relapsed or refractory acute leukemias or myelodysplastic syndrome: A Pediatric Oncology Experimental Therapeutics Investigators' Consortium study (POE 10-03). *Pediatr. Blood Cancer* 64. <https://doi.org/10.1002/pbc.26414>
- Coyle, A.J., Gutierrez-Ramos, J.C., 2001. The expanding B7 superfamily: increasing complexity in costimulatory signals regulating T cell function. *Nat. Immunol.* 2, 203–209. <https://doi.org/10.1038/85251>
- Curran, E.K., Godfrey, J., Kline, J., 2017. Mechanisms of Immune Tolerance in Leukemia and Lymphoma. *Trends Immunol.* 38, 513–525. <https://doi.org/10.1016/j.it.2017.04.004>

Daigle, S.R., Olhava, E.J., Therkelsen, C.A., Basavapathruni, A., Jin, L., Boriack-Sjodin, P.A., Allain, C.J., Klaus, C.R., Raimondi, A., Scott, M.P., Waters, N.J., Chesworth, R., Moyer, M.P., Copeland, R.A., Richon, V.M., Pollock, R.M., 2013. Potent inhibition of DOT1L as treatment of MLL-fusion leukemia. *Blood* 122, 1017–1025. <https://doi.org/10.1182/blood-2013-04-497644>

Daigle, S.R., Olhava, E.J., Therkelsen, C.A., Majer, C.R., Sneeringer, C.J., Song, J., Johnston, L.D., Scott, M.P., Smith, J.J., Xiao, Y., Jin, L., Kuntz, K.W., Chesworth, R., Moyer, M.P., Bernt, K.M., Tseng, J.-C., Kung, A.L., Armstrong, S.A., Copeland, R.A., Richon, V.M., Pollock, R.M., 2011. Selective killing of mixed lineage leukemia cells by a potent small-molecule DOT1L inhibitor. *Cancer Cell* 20, 53–65. <https://doi.org/10.1016/j.ccr.2011.06.009>

Davis, K.L., Fox, E., Merchant, M.S., Reid, J.M., Kudgus, R.A., Liu, X., Minard, C.G., Voss, S., Berg, S.L., Weigel, B.J., Mackall, C.L., 2020. Nivolumab in children and young adults with relapsed or refractory solid tumours or lymphoma (ADVL1412): a multicentre, open-label, single-arm, phase 1–2 trial. *Lancet Oncol.* 21, 541–550. [https://doi.org/10.1016/S1470-2045\(20\)30023-1](https://doi.org/10.1016/S1470-2045(20)30023-1)

Davis, S., Bozon, B., Laroche, S., 2003. How necessary is the activation of the immediate early gene *zif268* in synaptic plasticity and learning? *Behav. Brain Res.* 142, 17–30. [https://doi.org/10.1016/s0166-4328\(02\)00421-7](https://doi.org/10.1016/s0166-4328(02)00421-7)

Dawson, M.A., Prinjha, R.K., Dittmann, A., Giotopoulos, G., Bantscheff, M., Chan, W.-I., Robson, S.C., Chung, C., Hopf, C., Savitski, M.M., Huthmacher, C., Gudgin, E., Lugo, D., Beinke, S., Chapman, T.D., Roberts, E.J., Soden, P.E., Auger, K.R., Mirguet, O., Doehner, K., Delwel, R., Burnett, A.K., Jeffrey, P., Drewes, G., Lee, K., Huntly, B.J.P., Kouzarides, T., 2011. Inhibition of BET recruitment to chromatin as an effective treatment for MLL-fusion leukaemia. *Nature* 478, 529–533. <https://doi.org/10.1038/nature10509>

Day, M.L., Fahrner, T.J., Aykent, S., Milbrandt, J., 1990. The zinc finger protein NGFI-A exists in both nuclear and cytoplasmic forms in nerve growth factor-stimulated PC12 cells. *J. Biol. Chem.* 265, 15253–15260. [https://doi.org/10.1016/S0021-9258\(18\)77249-9](https://doi.org/10.1016/S0021-9258(18)77249-9)

de Boer, J., Walf-Vorderwülbecke, V., Williams, O., 2013. In focus: MLL-rearranged leukemia. *Leukemia* 27, 1224–1228. <https://doi.org/10.1038/leu.2013.78>

de Bruijn, M.F., Speck, N.A., Peeters, M.C., Dzierzak, E., 2000. Definitive hematopoietic stem cells first develop within the major arterial regions of the mouse embryo. *EMBO J.* 19, 2465–2474. <https://doi.org/10.1093/emboj/19.11.2465>

De Lorenzo, P., Moorman, A.V., Pieters, R., Dreyer, Z.E., Heerema, N.A., Carroll, A.J., Hunger, S.P., Harvey, R., Willman, C.L., Devidas, M., Valsecchi, M.-G., Harrison, C.J., 2014. Cytogenetics and outcome of infants with acute lymphoblastic leukemia and absence of MLL rearrangements. *Leukemia* 28, 428–430. <https://doi.org/10.1038/leu.2013.280>

Dege, C., Fegan, K.H., Creamer, J.P., Berrien-Elliott, M.M., Luff, S.A., Kim, D., Wagner, J.A., Kingsley, P.D., McGrath, K.E., Fehniger, T.A., Palis, J., Sturgeon, C.M., 2020. Potently Cytotoxic Natural Killer Cells Initially Emerge from Erythro-Myeloid Progenitors during Mammalian Development. *Dev. Cell* 53, 229–239.e7. <https://doi.org/10.1016/j.devcel.2020.02.016>

DeLigio, J.T., Zorio, D.A.R., 2009. Early growth response 1 (EGR1): A gene with as many names as biological functions. *Cancer Biol. Ther.* 8, 1889–1892. <https://doi.org/10.4161/cbt.8.20.9804>

Deshpande, A.J., Chen, L., Fazio, M., Sinha, A.U., Bernt, K.M., Banka, D., Dias, S., Chang, J., Olhava, E.J., Daigle, S.R., Richon, V.M., Pollock, R.M., Armstrong, S.A., 2013. Leukemic transformation by the MLL-AF6 fusion oncogene requires the H3K79 methyltransferase Dot1l. *Blood* 121, 2533–2541. <https://doi.org/10.1182/blood-2012-11-465120>

- Desmazières, A., Decker, L., Vallat, J.-M., Charnay, P., Gilardi-Hebenstreit, P., 2008. Disruption of Krox20–Nab Interaction in the Mouse Leads to Peripheral Neuropathy with Biphasic Evolution. *J. Neurosci.* 28, 5891–5900. <https://doi.org/10.1523/JNEUROSCI.5187-07.2008>
- Dobbins, S.E., Sherborne, A.L., Ma, Y.P., Bardini, M., Biondi, A., Cazzaniga, G., Lloyd, A., Chubb, D., Greaves, M.F., Houlston, R.S., 2013. The silent mutational landscape of infant MLL-AF4 pro-B acute lymphoblastic leukemia. *Genes. Chromosomes Cancer* 52, 954–960. <https://doi.org/10.1002/gcc.22090>
- Dou, Y., Milne, T.A., Ruthenburg, A.J., Lee, S., Lee, J.W., Verdine, G.L., Allis, C.D., Roeder, R.G., 2006. Regulation of MLL1 H3K4 methyltransferase activity by its core components. *Nat. Struct. Mol. Biol.* 13, 713–719. <https://doi.org/10.1038/nsmb1128>
- Dou, Y., Milne, T.A., Tackett, A.J., Smith, E.R., Fukuda, A., Wysocka, J., Allis, C.D., Chait, B.T., Hess, J.L., Roeder, R.G., 2005. Physical Association and Coordinate Function of the H3 K4 Methyltransferase MLL1 and the H4 K16 Acetyltransferase MOF. *Cell* 121, 873–885. <https://doi.org/10.1016/j.cell.2005.04.031>
- Dreyer, Z.E., Dinndorf, P.A., Camitta, B., Sather, H., La, M.K., Devidas, M., Hilden, J.M., Heerema, N.A., Sanders, J.E., McGlennen, R., Willman, C.L., Carroll, A.J., Behm, F., Smith, F.O., Woods, W.G., Godder, K., Reaman, G.H., 2011. Analysis of the role of hematopoietic stem-cell transplantation in infants with acute lymphoblastic leukemia in first remission and MLL gene rearrangements: a report from the Children’s Oncology Group. *J. Clin. Oncol. Off. J. Am. Soc. Clin. Oncol.* 29, 214–222. <https://doi.org/10.1200/JCO.2009.26.8938>
- Driessen, E.M.C., de Lorenzo, P., Campbell, M., Felice, M., Ferster, A., Hann, I., Vora, A., Hovi, L., Escherich, G., Li, C.K., Mann, G., Leblanc, T., Locatelli, F., Biondi, A., Rubnitz, J., Schrappe, M., Silverman, L., Stary, J., Suppiah, R., Szczepanski, T., Valsecchi, M., Pieters, R., 2016. Outcome of relapsed infant acute lymphoblastic leukemia treated on the interfant-99 protocol. *Leukemia* 30, 1184–1187. <https://doi.org/10.1038/leu.2015.246>
- Driessen, E.M.C., van Roon, E.H.J., Spijkers-Hagelstein, J.A.P., Schneider, P., de Lorenzo, P., Valsecchi, M.G., Pieters, R., Stam, R.W., 2013. Frequencies and prognostic impact of RAS mutations in MLL-rearranged acute lymphoblastic leukemia in infants. *Haematologica* 98, 937–944. <https://doi.org/10.3324/haematol.2012.067983>
- Du, J., He, H., Li, Z., He, J., Bai, Z., Liu, B., Lan, Y., 2021. Integrative transcriptomic analysis of developing hematopoietic stem cells in human and mouse at single-cell resolution. *Biochem. Biophys. Res. Commun.* 558, 161–167. <https://doi.org/10.1016/j.bbrc.2021.04.058>
- Du, M.-R., Guo, P.-F., Piao, H.-L., Wang, S.-C., Sun, C., Jin, L.-P., Tao, Y., Li, Y.-H., Zhang, D., Zhu, R., Fu, Q., Li, D.-J., 2014. Embryonic Trophoblasts Induce Decidual Regulatory T Cell Differentiation and Maternal–Fetal Tolerance through Thymic Stromal Lymphopoietin Instructing Dendritic Cells. *J. Immunol.* 192, 1502–1511. <https://doi.org/10.4049/jimmunol.1203425>
- Duan, C.-W., Shi, J., Chen, J., Wang, B., Yu, Y.-H., Qin, X., Zhou, X.-C., Cai, Y.-J., Li, Z.-Q., Zhang, F., Yin, M.-Z., Tao, Y., Mi, J.-Q., Li, L.-H., Enver, T., Chen, G.-Q., Hong, D.-L., 2014. Leukemia propagating cells rebuild an evolving niche in response to therapy. *Cancer Cell* 25, 778–793. <https://doi.org/10.1016/j.ccr.2014.04.015>
- Duhen, T., Duhen, R., Lanzavecchia, A., Sallusto, F., Campbell, D.J., 2012. Functionally distinct subsets of human FOXP3+ Treg cells that phenotypically mirror effector Th cells. *Blood* 119, 4430–4440. <https://doi.org/10.1182/blood-2011-11-392324>
- Easterbrook, J., Rybtsov, S., Gordon-Keylock, S., Ivanovs, A., Taoudi, S., Anderson, R.A., Medvinsky, A., 2019. Analysis of the Spatiotemporal Development of Hematopoietic Stem and Progenitor Cells in the Early Human Embryo. *Stem Cell Rep.* 12, 1056–1068. <https://doi.org/10.1016/j.stemcr.2019.03.003>

Ernst, P., Wang, J., Huang, M., Goodman, R.H., Korsmeyer, S.J., 2001. MLL and CREB Bind Cooperatively to the Nuclear Coactivator CREB-Binding Protein. *Mol. Cell. Biol.* 21, 2249–2258. <https://doi.org/10.1128/MCB.21.7.2249-2258.2001>

Faber, J., Krivtsov, A.V., Stubbs, M.C., Wright, R., Davis, T.N., van den Heuvel-Eibrink, M., Zwaan, C.M., Kung, A.L., Armstrong, S.A., 2009. HOXA9 is required for survival in human MLL-rearranged acute leukemias. *Blood* 113, 2375–2385. <https://doi.org/10.1182/blood-2007-09-113597>

Faget, J., Bendriss-Vermare, N., Gobert, M., Durand, I., Olive, D., Biota, C., Bachelot, T., Treilleux, I., Goddard-Leon, S., Lavergne, E., Chabaud, S., Blay, J.Y., Caux, C., Ménétrier-Caux, C., 2012. ICOS-ligand expression on plasmacytoid dendritic cells supports breast cancer progression by promoting the accumulation of immunosuppressive CD4+ T cells. *Cancer Res.* 72, 6130–6141. <https://doi.org/10.1158/0008-5472.CAN-12-2409>

Fair, K., Anderson, M., Bulanova, E., Mi, H., Tropschug, M., Diaz, M.O., 2001. Protein interactions of the MLL PHD fingers modulate MLL target gene regulation in human cells. *Mol. Cell. Biol.* 21, 3589–3597. <https://doi.org/10.1128/MCB.21.10.3589-3597.2001>

Ferrando, A.A., Armstrong, S.A., Neuberg, D.S., Sallan, S.E., Silverman, L.B., Korsmeyer, S.J., Look, A.T., 2003. Gene expression signatures in MLL-rearranged T-lineage and B-precursor acute leukemias: dominance of HOX dysregulation. *Blood* 102, 262–268. <https://doi.org/10.1182/blood-2002-10-3221>

Feuerer, M., Beckhove, P., Garbi, N., Mahnke, Y., Limmer, A., Hommel, M., Hämmerling, G.J., Kyewski, B., Hamann, A., Umansky, V., Schirmacher, V., 2003. Bone marrow as a priming site for T-cell responses to blood-borne antigen. *Nat. Med.* 9, 1151–1157. <https://doi.org/10.1038/nm914>

Feuerer, M., Rocha, M., Bai, L., Umansky, V., Solomayer, E.F., Bastert, G., Diel, I.J., Schirmacher, V., 2001. Enrichment of memory T cells and other profound immunological changes in the bone marrow from untreated breast cancer patients. *Int. J. Cancer* 92, 96–105.

Ford, A.M., Ridge, S.A., Cabrera, M.E., Mahmoud, H., Steel, C.M., Chan, L.C., Greaves, M., 1993. In utero rearrangements in the trithorax-related oncogene in infant leukaemias. *Nature* 363, 358–360. <https://doi.org/10.1038/363358a0>

Fos, C., Salles, A., Lang, V., Carrette, F., Audebert, S., Pastor, S., Ghiotto, M., Olive, D., Bismuth, G., Nunès, J.A., 2008. ICOS Ligation Recruits the p50 α PI3K Regulatory Subunit to the Immunological Synapse. *J. Immunol.* 181, 1969–1977. <https://doi.org/10.4049/jimmunol.181.3.1969>

Fujisaki, J., Wu, J., Carlson, A.L., Silberstein, L., Putheti, P., Larocca, R., Gao, W., Saito, T.I., Celso, C.L., Tsuyuzaki, H., Sato, T., Côté, D., Sykes, M., Strom, T.B., Scadden, D.T., Lin, C.P., 2011. In vivo imaging of Treg cells providing immune privilege to the haematopoietic stem-cell niche. *Nature* 474, 216–219. <https://doi.org/10.1038/nature10160>

Gale, K.B., Ford, A.M., Repp, R., Borkhardt, A., Keller, C., Eden, O.B., Greaves, M.F., 1997. Backtracking leukemia to birth: Identification of clonotypic gene fusion sequences in neonatal blood spots. *Proc. Natl. Acad. Sci. U. S. A.* 94, 13950–13954.

Gao, Y., Xu, B., Zhang, P., He, Y., Liang, X., Liu, J., Li, J., 2017. TNF- α Regulates Mast Cell Functions by Inhibiting Cell Degranulation. *Cell. Physiol. Biochem.* 44, 751–762. <https://doi.org/10.1159/000485288>

Gardner, R., Wu, D., Cherian, S., Fang, M., Hanafi, L.-A., Finney, O., Smithers, H., Jensen, M.C., Riddell, S.R., Maloney, D.G., Turtle, C.J., 2016. Acquisition of a CD19-negative myeloid phenotype allows immune escape of MLL-rearranged B-ALL from CD19 CAR-T-cell therapy. *Blood* 127, 2406–2410. <https://doi.org/10.1182/blood-2015-08-665547>

Garrido Castro, P., van Roon, E.H.J., Pinhaños, S.S., Trentin, L., Schneider, P., Kerstjens, M., Te Kronnie, G., Heidenreich, O., Pieters, R., Stam, R.W., 2018. The HDAC inhibitor panobinostat (LBH589) exerts in vivo anti-leukaemic activity against MLL-rearranged acute lymphoblastic leukaemia and involves the

RNF20/RNF40/WAC-H2B ubiquitination axis. *Leukemia* 32, 323–331. <https://doi.org/10.1038/leu.2017.216>

Geoerger, B., Kang, H.J., Yalon-Oren, M., Marshall, L.V., Vezina, C., Pappo, A., Laetsch, T.W., Petrilli, A.S., Ebinger, M., Toporski, J., Glade-Bender, J., Nicholls, W., Fox, E., DuBois, S.G., Macy, M.E., Cohn, S.L., Pathiraja, K., Diede, S.J., Ebbinghaus, S., Pinto, N., 2020. Pembrolizumab in paediatric patients with advanced melanoma or a PD-L1-positive, advanced, relapsed, or refractory solid tumour or lymphoma (KEYNOTE-051): interim analysis of an open-label, single-arm, phase 1–2 trial. *Lancet Oncol.* 21, 121–133. [https://doi.org/10.1016/S1470-2045\(19\)30671-0](https://doi.org/10.1016/S1470-2045(19)30671-0)

Ghosn, E., Yoshimoto, M., Nakauchi, H., Weissman, I.L., Herzenberg, L.A., 2019. Hematopoietic stem cell-independent hematopoiesis and the origins of innate-like B lymphocytes. *Dev. Camb. Engl.* 146, dev170571. <https://doi.org/10.1242/dev.170571>

Gillert, E., Leis, T., Repp, R., Reichel, M., Hösch, A., Breitenlohner, I., Angermüller, S., Borkhardt, A., Harbott, J., Lampert, F., Griesinger, F., Greil, J., Fey, G.H., Marschalek, R., 1999. A DNA damage repair mechanism is involved in the origin of chromosomal translocations t(4;11) in primary leukemic cells. *Oncogene* 18, 4663–4671. <https://doi.org/10.1038/sj.onc.1202842>

Goodman, A.M., Kato, S., Bazhenova, L., Patel, S.P., Frampton, G.M., Miller, V., Stephens, P.J., Daniels, G.A., Kurzrock, R., 2017. Tumor Mutational Burden as an Independent Predictor of Response to Immunotherapy in Diverse Cancers. *Mol. Cancer Ther.* 16, 2598–2608. <https://doi.org/10.1158/1535-7163.MCT-17-0386>

Greaves, M.F., Maia, A.T., Wiemels, J.L., Ford, A.M., 2003. Leukemia in twins: lessons in natural history. *Blood* 102, 2321–2333. <https://doi.org/10.1182/blood-2002-12-3817>

Greaves, M.F., Wiemels, J., 2003. Origins of chromosome translocations in childhood leukaemia. *Nat. Rev. Cancer* 3, 639–649. <https://doi.org/10.1038/nrc1164>

Greaves, P., Gribben, J.G., 2013. The role of B7 family molecules in hematologic malignancy. *Blood* 121, 734–744. <https://doi.org/10.1182/blood-2012-10-385591>

Green, M.R., Sambrook, J., 2019. Polymerase Chain Reaction (PCR) Amplification of GC-Rich Templates. *Cold Spring Harb. Protoc.* 2019. <https://doi.org/10.1101/pdb.prot095141>

Green, M.R., Sambrook, J., 2012. *Molecular cloning: a laboratory manual*, 4th ed. ed. Cold Spring Harbor Laboratory Press, Cold Spring Harbor, N.Y.

Greenwald, R.J., Freeman, G.J., Sharpe, A.H., 2005. The B7 family revisited. *Annu. Rev. Immunol.* 23, 515–548. <https://doi.org/10.1146/annurev.immunol.23.021704.115611>

Greil, J., Gramatzki, M., Burger, R., Marschalek, R., Peltner, M., Trautmann, U., Hansen-Hagge, T.E., Bartram, C.R., Fey, G.H., Stehr, K., 1994. The acute lymphoblastic leukaemia cell line SEM with t(4;11) chromosomal rearrangement is biphenotypic and responsive to interleukin-7. *Br. J. Haematol.* 86, 275–283. <https://doi.org/10.1111/j.1365-2141.1994.tb04726.x>

Hacein-Bey-Abina, S., Garrigue, A., Wang, G.P., Soulier, J., Lim, A., Morillon, E., Clappier, E., Caccavelli, L., Delabesse, E., Beldjord, K., Asnafi, V., MacIntyre, E., Dal Cortivo, L., Radford, I., Brousse, N., Sigaux, F., Moshous, D., Hauer, J., Borkhardt, A., Belohradsky, B.H., Wintergerst, U., Velez, M.C., Leiva, L., Sorensen, R., Wulffraat, N., Blanche, S., Bushman, F.D., Fischer, A., Cavazzana-Calvo, M., 2008. Insertional oncogenesis in 4 patients after retrovirus-mediated gene therapy of SCID-X1. *J. Clin. Invest.* 118, 3132–3142. <https://doi.org/10.1172/JCI35700>

Hacein-Bey-Abina, S., Von Kalle, C., Schmidt, M., McCormack, M.P., Wulffraat, N., Leboulch, P., Lim, A., Osborne, C.S., Pawliuk, R., Morillon, E., Sorensen, R., Forster, A., Fraser, P., Cohen, J.I., de Saint Basile, G., Alexander, I., Wintergerst, U., Frebourg, T., Aurias, A., Stoppa-Lyonnet, D., Romana, S., Radford-Weiss, I., Gross, F., Valensi, F., Delabesse, E., Macintyre, E., Sigaux, F., Soulier, J., Leiva, L.E., Wissler,

M., Prinz, C., Rabbitts, T.H., Le Deist, F., Fischer, A., Cavazzana-Calvo, M., 2003. LMO2-associated clonal T cell proliferation in two patients after gene therapy for SCID-X1. *Science* 302, 415–419. <https://doi.org/10.1126/science.1088547>

Han, Y., Dong, Y., Yang, Q., Xu, W., Jiang, S., Yu, Z., Yu, K., Zhang, S., 2018. Acute Myeloid Leukemia Cells Express ICOS Ligand to Promote the Expansion of Regulatory T Cells. *Front. Immunol.* 9, 2227. <https://doi.org/10.3389/fimmu.2018.02227>

Healy, S., Khan, P., Davie, J.R., 2013. Immediate early response genes and cell transformation. *Pharmacol. Ther.* 137, 64–77. <https://doi.org/10.1016/j.pharmthera.2012.09.001>

Hernández-Malmierca, P., Vonficht, D., Schnell, A., Uckelmann, H.J., Bollhagen, A., Mahmoud, M.A.A., Landua, S.-L., Salm, E. van der, Trautmann, C.L., Raffel, S., Grünschläger, F., Lutz, R., Ghosh, M., Renders, S., Correia, N., Donato, E., Dixon, K.O., Hirche, C., Andresen, C., Robens, C., Werner, P.S., Boch, T., Eisel, D., Osen, W., Pilz, F., Przybylla, A., Klein, C., Buchholz, F., Milsom, M.D., Essers, M.A.G., Eichmüller, S.B., Hofmann, W.-K., Nowak, D., Hübschmann, D., Hundemer, M., Thiede, C., Bullinger, L., Müller-Tidow, C., Armstrong, S.A., Trumpp, A., Kuchroo, V.K., Haas, S., 2022. Antigen presentation safeguards the integrity of the hematopoietic stem cell pool. *Cell Stem Cell* 29, 760-775.e10. <https://doi.org/10.1016/j.stem.2022.04.007>

Hilden, J.M., Dinndorf, P.A., Meerbaum, S.O., Sather, H., Villaluna, D., Heerema, N.A., McGlennen, R., Smith, F.O., Woods, W.G., Salzer, W.L., Johnstone, H.S., Dreyer, Z., Reaman, G.H., Children’s Oncology Group, 2006. Analysis of prognostic factors of acute lymphoblastic leukemia in infants: report on CCG 1953 from the Children’s Oncology Group. *Blood* 108, 441–451. <https://doi.org/10.1182/blood-2005-07-3011>

Hinze, L., Pfirrmann, M., Karim, S., Degar, J., McGuckin, C., Vinjamur, D., Sacher, J., Stevenson, K.E., Neuberg, D.S., Orellana, E., Stanulla, M., Gregory, R.I., Bauer, D.E., Wagner, F.F., Stegmaier, K., Gutierrez, A., 2019. Synthetic Lethality of Wnt Pathway Activation and Asparaginase in Drug-Resistant Acute Leukemias. *Cancer Cell* 35, 664-676.e7. <https://doi.org/10.1016/j.ccell.2019.03.004>

Hirata, Y., Furuhashi, K., Ishii, H., Li, H.W., Pinho, S., Ding, L., Robson, S.C., Frenette, P.S., Fujisaki, J., 2018. CD150^{high} Bone Marrow Tregs Maintain Hematopoietic Stem Cell Quiescence and Immune Privilege via Adenosine. *Cell Stem Cell* 22, 445-453.e5. <https://doi.org/10.1016/j.stem.2018.01.017>

Hirata, Y., Kakiuchi, M., Robson, S.C., Fujisaki, J., 2019. CD150^{high} CD4 T cells and CD150^{high} regulatory T cells regulate hematopoietic stem cell quiescence via CD73. *Haematologica* 104, 1136–1142. <https://doi.org/10.3324/haematol.2018.198283>

Hogan, L.E., Meyer, J.A., Yang, J., Wang, J., Wong, N., Yang, W., Condos, G., Hunger, S.P., Raetz, E., Saffery, R., Relling, M.V., Bhojwani, D., Morrison, D.J., Carroll, W.L., 2011. Integrated genomic analysis of relapsed childhood acute lymphoblastic leukemia reveals therapeutic strategies. *Blood* 118, 5218–5226. <https://doi.org/10.1182/blood-2011-04-345595>

Hom, R.A., Chang, P.-Y., Roy, S., Musselman, C.A., Glass, K.C., Selezneva, A.I., Gozani, O., Ismagilov, R.F., Cleary, M.L., Kutateladze, T.G., 2010. Molecular mechanism of MLL PHD3 and RNA recognition by the Cyp33 RRM domain. *J. Mol. Biol.* 400, 145–154. <https://doi.org/10.1016/j.jmb.2010.04.067>

Hotfilder, M., Röttgers, S., Rosemann, A., Schrauder, A., Schrappe, M., Pieters, R., Jürgens, H., Harbott, J., Vormoor, J., 2005. Leukemic stem cells in childhood high-risk ALL/t(9;22) and t(4;11) are present in primitive lymphoid-restricted CD34⁺CD19⁻ cells. *Cancer Res.* 65, 1442–1449. <https://doi.org/10.1158/0008-5472.CAN-04-1356>

Howe, S.J., Mansour, M.R., Schwarzwaelder, K., Bartholomae, C., Hubank, M., Kempinski, H., Brugman, M.H., Pike-Overzet, K., Chatters, S.J., de Ridder, D., Gilmour, K.C., Adams, S., Thornhill, S.I., Parsley, K.L., Staal, F.J.T., Gale, R.E., Linch, D.C., Bayford, J., Brown, L., Quaye, M., Kinnon, C., Ancliff, P., Webb, D.K., Schmidt, M., von Kalle, C., Gaspar, H.B., Thrasher, A.J., 2008. Insertional mutagenesis combined

with acquired somatic mutations causes leukemogenesis following gene therapy of SCID-X1 patients. *J. Clin. Invest.* 118, 3143–3150. <https://doi.org/10.1172/JCI35798>

Hsieh, J.J.-D., Cheng, E.H.-Y., Korsmeyer, S.J., 2003. Taspase1: a threonine aspartase required for cleavage of MLL and proper HOX gene expression. *Cell* 115, 293–303. [https://doi.org/10.1016/s0092-8674\(03\)00816-x](https://doi.org/10.1016/s0092-8674(03)00816-x)

Hugo, W., Zaretsky, J.M., Sun, L., Song, C., Moreno, B.H., Hu-Lieskovan, S., Berent-Maoz, B., Pang, J., Chmielowski, B., Cherry, G., Seja, E., Lomeli, S., Kong, X., Kelley, M.C., Sosman, J.A., Johnson, D.B., Ribas, A., Lo, R.S., 2016. Genomic and Transcriptomic Features of Response to Anti-PD-1 Therapy in Metastatic Melanoma. *Cell* 165, 35–44. <https://doi.org/10.1016/j.cell.2016.02.065>

Hutloff, A., Dittrich, A.M., Beier, K.C., Eljaschewitsch, B., Kraft, R., Anagnostopoulos, I., Kroczeck, R.A., 1999. ICOS is an inducible T-cell co-stimulator structurally and functionally related to CD28. *Nature* 397, 263–266. <https://doi.org/10.1038/16717>

Ito, T., Hanabuchi, S., Wang, Y.-H., Park, W.R., Arima, K., Bover, L., Qin, F.X.-F., Gilliet, M., Liu, Y.-J., 2008. Two Functional Subsets of FOXP3+ Regulatory T Cells in Human Thymus and Periphery. *Immunity* 28, 870–880. <https://doi.org/10.1016/j.immuni.2008.03.018>

Ivanovs, A., Rybtsov, S., Anderson, R.A., Medvinsky, A., 2020. Vast Self-Renewal Potential of Human AGM Region HSCs Dramatically Declines in the Umbilical Cord Blood. *Stem Cell Rep.* 15, 811–816. <https://doi.org/10.1016/j.stemcr.2020.08.008>

Iwamoto, S., Mihara, K., Downing, J.R., Pui, C.-H., Campana, D., 2007. Mesenchymal cells regulate the response of acute lymphoblastic leukemia cells to asparaginase. *J. Clin. Invest.* 117, 1049–1057. <https://doi.org/10.1172/JCI30235>

Iwata, R., Lee, J.H., Hayashi, M., Dianzani, U., Ofune, K., Maruyama, M., Oe, S., Ito, T., Hashiba, T., Yoshimura, K., Nonaka, M., Nakano, Y., Norian, L., Nakano, I., Asai, A., 2019. ICOSLG-mediated regulatory T cell expansion and IL-10 production promote progression of glioblastoma. *Neuro-Oncol.* noz204. <https://doi.org/10.1093/neuonc/noz204>

Kang, H., Wilson, C.S., Harvey, R.C., Chen, I.-M., Murphy, M.H., Atlas, S.R., Bedrick, E.J., Devidas, M., Carroll, A.J., Robinson, B.W., Stam, R.W., Valsecchi, M.G., Pieters, R., Heerema, N.A., Hilden, J.M., Felix, C.A., Reaman, G.H., Camitta, B., Winick, N., Carroll, W.L., Dreyer, Z.E., Hunger, S.P., Willman, C.L., 2012. Gene expression profiles predictive of outcome and age in infant acute lymphoblastic leukemia: a Children’s Oncology Group study. *Blood* 119, 1872–1881. <https://doi.org/10.1182/blood-2011-10-382861>

Kebriaei, P., Izsvák, Z., Narayanavari, S.A., Singh, H., Ivics, Z., 2017. Gene Therapy with the Sleeping Beauty Transposon System. *Trends Genet.* 33, 852–870. <https://doi.org/10.1016/j.tig.2017.08.008>

Khapirova, E., Jardine, L., Coorens, T.H.H., Webb, S., Treger, T.D., Engelbert, J., Porter, T., Prigmore, E., Collord, G., Piapi, A., Teichmann, S.A., Inglott, S., Williams, O., Heidenreich, O., Young, M.D., Straathof, K., Bomken, S., Bartram, J., Haniffa, M., Behjati, S., 2022. Single-cell transcriptomics reveals a distinct developmental state of KMT2A-rearranged infant B-cell acute lymphoblastic leukemia. *Nat. Med.* 1–9. <https://doi.org/10.1038/s41591-022-01720-7>

Khayyamian, S., Hutloff, A., Büchner, K., Gräfe, M., Henn, V., Kroczeck, R.A., Mages, H.W., 2002. ICOS-ligand, expressed on human endothelial cells, costimulates Th1 and Th2 cytokine secretion by memory CD4+ T cells. *Proc. Natl. Acad. Sci.* 99, 6198–6203. <https://doi.org/10.1073/pnas.092576699>

Kingsley, P.D., Malik, J., Fantauzzo, K.A., Palis, J., 2004. Yolk sac-derived primitive erythroblasts enucleate during mammalian embryogenesis. *Blood* 104, 19–25. <https://doi.org/10.1182/blood-2003-12-4162>

Kissa, K., Herbomel, P., 2010. Blood stem cells emerge from aortic endothelium by a novel type of cell transition. *Nature* 464, 112–115. <https://doi.org/10.1038/nature08761>

Knapska, E., Kaczmarek, L., 2004. A gene for neuronal plasticity in the mammalian brain: Zif268/Egr-1/NGFI-A/Krox-24/TIS8/ZENK? *Prog. Neurobiol.* 74, 183–211. <https://doi.org/10.1016/j.pneurobio.2004.05.007>

Knudsen, A.M., Eilertsen, I., Kielland, S., Pedersen, M.W., Sørensen, M.D., Dahlrot, R.H., Boldt, H.B., Munthe, S., Poulsen, F.R., Kristensen, B.W., 2020. Expression and prognostic value of the transcription factors EGR1 and EGR3 in gliomas. *Sci. Rep.* 10, 9285. <https://doi.org/10.1038/s41598-020-66236-x>

Kong, Y., Yoshida, S., Saito, Y., Doi, T., Nagatoshi, Y., Fukata, M., Saito, N., Yang, S.M., Iwamoto, C., Okamura, J., Liu, K.Y., Huang, X.J., Lu, D.P., Shultz, L.D., Harada, M., Ishikawa, F., 2008. CD34+CD38+CD19+ as well as CD34+CD38-CD19+ cells are leukemia-initiating cells with self-renewal capacity in human B-precursor ALL. *Leukemia* 22, 1207–1213. <https://doi.org/10.1038/leu.2008.83>

Kornete, M., Mason, E.S., Girouard, J., Lafferty, E.I., Qureshi, S., Piccirillo, C.A., 2015. Th1-Like ICOS+ Foxp3+ Treg Cells Preferentially Express CXCR3 and Home to β -Islets during Pre-Diabetes in BDC2.5 NOD Mice. *PLOS ONE* 10, e0126311. <https://doi.org/10.1371/journal.pone.0126311>

Kornete, M., Sgouroudis, E., Piccirillo, C.A., 2012. ICOS-dependent homeostasis and function of Foxp3+ regulatory T cells in islets of nonobese diabetic mice. *J. Immunol. Baltim. Md 1950* 188, 1064–1074. <https://doi.org/10.4049/jimmunol.1101303>

Kowarz, E., Burmeister, T., Lo Nigro, L., Jansen, M.W.J.C., Delabesse, E., Klingebiel, T., Dinger, M., Meyer, C., Marschalek, R., 2007. Complex MLL rearrangements in t(4;11) leukemia patients with absent AF4.MLL fusion allele. *Leukemia* 21, 1232–1238. <https://doi.org/10.1038/sj.leu.2404686>

Kowarz, E., Löscher, D., Marschalek, R., 2015. Optimized Sleeping Beauty transposons rapidly generate stable transgenic cell lines. *Biotechnol. J.* 10, 647–653. <https://doi.org/10.1002/biot.201400821>

Kühn, A., Löscher, D., Marschalek, R., 2016. The IRX1/HOXA connection: insights into a novel t(4;11)-specific cancer mechanism. *Oncotarget* 7, 35341–35352. <https://doi.org/10.18632/oncotarget.9241>

Kühn, A.C., 2017. Untersuchung der molekularbiologischen Relevanz des Transkriptionsfaktors IRX1 im Kontext einer MLL-AF4-assoziierten Leukämie.

Kumar, A.R., Yao, Q., Li, Q., Sam, T.A., Kersey, J.H., 2011. t(4;11) leukemias display addiction to MLL-AF4 but not to AF4-MLL. *Leuk. Res.* 35, 305–309. <https://doi.org/10.1016/j.leukres.2010.08.011>

Kumar, B., Garcia, M., Weng, L., Jung, X., Murakami, J.L., Hu, X., McDonald, T., Lin, A., Kumar, A.R., DiGiusto, D.L., Stein, A.S., Pullarkat, V.A., Hui, S.K., Carlesso, N., Kuo, Y.-H., Bhatia, R., Marcucci, G., Chen, C.-C., 2018. Acute myeloid leukemia transforms the bone marrow niche into a leukemia-permissive microenvironment through exosome secretion. *Leukemia* 32, 575–587. <https://doi.org/10.1038/leu.2017.259>

Kumaravelu, P., Hook, L., Morrison, A.M., Ure, J., Zhao, S., Zuyev, S., Ansell, J., Medvinsky, A., 2002. Quantitative developmental anatomy of definitive haematopoietic stem cells/long-term repopulating units (HSC/RUs): role of the aorta-gonad-mesonephros (AGM) region and the yolk sac in colonisation of the mouse embryonic liver. *Development* 129, 4891–4899. <https://doi.org/10.1242/dev.129.21.4891>

Le, N., Nagarajan, R., Wang, J.Y.T., Svaren, J., LaPash, C., Araki, T., Schmidt, R.E., Milbrandt, J., 2005. Nab proteins are essential for peripheral nervous system myelination. *Nat. Neurosci.* 8, 932–940. <https://doi.org/10.1038/nn1490>

le Viseur, C., Hotfilder, M., Bomken, S., Wilson, K., Röttgers, S., Schrauder, A., Rosemann, A., Irving, J., Stam, R.W., Shultz, L.D., Harbott, J., Jürgens, H., Schrappe, M., Pieters, R., Vormoor, J., 2008. In childhood acute lymphoblastic leukemia, blasts at different stages of immunophenotypic maturation have stem cell properties. *Cancer Cell* 14, 47–58. <https://doi.org/10.1016/j.ccr.2008.05.015>

- Lee, H.-J., Kim, S.-N., Jeon, M.-S., Yi, T., Song, S.U., 2017. ICOSL expression in human bone marrow-derived mesenchymal stem cells promotes induction of regulatory T cells. *Sci. Rep.* 7, 44486. <https://doi.org/10.1038/srep44486>
- Lengauer, C., 2001. How do tumors make ends meet? *Proc. Natl. Acad. Sci.* 98, 12331–12333. <https://doi.org/10.1073/pnas.231485898>
- Li, B., Brady, S.W., Ma, X., Shen, S., Zhang, Y., Li, Y., Szlachta, K., Dong, L., Liu, Yu, Yang, F., Wang, N., Flasch, D.A., Myers, M.A., Mulder, H.L., Ding, L., Liu, Yanling, Tian, L., Hagiwara, K., Xu, K., Zhou, X., Sioson, E., Wang, T., Yang, L., Zhao, J., Zhang, H., Shao, Y., Sun, H., Sun, L., Cai, J., Sun, H.-Y., Lin, T.-N., Du, L., Li, H., Rusch, M., Edmonson, M.N., Easton, J., Zhu, X., Zhang, Jingliao, Cheng, C., Raphael, B.J., Tang, J., Downing, J.R., Alexandrov, L.B., Zhou, B.-B.S., Pui, C.-H., Yang, J.J., Zhang, Jinghui, 2020. Therapy-induced mutations drive the genomic landscape of relapsed acute lymphoblastic leukemia. *Blood* 135, 41–55. <https://doi.org/10.1182/blood.2019002220>
- Li, D.-Y., Xiong, X.-Z., 2020. ICOS+ Tregs: A Functional Subset of Tregs in Immune Diseases. *Front. Immunol.* 11, 2104. <https://doi.org/10.3389/fimmu.2020.02104>
- Li, S., Miao, T., Sebastian, M., Bhullar, P., Ghaffari, E., Liu, M., Symonds, A.L.J., Wang, P., 2012. The Transcription Factors Egr2 and Egr3 Are Essential for the Control of Inflammation and Antigen-Induced Proliferation of B and T Cells. *Immunity* 37, 685–696. <https://doi.org/10.1016/j.immuni.2012.08.001>
- Li, S., Symonds, A.L.J., Zhu, B., Liu, M., Raymond, M.V., Miao, T., Wang, P., 2011. Early Growth Response Gene-2 (Egr-2) Regulates the Development of B and T Cells. *PLOS ONE* 6, e18498. <https://doi.org/10.1371/journal.pone.0018498>
- Li, Y., Rong, G., Kang, H., 2017. Taxotere-induced elevated expression of IL8 in carcinoma-associated fibroblasts of breast invasive ductal cancer. *Oncol. Lett.* 13, 1856–1860. <https://doi.org/10.3892/ol.2017.5612>
- Li, Z., Lan, Y., He, W., Chen, D., Wang, J., Zhou, F., Wang, Y., Sun, H., Chen, X., Xu, C., Li, S., Pang, Y., Zhang, G., Yang, L., Zhu, L., Fan, M., Shang, A., Ju, Z., Luo, L., Ding, Y., Guo, W., Yuan, W., Yang, X., Liu, B., 2012. Mouse embryonic head as a site for hematopoietic stem cell development. *Cell Stem Cell* 11, 663–675. <https://doi.org/10.1016/j.stem.2012.07.004>
- Lin, C., Smith, E.R., Takahashi, H., Lai, K.C., Martin-Brown, S., Florens, L., Washburn, M.P., Conaway, J.W., Conaway, R.C., Shilatifard, A., 2010. AFF4, a Component of the ELL/P-TEFb Elongation Complex and a Shared Subunit of MLL Chimeras, Can Link Transcription Elongation to Leukemia. *Mol. Cell* 37, 429–437. <https://doi.org/10.1016/j.molcel.2010.01.026>
- Lin, J.T., Kornhauser, J.M., Singh, N.P., Mayo, K.E., Takahashi, J.S., 1997. Visual sensitivities of nur77 (NGFI-B) and zif268 (NGFI-A) induction in the suprachiasmatic nucleus are dissociated from c-fos induction and behavioral phase-shifting responses. *Mol. Brain Res.* 46, 303–310. [https://doi.org/10.1016/S0169-328X\(97\)00005-3](https://doi.org/10.1016/S0169-328X(97)00005-3)
- Linden, M.H. van der, Boer, J.M., Schneider, P., Willekes, M., Seslija, L., Lorenzo, P.D., Valsecchi, M.G., Cazzaniga, G., Biondi, A., Boer, M.L. den, Pieters, R., Stam, R.W., 2016. Clinical and molecular genetic characterization of wild-type MLL infant acute lymphoblastic leukemia identifies few recurrent abnormalities. *Haematologica* 101, e95–e99. <https://doi.org/10.3324/haematol.2014.122119>
- Luo, Z., Lin, C., Shilatifard, A., 2012. The super elongation complex (SEC) family in transcriptional control. *Nat. Rev. Mol. Cell Biol.* 13, 543–547. <https://doi.org/10.1038/nrm3417>
- Manente, A.G., Pinton, G., Tavian, D., Lopez-Rodas, G., Brunelli, E., Moro, L., 2011. Coordinated Sumoylation and Ubiquitination Modulate EGF Induced EGR1 Expression and Stability. *PLoS ONE* 6, e25676. <https://doi.org/10.1371/journal.pone.0025676>

Mann, G., Attarbaschi, A., Schrappe, M., De Lorenzo, P., Peters, C., Hann, I., De Rossi, G., Felice, M., Lausen, B., Leblanc, T., Szczepanski, T., Ferster, A., Janka-Schaub, G., Rubnitz, J., Silverman, L.B., Stary, J., Campbell, M., Li, C.K., Suppiah, R., Biondi, A., Vora, A., Valsecchi, M.G., Pieters, R., Interfant-99 Study Group, 2010. Improved outcome with hematopoietic stem cell transplantation in a poor prognostic subgroup of infants with mixed-lineage-leukemia (MLL)-rearranged acute lymphoblastic leukemia: results from the Interfant-99 Study. *Blood* 116, 2644–2650. <https://doi.org/10.1182/blood-2010-03-273532>

Mariette, X., Bombardieri, M., Alevizos, I., Moate, R., Sullivan, B., Noaiseh, G., Kvarnström, M., Rees, W., Wang, L., Illei, G., 2019. A Phase 2a Study of MEDI5872 (AMG557), a Fully Human Anti-ICOS Ligand Monoclonal Antibody in Patients with Primary Sjögren’s Syndrome. *ACR Meet. Abstr.* URL <https://acrabstracts.org/abstract/a-phase-2a-study-of-medi5872-amg557-a-fully-human-anti-icos-ligand-monoclonal-antibody-in-patients-with-primary-sjogrens-syndrome/> (accessed 1.25.22).

Marlein, C.R., Zaitseva, L., Piddock, R.E., Robinson, S.D., Edwards, D.R., Shafat, M.S., Zhou, Z., Lawes, M., Bowles, K.M., Rushworth, S.A., 2017. NADPH oxidase-2 derived superoxide drives mitochondrial transfer from bone marrow stromal cells to leukemic blasts. *Blood* 130, 1649–1660. <https://doi.org/10.1182/blood-2017-03-772939>

Marschalek, R., 2011. Mechanisms of leukemogenesis by MLL fusion proteins. *Br. J. Haematol.* 152, 141–154. <https://doi.org/10.1111/j.1365-2141.2010.08459.x>

Martin-Orozco, N., Li, Y., Wang, Y., Liu, S., Hwu, P., Liu, Y.-J., Dong, C., Radvanyi, L., 2010. Melanoma Cells Express ICOS Ligand to Promote the Activation and Expansion of T-Regulatory Cells. *Cancer Res.* 70, 9581–9590. <https://doi.org/10.1158/0008-5472.CAN-10-1379>

Maude, S.L., Laetsch, T.W., Buechner, J., Rives, S., Boyer, M., Bittencourt, H., Bader, P., Verneris, M.R., Stefanski, H.E., Myers, G.D., Qayed, M., De Moerloose, B., Hiramatsu, H., Schlis, K., Davis, K.L., Martin, P.L., Nemecek, E.R., Yanik, G.A., Peters, C., Baruchel, A., Boissel, N., Mechinaud, F., Balduzzi, A., Krueger, J., June, C.H., Levine, B.L., Wood, P., Taran, T., Leung, M., Mueller, K.T., Zhang, Y., Sen, K., Leblwohl, D., Pulsipher, M.A., Grupp, S.A., 2018. Tisagenlecleucel in Children and Young Adults with B-Cell Lymphoblastic Leukemia. *N. Engl. J. Med.* 378, 439–448. <https://doi.org/10.1056/NEJMoa1709866>

Maurer, D.M., Adamik, J., Santos, P.M., Shi, J., Shurin, M.R., Kirkwood, J.M., Storkus, W.J., Butterfield, L.H., 2020. Dysregulated NF-κB–Dependent ICOSL Expression in Human Dendritic Cell Vaccines Impairs T-cell Responses in Patients with Melanoma. *Cancer Immunol. Res.* 8, 1554–1567. <https://doi.org/10.1158/2326-6066.CIR-20-0274>

Maynard, C.L., Harrington, L.E., Janowski, K.M., Oliver, J.R., Zindl, C.L., Rudensky, A.Y., Weaver, C.T., 2007. Regulatory T cells expressing interleukin 10 develop from Foxp3+ and Foxp3- precursor cells in the absence of interleukin 10. *Nat. Immunol.* 8, 931–941. <https://doi.org/10.1038/ni1504>

McGrath, K.E., Frame, J.M., Fegan, K.H., Bowen, J.R., Conway, S.J., Catherman, S.C., Kingsley, P.D., Koniski, A.D., Palis, J., 2015. Distinct Sources of Hematopoietic Progenitors Emerge before HSCs and Provide Functional Blood Cells in the Mammalian Embryo. *Cell Rep.* 11, 1892–1904. <https://doi.org/10.1016/j.celrep.2015.05.036>

Medvinsky, A., Dzierzak, E., 1996. Definitive Hematopoiesis Is Autonomously Initiated by the AGM Region. *Cell* 86, 897–906. [https://doi.org/10.1016/S0092-8674\(00\)80165-8](https://doi.org/10.1016/S0092-8674(00)80165-8)

Medyouf, H., 2017. The microenvironment in human myeloid malignancies: emerging concepts and therapeutic implications. *Blood* 129, 1617–1626. <https://doi.org/10.1182/blood-2016-11-696070>

Mejstříková, E., Hrusak, O., Borowitz, M.J., Whitlock, J.A., Brethon, B., Trippett, T.M., Zugmaier, G., Gore, L., von Stackelberg, A., Locatelli, F., 2017. CD19-negative relapse of pediatric B-cell precursor acute lymphoblastic leukemia following blinatumomab treatment. *Blood Cancer J.* 7, 659. <https://doi.org/10.1038/s41408-017-0023-x>

- Menendez, P., Catalina, P., Rodríguez, R., Melen, G.J., Bueno, C., Arriero, M., García-Sánchez, F., Las-saletta, A., García-Sanz, R., García-Castro, J., 2009. Bone marrow mesenchymal stem cells from infants with MLL-AF4+ acute leukemia harbor and express the MLL-AF4 fusion gene. *J. Exp. Med.* 206, 3131–3141. <https://doi.org/10.1084/jem.20091050>
- Metsalu, T., Vilo, J., 2015. ClustVis: a web tool for visualizing clustering of multivariate data using Principal Component Analysis and heatmap. *Nucleic Acids Res.* 43, W566-570. <https://doi.org/10.1093/nar/gkv468>
- Meyer, C., Burmeister, T., Gröger, D., Tsauro, G., Fechina, L., Renneville, A., Sutton, R., Venn, N.C., Emerenciano, M., Pombo-de-Oliveira, M.S., Barbieri Blunck, C., Almeida Lopes, B., Zuna, J., Trka, J., Ballerini, P., Lapillonne, H., De Braekeleer, M., Cazzaniga, G., Corral Abascal, L., van der Velden, V.H.J., Delabesse, E., Park, T.S., Oh, S.H., Silva, M.L.M., Lund-Aho, T., Juvonen, V., Moore, A.S., Heidenreich, O., Vormoor, J., Zerkalenkova, E., Olshanskaya, Y., Bueno, C., Menendez, P., Teigler-Schlegel, A., zur Stadt, U., Lentès, J., Göhring, G., Kustanovich, A., Aleinikova, O., Schäfer, B.W., Kubetzko, S., Madsen, H.O., Gruhn, B., Duarte, X., Gameiro, P., Lippert, E., Bidet, A., Cayuela, J.M., Clappier, E., Alonso, C.N., Zwaan, C.M., van den Heuvel-Eibrink, M.M., Izraeli, S., Trakhtenbrot, L., Archer, P., Hancock, J., Möricke, A., Alten, J., Schrappe, M., Stanulla, M., Strehl, S., Attarbaschi, A., Dworzak, M., Haas, O.A., Panzer-Grümayer, R., Sedék, L., Szczepański, T., Caye, A., Suarez, L., Cavé, H., Marschalek, R., 2018. The MLL recombinome of acute leukemias in 2017. *Leukemia* 32, 273–284. <https://doi.org/10.1038/leu.2017.213>
- Milne, T.A., 2017. Mouse models of MLL leukemia: recapitulating the human disease. *Blood* 129, 2217–2223. <https://doi.org/10.1182/blood-2016-10-691428>
- Milne, T.A., Briggs, S.D., Brock, H.W., Martin, M.E., Gibbs, D., Allis, C.D., Hess, J.L., 2002. MLL Targets SET Domain Methyltransferase Activity to Hox Gene Promoters. *Mol. Cell* 10, 1107–1117. [https://doi.org/10.1016/S1097-2765\(02\)00741-4](https://doi.org/10.1016/S1097-2765(02)00741-4)
- Milne, T.A., Kim, J., Wang, G.G., Stadler, S.C., Basrur, V., Whitcomb, S.J., Wang, Z., Ruthenburg, A.J., Elenitoba-Johnson, K.S.J., Roeder, R.G., Allis, C.D., 2010. Multiple interactions recruit MLL1 and MLL1 fusion proteins to the HOXA9 locus in leukemogenesis. *Mol. Cell* 38, 853–863. <https://doi.org/10.1016/j.molcel.2010.05.011>
- Min, I.M., Pietramaggiore, G., Kim, F.S., Passequé, E., Stevenson, K.E., Wagers, A.J., 2008. The Transcription Factor EGR1 Controls Both the Proliferation and Localization of Hematopoietic Stem Cells. *Cell Stem Cell* 2, 380–391. <https://doi.org/10.1016/j.stem.2008.01.015>
- Mittelstadt, P.R., Ashwell, J.D., 1999. Role of Egr-2 in Up-regulation of Fas Ligand in Normal T Cells and Aberrant Double-negative Ipr and gld T Cells *. *J. Biol. Chem.* 274, 3222–3227. <https://doi.org/10.1074/jbc.274.5.3222>
- Mittelstadt, P.R., Ashwell, J.D., 1998. Cyclosporin A-sensitive transcription factor Egr-3 regulates Fas ligand expression. *Mol. Cell. Biol.* 18, 3744–3751. <https://doi.org/10.1128/MCB.18.7.3744>
- Mold, J.E., Venkatasubrahmanyam, S., Burt, T.D., Michaëlsson, J., Rivera, J.M., Galkina, S.A., Weinberg, K., Stoddart, C.A., McCune, J.M., 2010. Fetal and Adult Hematopoietic Stem Cells Give Rise to Distinct T Cell Lineages in Humans. *Science* 330, 1695–1699. <https://doi.org/10.1126/science.1196509>
- Morrison, S.J., Scadden, D.T., 2014. The bone marrow niche for haematopoietic stem cells. *Nature* 505, 327–334. <https://doi.org/10.1038/nature12984>
- Morrison, S.J., Uchida, N., Weissman, I.L., 1995. The biology of hematopoietic stem cells. *Annu. Rev. Cell Dev. Biol.* 11, 35–71. <https://doi.org/10.1146/annurev.cb.11.110195.000343>
- Moudgil, A., Wilkinson, M.N., Chen, X., He, J., Cammack, A.J., Vasek, M.J., Lagunas, T., Qi, Z., Lalli, M.A., Guo, C., Morris, S.A., Dougherty, J.D., Mitra, R.D., 2020. Self-Reporting Transposons Enable

Simultaneous Readout of Gene Expression and Transcription Factor Binding in Single Cells. *Cell* 182, 992–1008.e21. <https://doi.org/10.1016/j.cell.2020.06.037>

Mrózek, K., Heerema, N.A., Bloomfield, C.D., 2004. Cytogenetics in acute leukemia. *Blood Rev.* 18, 115–136. [https://doi.org/10.1016/S0268-960X\(03\)00040-7](https://doi.org/10.1016/S0268-960X(03)00040-7)

Müller, A.M., Medvinsky, A., Strouboulis, J., Grosveld, F., Dzierzakt, E., 1994. Development of hematopoietic stem cell activity in the mouse embryo. *Immunity* 1, 291–301. [https://doi.org/10.1016/1074-7613\(94\)90081-7](https://doi.org/10.1016/1074-7613(94)90081-7)

Mullighan, C.G., Goorha, S., Radtke, I., Miller, C.B., Coustan-Smith, E., Dalton, J.D., Girtman, K., Mathew, S., Ma, J., Pounds, S.B., Su, X., Pui, C.-H., Relling, M.V., Evans, W.E., Shurtleff, S.A., Downing, J.R., 2007. Genome-wide analysis of genetic alterations in acute lymphoblastic leukaemia. *Nature* 446, 758–764. <https://doi.org/10.1038/nature05690>

Muntean, A.G., Tan, J., Sitwala, K., Huang, Y., Bronstein, J., Connelly, J.A., Basrur, V., Elenitoba-Johnson, K.S.J., Hess, J.L., 2010. The PAF complex synergizes with MLL fusion proteins at HOX loci to promote leukemogenesis. *Cancer Cell* 17, 609–621. <https://doi.org/10.1016/j.ccr.2010.04.012>

Nakamura, T., Mori, T., Tada, S., Krajewski, W., Rozovskaia, T., Wassell, R., Dubois, G., Mazo, A., Croce, C.M., Canaani, E., 2002. ALL-1 Is a Histone Methyltransferase that Assembles a Supercomplex of Proteins Involved in Transcriptional Regulation. *Mol. Cell* 10, 1119–1128. [https://doi.org/10.1016/S1097-2765\(02\)00740-2](https://doi.org/10.1016/S1097-2765(02)00740-2)

Nguyen, A.T., Taranova, O., He, J., Zhang, Y., 2011. DOT1L, the H3K79 methyltransferase, is required for MLL-AF9-mediated leukemogenesis. *Blood* 117, 6912–6922. <https://doi.org/10.1182/blood-2011-02-334359>

Notta, F., Zandi, S., Takayama, N., Dobson, S., Gan, O.I., Wilson, G., Kaufmann, K.B., McLeod, J., Laurenti, E., Dunant, C.F., McPherson, J.D., Stein, L.D., Dror, Y., Dick, J.E., 2016. Distinct routes of lineage development reshape the human blood hierarchy across ontogeny. *Science* 351, aab2116. <https://doi.org/10.1126/science.aab2116>

O’Brien, M.M., Ji, L., Shah, N.N., Rheingold, S.R., Bhojwani, D., Yuan, C.M., Xu, X., Yi, J.S., Harris, A.C., Brown, P.A., Borowitz, M.J., Militano, O., Kairalla, J., Devidas, M., Raetz, E.A., Gore, L., Loh, M.L., 2022. Phase II Trial of Inotuzumab Ozogamicin in Children and Adolescents With Relapsed or Refractory B-Cell Acute Lymphoblastic Leukemia: Children’s Oncology Group Protocol AALL1621. *J. Clin. Oncol. Off. J. Am. Soc. Clin. Oncol.* 40, 956–967. <https://doi.org/10.1200/JCO.21.01693>

O’Donovan, K.J., Levkovitz, Y., Ahn, D., Baraban, J.M., 2000. Functional Comparison of Egr3 Transcription Factor Isoforms. *J. Neurochem.* 75, 1352–1357. <https://doi.org/10.1046/j.1471-4159.2000.0751352.x>

Okkenhaug, K., Vanhaesebroeck, B., 2003. PI3K in lymphocyte development, differentiation and activation. *Nat. Rev. Immunol.* 3, 317–330. <https://doi.org/10.1038/nri1056>

Okuda, H., Kanai, A., Ito, S., Matsui, H., Yokoyama, A., 2015. AF4 uses the SL1 components of RNAP1 machinery to initiate MLL fusion- and AEP-dependent transcription. *Nat. Commun.* 6, 8869. <https://doi.org/10.1038/ncomms9869>

Osmond, D.G., 1994. Production and selection of B lymphocytes in bone marrow: lymphostromal interactions and apoptosis in normal, mutant and transgenic mice. *Adv. Exp. Med. Biol.* 355, 15–20. https://doi.org/10.1007/978-1-4615-2492-2_3

Ottersbach, K., 2019. Endothelial-to-haematopoietic transition: an update on the process of making blood. *Biochem. Soc. Trans.* 47, 591–601. <https://doi.org/10.1042/BST20180320>

Ottersbach, K., Dzierzak, E., 2005. The murine placenta contains hematopoietic stem cells within the vascular labyrinth region. *Dev. Cell* 8, 377–387. <https://doi.org/10.1016/j.devcel.2005.02.001>

Palis, J., 2014. Primitive and definitive erythropoiesis in mammals. *Front. Physiol.* 5.

Palis, J., Robertson, S., Kennedy, M., Wall, C., Keller, G., 1999. Development of erythroid and myeloid progenitors in the yolk sac and embryo proper of the mouse. *Dev. Camb. Engl.* 126, 5073–5084. <https://doi.org/10.1242/dev.126.22.5073>

Park, S., Osmer, U., Raman, G., Schwantes, R.H., Diaz, M.O., Bushweller, J.H., 2010. The PHD3 domain of MLL acts as a CYP33-regulated switch between MLL-mediated activation and repression. *Biochemistry* 49, 6576–6586. <https://doi.org/10.1021/bi1009387>

Parkinson, R.M., Collins, S.L., Horton, M.R., Powell, J.D., 2014. Egr3 Induces a Th17 Response by Promoting the Development of $\gamma\delta$ T Cells. *PLOS ONE* 9, e87265. <https://doi.org/10.1371/journal.pone.0087265>

Pastorczyk, A., Domka, K., Fidyk, K., Poprzeczko, M., Firczuk, M., 2021. Mechanisms of Immune Evasion in Acute Lymphoblastic Leukemia. *Cancers* 13, 1536. <https://doi.org/10.3390/cancers13071536>

Patel, A., Dharmarajan, V., Vought, V.E., Cosgrove, M.S., 2009. On the Mechanism of Multiple Lysine Methylation by the Human Mixed Lineage Leukemia Protein-1 (MLL1) Core Complex*♦. *J. Biol. Chem.* 284, 24242–24256. <https://doi.org/10.1074/jbc.M109.014498>

Perner, F., Gadrey, J.Y., Xiong, Y., Hatton, C., Eschle, B.K., Weiss, A., Stauffer, F., Gaul, C., Tiedt, R., Perry, J.A., Armstrong, S.A., Krivtsov, A.V., 2020. Novel inhibitors of the histone methyltransferase DOT1L show potent antileukemic activity in patient-derived xenografts. *Blood* 136, 1983–1988. <https://doi.org/10.1182/blood.2020006113>

Petroff, M.G., Kharatyan, E., Torry, D.S., Holets, L., 2005. The immunomodulatory proteins B7-DC, B7-H2, and B7-H3 are differentially expressed across gestation in the human placenta. *Am. J. Pathol.* 167, 465–473. [https://doi.org/10.1016/S0002-9440\(10\)62990-2](https://doi.org/10.1016/S0002-9440(10)62990-2)

Pierson, W., Cauwe, B., Policheni, A., Schlenner, S.M., Franckaert, D., Berges, J., Humblet-Baron, S., Schönefeldt, S., Herold, M.J., Hildeman, D., Strasser, A., Bouillet, P., Lu, L.-F., Matthys, P., Freitas, A.A., Luther, R.J., Weaver, C.T., Dooley, J., Gray, D.H.D., Liston, A., 2013. Antiapoptotic Mcl-1 is critical for the survival and niche-filling capacity of Foxp3⁺ regulatory T cells. *Nat. Immunol.* 14, 959–965. <https://doi.org/10.1038/ni.2649>

Pieters, R., De Lorenzo, P., Ancliffe, P., Aversa, L.A., Brethon, B., Biondi, A., Campbell, M., Escherich, G., Ferster, A., Gardner, R.A., Kotecha, R.S., Lausen, B., Li, C.K., Locatelli, F., Attarbaschi, A., Peters, C., Rubnitz, J.E., Silverman, L.B., Stary, J., Szczepanski, T., Vora, A., Schrappe, M., Valsecchi, M.G., 2019. Outcome of Infants Younger Than 1 Year With Acute Lymphoblastic Leukemia Treated With the Interfant-06 Protocol: Results From an International Phase III Randomized Study. *J. Clin. Oncol. Off. J. Am. Soc. Clin. Oncol.* 37, 2246–2256. <https://doi.org/10.1200/JCO.19.00261>

Pieters, R., Schrappe, M., De Lorenzo, P., Hann, I., De Rossi, G., Felice, M., Hovi, L., LeBlanc, T., Szczepanski, T., Ferster, A., Janka, G., Rubnitz, J., Silverman, L., Stary, J., Campbell, M., Li, C.-K., Mann, G., Suppiah, R., Biondi, A., Vora, A., Valsecchi, M.G., 2007. A treatment protocol for infants younger than 1 year with acute lymphoblastic leukaemia (Interfant-99): an observational study and a multicentre randomised trial. *Lancet Lond. Engl.* 370, 240–250. [https://doi.org/10.1016/S0140-6736\(07\)61126-X](https://doi.org/10.1016/S0140-6736(07)61126-X)

Pinho, S., Frenette, P.S., 2019. Haematopoietic stem cell activity and interactions with the niche. *Nat. Rev. Mol. Cell Biol.* 20, 303–320. <https://doi.org/10.1038/s41580-019-0103-9>

Pokholok, D.K., Harbison, C.T., Levine, S., Cole, M., Hannett, N.M., Lee, T.I., Bell, G.W., Walker, K., Rolfe, P.A., Herbolzheimer, E., Zeitlinger, J., Lewitter, F., Gifford, D.K., Young, R.A., 2005. Genome-wide Map of Nucleosome Acetylation and Methylation in Yeast. *Cell* 122, 517–527. <https://doi.org/10.1016/j.cell.2005.06.026>

Pontarini, E., Verstappen, G.M., Grigoriadou, S., Kroese, F.G.M., Bootsma, H., Bombardieri, M., 2020. Blocking T cell co-stimulation in primary Sjögren's syndrome: rationale, clinical efficacy and modulation of peripheral and salivary gland biomarkers. *Clin. Exp. Rheumatol.* 38 Suppl 126, 222–227.

Prange, K.H.M., Mandoli, A., Kuznetsova, T., Wang, S.-Y., Sotoca, A.M., Marneth, A.E., van der Reijden, B.A., Stunnenberg, H.G., Martens, J.H.A., 2017. MLL-AF9 and MLL-AF4 oncofusion proteins bind a distinct enhancer repertoire and target the RUNX1 program in 11q23 acute myeloid leukemia. *Oncogene* 36, 3346–3356. <https://doi.org/10.1038/onc.2016.488>

Prelich, G., 2012. Gene Overexpression: Uses, Mechanisms, and Interpretation. *Genetics* 190, 841–854. <https://doi.org/10.1534/genetics.111.136911>

Prelle, C., Bursen, A., Dingeramn, T., Marschalek, R., 2013. Secondary mutations in t(4;11) leukemia patients. *Leukemia* 27, 1425–1427. <https://doi.org/10.1038/leu.2012.365>

Prieto, C., Marschalek, R., Kühn, A., Bursen, A., Bueno, C., Menéndez, P., 2017. The AF4-MLL fusion transiently augments multilineage hematopoietic engraftment but is not sufficient to initiate leukemia in cord blood CD34+ cells. *Oncotarget* 8, 81936–81941. <https://doi.org/10.18632/oncotarget.19567>

Qasim, W., Zhan, H., Samarasinghe, S., Adams, S., Amrolia, P., Stafford, S., Butler, K., Rivat, C., Wright, G., Somana, K., Ghorashian, S., Pinner, D., Ahsan, G., Gilmour, K., Lucchini, G., Inglott, S., Mifsud, W., Chiesa, R., Peggs, K.S., Chan, L., Farzeneh, F., Thrasher, A.J., Vora, A., Pule, M., Veys, P., 2017. Molecular remission of infant B-ALL after infusion of universal TALEN gene-edited CAR T cells. *Sci. Transl. Med.* 9, eaaj2013. <https://doi.org/10.1126/scitranslmed.aaj2013>

Quessada, J., Cucchini, W., Saultier, P., Loosveld, M., Harrison, C.J., Lafage-Pochitaloff, M., 2021. Cytogenetics of Pediatric Acute Myeloid Leukemia: A Review of the Current Knowledge. *Genes* 12, 924. <https://doi.org/10.3390/genes12060924>

Raineri, D., Dianzani, C., Cappellano, G., Maione, F., Baldanzi, G., Iacobucci, I., Clemente, N., Baldone, G., Boggio, E., Gigliotti, C.L., Boldorini, R., Rojo, J.M., Monti, M., Birolo, L., Dianzani, U., Chiocchetti, A., 2020. Osteopontin binds ICOSL promoting tumor metastasis. *Commun. Biol.* 3, 1–15. <https://doi.org/10.1038/s42003-020-01333-1>

Ramakers-van Woerden, N.L., Beverloo, H.B., Veerman, A.J.P., Camitta, B.M., Loonen, A.H., van Wering, E.R., Slater, R.M., Harbott, J., den Boer, M.L., Ludwig, W.D., Haas, O.A., Janka-Schaub, G.E., Pieters, R., 2004. In vitro drug-resistance profile in infant acute lymphoblastic leukemia in relation to age, MLL rearrangements and immunophenotype. *Leukemia* 18, 521–529. <https://doi.org/10.1038/sj.leu.2403253>

Rayes, A., McMasters, R.L., O'Brien, M.M., 2016. Lineage Switch in MLL-Rearranged Infant Leukemia Following CD19-Directed Therapy. *Pediatr. Blood Cancer* 63, 1113–1115. <https://doi.org/10.1002/pbc.25953>

Reichel, M., Gillert, E., Angermüller, S., Hensel, J.P., Heidel, F., Lode, M., Leis, T., Biondi, A., Haas, O.A., Strehl, S., Panzer-Grümayer, E.R., Griesinger, F., Beck, J.D., Greil, J., Fey, G.H., Uckun, F.M., Marschalek, R., 2001. Biased distribution of chromosomal breakpoints involving the MLL gene in infants versus children and adults with t(4;11) ALL. *Oncogene* 20, 2900–2907. <https://doi.org/10.1038/sj.onc.1204401>

Reichel, M., Gillert, E., Nilson, I., Siegler, G., Greil, J., Fey, G.H., Marschalek, R., 1998. Fine structure of translocation breakpoints in leukemic blasts with chromosomal translocation t(4;11): the DNA damage-repair model of translocation. *Oncogene* 17, 3035–3044. <https://doi.org/10.1038/sj.onc.1202229>

Rice, S., Jackson, T., Crump, N.T., Fordham, N., Elliott, N., O'Byrne, S., Fanego, M. del M.L., Addy, D., Crabb, T., Dryden, C., Inglott, S., Ladon, D., Wright, G., Bartram, J., Ancliff, P., Mead, A.J., Halsey, C., Roberts, I., Milne, T.A., Roy, A., 2021. A human fetal liver-derived infant MLL-AF4 acute lymphoblastic leukemia model reveals a distinct fetal gene expression program. *Nat. Commun.* 12, 6905. <https://doi.org/10.1038/s41467-021-27270-z>

- Rice, S., Roy, A., 2020. MLL-rearranged infant leukaemia: A “thorn in the side” of a remarkable success story. *Biochim. Biophys. Acta Gene Regul. Mech.* 1863, 194564. <https://doi.org/10.1016/j.bbagr.2020.194564>
- Riddick, G., Kotliarova, S., Rodriguez, V., Kim, H.S., Linkous, A., Storaska, A.J., Ahn, S., Walling, J., Belova, G., Fine, H.A., 2017. A Core Regulatory Circuit in Glioblastoma Stem Cells Links MAPK Activation to a Transcriptional Program of Neural Stem Cell Identity. *Sci. Rep.* 7, 43605. <https://doi.org/10.1038/srep43605>
- Riella, L.V., Dada, S., Chabtini, L., Smith, B., Huang, L., Dakle, P., Mfarrej, B., D’Addio, F., Adams, L.-T., Kochupurakkal, N., Vergani, A., Fiorina, P., Mellor, A.L., Sharpe, A.H., Yagita, H., Guleria, I., 2013. B7h (ICOS-L) Maintains Tolerance at the Fetomaternal Interface. *Am. J. Pathol.* 182, 2204–2213. <https://doi.org/10.1016/j.ajpath.2013.02.014>
- Rizvi, N.A., Hellmann, M.D., Snyder, A., Kvistborg, P., Makarov, V., Havel, J.J., Lee, W., Yuan, J., Wong, P., Ho, T.S., Miller, M.L., Rekhtman, N., Moreira, A.L., Ibrahim, F., Bruggeman, C., Gasmir, B., Zappasodi, R., Maeda, Y., Sander, C., Garon, E.B., Merghoub, T., Wolchok, J.D., Schumacher, T.N., Chan, T.A., 2015. Mutational landscape determines sensitivity to PD-1 blockade in non-small cell lung cancer. *Science* 348, 124–128. <https://doi.org/10.1126/science.aaa1348>
- Roelf, C., Richter, A., Konkolefski, C., Knuebel, G., Sekora, A., Krohn, S., Stenzel, J., Krause, B.J., Vollmar, B., Murua Escobar, H., Junghanss, C., 2018. Decitabine demonstrates antileukemic activity in B cell precursor acute lymphoblastic leukemia with MLL rearrangements. *J. Hematol. Oncol.* 11, 62. <https://doi.org/10.1186/s13045-018-0607-3>
- Ropero, S., Esteller, M., 2007. The role of histone deacetylases (HDACs) in human cancer. *Mol. Oncol.* 1, 19–25. <https://doi.org/10.1016/j.molonc.2007.01.001>
- Rössler, T., Marschalek, R., 2013. An alternative splice process renders the MLL protein either into a transcriptional activator or repressor. *Pharm.* 68, 601–607. <https://doi.org/10.1055/s-0033-1343653>
- Rozovskaia, T., Feinstein, E., Mor, O., Foa, R., Blechman, J., Nakamura, T., Croce, C.M., Cimino, G., Canaani, E., 2001. Upregulation of Meis1 and HoxA9 in acute lymphocytic leukemias with the t(4 : 11) abnormality. *Oncogene* 20, 874–878. <https://doi.org/10.1038/sj.onc.1204174>
- Rudensky, A.Y., Gavin, M., Zheng, Y., 2006. FOXP3 and NFAT: partners in tolerance. *Cell* 126, 253–256. <https://doi.org/10.1016/j.cell.2006.07.005>
- Russo, M.W., Severson, B.R., Milbrandt, J., 1995. Identification of NAB1, a repressor of NGFI-A- and Krox20-mediated transcription. *Proc. Natl. Acad. Sci. U. S. A.* 92, 6873–6877. <https://doi.org/10.1073/pnas.92.15.6873>
- Sabiani, S., Geppert, T., Engelbrecht, C., Kowarz, E., Schneider, G., Marschalek, R., 2015. Unraveling the Activation Mechanism of Taspase1 which Controls the Oncogenic AF4-MLL Fusion Protein. *EBioMedicine* 2, 386–395. <https://doi.org/10.1016/j.ebiom.2015.04.009>
- Safford, M., Collins, S., Lutz, M.A., Allen, A., Huang, C.-T., Kowalski, J., Blackford, A., Horton, M.R., Drake, C., Schwartz, R.H., Powell, J.D., 2005. Egr-2 and Egr-3 are negative regulators of T cell activation. *Nat. Immunol.* 6, 472–480. <https://doi.org/10.1038/ni1193>
- Saito, K., Zhang, Q., Yang, H., Yamatani, K., Ai, T., Ruvolo, V., Baran, N., Cai, T., Ma, H., Jacamo, R., Kuruvilla, V., Imoto, J., Kinjo, S., Ikeo, K., Moriya, K., Suzuki, K., Miida, T., Kim, Y.-M., Vellano, C.P., Andreeff, M., Marszalek, J.R., Tabe, Y., Konopleva, M., 2021. Exogenous mitochondrial transfer and endogenous mitochondrial fission facilitate AML resistance to OxPhos inhibition. *Blood Adv.* 5, 4233–4255. <https://doi.org/10.1182/bloodadvances.2020003661>
- Sakakini, N., Turchi, L., Bergon, A., Holota, H., Rekima, S., Lopez, F., Paquis, P., Almairac, F., Fontaine, D., Baeza-Kallee, N., Van Obberghen-Schilling, E., Junier, M.-P., Chneiweiss, H., Figarella-Branger, D.,

Burel-Vandenbos, F., Imbert, J., Virolle, T., 2016. A Positive Feed-forward Loop Associating EGR1 and PDGFA Promotes Proliferation and Self-renewal in Glioblastoma Stem Cells. *J. Biol. Chem.* 291, 10684–10699. <https://doi.org/10.1074/jbc.M116.720698>

Salvany-Celades, M., van der Zwan, A., Benner, M., Setrajcic-Dragos, V., Bougleux Gomes, H.A., Iyer, V., Norwitz, E.R., Strominger, J.L., Tilburgs, T., 2019. Three Types of Functional Regulatory T Cells Control T Cell Responses at the Human Maternal-Fetal Interface. *Cell Rep.* 27, 2537-2547.e5. <https://doi.org/10.1016/j.celrep.2019.04.109>

Salzer, W.L., Jones, T.L., Devidas, M., Dreyer, Z.E., Gore, L., Winick, N.J., Sung, L., Raetz, E., Loh, M.L., Wang, C.Y., De Lorenzo, P., Valsecchi, M.G., Pieters, R., Carroll, W.L., Hunger, S.P., Hilden, J.M., Brown, P., 2015. Decreased induction morbidity and mortality following modification to induction therapy in infants with acute lymphoblastic leukemia enrolled on AALL0631: a report from the Children’s Oncology Group. *Pediatr. Blood Cancer* 62, 414–418. <https://doi.org/10.1002/pbc.25311>

Sandelin, A., Alkema, W., Engström, P., Wasserman, W.W., Lenhard, B., 2004. JASPAR: an open-access database for eukaryotic transcription factor binding profiles. *Nucleic Acids Res.* 32, D91–D94. <https://doi.org/10.1093/nar/gkh012>

Sanjuan-Pla, A., Bueno, C., Prieto, C., Acha, P., Stam, R.W., Marschalek, R., Menéndez, P., 2015. Revisiting the biology of infant t(4;11)/MLL-AF4+ B-cell acute lymphoblastic leukemia. *Blood* 126, 2676–2685. <https://doi.org/10.1182/blood-2015-09-667378>

Santos-Rosa, H., Schneider, R., Bannister, A.J., Sherriff, J., Bernstein, B.E., Emre, N.C.T., Schreiber, S.L., Mellor, J., Kouzarides, T., 2002. Active genes are tri-methylated at K4 of histone H3. *Nature* 419, 407–411. <https://doi.org/10.1038/nature01080>

Schafer, E., Irizarry, R., Negi, S., McIntyre, E., Small, D., Figueroa, M.E., Melnick, A., Brown, P., 2010. Promoter hypermethylation in MLL-r infant acute lymphoblastic leukemia: biology and therapeutic targeting. *Blood* 115, 4798–4809. <https://doi.org/10.1182/blood-2009-09-243634>

Schneider-Maunoury, S., Topilko, P., Seitandou, T., Levi, G., Cohen-Tannoudji, M., Pournin, S., Babinet, C., Charnay, P., 1993. Disruption of Krox-20 results in alteration of rhombomeres 3 and 5 in the developing hindbrain. *Cell* 75, 1199–1214. [https://doi.org/10.1016/0092-8674\(93\)90329-o](https://doi.org/10.1016/0092-8674(93)90329-o)

Schraets, D., Lehmann, T., Dingermann, T., Marschalek, R., 2003. MLL-mediated transcriptional gene regulation investigated by gene expression profiling. *Oncogene* 22, 3655–3668. <https://doi.org/10.1038/sj.onc.1206438>

Shah, N.N., Stevenson, M.S., Yuan, C.M., Richards, K., Delbrook, C., Kreitman, R.J., Pastan, I., Wayne, A.S., 2015. Characterization of CD22 expression in acute lymphoblastic leukemia. *Pediatr. Blood Cancer* 62, 964–969. <https://doi.org/10.1002/pbc.25410>

Shenghui, Z., Yixiang, H., Jianbo, W., Kang, Y., Laixi, B., Yan, Z., Xi, X., 2011. Elevated frequencies of CD4⁺ CD25⁺ CD127^{lo} regulatory T cells is associated to poor prognosis in patients with acute myeloid leukemia. *Int. J. Cancer* 129, 1373–1381. <https://doi.org/10.1002/ijc.25791>

Shukla, N., Wetmore, C., O’Brien, M.M., Silverman, L.B., Brown, P., Cooper, T.M., Thomson, B., Blake-more, S.J., Daigle, S., Suttle, B., Waters, N.J., Krivstov, A.V., Armstrong, S.A., Ho, P.T., Gore, L., 2016. Final Report of Phase 1 Study of the DOT1L Inhibitor, Pinometostat (EPZ-5676), in Children with Relapsed or Refractory MLL-r Acute Leukemia. *Blood* 128, 2780. <https://doi.org/10.1182/blood.V128.22.2780.2780>

Sison, E.A.R., Magoon, D., Li, L., Annesley, C.E., Rau, R.E., Small, D., Brown, P., 2014. Plerixafor as a chemosensitizing agent in pediatric acute lymphoblastic leukemia: efficacy and potential mechanisms of resistance to CXCR4 inhibition. *Oncotarget* 5, 8947–8958.

Sison, E.A.R., Magoon, D., Li, L., Annesley, C.E., Romagnoli, B., Douglas, G.J., Tuffin, G., Zimmermann, J., Brown, P., 2015. POL5551, a novel and potent CXCR4 antagonist, enhances sensitivity to chemotherapy in pediatric ALL. *Oncotarget* 6, 30902–30918. <https://doi.org/10.18632/oncotarget.5094>

Sison, E.A.R., McIntyre, E., Magoon, D., Brown, P., 2013a. Dynamic chemotherapy-induced upregulation of CXCR4 expression: a mechanism of therapeutic resistance in pediatric AML. *Mol. Cancer Res. MCR* 11, 1004–1016. <https://doi.org/10.1158/1541-7786.MCR-13-0114>

Sison, E.A.R., Rau, R.E., McIntyre, E., Li, L., Small, D., Brown, P., 2013b. MLL-rearranged acute lymphoblastic leukaemia stem cell interactions with bone marrow stroma promote survival and therapeutic resistance that can be overcome with CXCR4 antagonism. *Br. J. Haematol.* 160, 785–797. <https://doi.org/10.1111/bjh.12205>

Smigiel, K.S., Richards, E., Srivastava, S., Thomas, K.R., Dudda, J.C., Klonowski, K.D., Campbell, D.J., 2014. CCR7 provides localized access to IL-2 and defines homeostatically distinct regulatory T cell subsets. *J. Exp. Med.* 211, 121–136. <https://doi.org/10.1084/jem.20131142>

Southall, S.M., Wong, P.-S., Odho, Z., Roe, S.M., Wilson, J.R., 2009. Structural basis for the requirement of additional factors for MLL1 SET domain activity and recognition of epigenetic marks. *Mol. Cell* 33, 181–191. <https://doi.org/10.1016/j.molcel.2008.12.029>

Stam, R.W., den Boer, M.L., Meijerink, J.P.P., Ebus, M.E.G., Peters, G.J., Noordhuis, P., Janka-Schaub, G.E., Armstrong, S.A., Korsmeyer, S.J., Pieters, R., 2003. Differential mRNA expression of Ara-C-metabolizing enzymes explains Ara-C sensitivity in MLL gene-rearranged infant acute lymphoblastic leukemia. *Blood* 101, 1270–1276. <https://doi.org/10.1182/blood-2002-05-1600>

Stam, R.W., Schneider, P., de Lorenzo, P., Valsecchi, M.G., den Boer, M.L., Pieters, R., 2007. Prognostic significance of high-level FLT3 expression in MLL-rearranged infant acute lymphoblastic leukemia. *Blood* 110, 2774–2775. <https://doi.org/10.1182/blood-2007-05-091934>

Stam, R.W., Schneider, P., Hagelstein, J.A.P., van der Linden, M.H., Stumpel, D.J.P.M., de Menezes, R.X., de Lorenzo, P., Valsecchi, M.G., Pieters, R., 2010. Gene expression profiling-based dissection of MLL translocated and MLL germline acute lymphoblastic leukemia in infants. *Blood* 115, 2835–2844. <https://doi.org/10.1182/blood-2009-07-233049>

Stanulla, M., Wang, J., Chervinsky, D.S., Thandla, S., Aplan, P.D., 1997. DNA cleavage within the MLL breakpoint cluster region is a specific event which occurs as part of higher-order chromatin fragmentation during the initial stages of apoptosis. *Mol. Cell. Biol.* 17, 4070–4079. <https://doi.org/10.1128/MCB.17.7.4070>

Stein, E.M., Garcia-Manero, G., Rizzieri, D.A., Tibes, R., Berdeja, J.G., Savona, M.R., Jongen-Lavrenic, M., Altman, J.K., Thomson, B., Blakemore, S.J., Daigle, S.R., Waters, N.J., Suttle, A.B., Clawson, A., Pollock, R., Krivtsov, A., Armstrong, S.A., DiMartino, J., Hedrick, E., Löwenberg, B., Tallman, M.S., 2018. The DOT1L inhibitor pinometostat reduces H3K79 methylation and has modest clinical activity in adult acute leukemia. *Blood* 131, 2661–2669. <https://doi.org/10.1182/blood-2017-12-818948>

Stumpel, D.J.P.M., Schneider, P., Seslija, L., Osaki, H., Williams, O., Pieters, R., Stam, R.W., 2012. Connectivity mapping identifies HDAC inhibitors for the treatment of t(4;11)-positive infant acute lymphoblastic leukemia. *Leukemia* 26, 682–692. <https://doi.org/10.1038/leu.2011.278>

Stumpel, D.J.P.M., Schneider, P., van Roon, E.H.J., Boer, J.M., de Lorenzo, P., Valsecchi, M.G., de Menezes, R.X., Pieters, R., Stam, R.W., 2009. Specific promoter methylation identifies different subgroups of MLL-rearranged infant acute lymphoblastic leukemia, influences clinical outcome, and provides therapeutic options. *Blood* 114, 5490–5498. <https://doi.org/10.1182/blood-2009-06-227660>

Stumpel, D.J.P.M., Schotte, D., Lange-Turenhout, E. a. M., Schneider, P., Seslija, L., de Menezes, R.X., Marquez, V.E., Pieters, R., den Boer, M.L., Stam, R.W., 2011. Hypermethylation of specific microRNA

genes in MLL-rearranged infant acute lymphoblastic leukemia: major matters at a micro scale. *Leukemia* 25, 429–439. <https://doi.org/10.1038/leu.2010.282>

Stutterheim, J., van der Sluis, I.M., de Lorenzo, P., Alten, J., Ancliffe, P., Attarbaschi, A., Brethon, B., Biondi, A., Campbell, M., Cazzaniga, G., Escherich, G., Ferster, A., Kotecha, R.S., Lausen, B., Li, C.K., Lo Nigro, L., Locatelli, F., Marschalek, R., Meyer, C., Schrappe, M., Stary, J., Vora, A., Zuna, J., van der Velden, V.H.J., Szczepanski, T., Valsecchi, M.G., Pieters, R., 2021. Clinical Implications of Minimal Residual Disease Detection in Infants With KMT2A-Rearranged Acute Lymphoblastic Leukemia Treated on the Interfant-06 Protocol. *J. Clin. Oncol. Off. J. Am. Soc. Clin. Oncol.* 39, 652–662. <https://doi.org/10.1200/JCO.20.02333>

Sullivan, B.A., Tsuji, W., Kivitz, A., Peng, J., Arnold, G.E., Boedigheimer, M.J., Chiu, K., Green, C.L., Kaliyaperumal, A., Wang, C., Ferbas, J., Chung, J.B., 2016. Inducible T-cell co-stimulator ligand (ICOSL) blockade leads to selective inhibition of anti-KLH IgG responses in subjects with systemic lupus erythematosus. *Lupus Sci. Med.* 3, e000146. <https://doi.org/10.1136/lupus-2016-000146>

Svaren, J., Sevetson, B.R., Apel, E.D., Zimonjic, D.B., Popescu, N.C., Milbrandt, J., 1996. NAB2, a corepressor of NGFI-A (Egr-1) and Krox20, is induced by proliferative and differentiative stimuli. *Mol. Cell. Biol.* 16, 3545–3553.

Svensson-Arvelund, J., Mehta, R.B., Lindau, R., Mirrasekhian, E., Rodriguez-Martinez, H., Berg, G., Lash, G.E., Jenmalm, M.C., Ernerudh, J., 2015. The Human Fetal Placenta Promotes Tolerance against the Semiallogeneic Fetus by Inducing Regulatory T Cells and Homeostatic M2 Macrophages. *J. Immunol.* 194, 1534–1544. <https://doi.org/10.4049/jimmunol.1401536>

Swirnoff, A.H., Apel, E.D., Svaren, J., Sevetson, B.R., Zimonjic, D.B., Popescu, N.C., Milbrandt, J., 1998. Nab1, a corepressor of NGFI-A (Egr-1), contains an active transcriptional repression domain. *Mol. Cell. Biol.* 18, 512–524. <https://doi.org/10.1128/MCB.18.1.512>

Symeonidou, V., Ottersbach, K., 2021. HOXA9/IRX1 expression pattern defines two subgroups of infant MLL-AF4-driven acute lymphoblastic leukemia. *Exp. Hematol.* 93, 38–43.e5. <https://doi.org/10.1016/j.exphem.2020.10.002>

Takachi, T., Watanabe, T., Miyamura, T., Moriya Saito, A., Deguchi, T., Hori, T., Yamada, T., Ohmori, S., Haba, M., Aoki, Y., Ishimaru, S., Sasaki, S., Ohshima, J., Iguchi, A., Takahashi, Y., Hyakuna, N., Manabe, A., Horibe, K., Ishii, E., Koh, K., Tomizawa, D., 2021. Hematopoietic stem cell transplantation for infants with high-risk KMT2A gene-rearranged acute lymphoblastic leukemia. *Blood Adv.* 5, 3891–3899. <https://doi.org/10.1182/bloodadvances.2020004157>

Takahata, Y., Nomura, A., Takada, H., Ohga, S., Furuno, K., Hikino, S., Nakayama, H., Sakaguchi, S., Hara, T., 2004. CD25+CD4+ T cells in human cord blood: an immunoregulatory subset with naive phenotype and specific expression of forkhead box p3 (Foxp3) gene. *Exp. Hematol.* 32, 622–629. <https://doi.org/10.1016/j.exphem.2004.03.012>

Taketani, T., Taki, T., Sugita, Kanji, Furuichi, Y., Ishii, E., Hanada, R., Tsuchida, M., Sugita, Kenichi, Ida, K., Hayashi, Y., 2004. FLT3 mutations in the activation loop of tyrosine kinase domain are frequently found in infant ALL with MLL rearrangements and pediatric ALL with hyperdiploidy. *Blood* 103, 1085–1088. <https://doi.org/10.1182/blood-2003-02-0418>

Tallen, G., Ratei, R., Mann, G., Kaspers, G., Niggli, F., Karachunsky, A., Ebell, W., Escherich, G., Schrappe, M., Klingebiel, T., Fengler, R., Henze, G., Stackelberg, A. von, 2010. Long-Term Outcome in Children With Relapsed Acute Lymphoblastic Leukemia After Time-Point and Site-of-Relapse Stratification and Intensified Short-Course Multidrug Chemotherapy: Results of Trial ALL-REZ BFM 90. *J. Clin. Oncol.* <https://doi.org/10.1200/JCO.2009.25.1983>

Tang, C., Li, M.-H., Chen, Y.-L., Sun, H.-Y., Liu, S.-L., Zheng, W.-W., Zhang, M.-Y., Li, H., Fu, W., Zhang, W.-J., Liang, A.-B., Tang, Z.-H., Hong, D.-L., Zhou, B.-B.S., Duan, C.-W., 2018. Chemotherapy-induced

niche perturbs hematopoietic reconstitution in B-cell acute lymphoblastic leukemia. *J. Exp. Clin. Cancer Res.* 37, 204. <https://doi.org/10.1186/s13046-018-0859-3>

Tilburgs, T., Roelen, D.L., Mast, B.J. van der, Groot-Swings, G.M. de, Kleijburg, C., Scherjon, S.A., Claas, F.H., 2008. Evidence for a Selective Migration of Fetus-Specific CD4+CD25bright Regulatory T Cells from the Peripheral Blood to the Decidua in Human Pregnancy. *J. Immunol.* 180, 5737–5745. <https://doi.org/10.4049/jimmunol.180.8.5737>

Tomizawa, D., Koh, K., Hirayama, M., Miyamura, T., Hatanaka, M., Saikawa, Y., Ishii, E., 2009. Outcome of recurrent or refractory acute lymphoblastic leukemia in infants with MLL gene rearrangements: A report from the Japan Infant Leukemia Study Group. *Pediatr. Blood Cancer* 52, 808–813. <https://doi.org/10.1002/pbc.21975>

Tomizawa, D., Miyamura, T., Imamura, T., Watanabe, T., Moriya Saito, A., Ogawa, A., Takahashi, Y., Hirayama, M., Taki, T., Deguchi, T., Hori, T., Sanada, M., Ohmori, S., Haba, M., Iguchi, A., Arakawa, Y., Koga, Y., Manabe, A., Horibe, K., Ishii, E., Koh, K., 2020. A risk-stratified therapy for infants with acute lymphoblastic leukemia: a report from the JPLSG MLL-10 trial. *Blood* 136, 1813–1823. <https://doi.org/10.1182/blood.2019004741>

Trentin, L., Giordan, M., Dingermann, T., Basso, G., Te Kronnie, G., Marschalek, R., 2009. Two independent gene signatures in pediatric t(4;11) acute lymphoblastic leukemia patients. *Eur. J. Haematol.* 83, 406–419. <https://doi.org/10.1111/j.1600-0609.2009.01305.x>

Usmani, S., Sivagnalingam, U., Tkachenko, O., Nunez, L., Shand, J.C., Mullen, C.A., 2019. Support of acute lymphoblastic leukemia cells by nonmalignant bone marrow stromal cells. *Oncol. Lett.* 17, 5039–5049. <https://doi.org/10.3892/ol.2019.10188>

Varešlija, D., McBryan, J., Fagan, A., Redmond, A.M., Hao, Y., Sims, A.H., Turnbull, A., Dixon, J.M., Ó Gaora, P., Hudson, L., Purcell, S., Hill, A.D.K., Young, L.S., 2016. Adaptation to AI Therapy in Breast Cancer Can Induce Dynamic Alterations in ER Activity Resulting in Estrogen-Independent Metastatic Tumors. *Clin. Cancer Res. Off. J. Am. Assoc. Cancer Res.* 22, 2765–2777. <https://doi.org/10.1158/1078-0432.CCR-15-1583>

Velten, L., Haas, S.F., Raffel, S., Blaszkiewicz, S., Islam, S., Hennig, B.P., Hirche, C., Lutz, C., Buss, E.C., Nowak, D., Boch, T., Hofmann, W.-K., Ho, A.D., Huber, W., Trumpp, A., Essers, M.A.G., Steinmetz, L.M., 2017. Human haematopoietic stem cell lineage commitment is a continuous process. *Nat. Cell Biol.* 19, 271–281. <https://doi.org/10.1038/ncb3493>

Vocanson, M., Rozieres, A., Hennino, A., Poyet, G., Gaillard, V., Renaudineau, S., Achachi, A., Benetiere, J., Kaiserlian, D., Dubois, B., Nicolas, J.-F., 2010. Inducible costimulator (ICOS) is a marker for highly suppressive antigen-specific T cells sharing features of TH17/TH1 and regulatory T cells. *J. Allergy Clin. Immunol.* 126, 280-289.e7. <https://doi.org/10.1016/j.jaci.2010.05.022>

von Stackelberg, A., Locatelli, F., Zugmaier, G., Handgretinger, R., Trippett, T.M., Rizzari, C., Bader, P., O'Brien, M.M., Brethon, B., Bhojwani, D., Schlegel, P.G., Borkhardt, A., Rheingold, S.R., Cooper, T.M., Zwaan, C.M., Barnette, P., Messina, C., Michel, G., DuBois, S.G., Hu, K., Zhu, M., Whitlock, J.A., Gore, L., 2016. Phase I/Phase II Study of Blinatumomab in Pediatric Patients With Relapsed/Refractory Acute Lymphoblastic Leukemia. *J. Clin. Oncol. Off. J. Am. Soc. Clin. Oncol.* 34, 4381–4389. <https://doi.org/10.1200/JCO.2016.67.3301>

Wang, Z., Song, J., Milne, T.A., Wang, G.G., Li, H., Allis, C.D., Patel, D.J., 2010. Pro isomerization in MLL1 PHD3-bromo cassette connects H3K4me readout to CyP33 and HDAC-mediated repression. *Cell* 141, 1183–1194. <https://doi.org/10.1016/j.cell.2010.05.016>

Wilhelm, A., Marschalek, R., 2021. The role of reciprocal fusions in MLL-r acute leukemia: studying the chromosomal translocation t(4;11). *Oncogene* 40, 6093–6102. <https://doi.org/10.1038/s41388-021-02001-2>

Wilkinson, A.C., Ballabio, E., Geng, H., North, P., Tapia, M., Kerry, J., Biswas, D., Roeder, R.G., Allis, C.D., Melnick, A., de Bruijn, M.F.T.R., Milne, T.A., 2013. RUNX1 is a key target in t(4;11) leukemias that contributes to gene activation through an AF4-MLL complex interaction. *Cell Rep.* 3, 116–127. <https://doi.org/10.1016/j.celrep.2012.12.016>

Williams, J., Dragunow, M., Lawlor, P., Mason, S., Abraham, W.C., Leah, J., Bravo, R., Demmer, J., Tate, W., 1995. Krox20 may play a key role in the stabilization of long-term potentiation. *Mol. Brain Res.* 28, 87–93. [https://doi.org/10.1016/0169-328X\(94\)00187-J](https://doi.org/10.1016/0169-328X(94)00187-J)

Wisden, W., Errington, M.L., Williams, S., Dunnett, S.B., Waters, C., Hitchcock, D., Evan, G., Bliss, T.V.P., Hunt, S.P., 1990. Differential expression of immediate early genes in the hippocampus and spinal cord. *Neuron* 4, 603–614. [https://doi.org/10.1016/0896-6273\(90\)90118-Y](https://doi.org/10.1016/0896-6273(90)90118-Y)

Wu, Y., Borde, M., Heissmeyer, V., Feuerer, M., Lapan, A.D., Stroud, J.C., Bates, D.L., Guo, L., Han, A., Ziegler, S.F., Mathis, D., Benoist, C., Chen, L., Rao, A., 2006. FOXP3 Controls Regulatory T Cell Function through Cooperation with NFAT. *Cell* 126, 375–387. <https://doi.org/10.1016/j.cell.2006.05.042>

Wysocka, J., Swigut, T., Milne, T.A., Dou, Y., Zhang, X., Burlingame, A.L., Roeder, R.G., Brivanlou, A.H., Allis, C.D., 2005. WDR5 associates with histone H3 methylated at K4 and is essential for H3 K4 methylation and vertebrate development. *Cell* 121, 859–872. <https://doi.org/10.1016/j.cell.2005.03.036>

Xia, Z.-B., Anderson, M., Diaz, M.O., Zeleznik-Le, N.J., 2003. MLL repression domain interacts with histone deacetylases, the polycomb group proteins HPC2 and BMI-1, and the corepressor C-terminal-binding protein. *Proc. Natl. Acad. Sci.* 100, 8342–8347. <https://doi.org/10.1073/pnas.1436338100>

Yamagata, K., Kaufmann, W.E., Lanahan, A., Papapavlou, M., Barnes, C.A., Andreasson, K.I., Worley, P.F., 1994. Egr3/Pilot, a zinc finger transcription factor, is rapidly regulated by activity in brain neurons and colocalizes with Egr1/zif268. *Learn. Mem.* 1, 140–152. <https://doi.org/10.1101/lm.1.2.140>

Yang, W., Lee, K.-W., Srivastava, R.M., Kuo, F., Krishna, C., Chowell, D., Makarov, V., Hoen, D., Dalin, M.G., Wexler, L., Ghossein, R., Katabi, N., Nadeem, Z., Cohen, M.A., Tian, S.K., Robine, N., Arora, K., Geiger, H., Agius, P., Bouvier, N., Huberman, K., Vanness, K., Havel, J.J., Sims, J.S., Samstein, R.M., Mandal, R., Tepe, J., Ganly, I., Ho, A.L., Riaz, N., Wong, R.J., Shukla, N., Chan, T.A., Morris, L.G.T., 2019. Immunogenic neoantigens derived from gene fusions stimulate T cell responses. *Nat. Med.* 25, 767–775. <https://doi.org/10.1038/s41591-019-0434-2>

Yeoh, E.-J., Ross, M.E., Shurtleff, S.A., Williams, W.K., Patel, D., Mahfouz, R., Behm, F.G., Raimondi, S.C., Relling, M.V., Patel, A., Cheng, C., Campana, D., Wilkins, D., Zhou, X., Li, J., Liu, H., Pui, C.-H., Evans, W.E., Naeve, C., Wong, L., Downing, J.R., 2002. Classification, subtype discovery, and prediction of outcome in pediatric acute lymphoblastic leukemia by gene expression profiling. *Cancer Cell* 1, 133–143. [https://doi.org/10.1016/S1535-6108\(02\)00032-6](https://doi.org/10.1016/S1535-6108(02)00032-6)

Yokoyama, A., 2021. Role of the MOZ/MLL-mediated transcriptional activation system for self-renewal in normal hematopoiesis and leukemogenesis. *FEBS J.* <https://doi.org/10.1111/febs.16180>

Yokoyama, A., Kitabayashi, I., Ayton, P.M., Cleary, M.L., Ohki, M., 2002. Leukemia proto-oncoprotein MLL is proteolytically processed into 2 fragments with opposite transcriptional properties. *Blood* 100, 3710–3718. <https://doi.org/10.1182/blood-2002-04-1015>

Yokoyama, A., Lin, M., Naresh, A., Kitabayashi, I., Cleary, M.L., 2010. A Higher-Order Complex Containing AF4 and ENL Family Proteins with P-TEFb Facilitates Oncogenic and Physiologic MLL-Dependent Transcription. *Cancer Cell* 17, 198–212. <https://doi.org/10.1016/j.ccr.2009.12.040>

Yokoyama, A., Wang, Z., Wysocka, J., Sanyal, M., Aufiero, D.J., Kitabayashi, I., Herr, W., Cleary, M.L., 2004. Leukemia proto-oncoprotein MLL forms a SET1-like histone methyltransferase complex with menin to regulate Hox gene expression. *Mol. Cell. Biol.* 24, 5639–5649. <https://doi.org/10.1128/MCB.24.13.5639-5649.2004>

- Yoshinaga, S.K., Whoriskey, J.S., Khare, S.D., Sarmiento, U., Guo, J., Horan, T., Shih, G., Zhang, M., Coccia, M.A., Kohno, T., Tafuri-Bladt, A., Brankow, D., Campbell, P., Chang, D., Chiu, L., Dai, T., Duncan, G., Elliott, G.S., Hui, A., McCabe, S.M., Scully, S., Shahinian, A., Shaklee, C.L., Van, G., Mak, T.W., Senaldi, G., 1999. T-cell co-stimulation through B7RP-1 and ICOS. *Nature* 402, 827–832. <https://doi.org/10.1038/45582>
- Zamora, A.E., Crawford, J.C., Allen, E.K., Guo, X.J., Bakke, J., Carter, R.A., Abdelsamed, H.A., Moustaki, A., Li, Y., Chang, T.-C., Awad, W., Dallas, M.H., Mullighan, C.G., Downing, J.R., Geiger, T.L., Chen, T., Green, D.R., Youngblood, B.A., Zhang, J., Thomas, P.G., 2019. Pediatric patients with acute lymphoblastic leukemia generate abundant and functional neoantigen-specific CD8⁺ T cell responses. *Sci. Transl. Med.* 11, eaat8549. <https://doi.org/10.1126/scitranslmed.aat8549>
- Zeleznik-Le, N.J., Harden, A.M., Rowley, J.D., 1994. 11q23 translocations split the “AT-hook” cruciform DNA-binding region and the transcriptional repression domain from the activation domain of the mixed-lineage leukemia (MLL) gene. *Proc. Natl. Acad. Sci.* 91, 10610–10614. <https://doi.org/10.1073/pnas.91.22.10610>
- Zeng, H., Yang, K., Cloer, C., Neale, G., Vogel, P., Chi, H., 2013. mTORC1 couples immune signals and metabolic programming to establish T(reg)-cell function. *Nature* 499, 485–490. <https://doi.org/10.1038/nature12297>
- Zheng, J., Chan, P.-L., Liu, Y., Qin, G., Xiang, Z., Lam, K.-T., Lewis, D.B., Lau, Y.-L., Tu, W., 2013. ICOS regulates the generation and function of human CD4⁺ Treg in a CTLA-4 dependent manner. *PloS One* 8, e82203. <https://doi.org/10.1371/journal.pone.0082203>
- Zou, L., Barnett, B., Safah, H., LaRussa, V.F., Evdemon-Hogan, M., Mottram, P., Wei, S., David, O., Curiel, T.J., Zou, W., 2004. Bone Marrow Is a Reservoir for CD4⁺CD25⁺ Regulatory T Cells that Traffic through CXCL12/CXCR4 Signals. *Cancer Res.* 64, 8451–8455. <https://doi.org/10.1158/0008-5472.CAN-04-1987>

6 List of figures

Figure no.	Title/Description	Page
1	The mouse and human multistep hematopoietic system	1
2	The standard model of hematopoietic hierarchy compared to the proposed re-defined model in FL and adult BM	2
3	Epidemiology and clinical characteristics of infant <i>KMT2A-r</i> ALL	4
4	Interfant induction protocol	6
5	Interfant-99 protocol	7
6	The <i>KMT2A</i> recombinome of acute leukemia	12
7	Schematic protein structure and consensus binding sequence of EGR1, EGR2 and EGR3	16
8	Generation of EGR1-3 overexpressing HEK293T cell culture models	30
9	Principal component analysis (PCA) comparing the grade of similarity between the IRX1 and EGR1-3 gene expression data sets	35
10	Establishment of stable cell culture models SEM:: <i>EGR3</i> and SEM:: <i>IRX1</i>	36
11	Proof of transgene expression for cell lines SEM::mock, SEM:: <i>EGR3</i> and SEM:: <i>IRX1</i>	37
12	Gene and protein expression analysis of SEM:: <i>EGR3</i> and SEM:: <i>IRX1</i> cell culture models	38
13	ChIP-qRT-PCR of predicted EGR3 binding sites at <i>ICOSLG</i> promoter	39
14	ChIP-Seq	40
15	Patient age distribution	41
16	Pearson correlation matrix	45
17	Pearson correlations of <i>IRX1</i> , <i>EGR3</i> and <i>ICOSLG</i>	45
18	EFS depending on <i>HOXA9</i> gene expression	46
19	EFS depending on <i>ICOSLG</i> gene expression	47
20	Gene expression comparison of “relapse” and “diagnosis” cohort	49
21	Principal component analysis (PCA) comparing the grade of similarity between “dx” <i>ICOSLG</i> ^{hi} , “dx” <i>ICOSLG</i> ^{lo} , and “rel”	50
22	T-cell co-culture: experimental procedure	51
23	Results of co-culture experiments	52
24	Consequences of <i>ICOSLG</i> blockade on Treg development	53
25	ICOS surface expression among different T-cell subsets	54
26	Patient age distribution of Stam <i>et al.</i> , 2010 compared to own data	58
27	<i>ICOSLG</i> expression in cells of the hematopoietic system	61
28	Signaling pathways activated in Tregs upon <i>ICOSLG/ICOS</i> binding	62
29	Proposed immune-evasion relapse mechanism	64

7 List of tables

Table no.	Title/Description	Page
1	Risk stratification of Interfant-06, COG (AALL0631) and JPLSG (MLL-10)	5
2	Stable cell lines established using the sleeping beauty (SB) transposon system	18
3	Recombinant DNA used in this thesis	18
4	Oligonucleotides used in this thesis	18
5	Media and solutions used in this thesis	19
6	Antibodies used in this thesis	20
7	Chemicals and recombinant proteins used in this thesis	21
8	Commercial assays and kits used in this thesis	22
9	Consumables used in this thesis	22
10	Devices used in this thesis	23
11	Software used in this thesis	24
12	Patients assigned to study centers that provided RNA samples	27
13	Summary of RNA sample characteristics for MACE-Seq	31
14	Selected genes and respective log ₂ fc values of IRX1 and EGR1-3 data sets	32
15	Individual and cumulative variance expressed by three dimensions	34
16	Principal component coordinates of each data set	34
17	Immune related genes upregulated in EGR3 MACE data and IRX1 Affymetrix data	35
18	Predicted binding sites of EGR3	39
19	Patient characteristics of the “diagnosis cohort”	42
20	Patient characteristics of the “relapse cohort”	48
21	Individual and cumulative variance expressed by three dimensions	50

8 Acknowledgements

I would like to thank all the amazing people in- and outside the Marschalek lab who excessively supported me throughout this project – scientifically and personally.

First, I would like to thank Prof. Dr. Rolf Marschalek for the wonderful opportunity to work on this fascinating project and to intensively study the biology of childhood hematologic malignancy. It was a pleasure!

Second, I acknowledge all the great minds which inspired my understanding of science and fostered my curiosity in research: Dr. Anna Lena Siemund, Prof. Dr. Rolf Marschalek, Dr. Claus Meyer, Dr. Patrizia Larghero, Prof. Dr. Halvard Bönig and Prof. Dr. Gunnar Cario.

Moreover, I would like to thank the collaborators and co-workers of the project for contributing expertise, advice and patient samples: Dr. Anna Lena Siemund, Dr. Claus Meyer, Dr. Patrizia Larghero, Alissa Dietz, Robin Jaskosch, Dr. Julia Alten, Prof. Dr. Gunnar Cario, Birthe Fedders, PD Dr. Cornelia Eckert, Dr. Aurélie Caye-Eude, Prof. Dr. Hélène Cavé, Dr. Michela Bardini, Prof. Dr. Gianni Cazzaniga, Dr. Paola De Lorenzo, Prof. Dr. Maria Grazia Valsecchi, Laura Diehl, Prof. Dr. Halvard Bönig and Dr. Phillip Grote.

Thank you for so wonderful times in the lab Anna, Vanessa, Patrick, Claus, Patrizia, Alissa, Robin, Silvia, Eric, Jenny, Arpita, Bruno, Lisa, Tamara, Freia, Valerie, Thomas and the Fürst group members!

I especially thank Prof. Dr. Robert Fürst for undertaking the second evaluation of this PhD thesis.

Finally, I thank my amazing family Bettina, Michael, Alex, Gabi and Paula for their compelling personal support during, before and after my PhD studies! Without you, this would have been impossible.

9 Declaration

Except where stated otherwise by reference or acknowledgment, the work presented was generated by myself under the supervision of my advisors during my doctoral studies. All contributions from colleagues are explicitly referenced in the thesis. The material listed below was obtained in the context of collaborative research.

Patient RNA samples extracted from PB biopsies as well as corresponding clinical data including age, treatment protocol, sex, time to event, and last follow up were derived from the following collaborators:

Patient no.	Study center	Contact
1 -14	Centro Ricerca Tettamanti, Pediatrics, University of Milano-Bicocca, San Gerardo Hospital, Monza, Italy	Dr. Michela Bardini, Prof. Dr. Gianni Cazzaniga
15-29	Department of Genetics, University Hospital Robert Debré, Paris, France	Dr. Aurélie Caye-Eude, Prof. Dr. Hélène Cavé
30 - 50	Department of Pediatrics, University Medical Center Schleswig-Holstein, Kiel, Germany	Dr. Julia Alten, Prof. Dr. Gunnar Cario
REZ1 – REZ18	Department of Pediatric Oncology and Hematology, Charité Campus Virchow Clinic, Berlin, Germany	PD Dr. Cornelia Eckert

Further gene expression and clinical data analyses were performed by myself.

The following parts of the thesis have been accepted for publication and copyright permission and/or co-author agreement has been obtained:

- Figures 13C, 14, 15, 16, 17D-F, 18, 19, 20, 21, 23, 24, 25, 29
- Tables 19, 20

I herewith declare that I have not previously participated in any doctoral examination procedure in a mathematics or natural science discipline.

Frankfurt am Main, 31 May 2022

Author's declaration

I hereby declare that I have produced my doctoral dissertation on the topic of

EGR-mediated relapse mechanisms in infant t(4;11) acute lymphoblastic leukemia

independently and using only the tools indicated therein. In particular, all references borrowed from external sources are clearly acknowledged and identified.

I confirm that I have respected the principles of good scientific practice and have not made use of the services of any commercial agency in respect of my doctorate.

Frankfurt am Main, 31 May 2022
